AD

USAAVLABS TECHNICAL REPORT 68-22C

IN-FLIGHT MEASUREMENT AND CORRELATION WITH THEORY OF BLADE AIRLOADS AND RESPONSES ON THE XH-51A COMPOUND HELICOPTER ROTOR

VOLUME III
THEORETICAL PREDICTION OF AIRLOADS AND STRUCTURAL LOADS AND CORRELATION WITH FLIGHT TEST MEASUREMENTS

By

J. E. Sweers

May 1968

U. S. ARMY AVIATION MATERIEL LABORATORIES
FORT EUSTIS, VIRGINIA

CONTRACT DA 44-177-AMC-357(T)

LOCKHEED-CALIFORNIA COMPANY
BURBANK, CALIFORNIA

SEP 9 1968

Disclaimers

Under Army contract, the Lockheed Aircraft Corporation has con-
ducted an investigation of blade aerodynamic pressures and strains
and other associated flight characteristics on an XH-51A compound
helicopter. The flight tests and theoretical analyses which were
performed during the program were monitored by Army personnel, and
the final report has been reviewed to ensure basic technical
accuracy.

This report is published for the dissemination of information
and the stimulation of further research.

IN-FLIGHT MEASUREMENT AND CORRELATION WITH THEORY OF BLADE AIRLOADS AND RESPONSES ON THE XH-51A COMPOUND HELICOPTER ROTOR

LR 21072

VOLUME III
THEORETICAL PREDICTION OF AIRLOADS AND STRUCTURAL LOADS AND CORRELATION WITH FLIGHT TEST MEASUREMENTS

By

J. E. Sweers

Prepared by

Lockheed-California Company
Burbank, California

for

U. S. ARMY AVIATION MATERIEL LABORATORIES
FORT EUSTIS, VIRGINIA

ABSTRACT

This report presents the results of a two-phase research program consisting of (1) in-flight measurement of aerodynamic pressures and structural loads on a compound, rigid-rotor helicopter and (2) correlation of these data with theoretical results.

Flight test data obtained in Phase I and recorded on an oscillograph were read on an oscillograph reading machine and were processed in an automatic data reduction program. This data processing consisted of integration of the pressure data to obtain the distribution of aerodynamic lift and pitching moments over the rotor blade, as functions of azimuth position. Airload and structural load data were harmonically analyzed.

Output of the data reduction program was used in Phase II as input to the correlation program. The measured airloads were used to compute the theoretical bending and torsion responses of the blade. The measured torsion moments were used in the theoretical prediction of the airloads. The results of the applied theories are compared with the flight measurements.

FOREWORD

This report describes a two-phase research program consisting of (1) flight
test measurements of helicopter rotor blade structural loads and aerody-
namic pressures and (2) correlation of these measurements with data obtained
from current theories. This research program was conducted by the Lockheed-
California Company under Contract DA 44-177-AMC-357(T) to the U.S. Army
Aviation Materiel Laboratories (USAAVLABS), Fort Eustis, Virginia.

The research program was performed during the period from June 1966 to
October 1967. Technical monitoring of the project for USAAVLABS was by
W. E. Nettles.

The report covering the program is presented in three volumes. Volume I
is entitled "Measurement and Data Reduction of Airloads and Structural
Loads". It contains the main body of the report plus Appendixes I through
IV. Volume II contains Appendixes V through IX, with all flight test data
in tabular form. The correlation of the measured airloads and structural
loads with theoretical data is covered in Volume III, "Theoretical
Prediction of Airloads and Structural Loads and Correlation with Flight
Test Measurements".

The Lockheed program was under the technical direction of A. W. Turner and
W. E. Spreuer, engineering managers, and J. E. Sweers, project leader. The
test pilot was R. Goudey. Additional Lockheed personnel associated with
the program included W. H. Foulke and R. A. Berry, flight test;
C. J. Buzzetti, E. A. Bartsch, S. H. Lomax, and T. H. Oglesby, structural
flight measurement; R. H. Cook and R. G. Murison, instrumentation;
R. D. Baker and W. C. Weddle, data processing; R. E. Donham and D. H. Janda,
rotary wing dynamics; C. H. Ranschau, programming; and R. P. Beal, editor.

Appreciation is due USAAVLABS for their help in providing assistance and
advice in planning and executing the entire research program.

CONTENTS

VOLUME I
Page

VOLUME II

VOLUME III

VOLUME III (Continued)

LIST OF ILLUSTRATIONS

x

xi

xiii

xv

LIST OF TABLES

LIST OF SYMBOLS

A   matrix of unit inertia forces: $A_{i,j}$ = generalized inertia force acting upon generalized coordinate i due to unit acceleration $\ddot{q}_j$

B   matrix of centrifugal forces: $-\Omega^2 B_{ij}$ generalized centrifugal force acting upon generalized coordinate i due to unit displacement q_j

C   stiffness matrix: C_{ij} = structural force acting upon generalized coordinate i due to unit displacement q_j

D   Coriolis force matrix: ΩD_{ij} = generalized Coriolis force acting upon generalized coordinate i due to unit velocity $\dot{q}_j$

$q_i, \dot{q}_i, \ddot{q}_i$ displacement, velocity, acceleration in generalized coordinate i

Q_i generalized force acting upon generalized coordinate i

T   kinetic energy

V   potential energy

x,y,z   right-hand Cartesian coordinate system, rotating about the z axis at angular velocity Ω of the rotor

θ_i rotation of blade element i (positive = leading edge up) relative to xy plane

$\dfrac{\partial x_i}{\partial q_n}, \dfrac{\partial y_i}{\partial q_n}, \dfrac{\partial z_i}{\partial q_n}, \dfrac{\partial \theta_i}{\partial q_n}$ mode shapes of generalized coordinate n; i.e.,

displacements in x, y, z direction, and rotation of blade element i for unit displacement in generalized coordinate n

$\theta_o, \theta_{1c}, \theta_{1s}$ collective and cyclic control angles

LIST OF SYMBOLS (Cont)

ψ azimuth position ($\psi=0$ is aft position of x axis) of x, y, z coordinate system

Z   vertical distance between rotor shaft plane and trailing tip vortex ring (positive when ring below rotor shaft plane)

ξ radius of trail. tip vortex ring

INTRODUCTION

The problem of analytically predicting loading conditions of helicopter rotor blades in high speed flight consists of three parts:

- To find the conditions for trim, i.e., vehicle attitude and blade control angles.

- To find the distribution of airloads over the blades as a function of azimuth position.

- To find the response of the rotor system to a given airload distribution.

The three parts of the analysis are interrelated, since the trimmed condition of blade control angles is determined by the airloads developed, and because the blade hub stiffness is normally low enough to result in blade motions of such magnitude as to affect the airloads distribution substantially. Furthermore, the airloads do not vary linearly with the control angles or the blade response. Starting with a given weight distribution and flight speed, therefore, requires an iteration procedure to obtain the structural loads on the blades.

Since in each of the steps in the analysis certain approximations and simplifying assumptions must be made, a considerable inaccuracy in the final result of bending and torsion moments can occur. It i, therefore of great value to obtain an intermediate result for comparison, such as measured airload distributions.

In the flight tests described in Volumes I and II, measurements of air pressures and blade stresses are used to determine airload distribution and blade response, while the blade control angles and flight attitude are also measured. This makes it possible to separate the three parts of the analysis from each other and to compare the results of each separable analysis with test data.

In the theoretical work, extensive use was made of the Cornell Aeronautical Laboratory's computer program for rotor blade loads analysis; in addition, two Lockheed computer programs were used.

1

ANALYTICAL METHODS

In this section a brief description is given of the theoretical methods used in the analysis of rotor loads.

LOCKHEED COMPUTER PROGRAMS

In the following discussion the two Lockheed rotor loads analysis programs used in the theoretical work are referred to as Program I and Program II. Similarity between the two programs makes it possible to give a parallel description of both.

Program I performs the computation of rotor blade responses from a given airload distribution. This airload distribution consists in general of the harmonics of lift, drag, and aerodynamic pitching moments, which are given as lumped loads at up to 20 blade stations. Program II performs similar computations but allows the use of a larger number of blade stations. In addition, Program II includes the computation of aerodynamic lift and drag at these blade stations. (A flow chart of Program II is given in Figure 1.)

In the airloads computations, the following assumptions are made:

- The induced velocity distribution can be obtained from a description of the wake. The wake is approximated by a number of Helmholtz ring vortexes representing the trailing tip vortexes of the rotor blades. The vertical displacements and the diameters of the ring vortexes are specified. (The vertical velocity of propagation of the vortex rings and the contraction depend upon wake-on-wake effects. A major contribution to the vertical velocity is the self-induced velocity of the vortex ring which is a function of vortex strength and core-radius to ring-radius ratio (Reference 2). For hovering conditions, an estimate of the ring spacing may be obtained from Reference 2. At low forward speed these estimates are assumed still to be valid. At higher forward speeds the rotor is essentially unloaded and the selection of ring vortex spacing is of lesser importance.)

- The strength of the ring vortexes is obtained from the total rotor thrust and is taken as constant around the azimuth. The shed vorticity is neglected.

- The induced velocity due to wake vorticity is approximated by using a number of simple algebraic expressions. This eliminates the very time-consuming evaluation of the elliptic integrals in the expressions for the exact velocities resulting from the Helmholtz ring vortex model.

- Optionally, the induced velocity can be taken as uniform over the rotor disc. In this case, it is obtained from momentum theory.

2
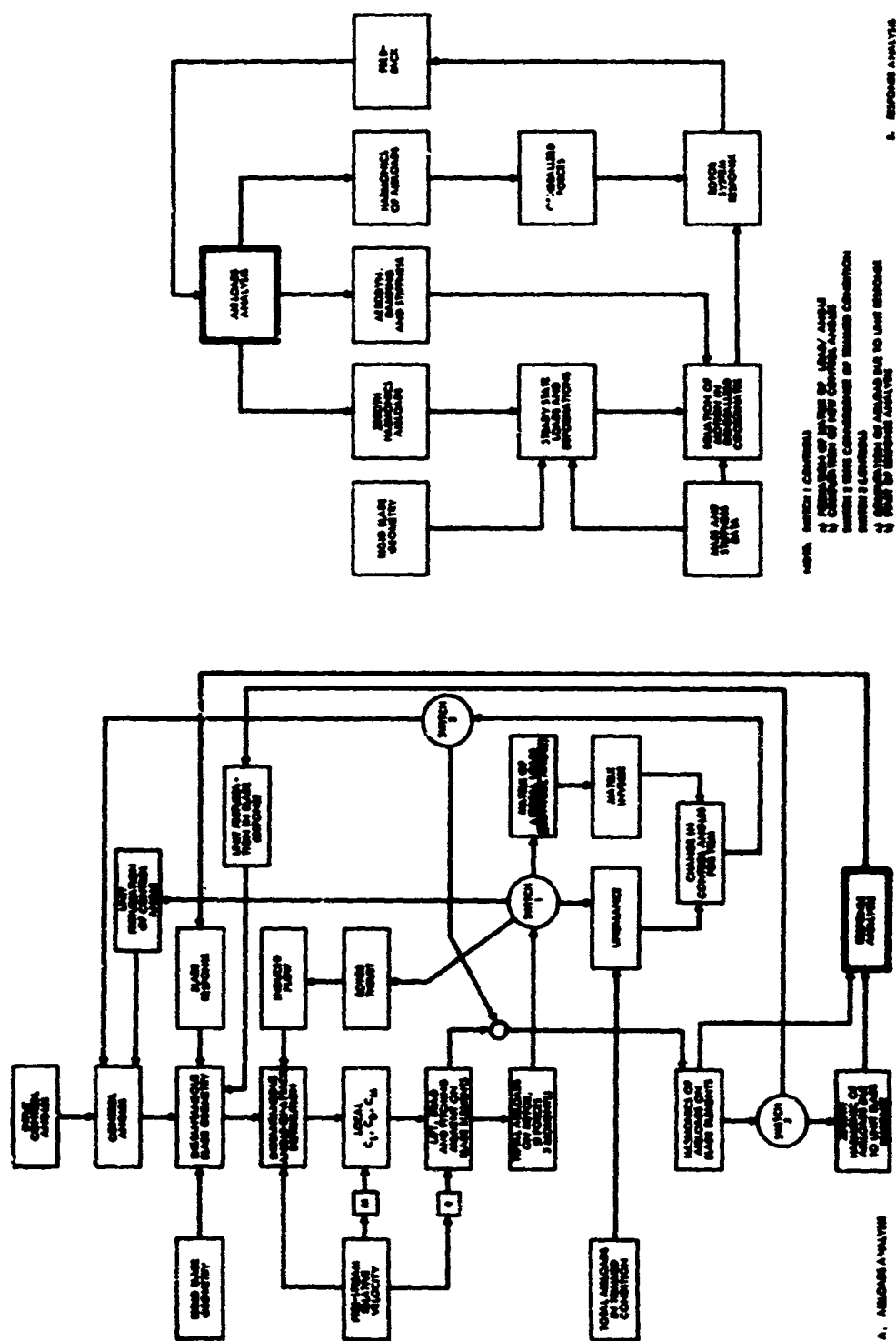
Figure 1. Schematic of Lockheed Computer Program

3

- The lift, drag, and pitching moment coefficients are expressed as functions of the local angle of attack and Mach number, as well as of the profile thickness. These expressions are given in tabular form. The local values of the coefficients are found by interpolation.

- Initially, the rigid blade geometry is used. The effects of blade element velocities parallel and perpendicular to the shaft, due to structural deformations, and of changes in local coning angle and blade twist due to elasticity are introduced in the next cycle, where, after the blade responses are computed, the airloads are reevaluated. The linear aeroelastic effects are, however, already introduced in closed form in the first cycle (i.e., without iteration) as shown below. (The term linear is used here to indicate that the aeroelastic effects acting upon each harmonic are produced by vibrations in the same harmonic, while the interaction between one harmonic and another is ignored at this point.)

The simplified theory for induced flow due to ring vortexes is obtained as follows.

The potential flow induced by a ring vortex of infinitesimal core thickness can be solved by an iterative procedure. The three-dimensional problem is first converted to a two-dimensional problem by using the apparent symmetry of the ring vortex model. Then, using a number of grid points in the plane of symmetry, the Laplace equation, expressing zero divergence, is solved at each of these grid points in succession (except for the grid points in the plane of the ring vortex, where the potential is constant).

The flow pattern resulting from these computations can be visualized as a system of equipotential lines and streamlines which intersect each other at right angles. This flow pattern is unique, i.e., it is independent of the vortex strength or the dimension of the ring vortex.

In order to arrive at a set of simple expressions for the computation of the induced flow components at an arbitrary point in the flow field, the flow pattern is modified by approximating the equipotential lines as well as the streamlines by circles, still intersecting each other at right angles. The equipotential lines are centered on the centerline of the ring; the streamlines are centered in the plane of the ring.

From the geometry of this simplified flow pattern, the induced velocities are easily obtained in terms of an arbitrary constant. This arbitrary constant is, of course, a linear function of the vortex strength. One more modification is needed. It appears that if the arbitrary constant is adjusted to give the correct value of the flow velocity in the vicinity of the vortex filament, the flow velocity at the center is underestimated by a factor $\pi/2$. The constant is therefore made a function of the radial distance at which the streamline passes through the plane of the vortex ring. This function is selected in such a manner that the exact flow velocities, both at the center and in the vicinity of the filament, are obtained.

4

One of the important features of the Lockheed airloads program is the
possibility of trimming the rotor to a given set of integrated airloads
acting on the shaft. Up to three forces and three moments can be selected to
which the rotor can be trimmed. These are: forward force, side force, rotor
thrust, roll moment, pitch moment, and torque. The trimmed conditions are
obtained by adjusting the same number of the following angles: collective
pitch, cyclic pitch (two components),shaft angle, flight path, and yaw
angle. Theoretically any combination of loads to be trimmed to and angles
to be computed can be made, with the obvious restriction that their respec-
tive numbers must be the same. The practical limitations of the method
are the same as those of the physical rotor system, e.g., in hover, changes
in the shaft angle will not effect any changes in the total loads. It
should also be noted that if it is attempted to trim the rotor to a load
or set of loads beyond its physical capability, the solution of the computer
program will not converge, and the computations will be terminated.

The method by which the trimmed conditions are obtained is briefly described
as follows.

In addition to the computation of the airloads on the blade elements using
the given starting values of the angles, the airloads are also evaluated
after making a small unit change in each of these angles in succession.
The total rotor loads (3 moments and 3 forces) are then computed,and those
found for the starting values are subtracted from each of the others. This
results in a 6 x 6 matrix of changes in total rotor loads due to changes
in angles. From this matrix the columns pertaining to loads to which
the system is not to be trimmed are removed. Also the rows pertain-
ing to angles which are not used for trimming (but are given as "fixed"
quantities) are removed. The resulting square matrix is inverted and
transposed, resulting in the "trim matrix".

The rotor loads computed with the starting values of the angles are sub-
tracted from the rotor loads, specified in the input, to which the rotor
must be trimmed. This results in a column matrix of six imbalances. The
imbalances in loads to which no trim is required are removed.

Finally, the column of imbalances is premultiplied by the trim matrix, and
the resulting column is scalar multiplied by the unit of change of the angles,
resulting in the changes in angles required for trim. These changes are
based on linear interpolation or extrapolation. The process is therefore
repeated until convergence.

After convergence, the final airloads on the blade are computed. These do
not yet include any aeroelastic effects. The linear aeroelastic effects
are found by repeating the airloads computations after making successive
unit changes in vertical (axial) air velocity, tangential air velocity,
collective pitch angle, collective pitch angular velocity, and uniform
coning angle. The difference between these airloads and the normal air-
loads is averaged over the azimuth, resulting in the "hovering" (linear)
aeroelastic effects for each blade station. This information is sub-
sequently used in the response calculations.

From this point on, the two Lockheed programs are similar, and the following description applies to both. However, some major differences exist and will be indicated where they occur.

Before entering the response part of the program, certain inertia forces are added to the lumped airloads on the blade elements. These are the effects of vertical acceleration, pitch and roll rate, pitch and roll acceleration, and rate of change of rotor rpm. In Program II the linear accelerations in fore-aft and side direction are also included. The total lumped loads are referred to as external loads in the following discussion.

The response to the steady-state part of the external loads is found by an iteration process. First, the bending moments about two axes and the torsion moments are computed, using rigid blade geometry. For the angular position of the structural principal axes of inertia of the blade section, the combination of collective pitch angle and built-in twist is used (the cyclic control angle is ignored at this point; however, the effect of cyclic angle is linearized and used later as it affects the first harmonic excitation). The deformed shape of the rotor blade is then computed based on the computed moments. The changes in deformation result in changes in centrifugal forces as well as in a new geometry. By using the new geometry and centrifugal forces, a new set of bending and torsion moments is computed. This process is repeated until convergence.

Normally the above process would not converge at all, but rather diverge very rapidly. Convergence is obtained by arbitrarily reducing the amount of change of the moments (in particular the normal bending moment) to a fraction of the computed change. Since at convergence the changes in moments are zero, this reduction does not alter the final results.

The response to oscillatory airloads (and gyroscopic forces in conditions with pitch and/or roll velocities) is obtained from the Lagrange equation:

$$\frac{d}{dt}\left(\frac{\partial T}{\partial \dot{q}}\right) - \frac{\partial T}{\partial q} + \frac{\partial V}{\partial q} = Q \tag{1}$$

where T is the kinetic energy, V is the potential energy and Q is the generalized force in the generalized coordinate, q. Acceleration forces are obtained from the first term, centrifugal forces are obtained from the second term, and Coriolis forces are obtained from both the first and the second term, while the third term gives rise to structural forces.

The generalized coordinates, q, used in the analysis are primitive bending and torsion modes which are of approximately the same shape as the natural modes of a nonrotating uniform beam. One advantage of the use of primitive mode shapes instead of natural modes is that the natural mode shapes are in general complex, i.e., vertical and horizontal displacements are not in phase, due to coupling by Coriolis forces between these displacements. Furthermore, experience shows that differences in the equilibrium position of

6

the blade under steady load can result in significant shifts of natural frequencies. This would make it necessary to compute new natural frequencies and mode shapes for each condition, which can be avoided by working with primitive modes only (which are not necessarily orthogonal) and accounting for all the coupling terms.

The Lagrange equations are expanded into matrix form by first writing the displacements in terms of generalized coordinates:

$$x_i = \sum_n \frac{\partial x_i}{\partial q_n} q_n \quad ; \quad y_i = \sum_n \frac{\partial y_i}{\partial q_n} q_n \quad ; \quad z_i = \sum_n \frac{\partial z_i}{\partial q_n} q_n \quad ;$$

$$\theta_i = \sum_n \frac{\partial \theta_i}{\partial q_n} q_n \tag{2}$$

then by writing the kinetic and potential energy in the rotor system in terms of displacements, velocities, and curvatures, and finally by taking second derivatives with respect to q_n and q_m as follows:

$$\frac{\partial}{\partial q_m}\left[\frac{d}{dt}\left(\frac{\partial T}{\partial \dot{q}}\right)\right] - \frac{\partial}{\partial q_m}\left(\frac{\partial T}{\partial q_n}\right) + \frac{\partial}{\partial q_m}\left(\frac{\partial V}{\partial q_n}\right) \tag{3}$$

to find the (n, m) elements of the matrices A, B, C, and D in the equation,

$$(-\omega^2[A] + i\omega\Omega [D] - \Omega^2 [B] + [C]) \quad \{q\} = \{Q\}, \tag{4}$$

where $\{Q\}$ is the column of generalized forces.

Feedback of rotor response into aerodynamics is accomplished as follows. As part of the airloads computations, the change in airload due to a change in relative velocities and angle of attack is included at each radial and azimuth position. These changes in airload are harmonically analyzed. The zeroth harmonic part is used to define the linear aerodynamic damping and stiffness terms in the above matrix equation, and these terms are added to matrices D and C. The harmonics of the airloads due to blade response cannot be used in a closed-form solution. Therefore the complete aerodynamic load distribution is recomputed using the blade response found in the previous cycle.

The computation of the total bending moments, shear loads, and torsion moments at each azimuth position is performed as follows:

From the harmonics of displacements in the primitive modes, the harmonics of displacements in x, y, and z directions and the rotation θ are computed; for example,

$$z_p(x) = \sum q_{i,p} \frac{\partial z(x)}{\partial q_i} \tag{5}$$

where i is the primitive mode number and p is the number of the harmonic.

7

The accelerations $\ddot{x}$, $\ddot{y}$, $\ddot{z}$, and $\ddot{\theta}$ are found from x, y, z, and θ by multiplying by $-(p-1)^2 \Omega^2$. Note that p=1 indicates the steady state, p=2 indicates the first harmonic, etc.

Inertia forces are computed on each blade element from the accelerations. Similarly the velocities $\dot{x}$ and $\dot{y}$ and the resulting Coriolis forces are computed. The inertia and Coriolis forces are added to the external loads, resulting in total forces on the blade elements.

The total moments are computed at each azimuth position from the total forces on the blade elements and the instantaneous blade geometry. Both the forces and the geometry at the selected azimuth positions are obtained from harmonic synthesis.

The output of the computer program consists of a listing of the two bending moments, torsion, two shears, axial load, and the y, z, and θ coordinates at each selected station and azimuth position. In addition the same data are given in harmonics at each blade station.

Optionally the same program can be used to compute natural frequencies and mode shapes. This consists of the solution of the eigenvalue problem:

$$(-\omega^2 [A] + i\omega\Omega[D] -\Omega^2 [B] + [C]) \{q\} = \{0\} \qquad (6)$$

If the linear aeroelastic effects are included in the D and C matrices, the eigenvalues ω consist of real and imaginary parts. The modulus of ω is the natural frequency; the ratio between the imaginary part and the real part represents the damping ratio.

If the linear aeroelastic effects are not included, the eigenvalues are found to be real.

The natural mode shapes consist of x, y, and z displacements and rotation θ. If the blade is rotating, the y and z displacements are coupled through coriolis forces and are therefore, in general, out of phase. It can be shown that each blade element describes an elliptical path, as illustrated in Figure 2.

CORNELL COMPUTER PROGRAM

This program is described in detail in Reference 3. In comparison with the Lockheed method, the following differences are of interest:

In the Cornell program the geometric blade angles are treated as known quantities, including the rotor angle of attack. It is therefore not possible to compute the collective and cyclic control angles and the rotor shaft angle required for a given trimmed condition in a single computer run. (A trimmed condition may be defined by given rotor thrust, shaft moments, and rotor torque.)

8

$\omega = 1.088 \, \Omega$

$\omega = 1.422 \, \Omega$

$\omega = 2.79 \, \Omega$

$\omega = 4.96 \, \Omega$
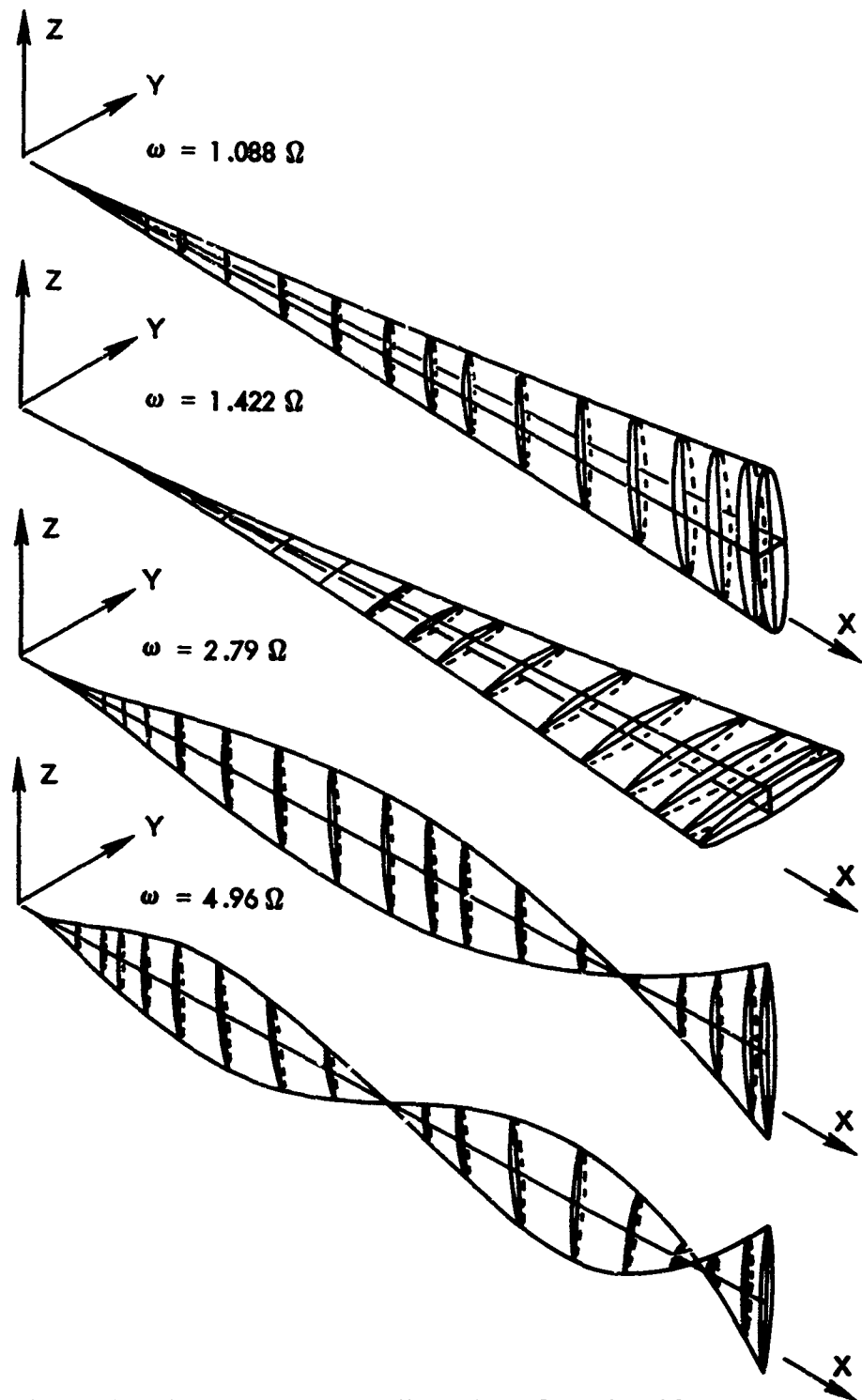
Figure 2. Natural Modes of Vibration, Rotating Blade

The description of the wake of the rotor blades is more elaborate in the Cornell program. The shed vorticity as well as the trailing vorticity is included in the analysis. At short distances behind each blade, the trailing vorticity is represented by a number of distinct (lumped) trailing vortexes rather than a single trailing tip vortex.

The wake geometry is specified by input values of the wake transport velocity, which can be selected differently at each station and azimuth position, but is constant with time. (The azimuthal differences in wake transport velocities are restricted by the method in which this input is defined to five harmonics only.) As a result, the wake spirals in this program do not contract and are located at equal distances from each other.

Only "flapping" degrees of freedom are considered in the Cornell programs. Torsional deformations of the blade are specified up to and including the fifth harmonic only.

A constant lift curve slope is used, which is cut off at stall. The effect of the Mach number is not included. Drag and aerodynamic pitching moments are not computed.

The structural responses computed in the Cornell program are limited to flapping bending moments. These are found as the summation of the bending moments in each of the natural modes.

APPLICATION OF THEORY

COMPUTATION OF NATURAL FREQUENCIES AND MODE SHAPES

The natural frequencies and mode shapes of the instrumented blade are mea-
sured by a shake test. In addition, the theoretical mode shapes and fre-
quencies are computed, using Lockheed Program I, for the cantilever-
nonrotating blade. The comparison of the test and analysis of these
frequencies and mode shapes is made in order to establish the validity
of the mathematical model used to represent the rotor system. This compari-
son is shown in Figure 3.

In the above analysis the blade is subjected to 1g gravity forces as it is
in the shake tests. In order to find the frequencies and mode shapes
which will be used in the Cornell program, the computations are repeated
without the 1g gravity forces and with the normal rotor rpm. The coupled
bending mode shapes are shown in Figure 2.

AIRLOADS COMPUTATIONS

A complete list of the flight conditions analyzed is contained in Table I.

Application of Lockheed Computer Program

The airloads computations performed with the Lockheed computer program are
to be considered separate airloads analyses, i.e., the airloads are com-
puted without iteration from a given blade geometry including the struc-
tural responses of the blades. Sample analyses showed that torsional
blade responses are of major importance in the determination of airloads
on the blade (Reference 4) and must be included in the computations.

The torsional deformation used in the analyses is based on the actual
measurements of the torsion moment on the blade (at a radial distance from
the shaft of 115 inches) in combination with the effective torsional stiff-
ness of the blade inboard of that station. The resulting twist angles
are used as constants over the blade. For the purpose of the separate
airloads analyses the computer program was modified in order to accept
the input of the torsion moment (at station 115) defined at 36 azimuth
positions. Theoretically this provides for the use of all the harmonics
of this torsion moment up to the seventeenth. However, it must be realized
that the distribution of the torsion moments over the blade span in the
higher harmonics will be quite different from that in the lower ones; hence
the higher harmonics of the torsional deformations could only be obtained
correctly if different effective stiffnesses were used in connection with
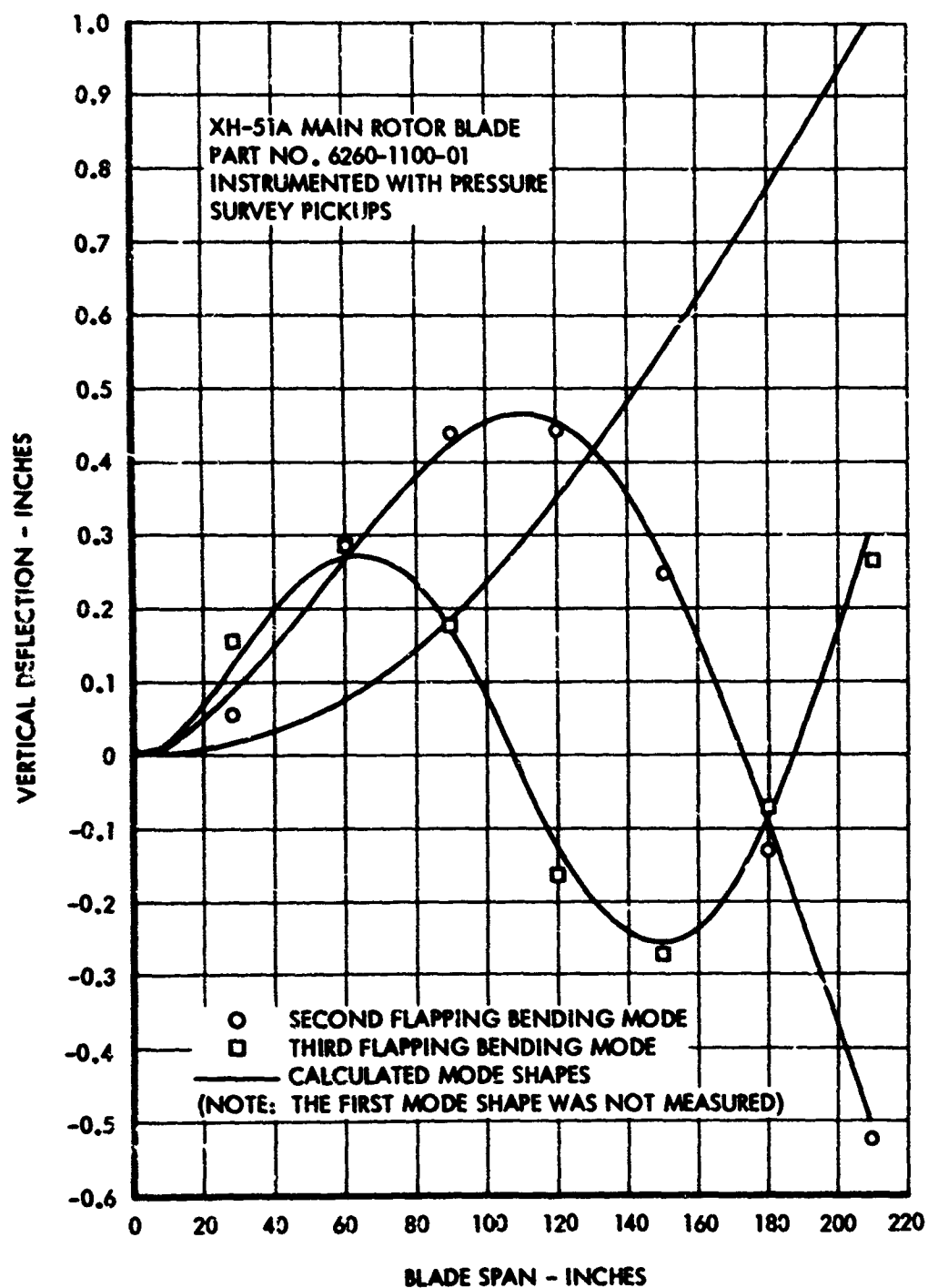
11

Figure 3. Natural Modes of Vibration, Nonrotating Blade

12

TABLE I. FLIGHT TEST CONDITIONS

TEST CONDITION NO.	DESCRIPTION OF TEST CONDITION	MEASURED ROTOR LOAD, LB	CG VERT ACCEL, G	ANGLE OF ATTACK, DEG	COLLECT. BLADE ANGLE, DEG	GROSS WT, LB	V_T, KT	ALT, FT	JET	INTEGRATED ROTOR LOAD, LB	TEST CONDITION ANALYSIS PERFORMED
1	HOVER	4480	1.00	-	10.41	4900	-	GROUND	OFF	4587	FULL
2	COLLECTIVE PULLUP	5180	1.19	-	11.1	4841	-	GROUND	OFF	4409	PARTIAL
3	COLLECTIVE PULLUP	5771	1.54	-	12.1	4830	-	GROUND	OFF	4752	PARTIAL
4	COLLECTIVE PULLUP	6850	1.54	-	13.27	4871	-	GROUND	OFF	5331	FULL
5	FORWARD FLIGHT	4720	1.02	3.02	7.50	5010	51	805	OFF	4145	FULL
6	FORWARD FLIGHT	4412	0.98	1.21	8.0	5006	59.5	1065	OFF	3748	PARTIAL
7	FORWARD FLIGHT	4883	0.98	-1.51	9.2	5051	80.4	1040	OFF	4739	PARTIAL
8	FORWARD FLIGHT	5330	1.04	-2.11	10.93	5010	105	1040	OFF	4454	FULL
9	LEFT TURN	6200	1.42	3.47	9.0	4920	91	975	OFF	5789	PARTIAL
10	RIGHT TURN	5990	1.32	2.20	6.9	4895	78	860	OFF	5500	PARTIAL
11	LEFT TURN	6490	1.33	1.51	9.54	5050	84	1025	OFF	9819	FULL
12	RIGHT TURN	5800	1.27	1.36	9.21	5040	82	1005	OFF	5317	PARTIAL
13	COLLECTIVE PULLUP	5773	1.36	2.27	9.3	5031	84.5	1005	OFF	9825	PARTIAL
14	COLLECTIVE PULLUP	7020	1.73	5.44	10.0	5031	86	1070	OFF	6972	PARTIAL
15	COLLECTIVE PULLUP	7700	2.06	6.84	9.0	4915	87	975	OFF	8015	PARTIAL
16	AUTOROTATION	4650	1.0	-	3.49	4900	-	115	OFF	3855	FULL
17	AUTOROTATION	3837	1.08	18.90	3.20	4986	63	1075	OFF	2780	PARTIAL
18	TRANSITION	5115	1.03	-	10.7	5241	-	GROUND	OFF	4670	PARTIAL
19	TRANSITION	5320	1.07	-	11.09	4990	-	1075	OFF	4138	FULL
20	TRANSITION	5134	1.05	-15.86	10.6	4861	60	GROUND	OFF	3817	PARTIAL
21	FLARE	4450	1.02	12.70	4.93	4891	-	1105	OFF	4295	FULL
22	FLARE	4442	1.07	-	9.7	5000	-	GROUND	OFF	4283	PARTIAL
23	LEVEL FLIGHT	2870	1.02	10.79	3.61	4940	109	1105	OFF	2129	FULL
24	LEVEL FLIGHT	2471	0.97	9.06	3.6	5156	124.5	1045	ON	1524	PARTIAL
25	LEVEL FLIGHT	1948	1.08	7.45	3.27	5100	163.5	1180	ON	1393	FULL
26	LEVEL FLIGHT	1040	1.05	5.47	3.15	4980	207	1245	ON	282	FULL
27	LEVEL FLIGHT	610	1.15	4.20	3.24	5110	227	1220	ON	-429	FULL
28	LEVEL FLIGHT	1636	1.03	6.80	3.70	4891	170	3530	ON	923	PARTIAL
29	LEVEL FLIGHT	1091	1.01	4.83	3.80	4936	215.5	3745	ON	-108	PARTIAL
30	LEVEL FLIGHT	663	1.10	5.13	3.86	4906	219.5	3720	ON	161	PARTIAL
31	LEVEL FLIGHT	654	1.13	4.80	3.34	4940	232	3655	ON	72	FULL
32	LEVEL FLIGHT	2280	1.05	10.50	3.37	5026	157	10100	ON	1063	FULL
33	LEVEL FLIGHT	1210	1.02	7.10	3.50	4996	202.5	10105	ON	395	PARTIAL
34	LEVEL FLIGHT	839	1.03	6.08	3.80	5011	219	10370	ON	276	PARTIAL
35	PULLUP	3290	1.32	11.63	3.52	5150	126	1025	ON	2966	FULL
36	PULLUP	3900	1.61	13.44	3.76	5150	124	1005	ON	3576	FULL
37	PULLUP	3183	1.02	10.35	4.00	5091	100	955	ON	2970	PARTIAL
38	PULLUP	1450	1.38	6.54	3.17	5030	206	1390	ON	651	FULL
39	PULLUP	1545	1.63	7.55	3.56	5096	83	1025	ON	727	FULL
40	PULLUP WITH VARIOUS RATES OF CONTROL APPLICATION	2311	1.39	8.85	3.80	4986	166	1075	ON	1810	FULL
41	LEFT TURNS	2616	1.56	9.75	3.70	5151	163	1290	ON	207	PARTIAL
42	LEFT TURNS	2854	1.54	9.27	3.60	5115	163	1110	ON	2666	PARTIAL
43	LEFT TURNS	2220	1.21	8.21	3.30	5100	162	1175	ON	1336	PARTIAL
44	LEFT TURNS	3078	1.25	10.72	3.40	5111	124	1040	ON	2344	PARTIAL
45	LEFT TURNS	2530	1.34	8.70	3.60	5140	161	1175	ON	1705	FULL
46	RIGHT TURNS	1495	1.37	6.08	3.50	5005	207.5	1385	ON	1036	PARTIAL
47	RIGHT TURNS	3338	1.36	11.33	3.70	5091	124	905	ON	2556	PARTIAL
48	RIGHT TURNS	2620	1.49	9.45	3.70	5110	164	1105	ON	1620	FULL
49	RIGHT TURNS	1536	1.38	6.23	3.23	4995	208	1265	ON	1212	PARTIAL

13

the higher harmonic torsion moments. Furthermore, in the higher harmonics the angular displacements could be expected to be different at the different stations.

The harmonics of the torsion moments at station 115 which are used in the separated airloads analysis are shown in Volume II. Comparison of the harmonic components at station 115 and station 185 confirms the above observations. The absence of any clear phase relationship between the torsion moments at these stations indicates that more than one mode participates in the torsion moment response. These uncertainties with regard to the finer details of the distribution of the torsional deformations must be borne in mind in the review of the comparisons of the results of the separated airloads analyses with the measured data.

No provisions were made to introduce a given normal or in-plane bending response into the separated airloads analysis. That the effect of in-plane bending on the airloads can safely be neglected is obvious. The effect of the normal bending response is evaluated on a sample basis by two different methods:

- In addition to the predicted airloads, the Lockheed computer program provides the change in lift, drag, and pitching moment due to a unit incremental relative vertical velocity. An estimate of the incremental relative vertical velocity due to blade bending response can be obtained from the response analyses.

- The Cornell computer program does include the effect of flapping bending on the airloads. Comparison of airloads computed with this program using three flapping modes and a modification where the displacements in the natural modes are zeroed out shows that the effect of blade bending response upon the airloads is relatively small.

In the Lockheed computer program the effect of not including the blade bending in the separated airloads analysis is largely compensated for, as far as the first harmonic is concerned, by making slight changes in the cyclic control angles, as will be discussed presently.

Since the Lockheed programs provide an option to trim the rotor to various selected forces and moments, it is interesting to look at the advantages of using this option.

Of the angles measured in the flight test, the collective and cyclic control angles are known with sufficient accuracy; the rotor angle of attack, however, is not, for a number of reasons. Among these are the possible effect of the wing and body on the free-stream velocity at the rotor disc and the fact that bending displacements of the rotor blade elements are neglected (the first harmonic of these changes the tip path plane).

Small variations in the cyclic control angle can compensate for neglecting the first harmonic of the vertical velocities of the blade elements due to blade bending.

The total rotor thrust is found from integration of the airloads on the rotor. The pitch and roll moments on the rotor can also be obtained in this way. It has been found, however, that these moments do not agree very well with the moments derived from the first harmonic of normal bending at station 6 in combination with gyroscopic and inertia moments based on measured roll and pitch rates and accelerations.

It may be assumed that the measurements of the normal bending moments at station 6 are highly reliable. Furthermore, substantial errors in the measurements of pitch and roll rates and pitch and roll accelerations are not to be expected. Therefore, in view of the fact that a very small error in the measured and integrated airload distribution can result in a substantial error in computed shaft moments, the trimmed solutions for the airloads computations are based upon the measured first harmonic of normal bending at station 6, extrapolated to the shaft, multiplied by 2 to account for four blades, and combined with the inertia and gyroscopic moments on the rotor due to the measured pitch and roll rates and accelerations.

The situation resulting from this method of analysis is that, as far as the steady-state and first harmonic airloads are concerned, the analytical results are believed to be quite accurate. The comparison of test and theory must therefore be considered as a check on the performance of the airloads measurements.

In addition to the trimmed analyses described above, analyses were made in which the rotor was not trimmed. In the untrimmed rotor analyses, the measured control angles and angle of attack were used. Also, the effect of the blade torsion was left out.

The Lockheed program provides for input of selected vertical displacements and contraction of the vortex rings. In the untrimmed analyses an assumed relationship between downward displacement and wake contraction is used, based on experimental work (Reference 5). The downward displacement is found from the uniform induced velocity based on momentum theory. This then determines the contraction, i.e., the wake radius. To the downward displacement is then added the vertical component of the free-stream velocity based on the measured angle of attack.

In the trimmed analyses the vertical displacement Z (positive down) and the vortex radii ξ were selected as follows:

Conditions	
1, 4, 19	$Z = 5, 12, 20, 28, 36, 44$
	$\xi = 205, 200, 195, 190, 185, 180$
Conditions	
5, 8, 11	$Z = 8, 25, 40$
	$\xi = 205, 200, 195$

15

Condition 16   Z = -10, -20, -30
                                      ξ = 205, 200, 195

Conditions
  21, 23, 25, 26, 27, 31, 33,   Z = 4, 10, 20
  36, 37, 39, 40, 46, 50   ξ = 205, 200, 195

Application of Cornell Program

In the analyses made using the Cornell A.L. computer program for rotor loads,
the following selections were made regarding the wake description, the
torsional response, and the blade dynamic properties and geometry:

A very important element in the computation of rotor loads using wake vorticity
is the placement of the wake elements with respect to the rotor. In the
Cornell program, the location of the wake elements is obtained from selected
inputs describing the downward velocity of the wake elements. In all com-
putations made with the Cornell program, this velocity was taken as the uni-
form inflow velocity obtained from momentum theory combined with the component
of the free-stream velocity perpendicular to the plane of the rotor. The
latter is found using the measured angle of attack. The wake is further
described as follows:

- Number of azimuth segments of the wake mesh
  behind each blade (i.e., number of shed vortices)   = 2

- Number of trailing vortexes in the rolled-up
  wake (tip vortex only)   = 1

- Number of wake revolutions   = 3

- Wake advance (i.e., fraction of $\Delta\Psi = 2^{\pi}$/no. of
  blades, by which the wake is advanced azimuthally)   = 0.7

- Distance rolled-up tip vortex is moved
  inboard from the blade tip   = 30 inches
  (Note: The radius of the tip vortex is then 180 inches.)

The torsional response is specified in the input. The Cornell program per-
mits a separate (different) input for the harmonics of the geometric blade
angle at each blade station. The responses used in the Cornell program were
obtained from Lockheed Program II and were computed from the measured airloads.
Since provisions are made for the input of the first five harmonics only, the
higher harmonics of the torsional response are not included.

The cone angle of the XH-51A rotor blade is not constant but varies between
3.2 degrees on the inboard blade and 2.2 degrees on the outboard blade. In
the Cornell program a single cone angle must be selected. This cone angle
was taken as the average, 2.7 degrees.

16

Since the rotor angle of attack is not found in the test data with sufficient reliability, and since this angle cannot be found from an internal trim procedure, the trimmed angle of attack computed with Lockheed Program II is used.

The natural frequencies and mode shapes computed with Lockheed Program I are used.

RESPONSE ANALYSES

Three different methods are used to compute the blade responses to the given measured airloads. It may be noted that since the total airloads are known, the damping forces and aeroelastic effects are included in the excitation. Therefore the only damping used in the computations is structural damping, which is estimated at .02 [complete damping, i.e., the stiffness matrix C is multiplied by (i = .02i)].

The response analyses are again considered as "separated analyses" since no feedback to airloads of the response need be considered.

The computations are performed with Lockheed Program I as described in the previous chapter. In these computations 7 harmonics are used and 18 azimuth positions (20° increments in azimuth). Thirteen primitive modes are used, consisting of five normal bending, five in-plane bending, and three torsion modes.

The same computations are performed with a simplified program. The difference between this new method and the method above is that the responses in the modes are computed for all harmonics including the steady state, thus ignoring the nonlinearities in the steady-state response. The normal bending moments are now found from a summation of bending moments in each of the modes. In these computations the same 13 primitive mode shapes are used as above. Also as above, the equilibrium position of the blade is taken as the steady-state deformed shape under the steady-state part of the load.

Since it is not practical to modify the Cornell program in such a way that a given airload distribution can be given as an input, the Cornell method for the computation of normal bending moments is simulated by a variation of the modified program. This consists of using only five primitive modes in normal bending and of using the undeflected blade shape as equilibrium position.

The measured distributions of differential pressures do not provide any information with regard to the chord forces. The integrated pressures (over the chord) give the normal force and aerodynamic moments only.

In view of the large chordwise bending moments measured, in particular at the blade root, it is apparent that the aerodynamic chord forces cannot be neglected. Furthermore, coupling between in-plane and normal bending results in an effect of the chordwise airloads on the normal bending as well as on the in-plane bending.

17

For the purpose of the present investigation, a modification was made to Lockheed Program I by which the chordwise airloads are derived from the normal forces as follows:

- The normal force coefficient is obtained from the measured normal force and the computed relative wind at each blade section.

- The chord force coefficient is found as a function of normal force coefficient and Mach number. This relationship is shown in Figure 4.

- The chordwise airload on each blade element is then computed from the relative wind velocity and the chord force coefficient.

The lumped normal forces and chord forces at each blade station and azimuth position are resolved in the directions parallel and perpendicular to the shaft axis. The angle of rotation used here is the instantaneous angle found from the collective and cyclic control angles

$$\theta = \theta_o + \theta_{1c} \cos \Psi + \theta_{1s} \sin \Psi$$

HARMONICS OF ROTOR LIFT

In the computations of the responses to measured airloads, using Lockheed Program I, the harmonics of normal shear force at each blade station are computed. It is assumed here that the responses of the noninstrumented blades are the same as those of the instrumented blade. From this it follows that the total vertical shear transmitted to the shaft contains only the fourth, eighth, twelfth, etc., harmonics, since these are the only harmonics to which the blades respond in phase with each other.

Of the seven harmonics used in the response analysis, only the fourth is therefore considered. In Table II the cosine and sine components and the amplitude of the fourth harmonic of rotor lift are given. These forces consist of the summation of the fourth harmonics of airloads and inertia forces on the blade elements, multiplied by four to account for the four blades. The cosine component is the instantaneous force acting at the time when the blades are at 0°, 90°, 180° and 270° azimuth positions; the sine component is the instantaneous force acting at the time when the blades are at 22.5°, 112.5° 202.5° and 292.5° azimuth positions.
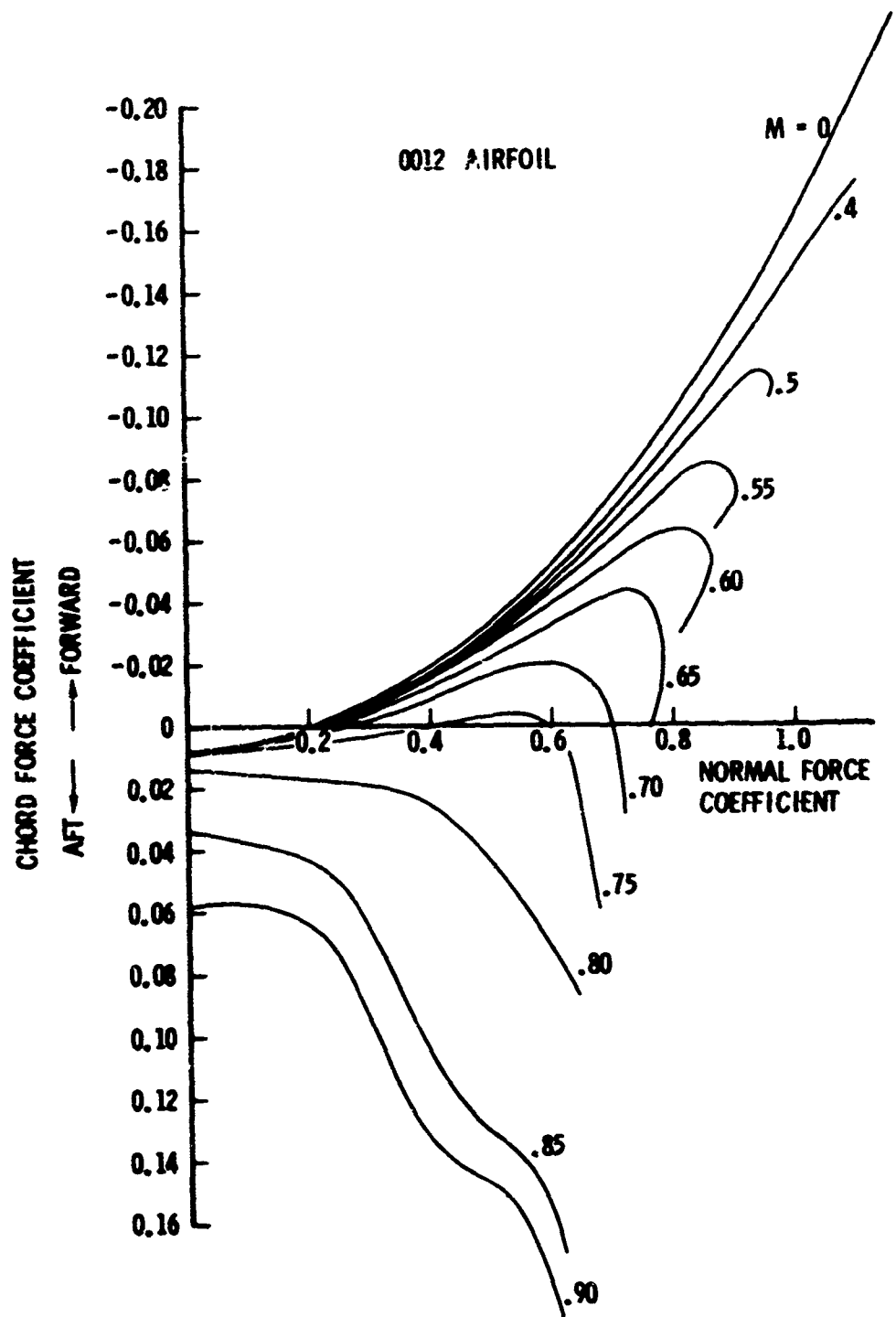
Figure 4. Chord Force Coefficient Versus Normal Force Coefficient, 0012 Profile

19

TABLE II. FOURTH HARMONIC COMPONENTS OF ROTOR LIFT, INCLUDING ROTOR INERTIA FORCES

Condition	Cosine Component	Sine Component	Amplitude	Condition	Cosine Component	Sine Component	Amplitude
1				26	-120	-16	120
2	-64	-128	144	27	-332	-536	632
3	64	4	64	28	- 60	- 28	68
4	0	60	60	29	-168	-200	260
5	-32	-108	112	30	-316	-368	488
6	- 8	- 96	96	31	-400	-740	840
7	8	-152	152				
8	224	- 52	228	33	-24	- 56	64
9	-108	-324	344	34	-56	-104	116
10	64	-264	272	35	-200	-400	448
11	-12	-288	288	36	-112	-128	168
12	28	-296	300	37	- 88	-124	152
13	48	-272	276	38	- 84	-120	148
14	140	-240	280	39	- 56	- 8	60
15	172	-292	340	40	- 12	- 96	96
16	-12	76	76	41	- 84	- 84	120
17	-80	-104	132	42	-100	-104	144
18	-76	- 68	104	43	- 44	-120	128
19	-12	- 84	84	44	-172	- 76	188
20	96	- 40	104	45	- 48	- 96	108
21	-12	- 60	60	46	- 36	- 64	76
22	412	-524	668	47	-124	- 32	128
23	-32	12	32	48	- 48	-104	112
24	-60	- 96	116	49	- 68	- 56	88
25	-64	- 32	72	50	- 76	- 24	80

COMPARISON OF THEORETICAL RESULTS WITH TEST DATA

Comparison of measured and computed responses (Figures 5 through 102) shows that on the outboard part of the blade the harmonics of the bending moments can be obtained with reasonable accuracy. Notable differences between test and theory exist, however, in the following areas:

- At the inboard stations the normal bending moments computed with Lockheed Program I show in many conditions a substantial difference in first harmonic content. This difference may be attributed to inaccuracy of the airloads measurements.

- . some conditions the steady-state part of the normal bending moments shows a considerable difference between test and theory.

- In several conditions the agreement between measured and computed in-plane bending moments is very poor. This indicates that the relationship between normal force and chord force coefficients, used to compute the drag loads (Figure 4), may be deficient in certain areas. This is in particular the case for the larger angles of attack; as shown in Figure 6, condition 4, which is a hovering pullup, the drag loads appear to be overestimated.

- The agreement between measured and computed torsion moments is rather poor, particularly at the lower flight speeds. The computed torsion moments show a large fourth harmonic response. This is to be expected, based on measured as well as computed torsion frequencies. It appears that the mechanism by which the torsion moments are produced is not fully known at this time. Improvements in the analytical methods should include the degrees of freedom of the control system and a more refined definition of the blade elastic axis and local cg.

- Comparison of results from Lockheed Program I and the modified Program I shows the improvement which is obtained by computing the bending moments from the summation of airloads and inertia forces, rather than from the summation of modal responses.

Comparison of measured and computed airloads shows that in most cases the basic shape of the airload distribution can be predicted (Figures 103 through 176).

For the 20 conditions for which a full data analysis is available, the trimmed rotor loads are computed using Lockheed Program II. The shaft

moments in these conditions are obtained from extrapolation of the first harmonic of normal bending at station 6, and include the gyroscopic and inertia moments on the rotor computed from the measured pitch and roll rates and accelerations. The rotor lift to which the rotor is trimmed is taken as the integrated airload. The angles used in the trimming procedure are the cyclic control angles and the rotor angle of attack, except in conditions 1, 4, and 19, which are essentially hovering conditions.

The rotor angle of attack found in the trimming procedure with Lockheed Program II is used in the same 20 conditions in the Cornell program (Figures 123 through 142). The other analyses with the Cornell program are performed using the angle of attack as measured in the flight tests (Figures 143 through 171).

In addition, the conditions for which a full analysis is made are analyzed untrimmed, using Lockheed computer Program II (Figures 105 through 122).

Comparison of the trimmed and untrimmed conditions shows the usefulness of the trim procedure. This also indicates that the measured angle of attack cannot be used for the computation of the rotor airloads. In some conditions this is quite obvious. In condition 16 for instance (Figure 108), which is an auto-rotation, the flight path angle is definitely nonzero and should be included in the analysis. The trimmed solution for this condition resulted in a rotor angle of attack of 14.5° relative to the free-stream velocity. It is also interesting to note that the computed rotor torque in the trimmed condition turned out to be a small negative value, as is to be expected in autorotation.

In condition 19 (transition to forward flight), an unsuccessful attempt was made to obtain a converging solution by trimming to the measured rotor thrust using a variation of the rotor angle of attack at a forward speed of 20 knots. The exact condition is not known, mainly because the forward speed was not specified. A converging solution was obtained by using the collective control angle for trim. The rotor angle of attack was estimated as -20°, and the forward speed was estimated as 40 knots. The airloads are shown in Figure 109. The trimmed collective control angle was found to be 11.13° as compared to the measured angle of 11.09°.

A good agreement was obtained using Lockheed Program II for the hovering condition, as shown in Figure 103. Figure 104 shows the effect of introducing a small forward velocity upon the airloads. This forward velocity was taken as 10 knots, which appears to be too high since it results in computed loads in the forward quadrants at the outboard stations which are too high. However, at the in-board stations a reasonable agreement with the test was obtained.

Encouraging results were obtained with the Lockheed Program II in trimmed analyses for the lower velocities (conditions 5, 8; see Figures 105 and 106). The fact that these analyses showed better agreement with the tests than

those with the Cornell program is attributed to an improvement in the description of the wake geometry (see Application of Theory, Airloads Computations, for the values of vertical displacements and radii of the ring vortexes).

All flight conditions of Table I were analyzed with the Cornell A.L. program of Reference 1.

Comparison of the tests and Cornell theory shows that at least at the outboard blade stations a good agreement is obtained in the shape of the airload curves at moderately high forward speeds (see Figures 131, 137, 138, and 141).

However, at the low speeds this agreement is very poor, as shown in Figures 125 and 127. It is likely that the computed deformation of the wake (as determined by the vertical wake transport velocity) should not be based on the uniform inflow velocity computed from momentum theory at the lower speeds. Particularly in hovering conditions (conditions 1 through 4), the computed steady-state part of the loads at the inboard stations is not in agreement with the test measurements.

In the course of the analytical work it became increasingly difficult to obtain convergence of the Cornell program at the higher forward speeds. No convergence was obtained in conditions 27, 29, 30, and 31.

Finally, for conditions 5, 8, 25, 31, and 37, the airloads were computed in trimmed flight, without an external input of torsional responses. In these analyses the responses were computed from the computed airloads and fed back into the airloads computations. The results are shown in Figures 172 through 176.

CONCLUSIONS

1. In most of the conditions analyzed, the computed bending moments were found to be in good agreement with the measured moments. The agreement between computed and measured torsion moments, however, was poor, indicating that improvements are required in the mathematical model as far as the torsional properties are concerned. (These may include the introduction of the control system degrees of freedom in the model.)

2. Comparison of measurements with airloads obtained with the Cornell program shows good agreement of the variations of the airloads over the azimuth.

3. At the lower forward speeds the rotor wake can be represented by a set of ring vortexes.

4. An urgent need exists for a method for predicting wake deformation and for programming this method.

5. Torsional responses are important in the computation of airloads.

6. A rotor trim procedure included in a rotor loads program has been shown to be useful in the prediction of rotor loads.

7. Based on the results obtained for chordwise bending moments, the relationship between normal force coefficient and chord force coefficient used in Lockheed Program I should be reexamined, particularly in high angle-of-attack areas. Such investigation may result in improved estimates of drag coefficients.

REFERENCES

1. PRANDTL, L., and TIETJENS, O. G., Fundamentals of Hydro and Aeromechanics, Dover Publications, Inc., New York, 1957

2. BRADY, W. G., and CRIMI, P., Representation of Propeller Wakes by Systems of Finite Core Vortices, CAR Report 88-1665-S-2, February 1965

3. PIZIALI, R. A., A Method for Predicting the Aerodynamic Loads and Dynamic Response of Rotor Blades, Cornell Aeronautical Laboratory, Inc., USAAVLABS TR 65-74, U. S. Army Aviation Materiel Laboratories, Fort Eustis, Virginia, January 1966

4. SISSINGH, G. J., and SWEERS, J. E., "Lifting Rotors Operating at High Speeds or Advance Ratios", Fluid Dynamics of Rotor and Fan Supported Aircraft at Subsonic Speeds, AGARD Conference Proceedings No. 22, September 1967

5. SIMMONS, I. A., PACIFICO, R. E., and JONES, J. P., "The Movement, Structure, and Breakdown of Trailing Vortices from a Rotor Blade", CAL/USAAVLABS Symposium Proceedings, Vol. 1, 22-24 June 1966
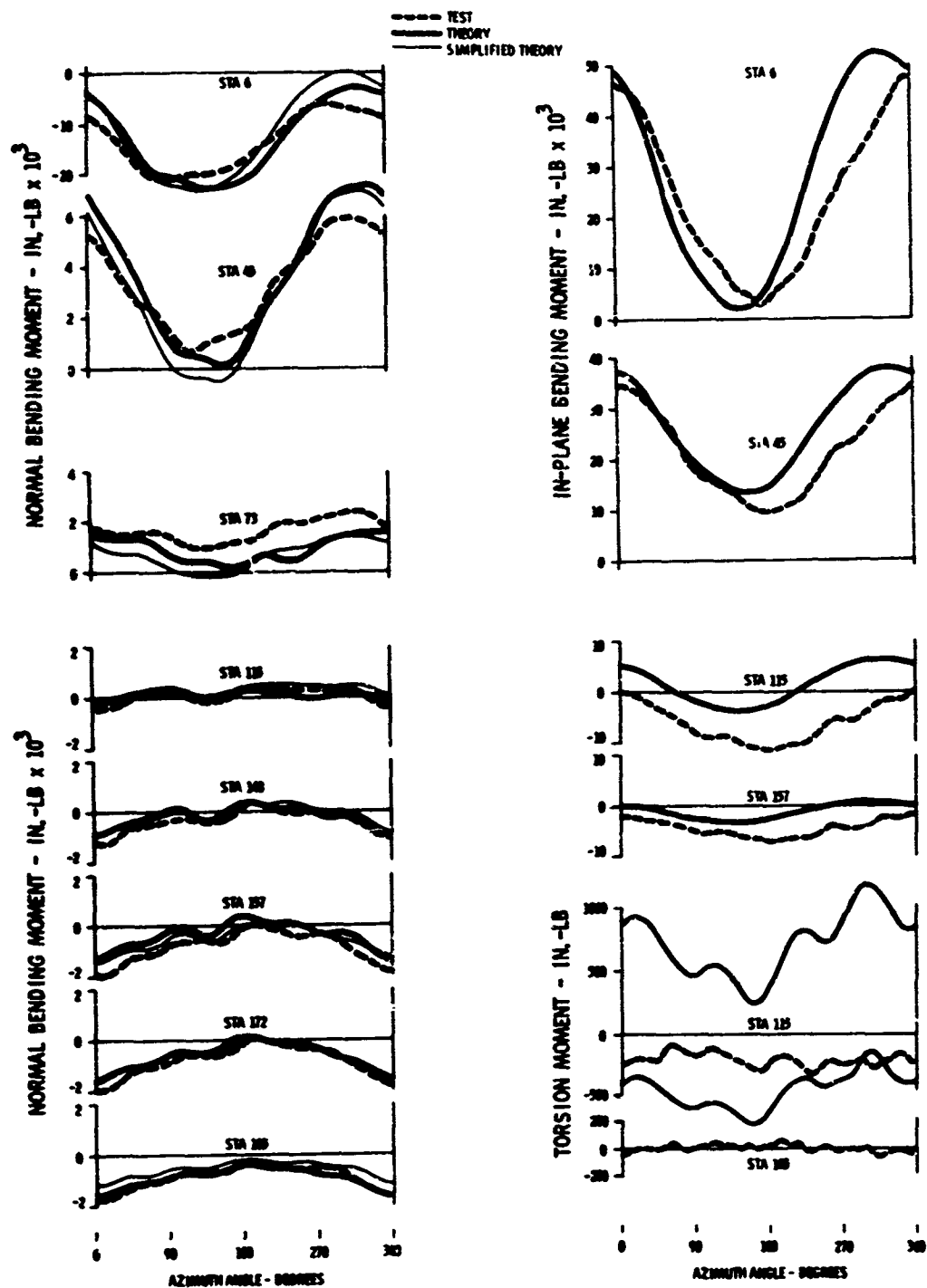
Figure 5. Response to Measured Airloads (13 Modes),
Condition 1 (Hover)
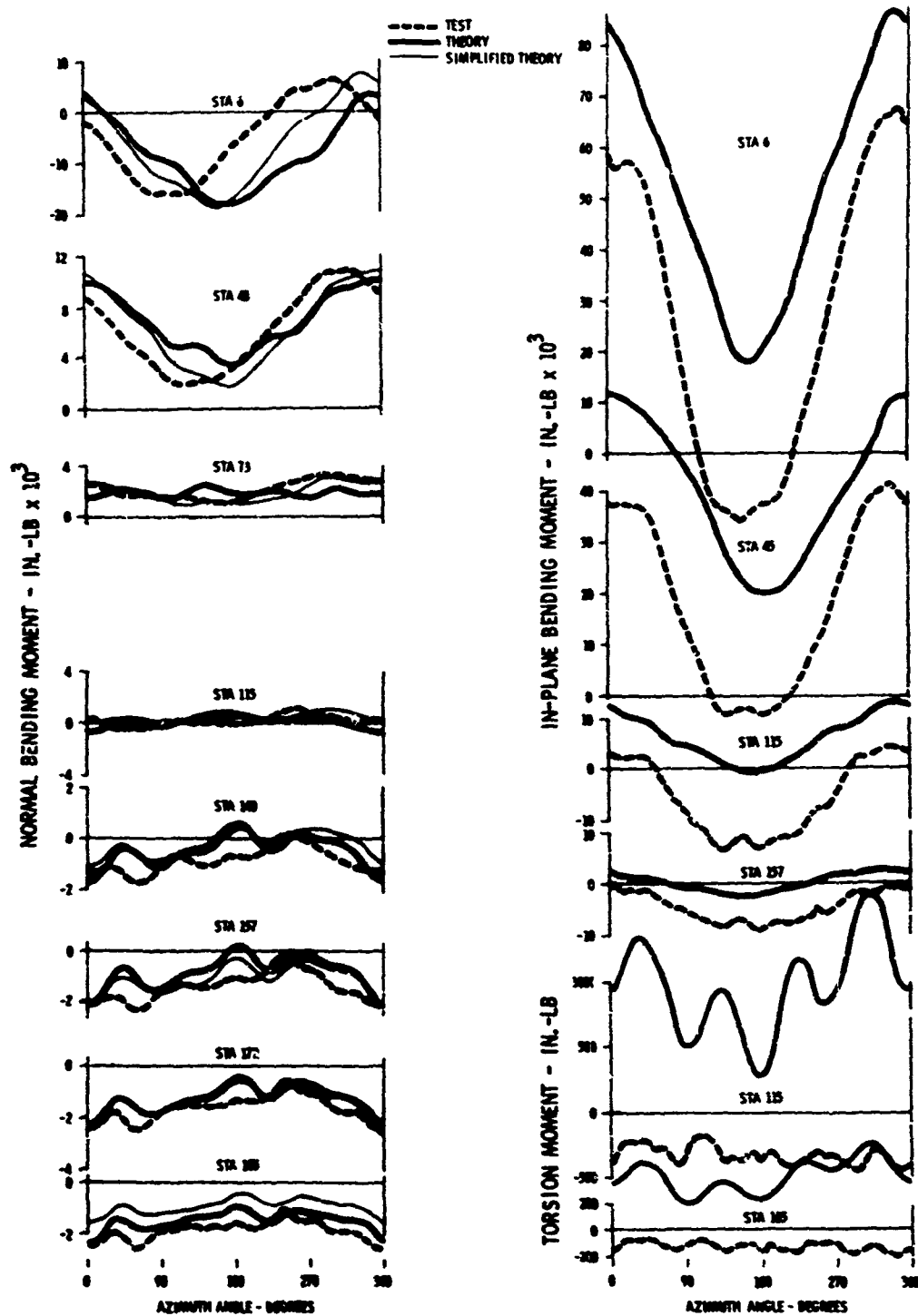
Figure 6. Response to Measured Airloads (13 Modes),
Condition 4 (Collective Pullup at 0 Knot TAS)
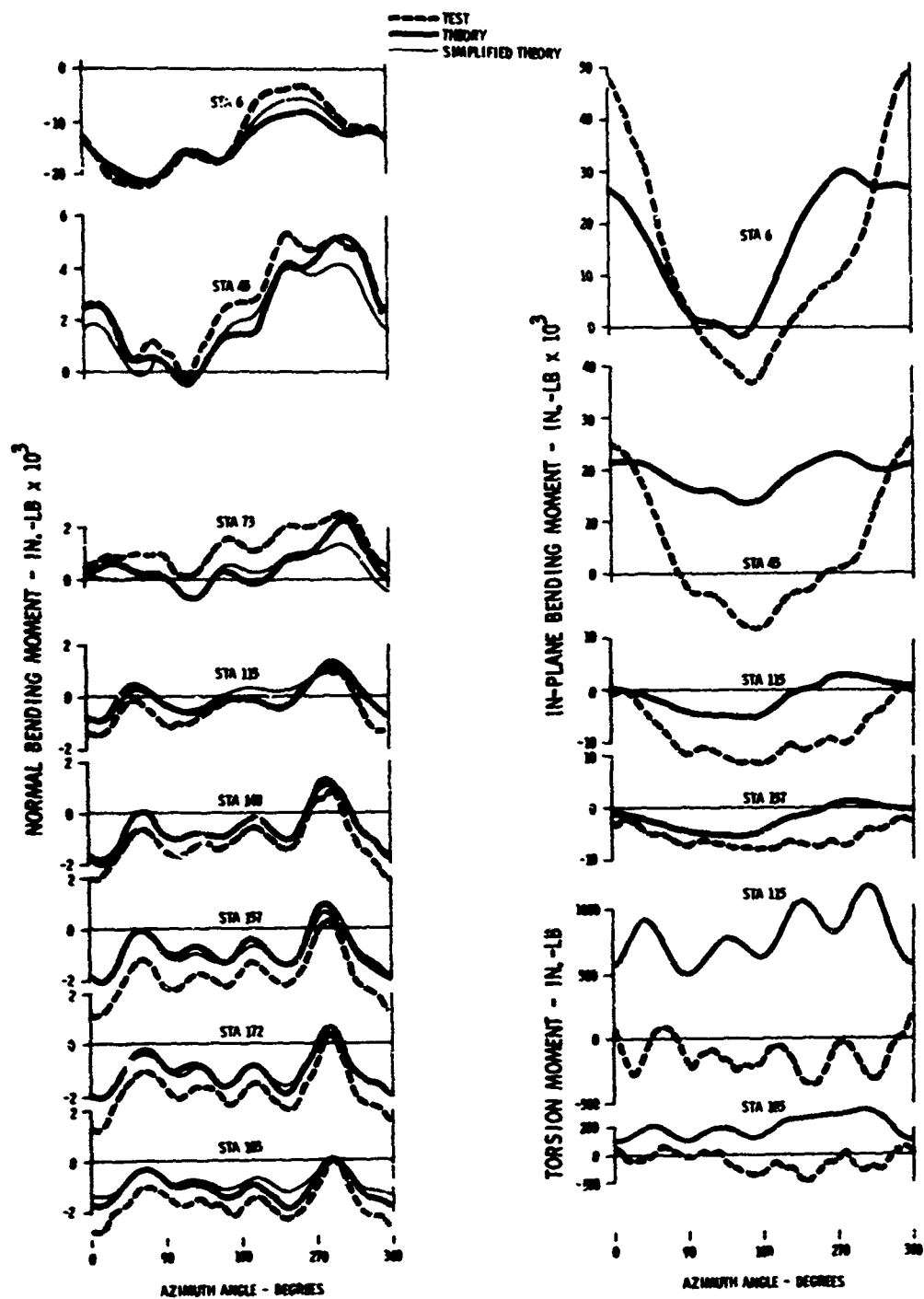
Figure 7. Response to Measured Airloads (13 Modes),
Condition 5 (Forward Flight at 51 . s TAS)

28
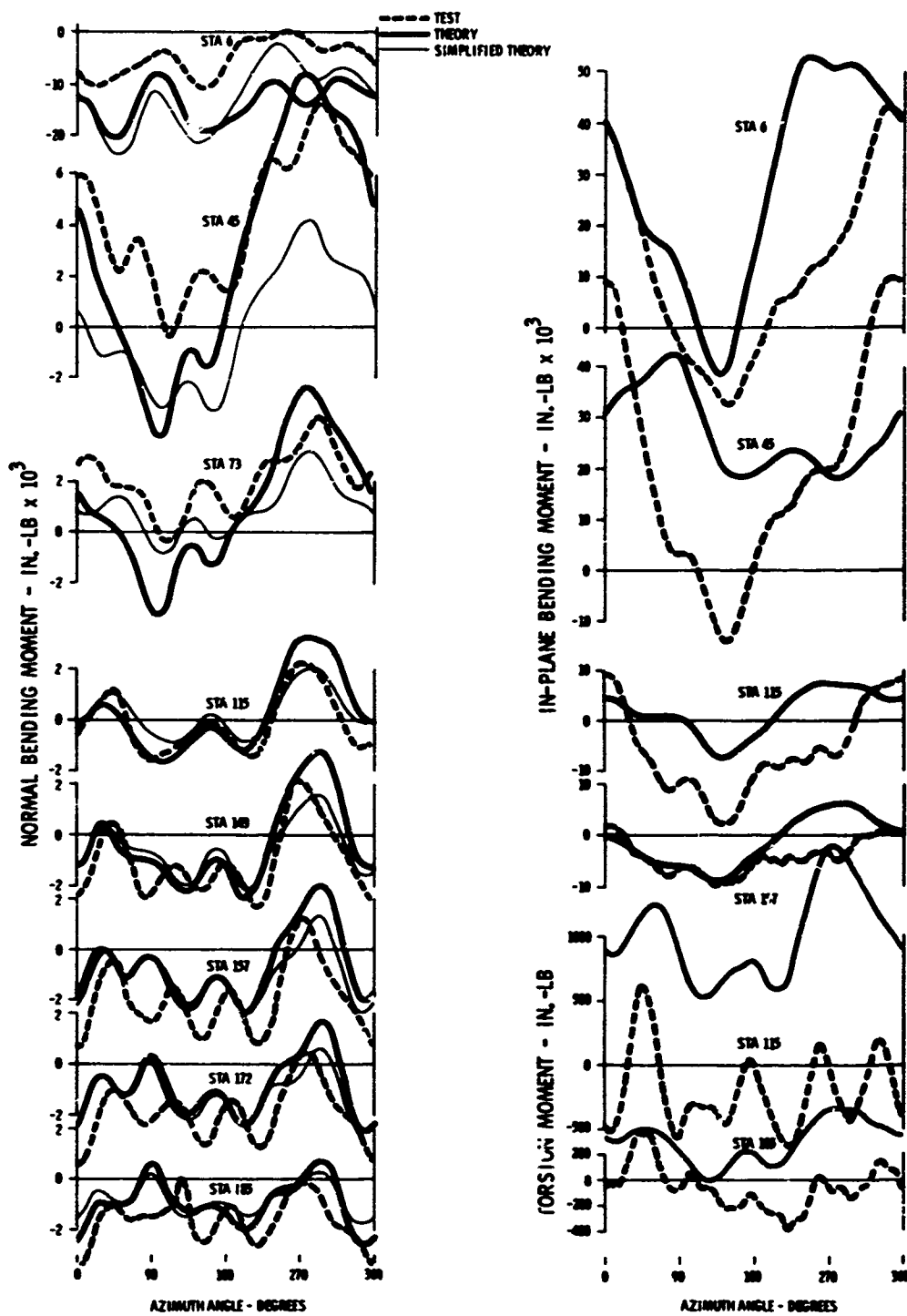
Figure 8. Response to Measured Airloads (13 Modes),
Condition 8 (Forward Flight at 105 Knots TAS)
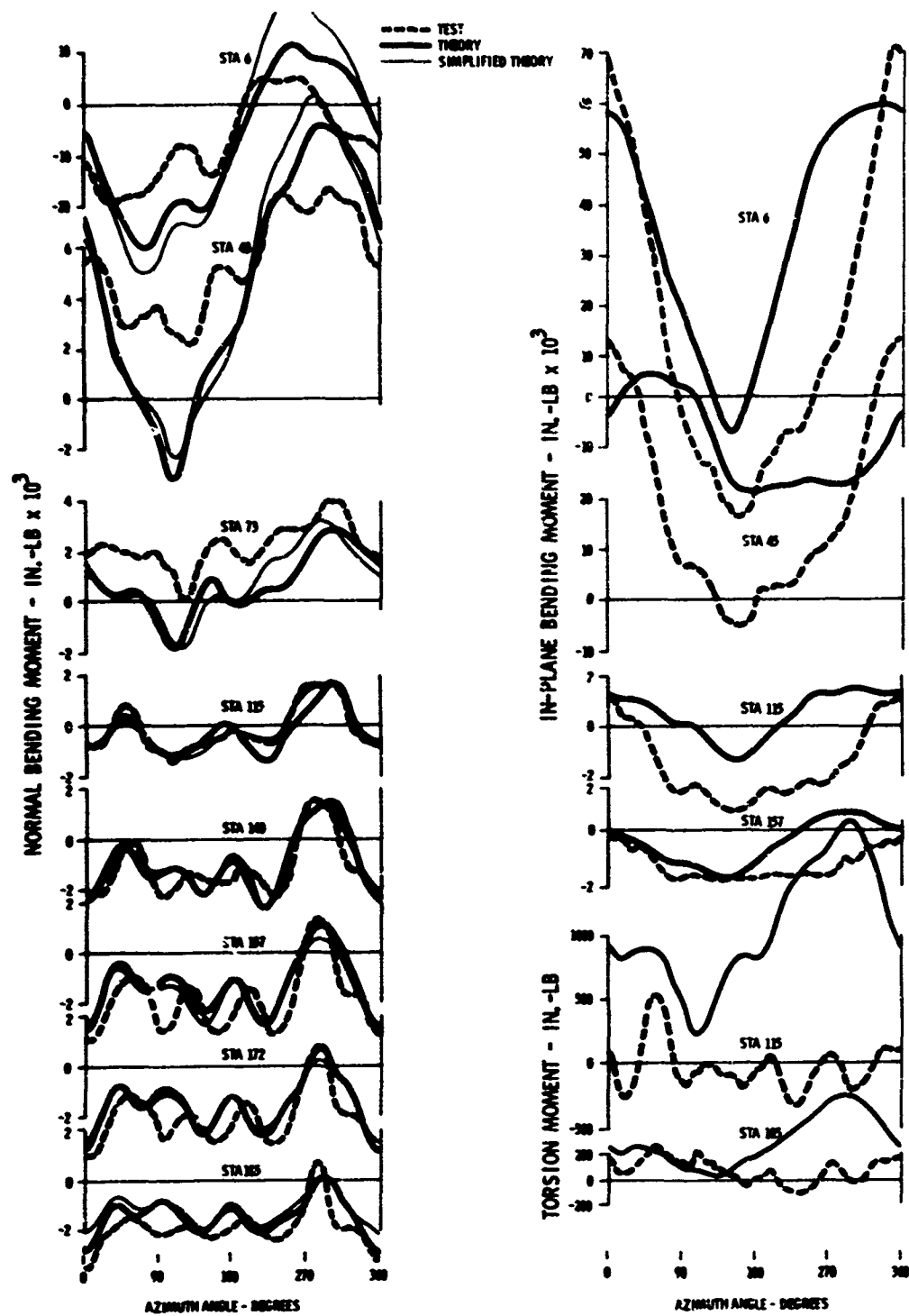
Figure 9. Response to Measured Airloads (13 Modes),
Condition 11 (Left Turn At 84 Knots TAS)
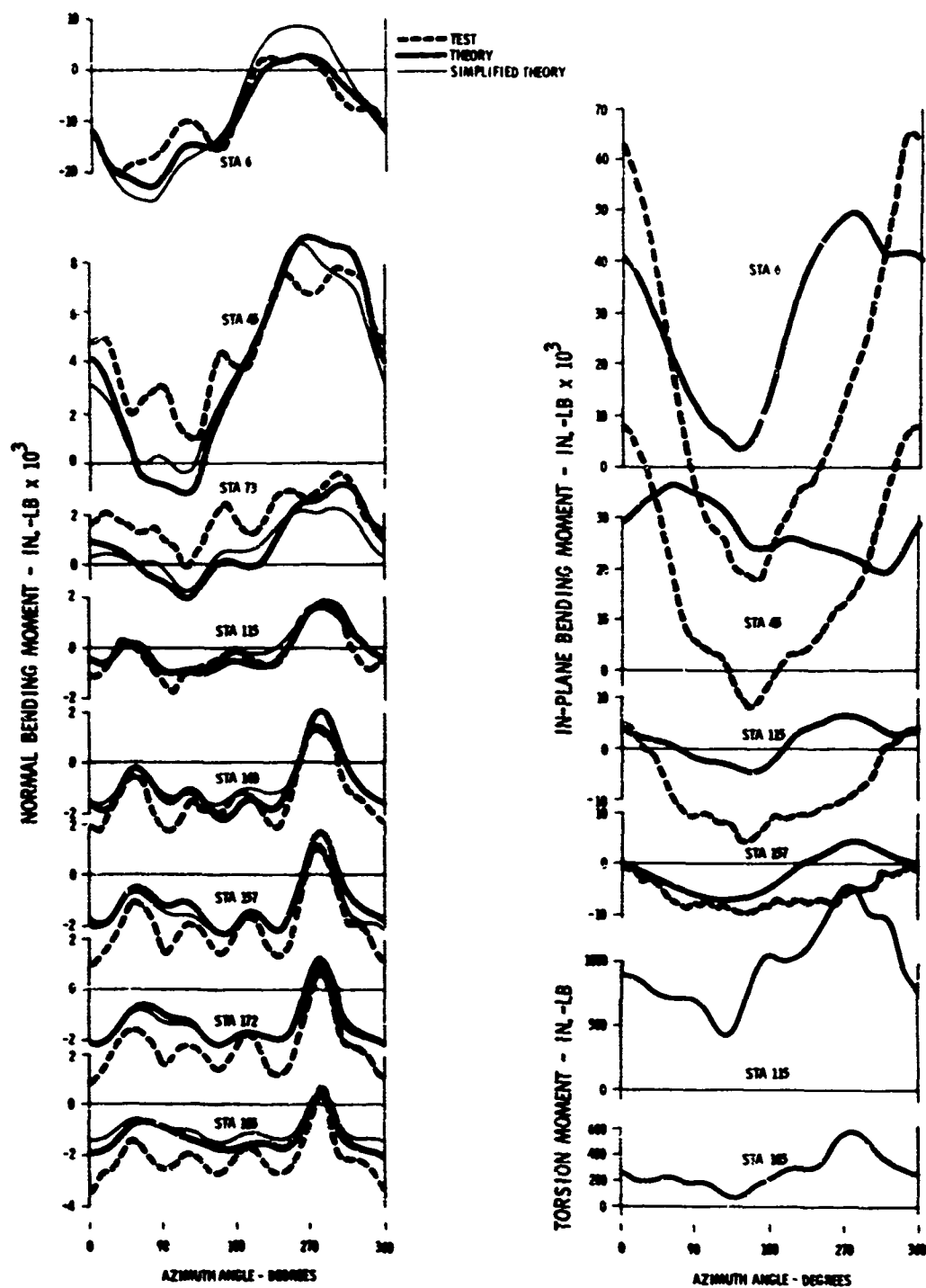
Figure 10. Response to Measured Airloads (13 Modes),
Condition 12 (Right Turn at 62 Knots TAS)

31
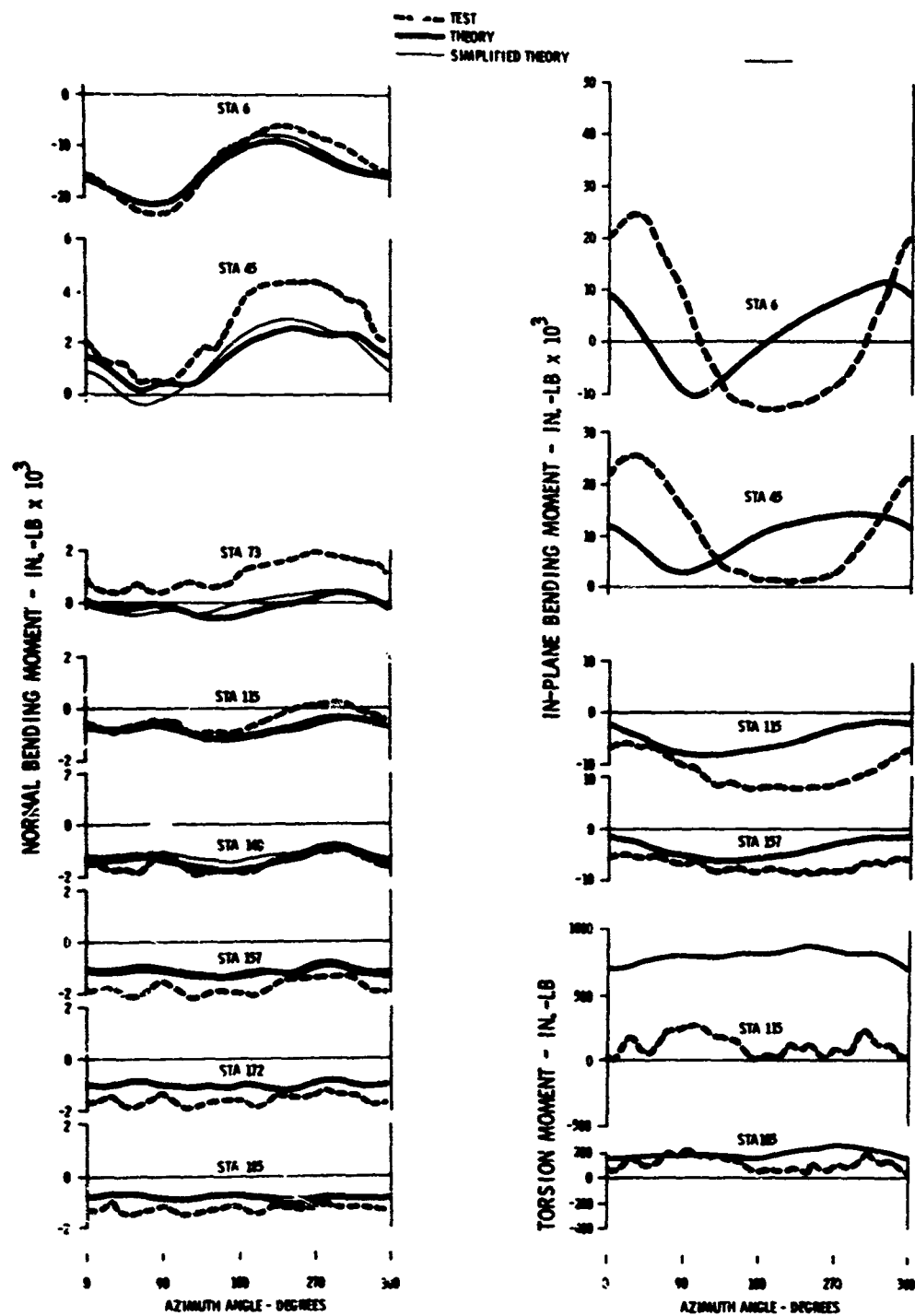
Figure 11.   Response to Measured Airloads (13 Modes),
Condition 16 (Autorotation)

32
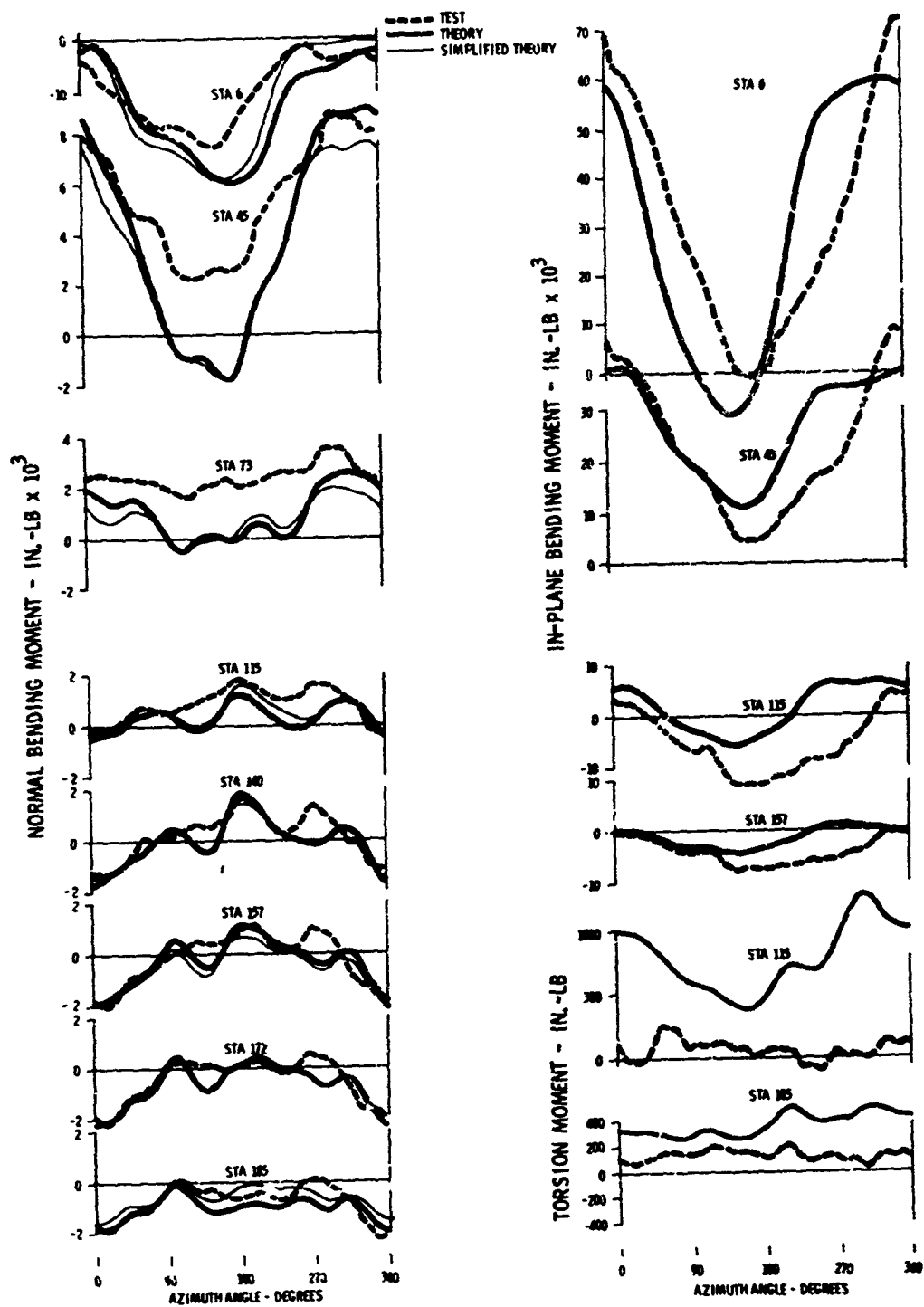
Figure 12. Response to Measured Airloads (13 Modes),
Condition 19 (Transition.)

33
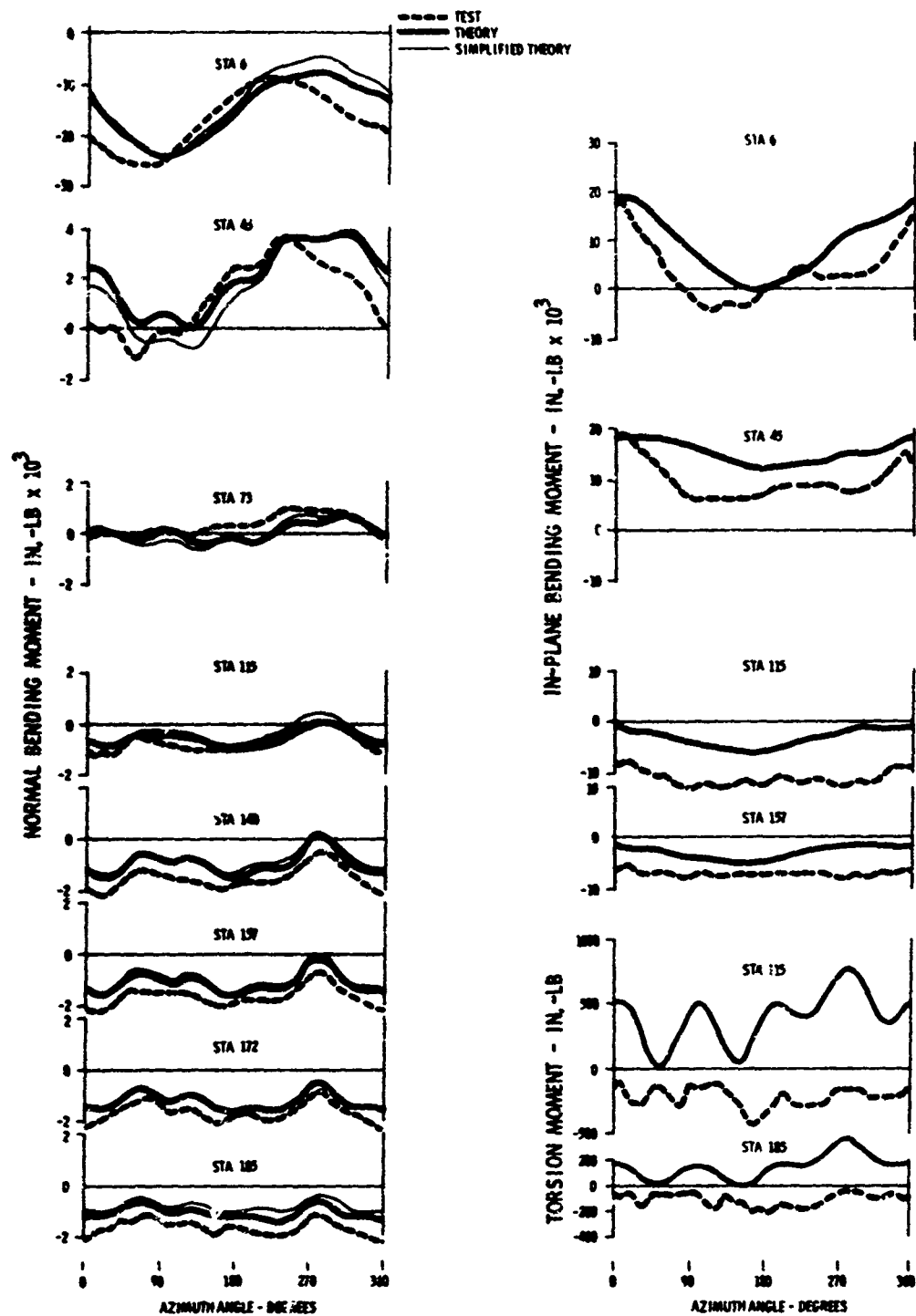
Figure 13. Response to Measured Airloads (13 Modes), Condition 21 (Flare at 60 Knots TAS)
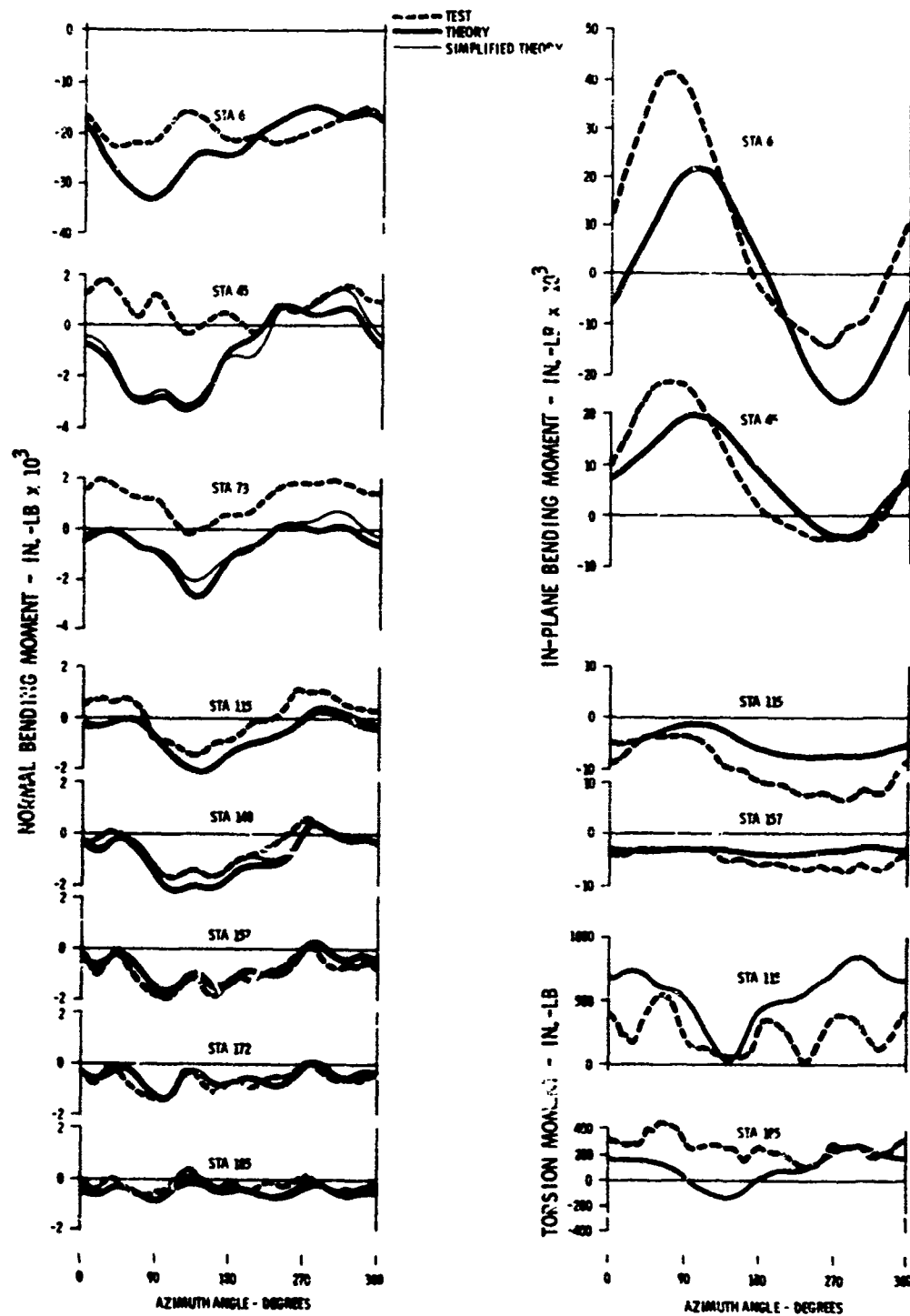
Figure 14. Response to Measured Airloads (13 Modes),
Condition 23 (Level Flight at 109 Knots TAS)
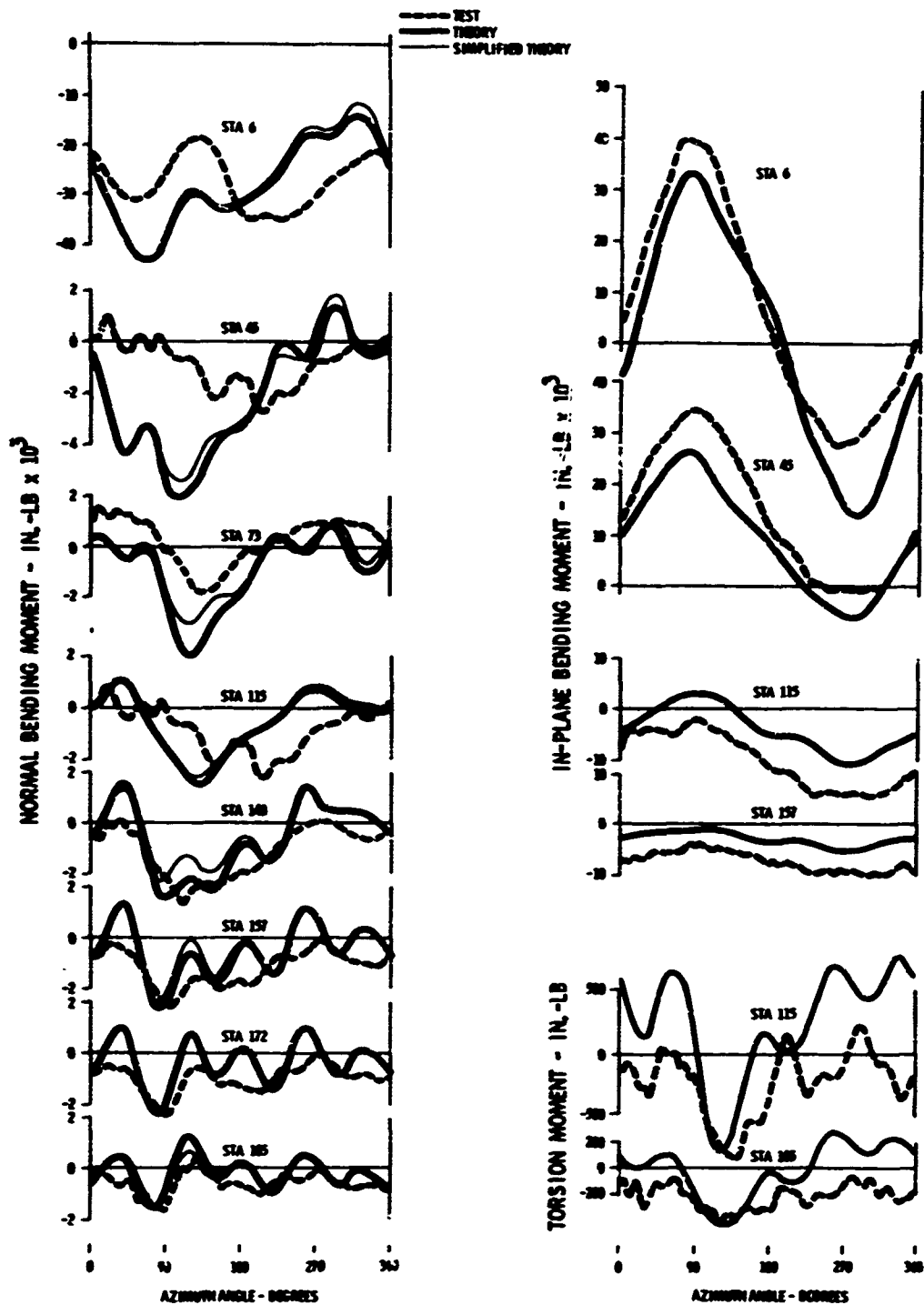
Figure 15. Response to Measured Airloads (13 Modes),
Condition 25 (Level Flight at 163.5 Knots TAS)

36
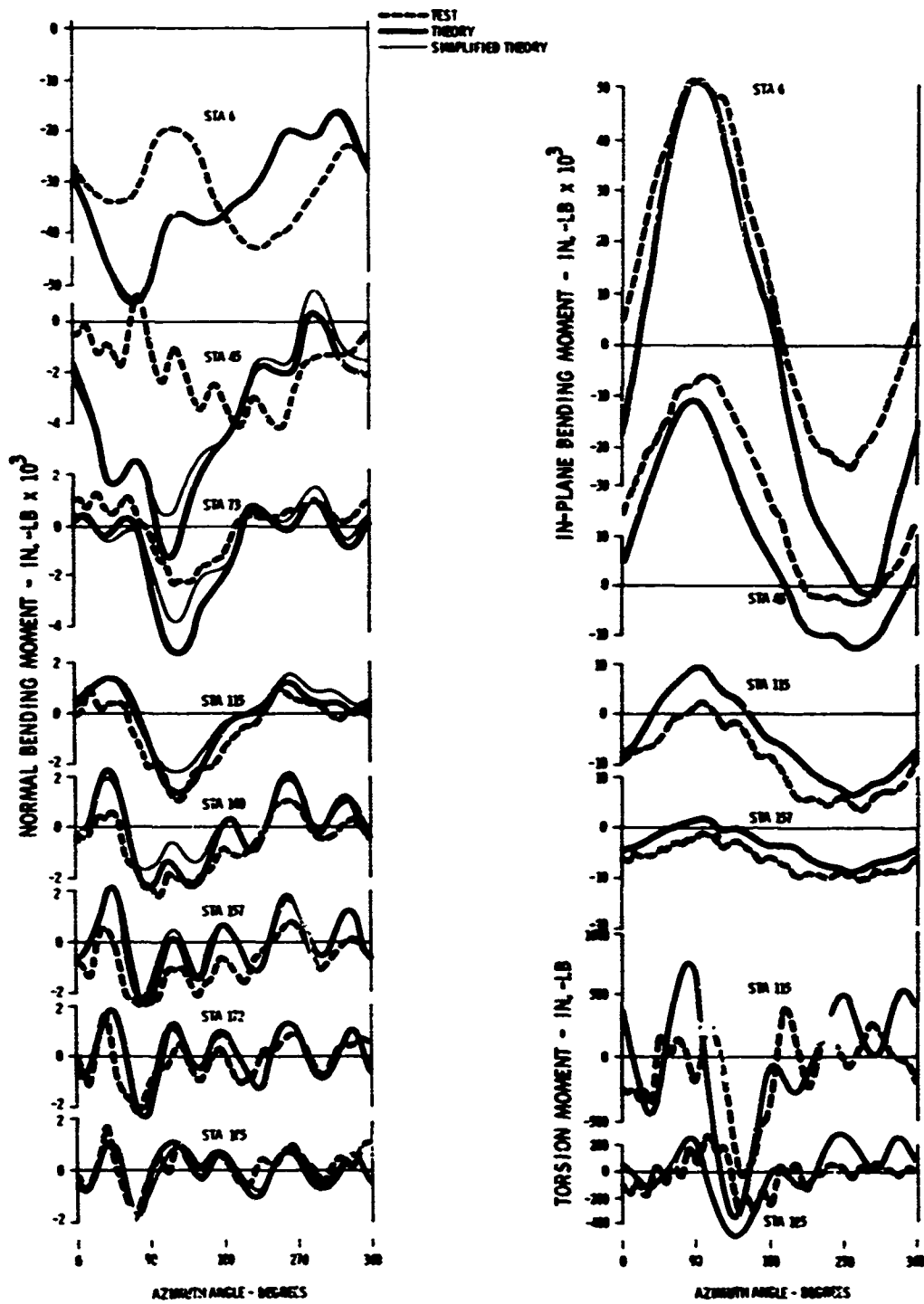
Figure 16. Response to Measured Airloads (13 Modes),
Condition 26 (Level Flight at 207 Knots TAS)

37
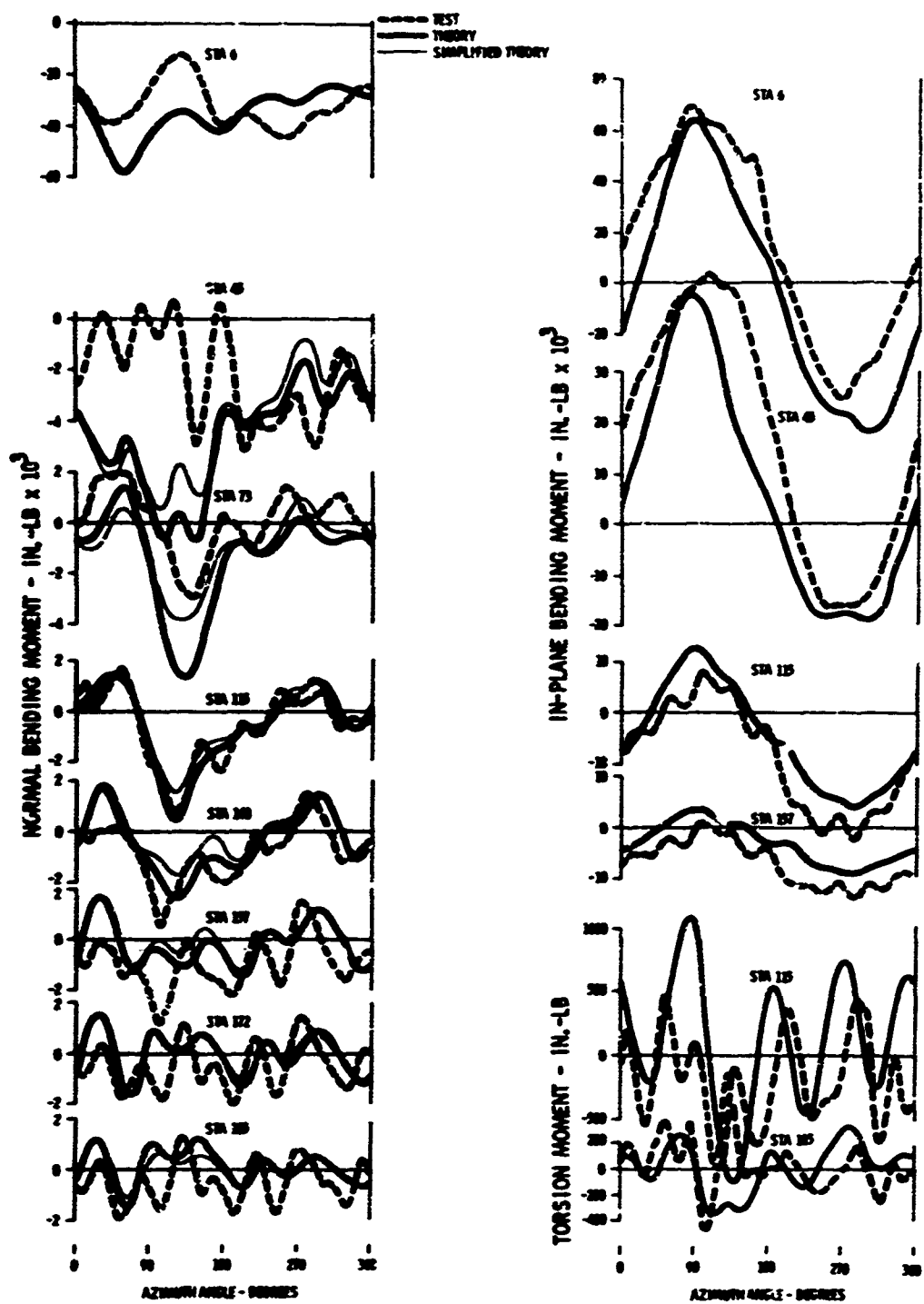
Figure 17. Response to Measured Airloads (13 Modes),
Condition 27 (Level Flight at 227 Knots TAS)

38
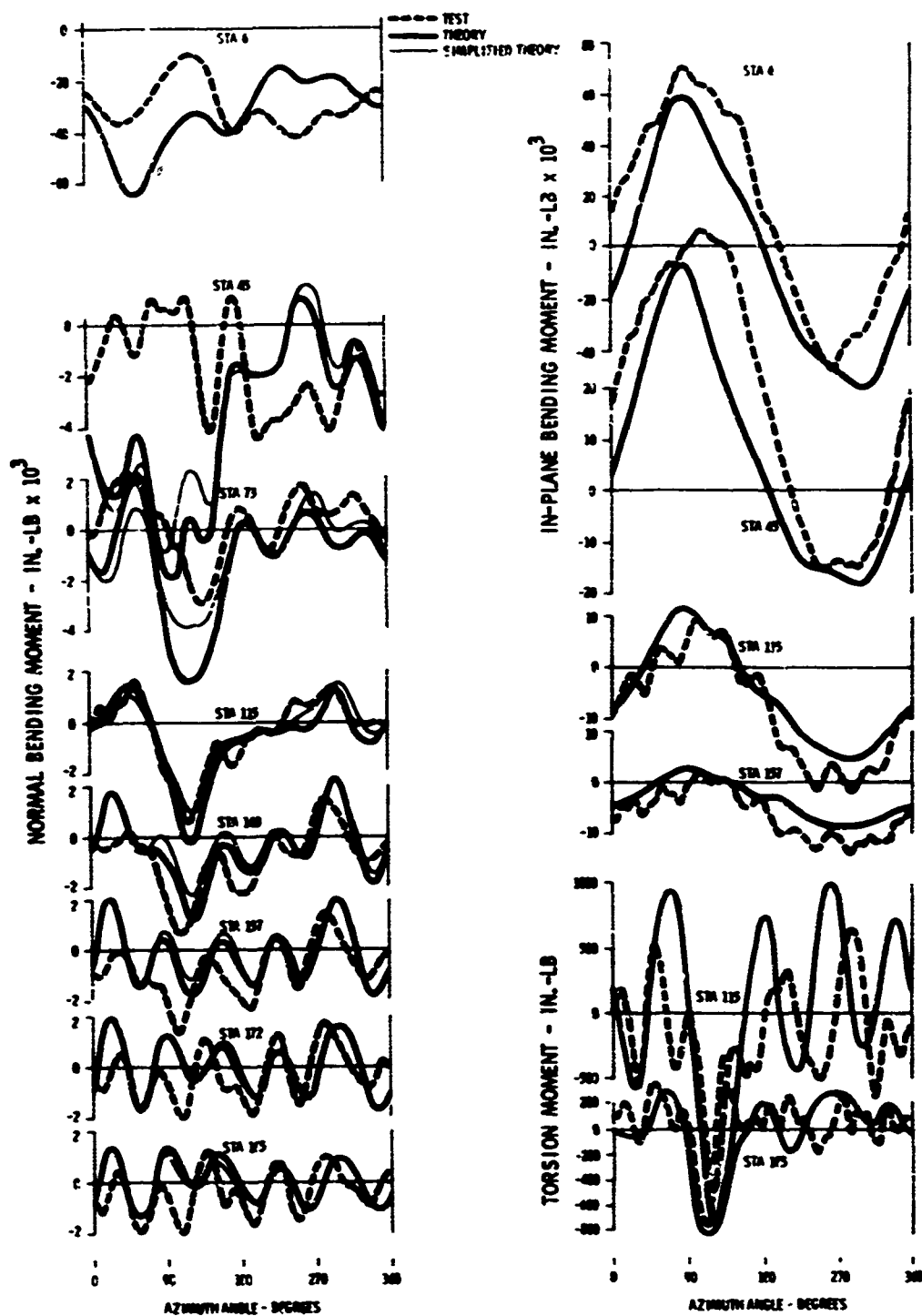
Figure 18. Response to Measured Airloads (13 Modes),
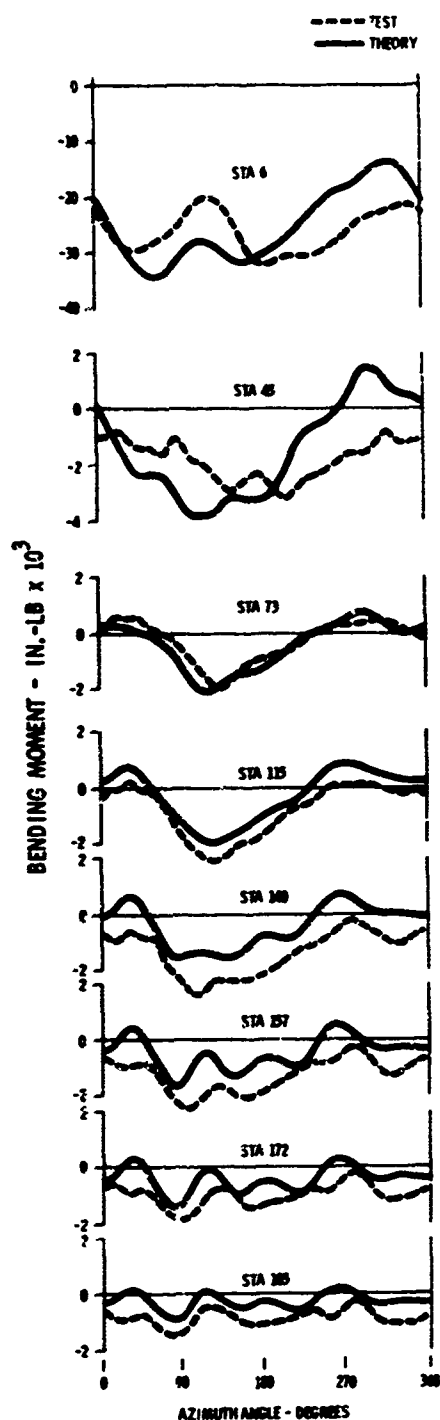Condition 31 (Level Flight at 232 Knots TAS)
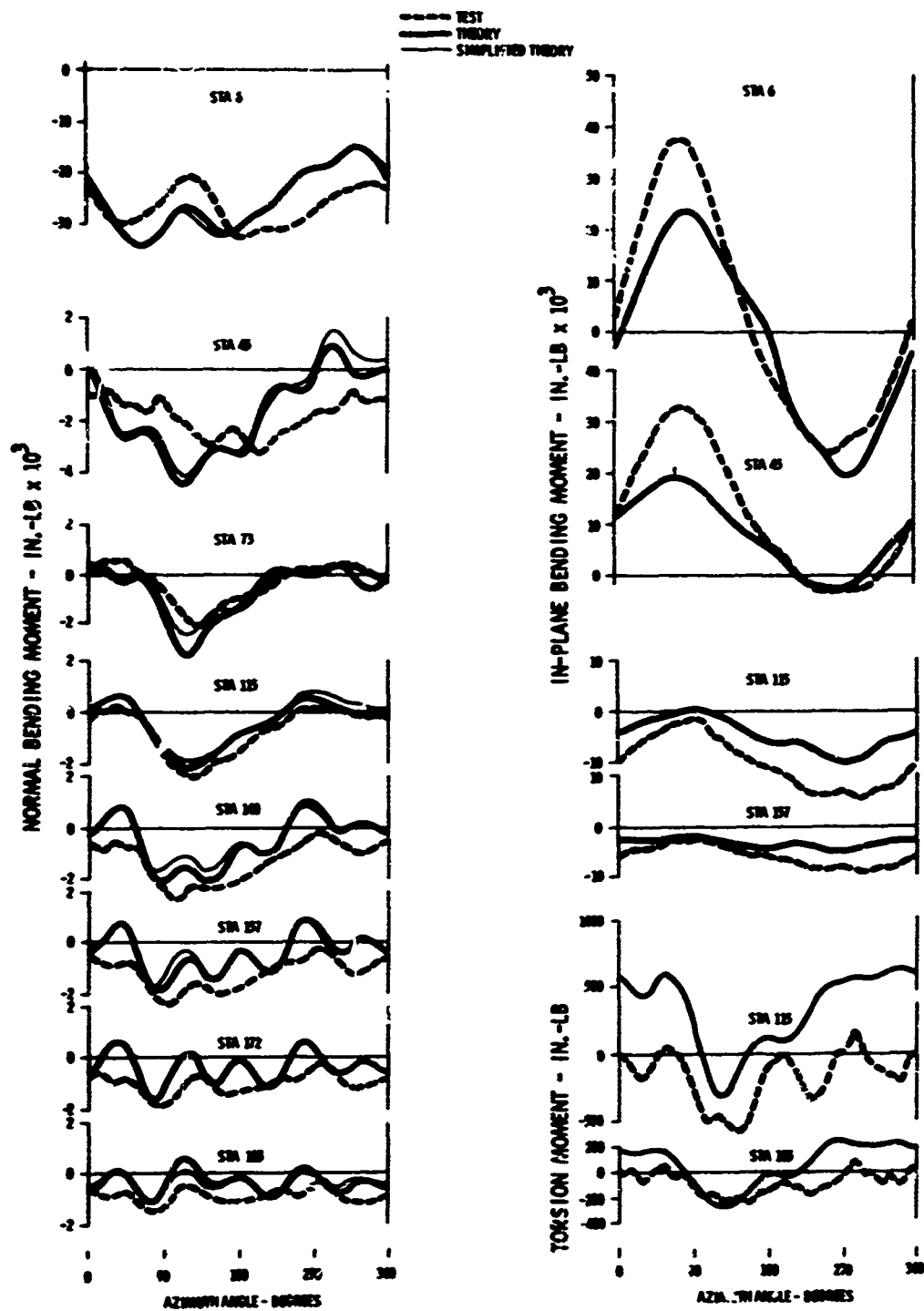
Figure 19. Response to Measured Airloads (13 Modes),
Condition 33 (Level Flight at 157 Knots TAS)

40
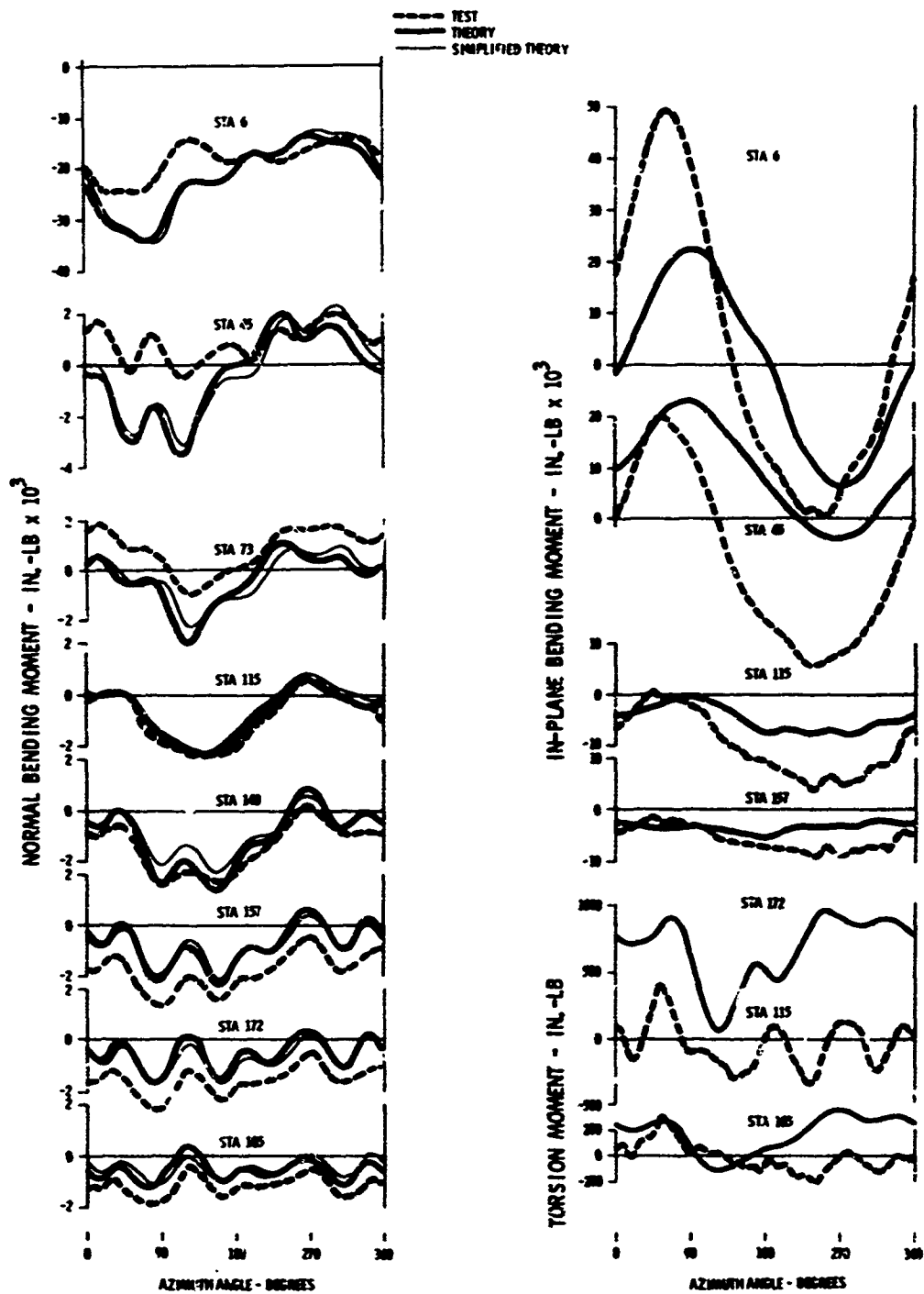
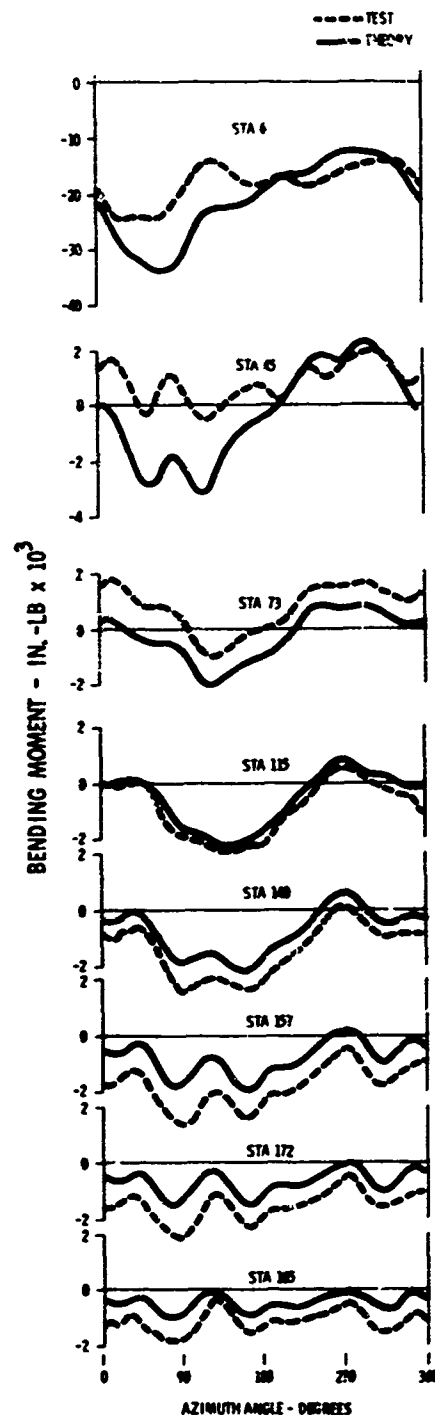Figure 20. Response to Measured Airloads (13 Modes),
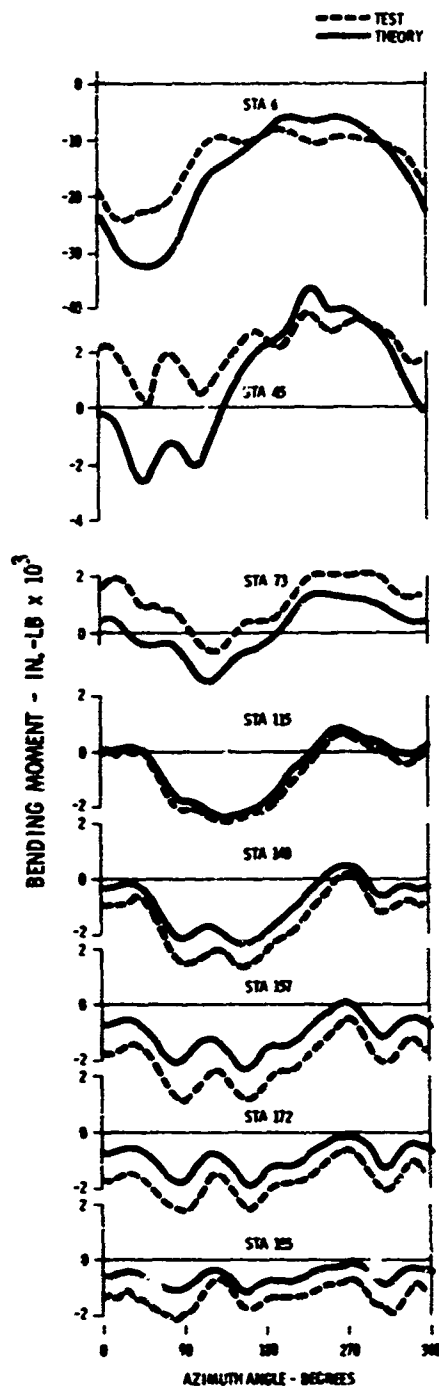Condition 36 (Pullup at 126 Knots TAS)

41
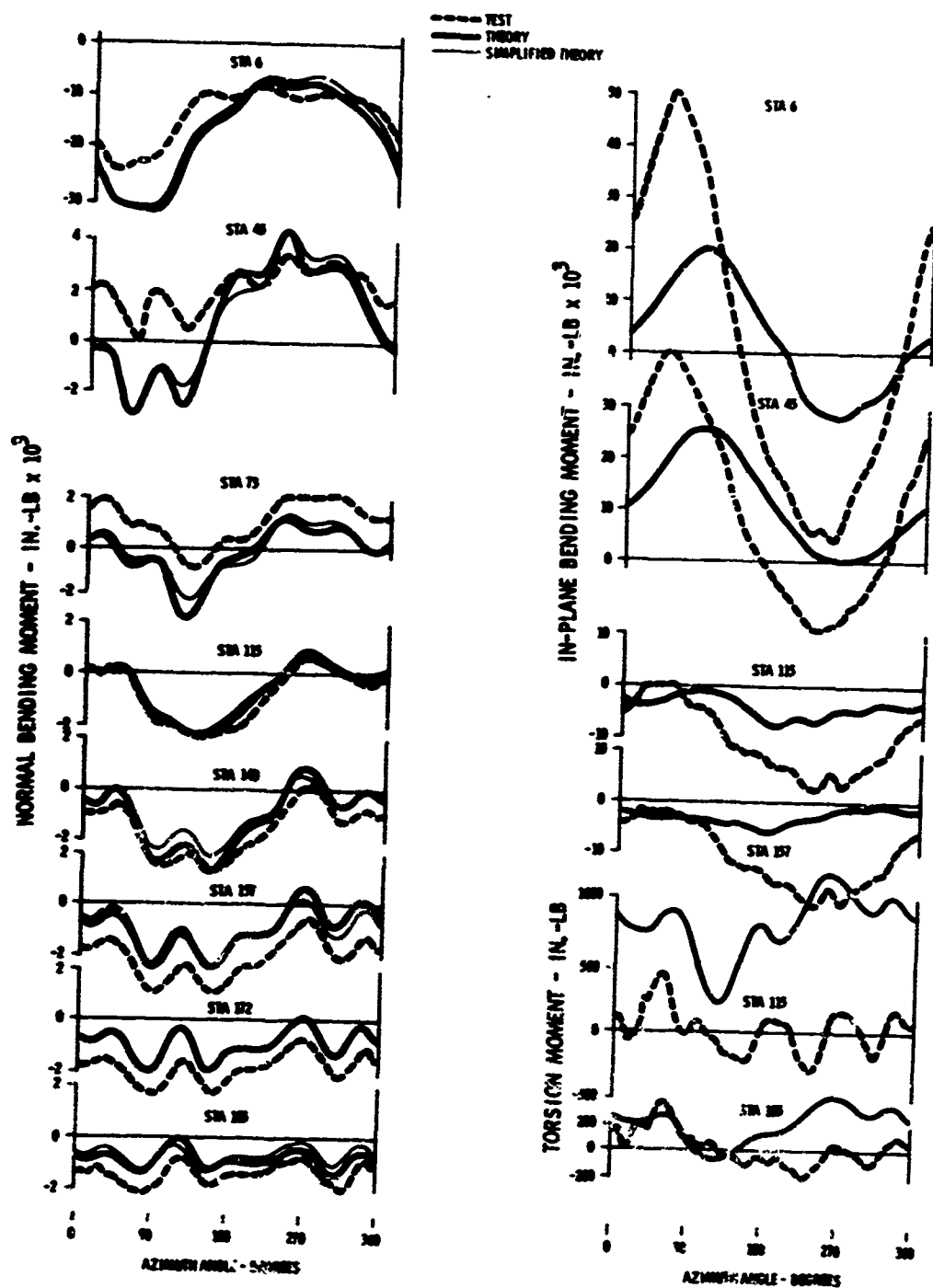
Figure 21. Response to Measured Airloads (13 Modes),
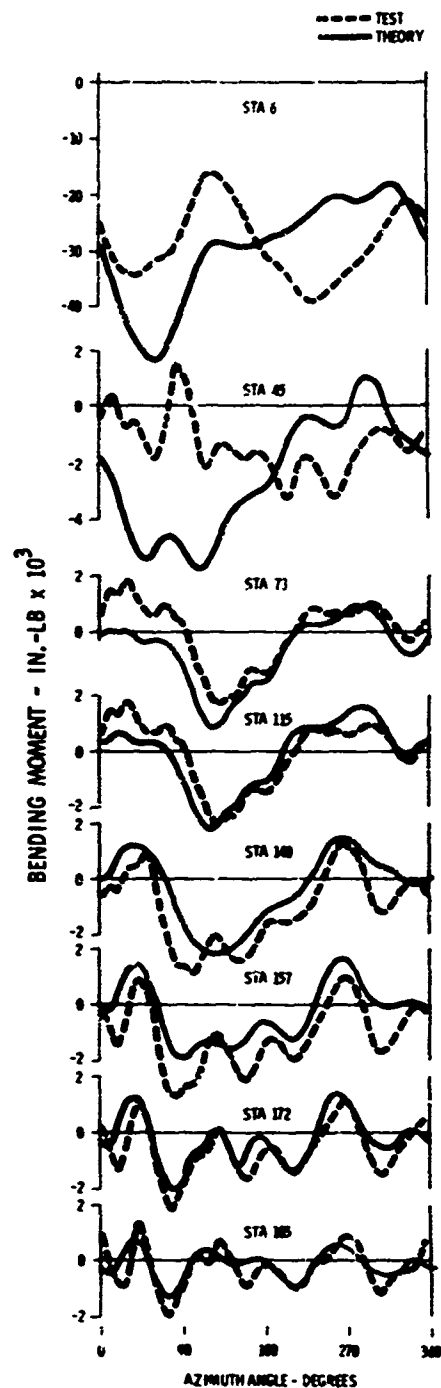Condition 37 (Pullup at 124 Knots TAS)
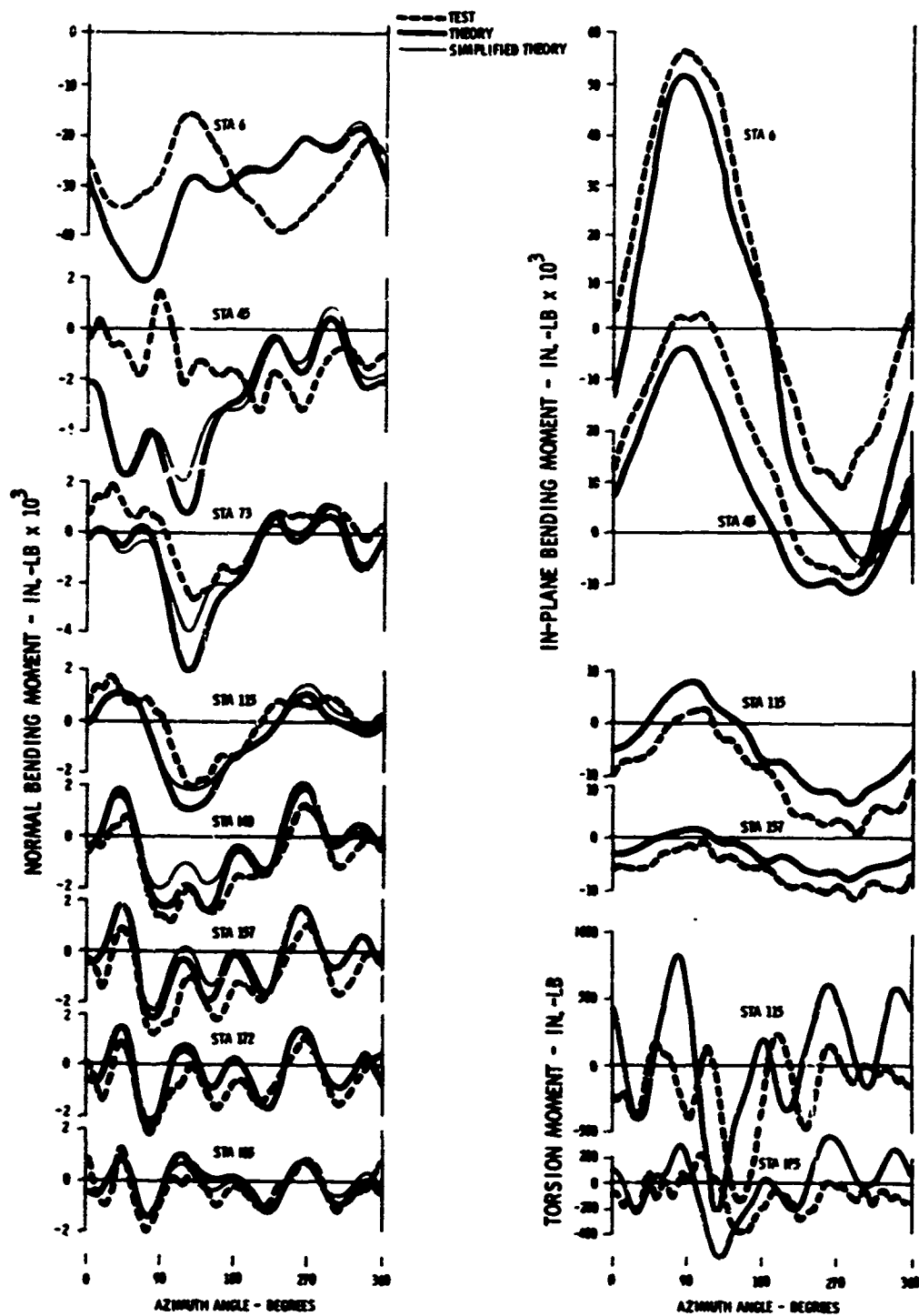
Figure 22. Response to Measured Airloads (13 Modes),
Condition 39 (Pullup at 206 Knots TAS)
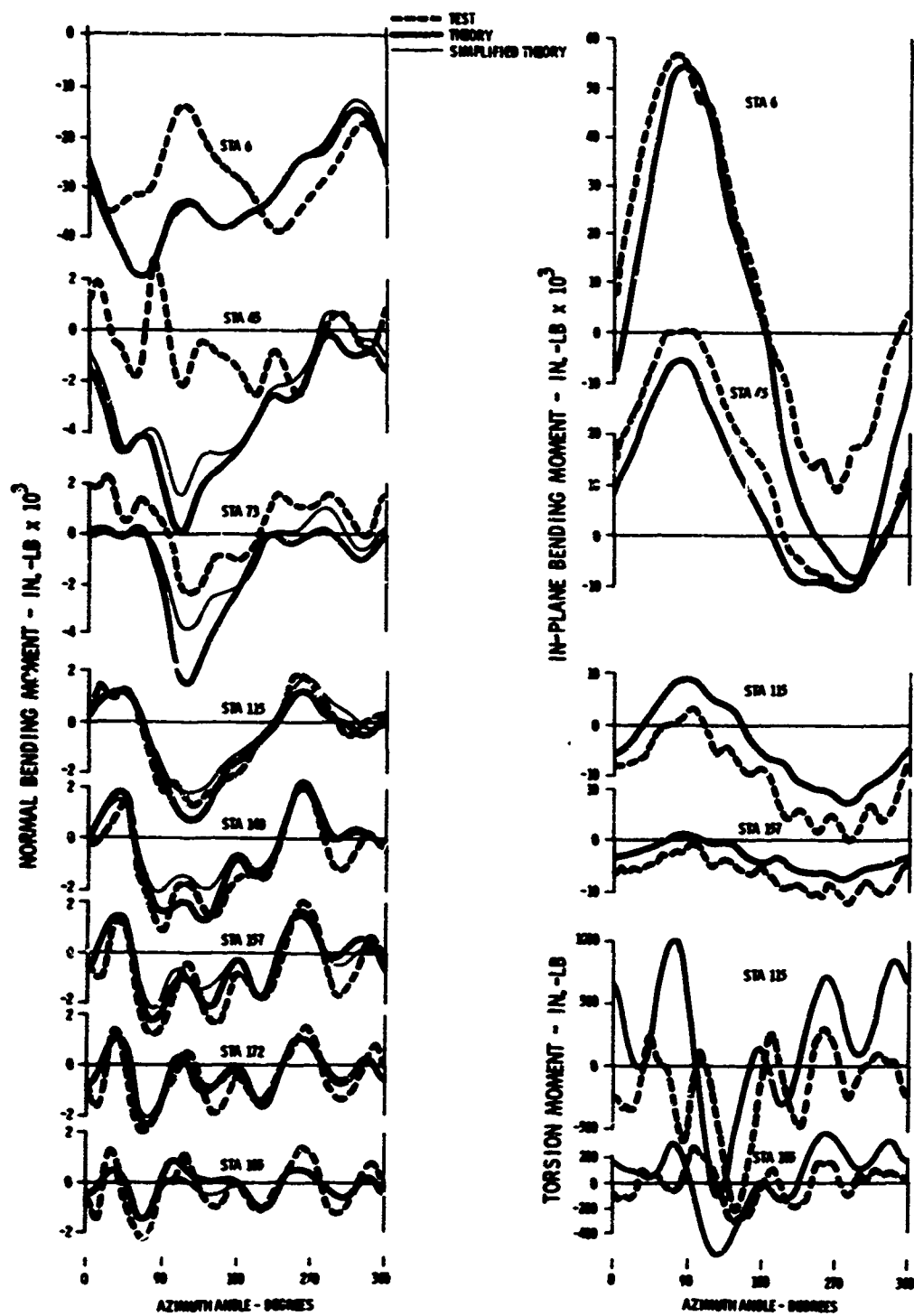
Figure 23. Response to Measured Airloads (13 Modes),
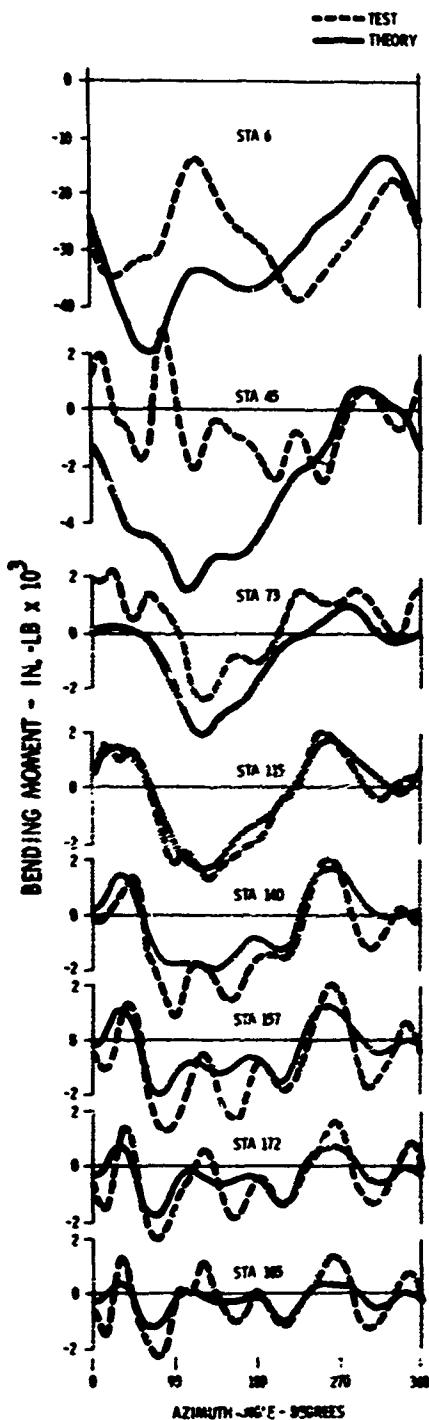Condition 40 (Pullup at 206 Knots TAS)

44
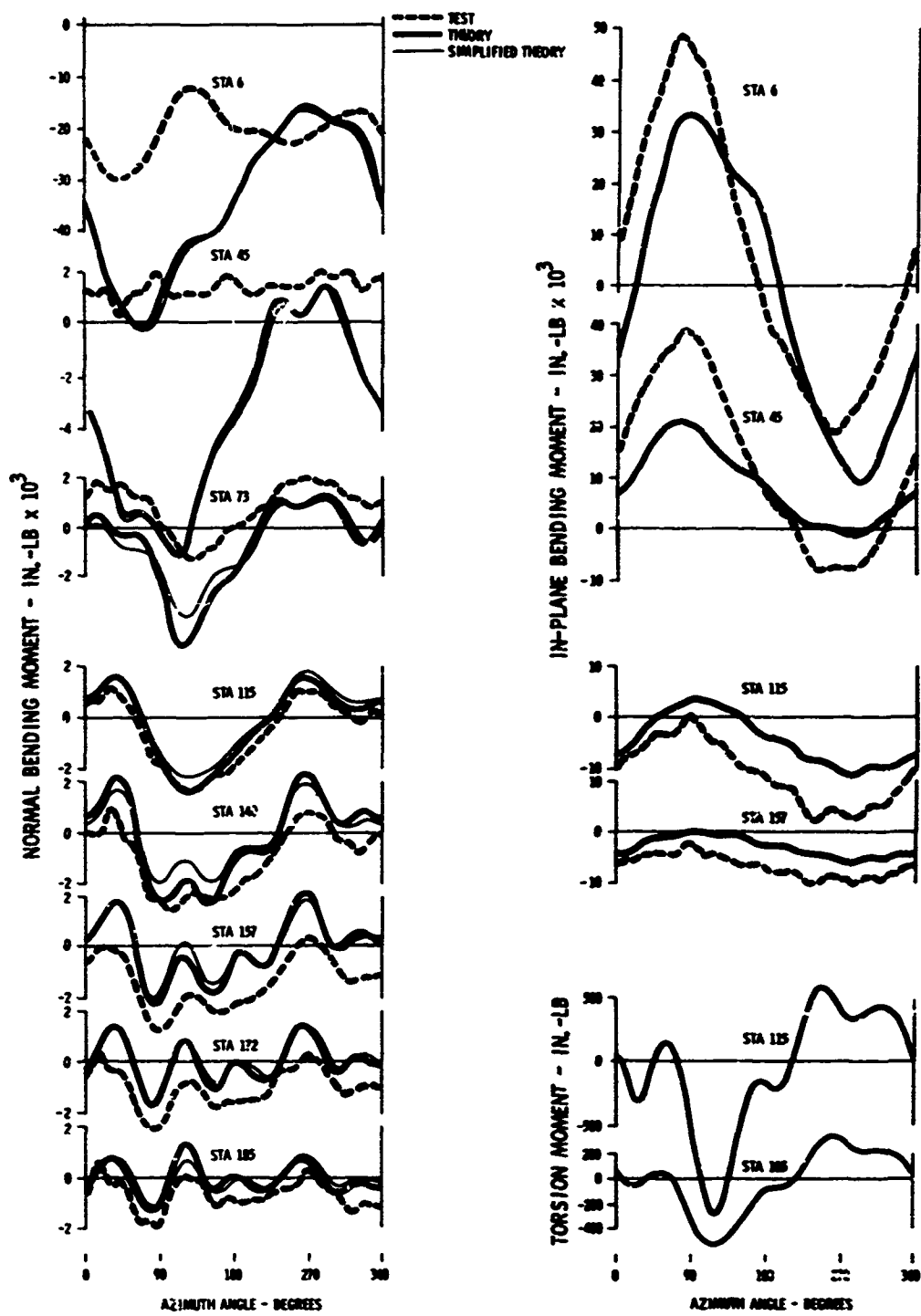
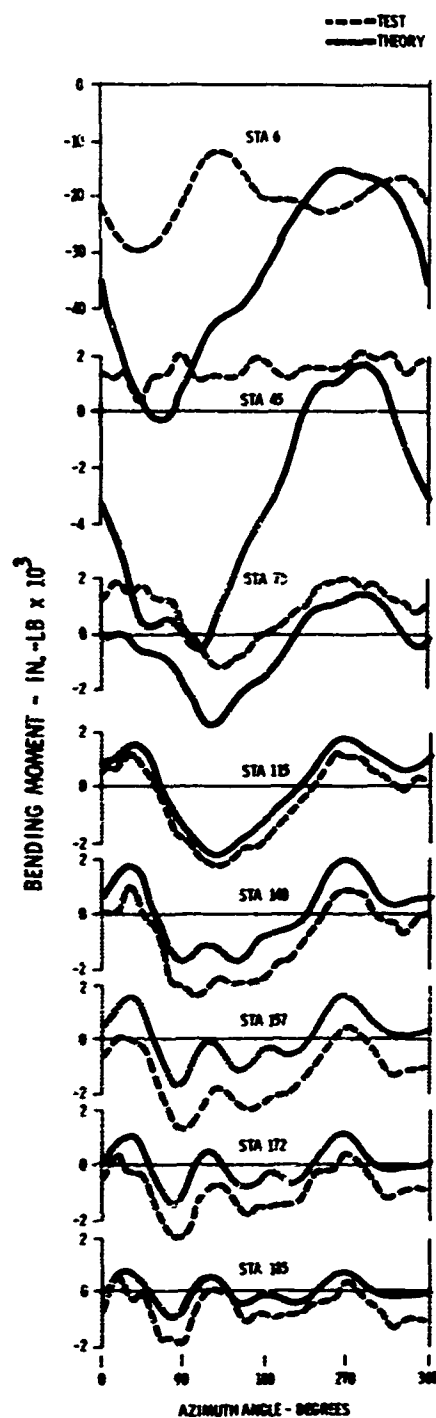Figure 24. Response to Measured Airloads (13 Modes),
Condition 43 (Pullup at 163 Knots TAS)
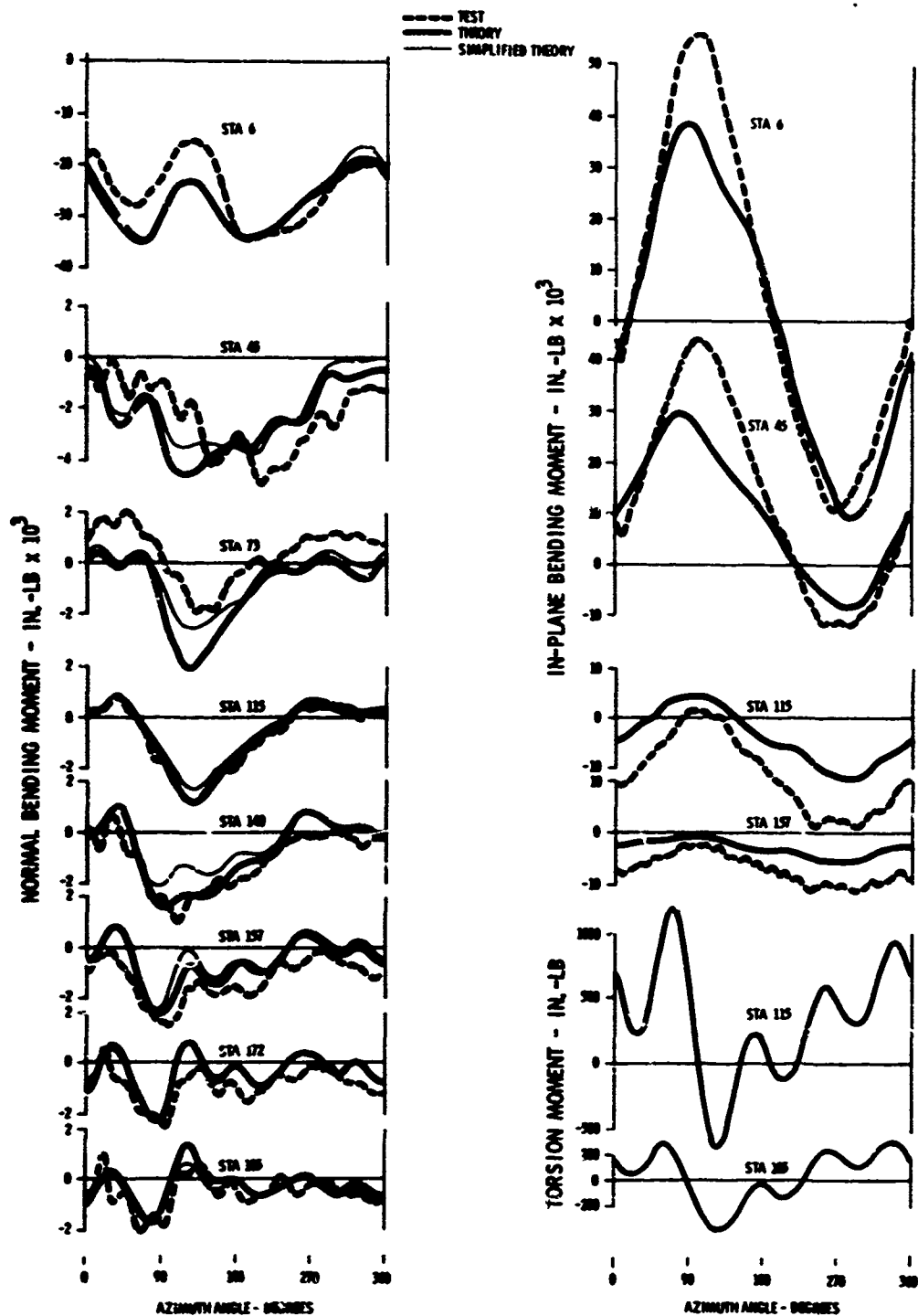
Figure 25. Response to Measured Airloads (13 Modes), Condition 44 (Pullup at 162 Knots TAS)

46
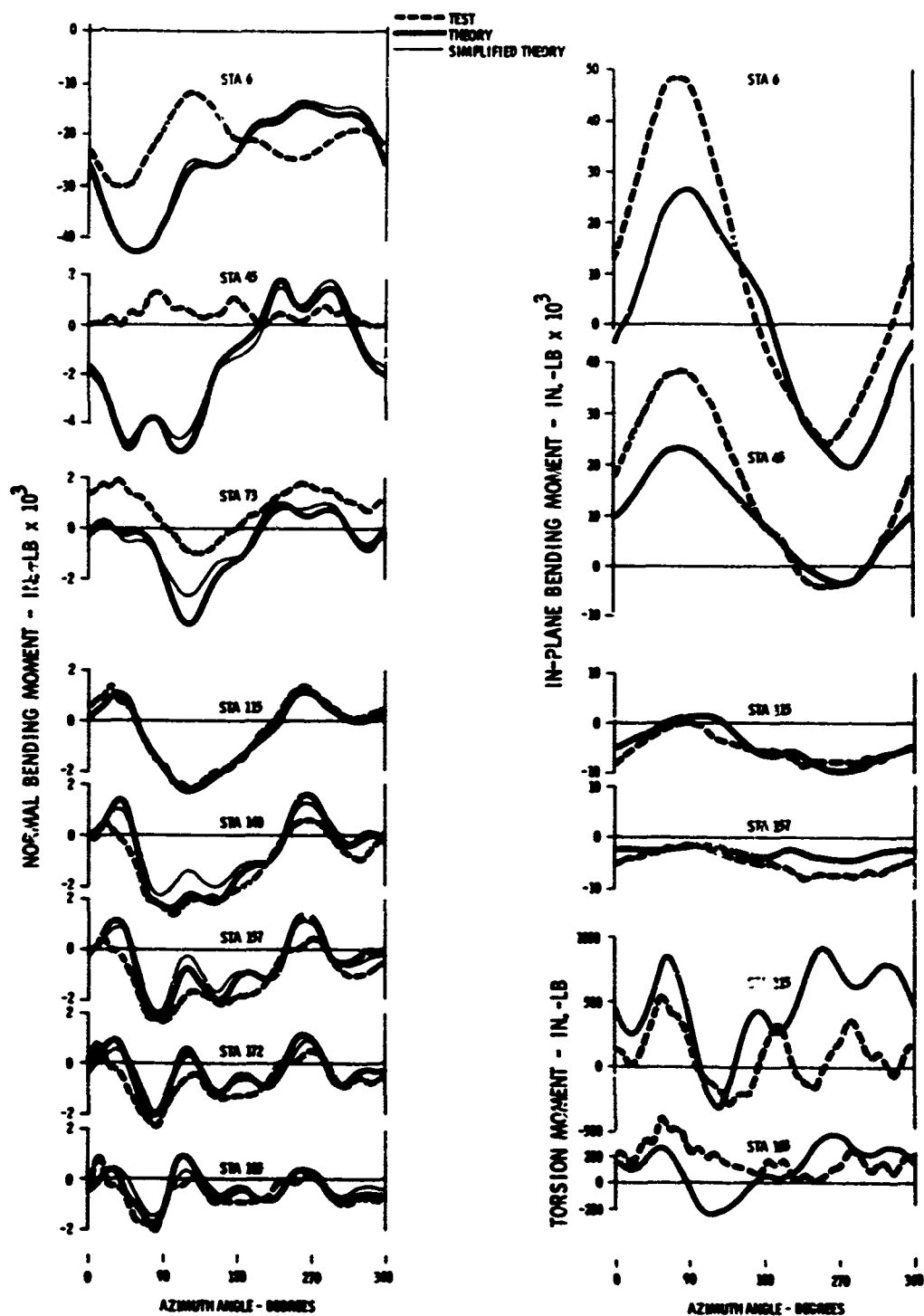
Figure 26. Response to Measured Airloads (13 Modes),
Condition 46 (Left Turn at 161 Knots TAS)

47
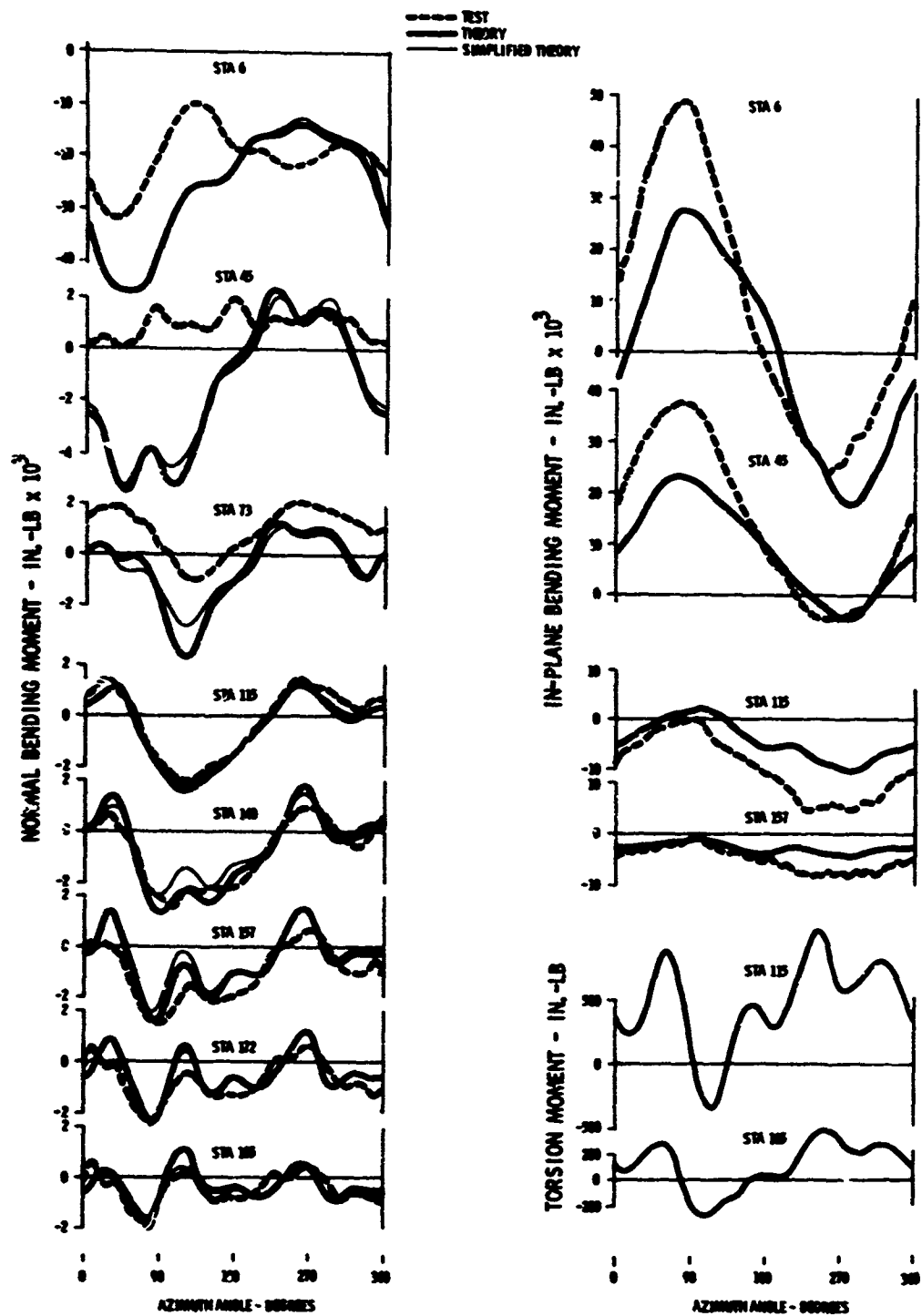
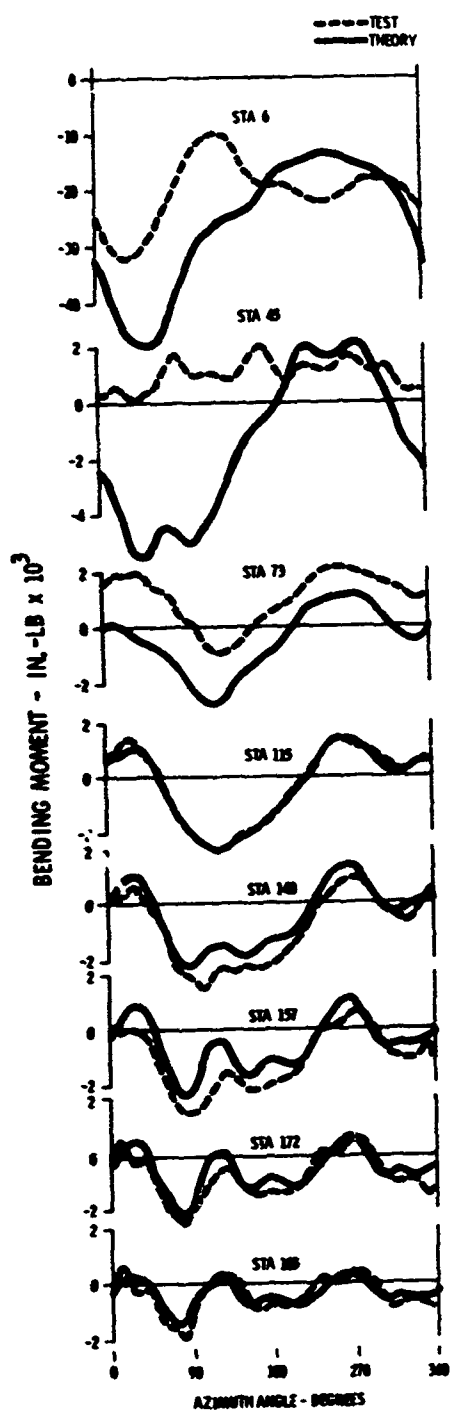Figure 27. Response to Measured Airloads (13 Modes),
Condition 49 (Right Turn at 164 Knots TAS)
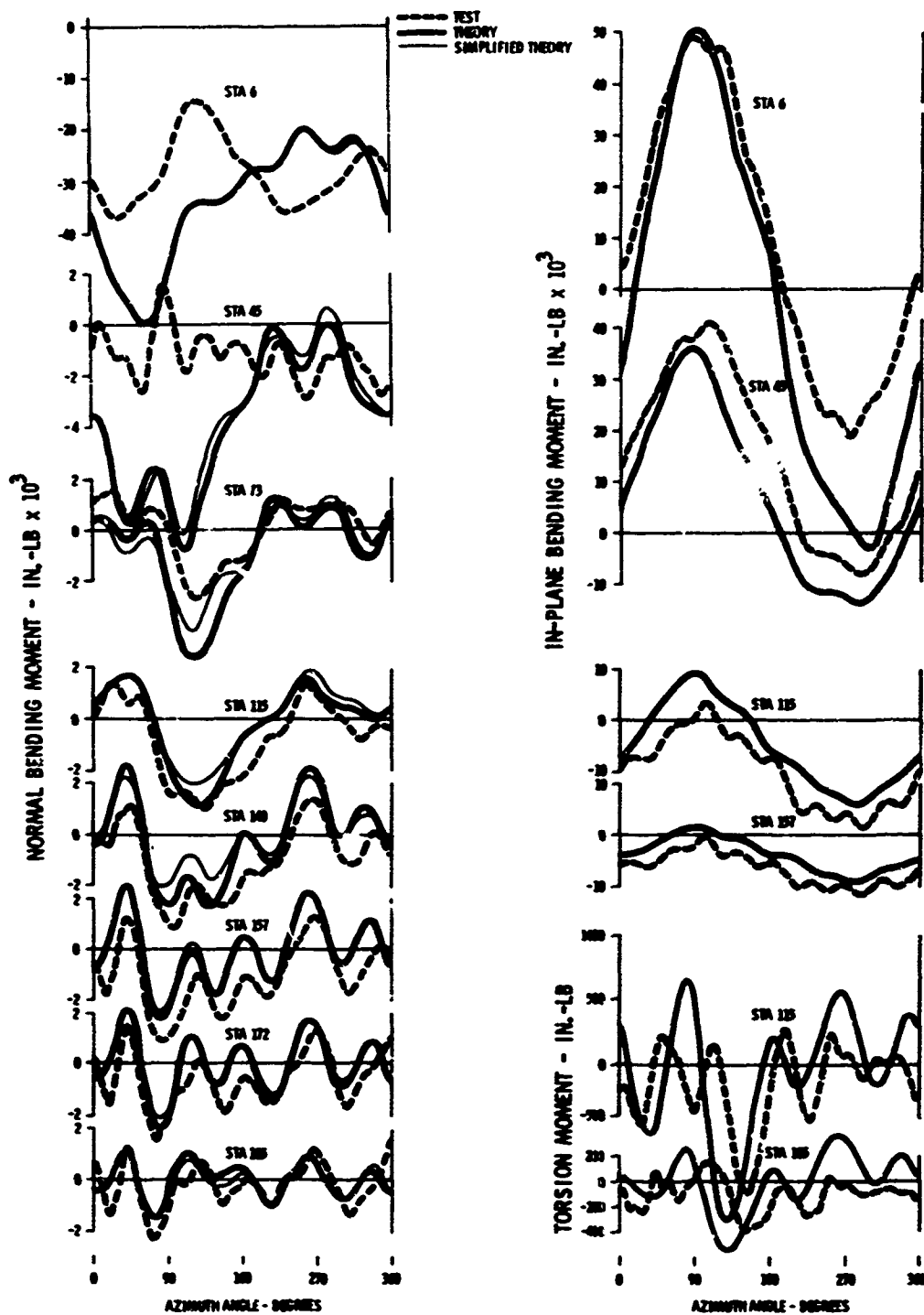
Figure 28. Response to Measured Airloads (13 Modes), Condition 50 (Right Turn at 208 Knots TAS)

49
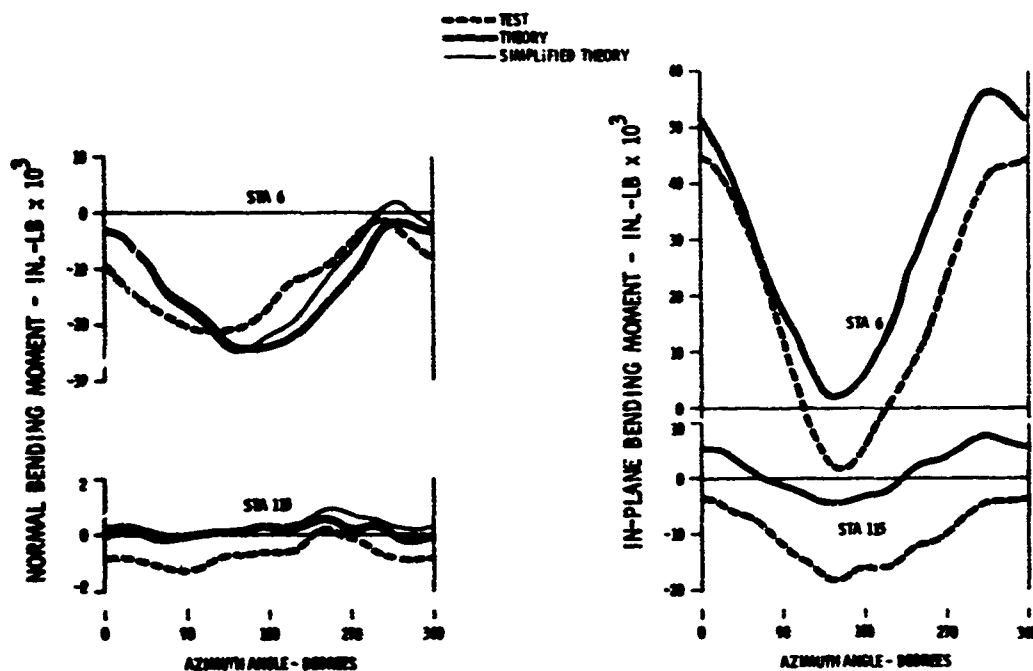
Figure 29. Response to Measured Airloads (13 Modes), Condition 2 (Collective Pullup at 0 Knot TAS)
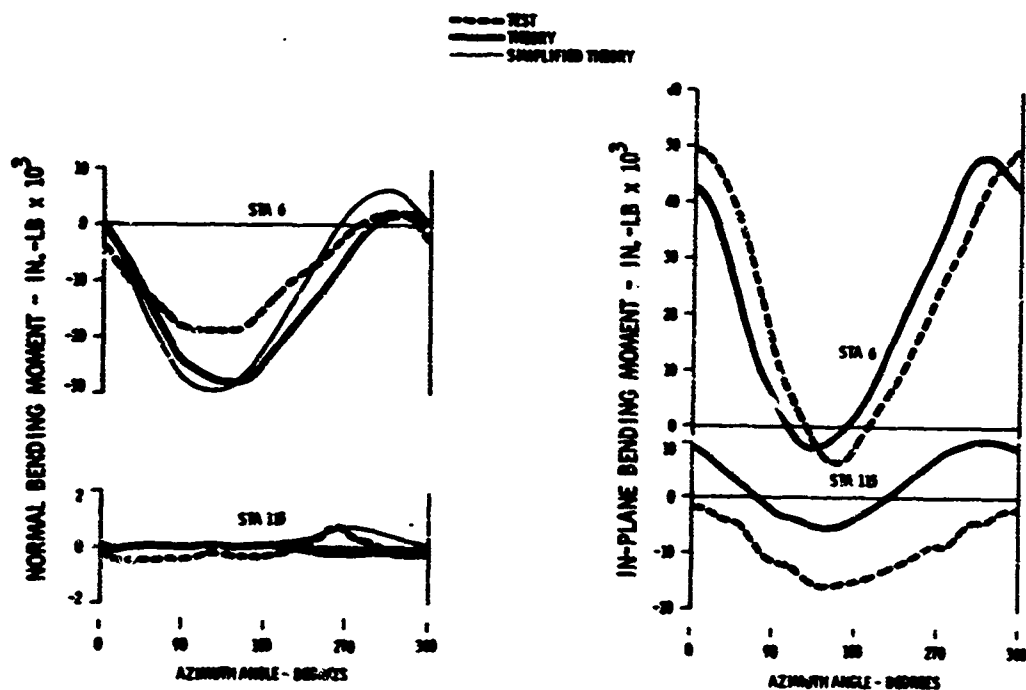
Figure 30. Response to Measured Airloads (13 Modes), Condition 3 (Collective Pullup at 0 Knot TAS)

50
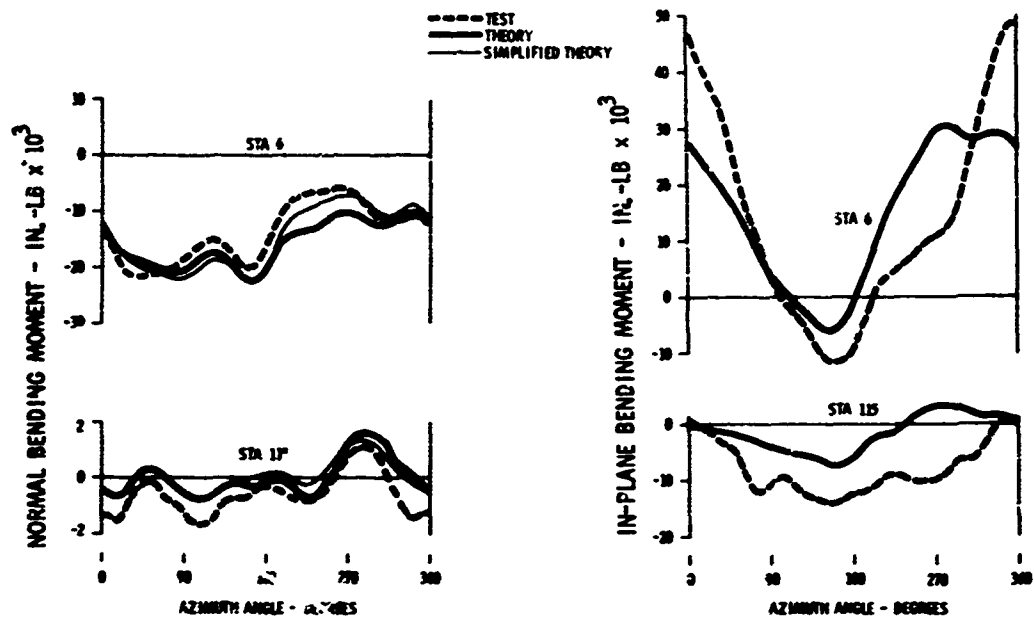
Figure 31. Response to Measured Airloads (13 Modes),
Condition 6 (Forward Flight at 59.5 Knots TAS)
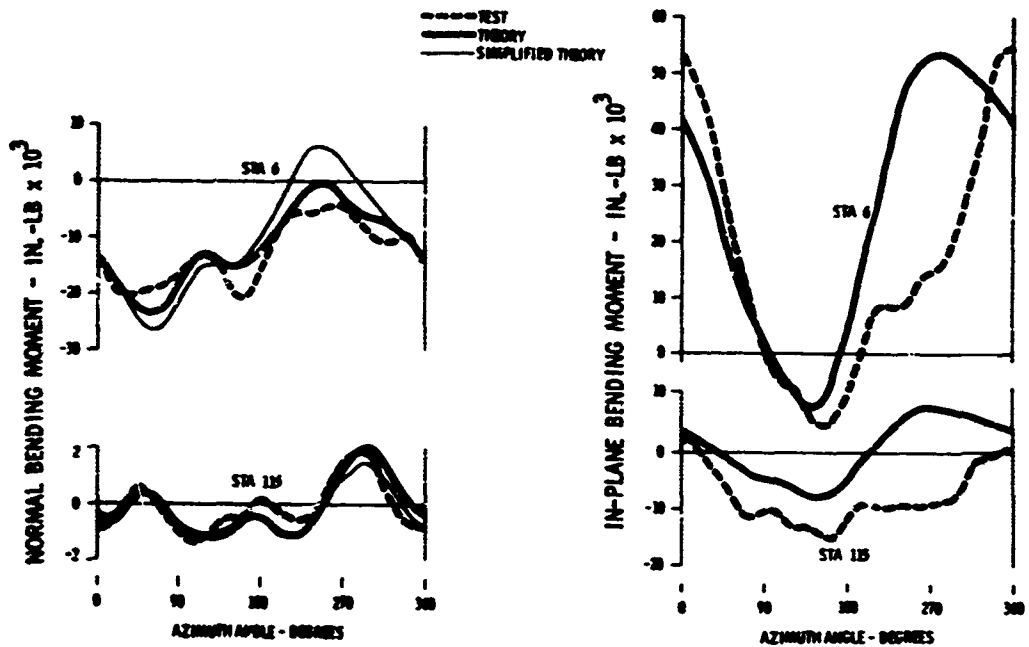
Figure 32. Response to Measured Airloads (13 Modes),
Condition 7 (Forward Flight at 80.5 Knots TAS)

51
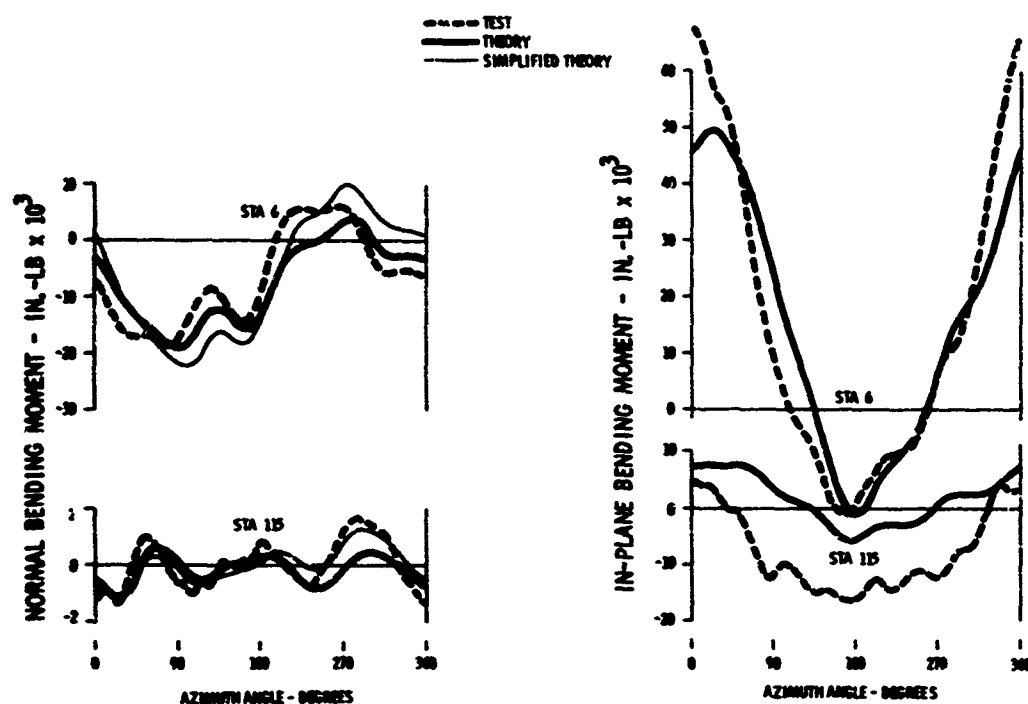
Figure 33. Response to Measured Airloads (13 Modes),
Condition 9 (Left Turn at 51 Knots TAS)
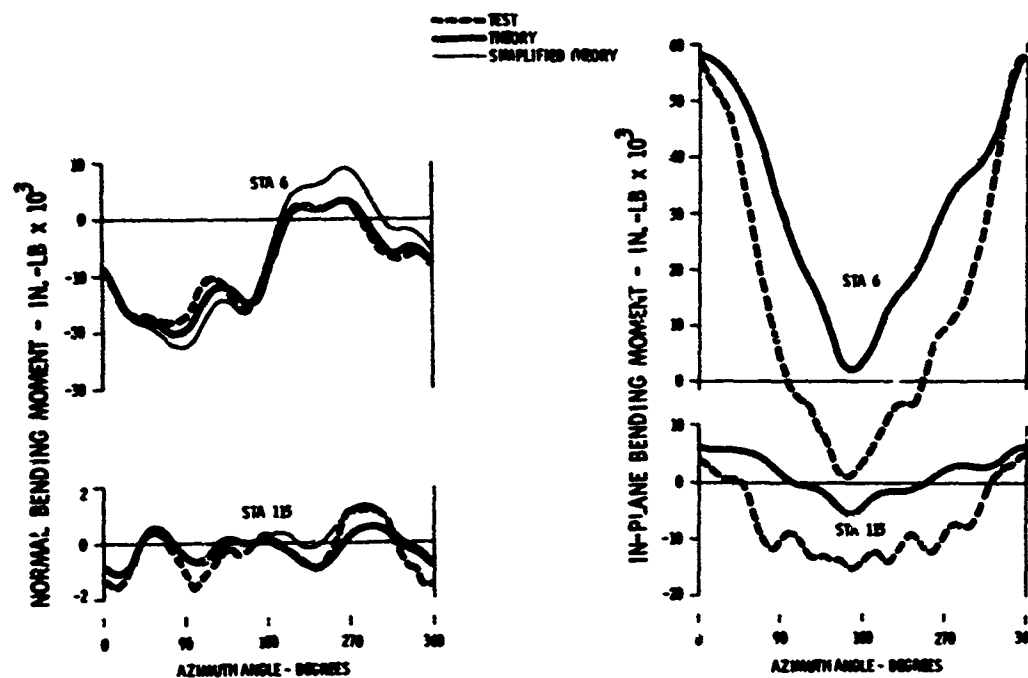
Figure 34. Response to Measured Airloads (13 Modes),
Condition 10 (Right Turn at 58 Knots TAS)

52
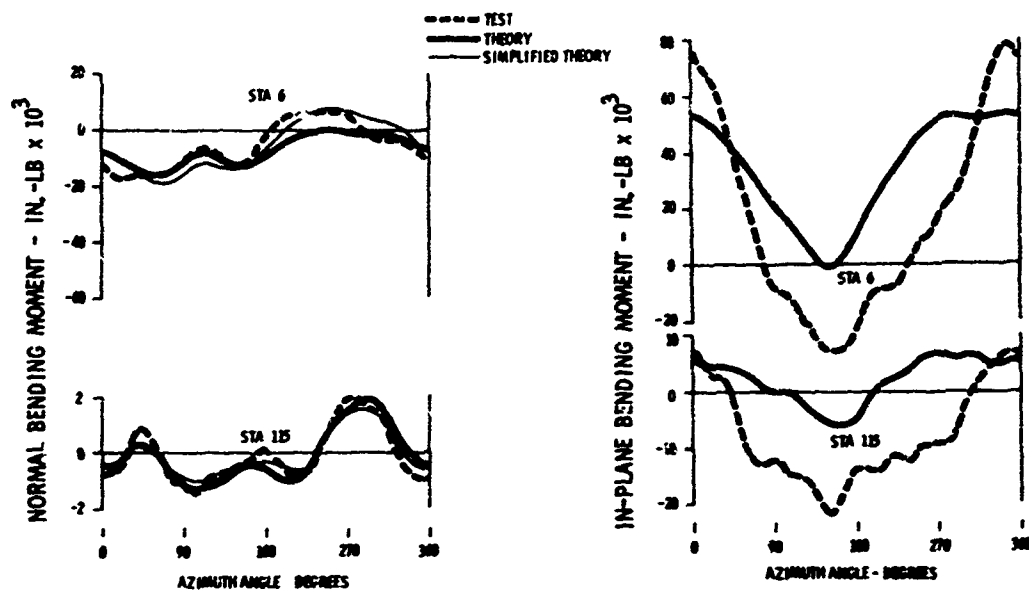
Figure 35. Response to Measured Airloads (13 Modes),
Condition 13 (Collective Pullup at 84.5 Knots TAS)
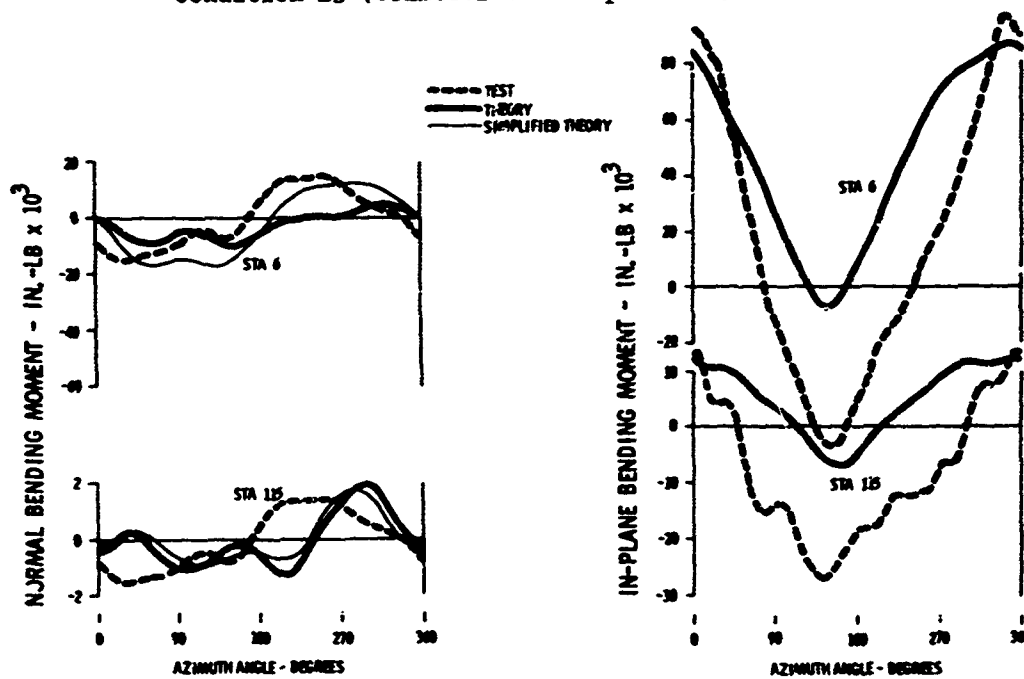
Figure 36. Response to Measured Airloads (13 Modes),
Condition 14 (Collective Pullup at 86 Knots TAS)

53
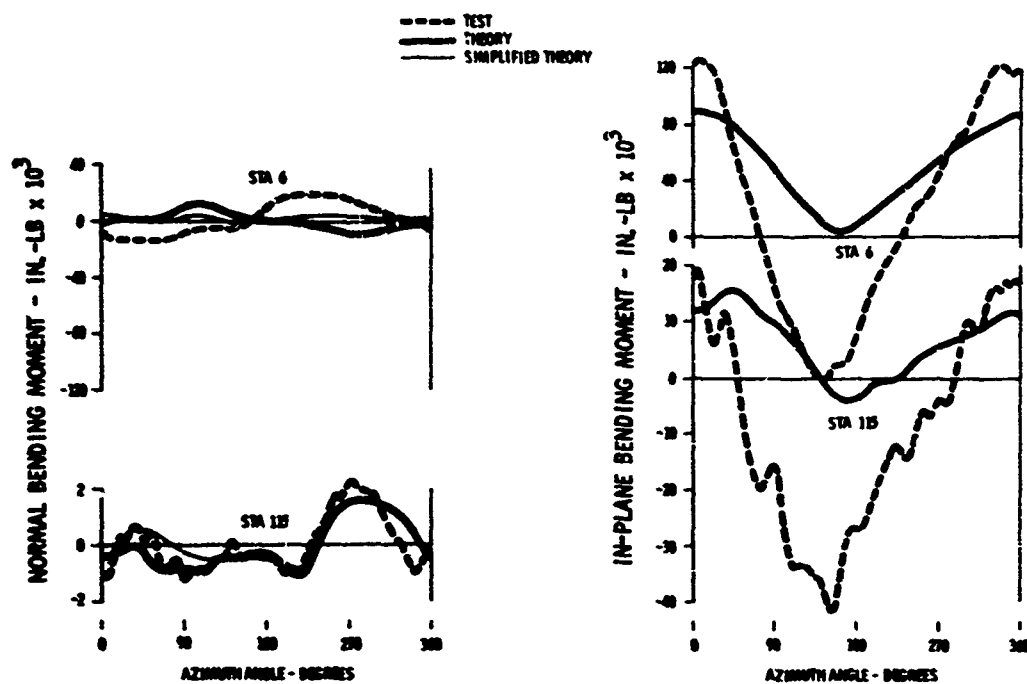
Figure 37. Response to Measured Airloads (13 Modes),
Condition 15 (Collective Pullup at 87 Knots TAS)
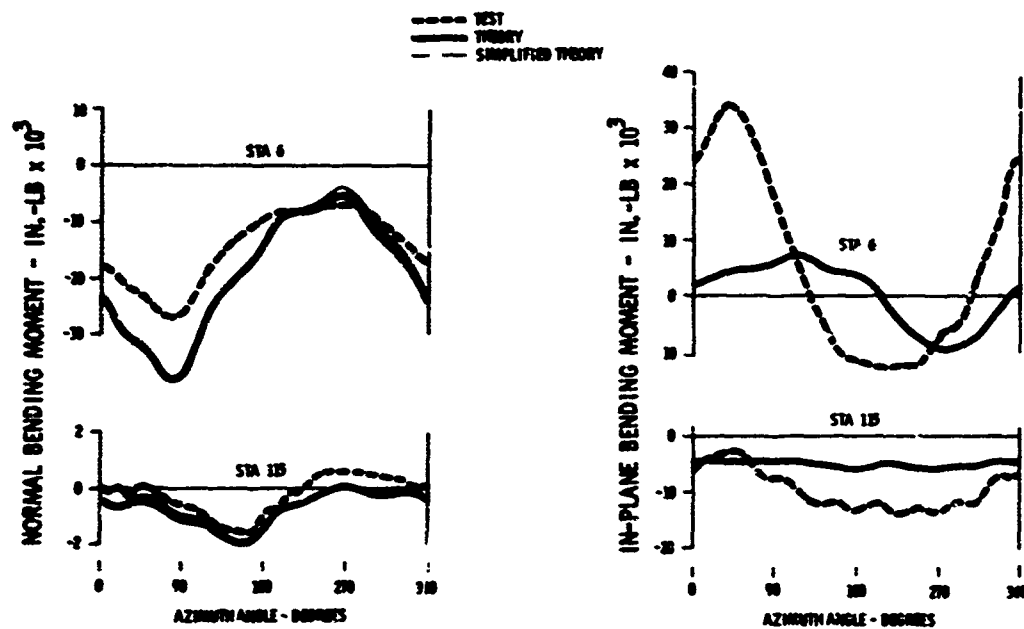
Figure 38. Response to Measured Airloads (13 Modes),
Condition 17 (Autorotation at 83 Knots TAS)
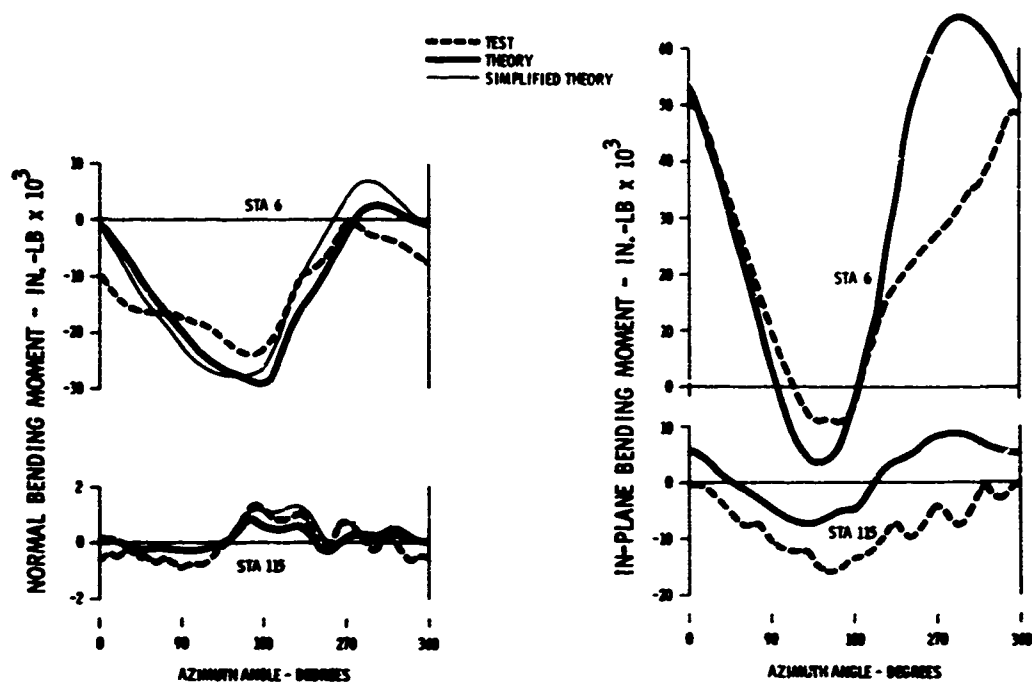
Figure 39. Response to Measured Airloads (13 Modes),
Condition 18 (Transition)
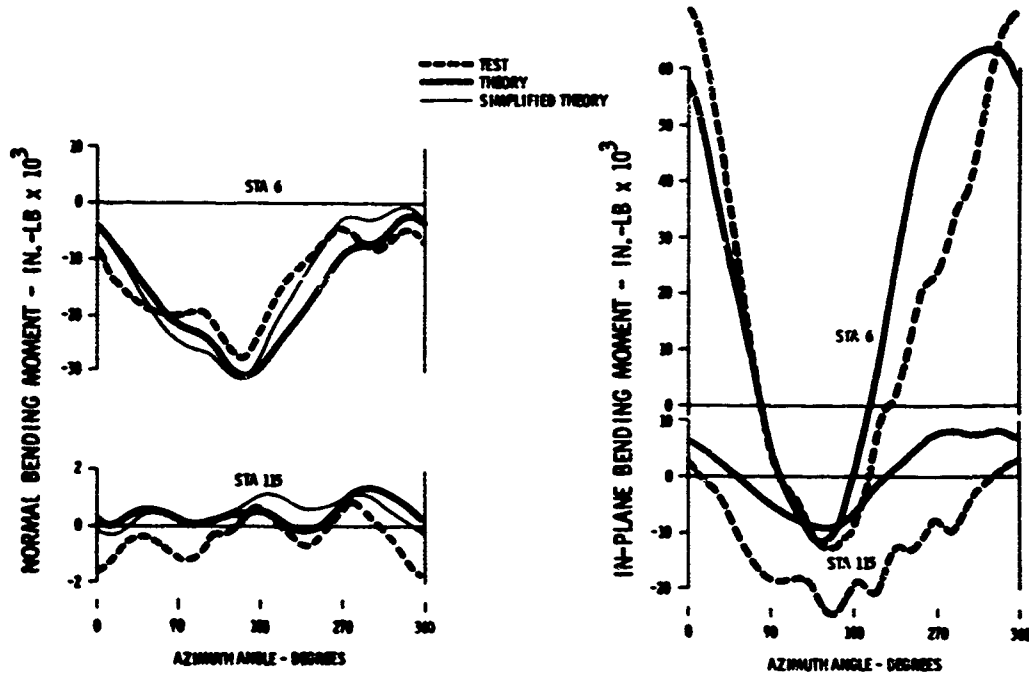
Figure 40. Response to Measured Airloads (13 Modes),
Condition 20 (Transition)
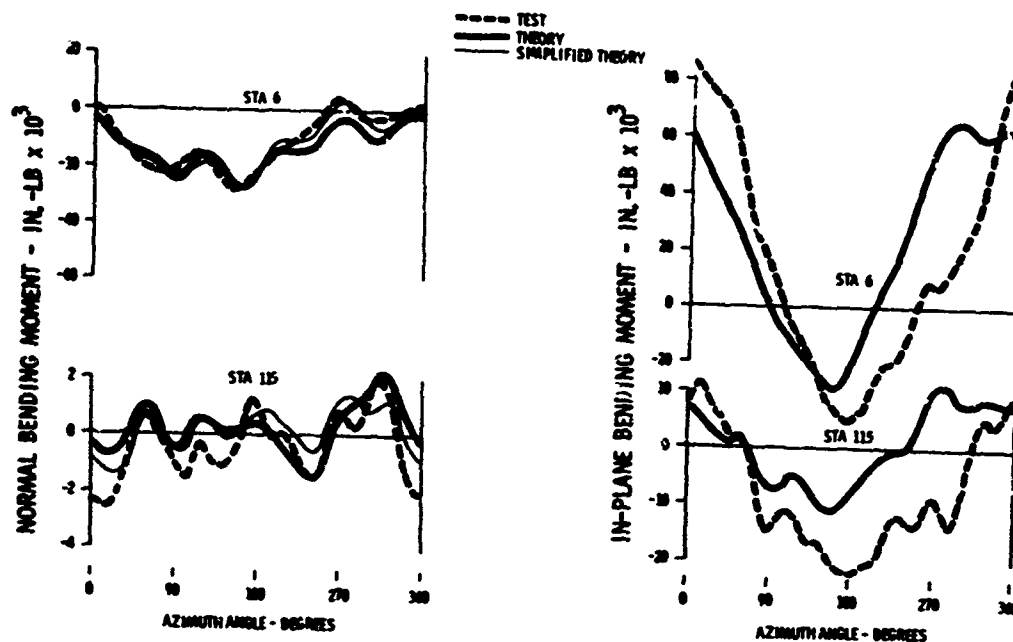
Figure 41.   Response to Measured Airloads (13 Modes),
Condition 22 (Flare)
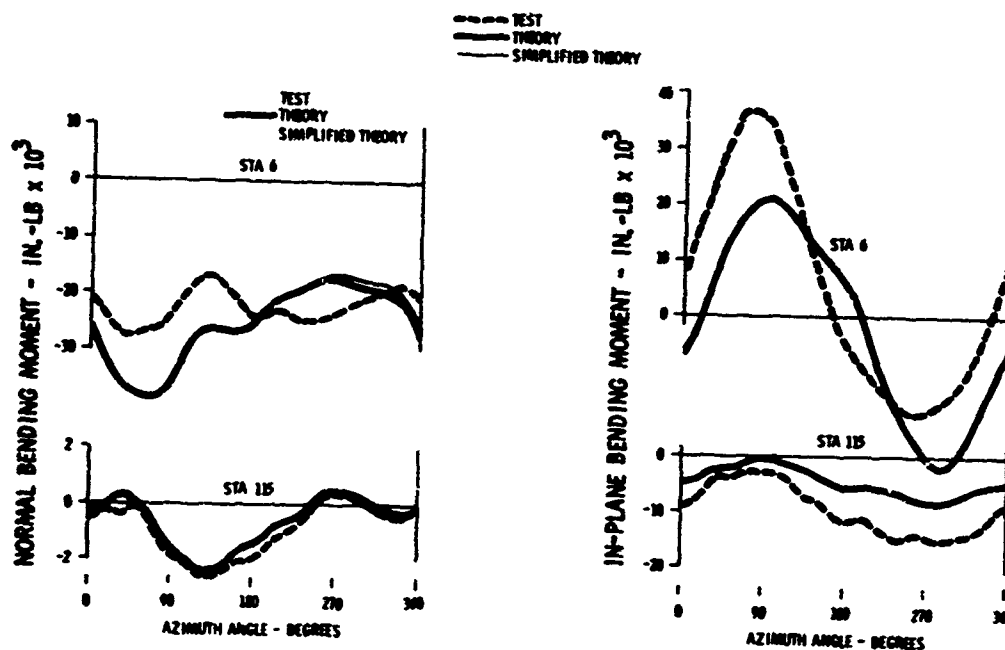
Figure 42.   Response to Measured Airloads (13 Modes),
Condition 24 (Level Flight at 124.5 Knots TAS)

56
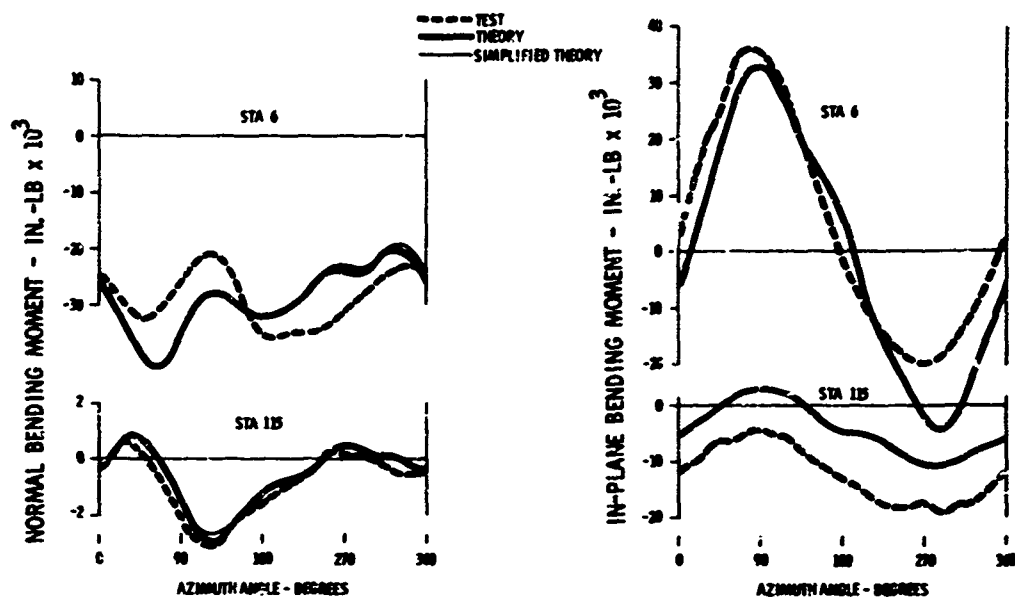
Figure 43. Response to Measured Airloads (13 Modes),
Condition 28 (Level Flight at 170 Knots TAS)
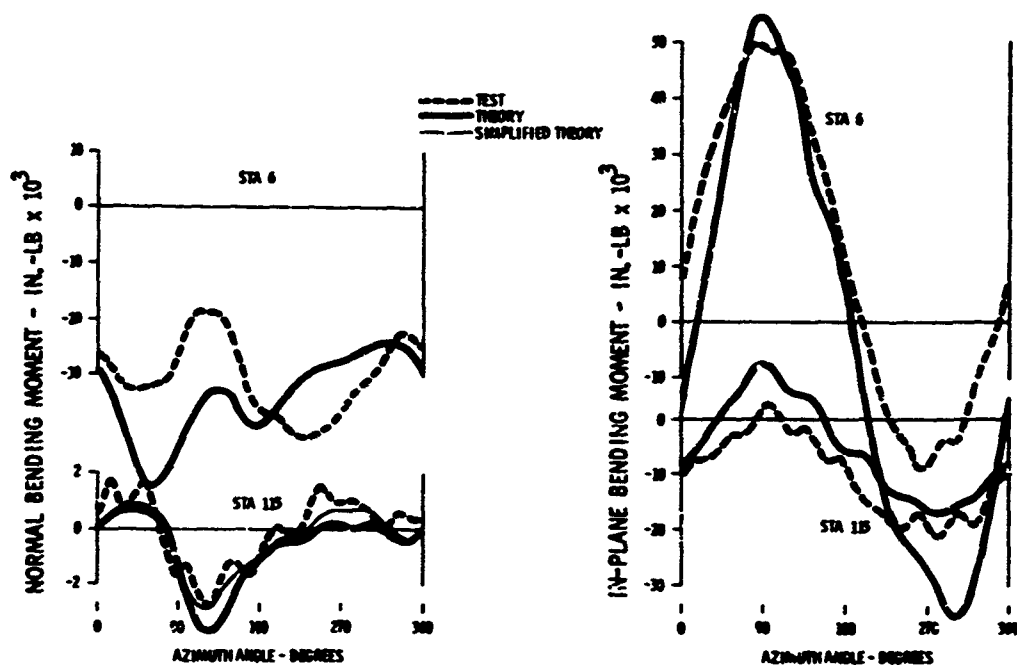
Figure 44. Response to Measured Airloads (13 Modes),
Condition 29 (Level Flight at 215.5 Knots TAS)
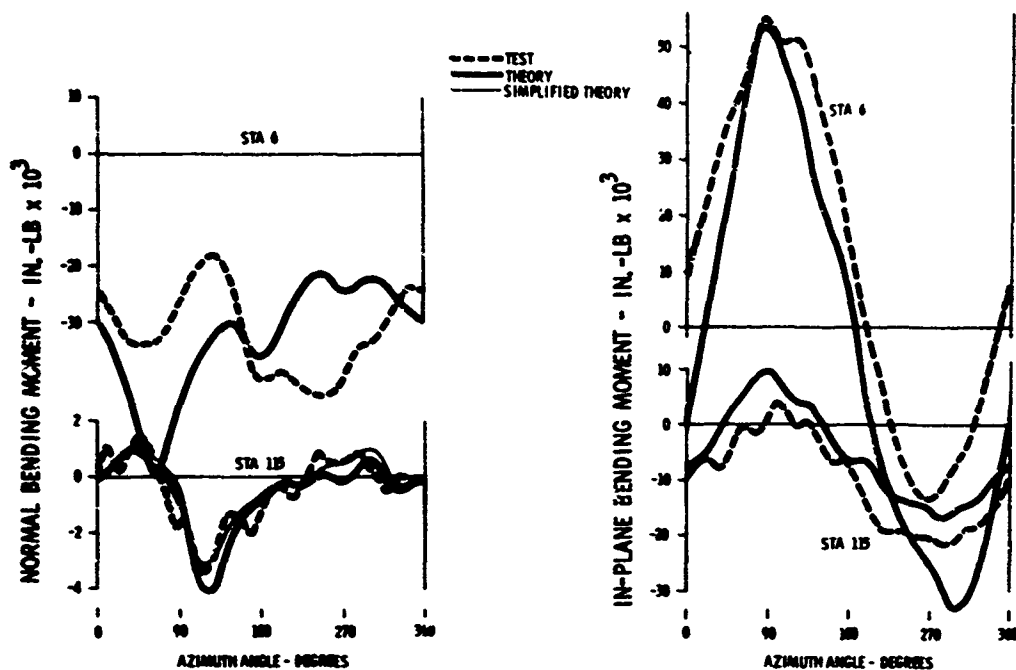
Figure 45. Response to Measured Airloads (13 Modes),
Condition 30 (Level Flight at 219.5 Knots TAS)
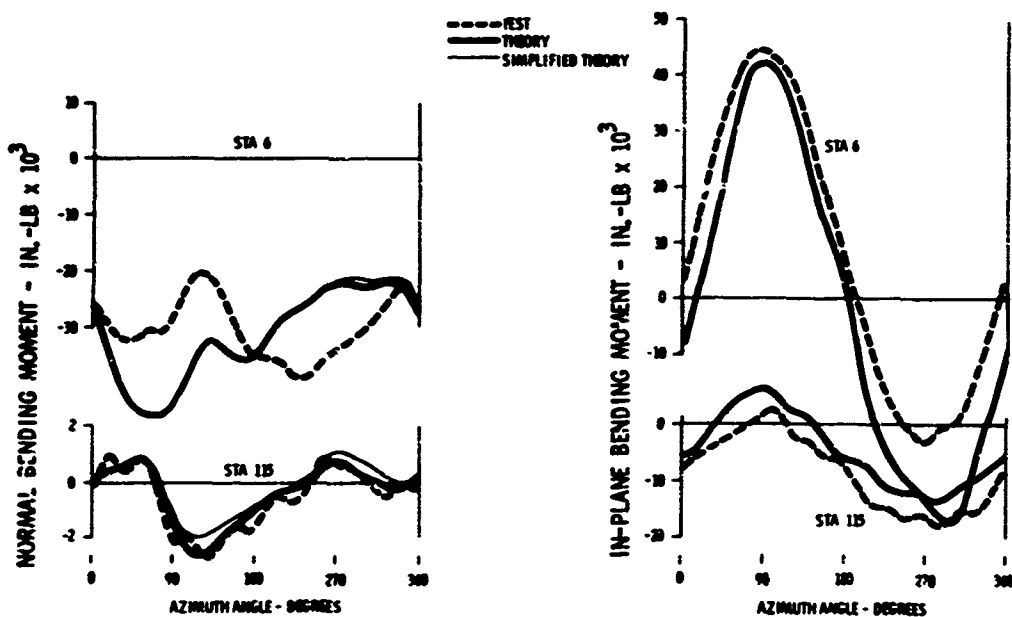
Figure 46. Response to Measured Airloads (13 Modes),
Condition 34 (Level Flight at 202.5 Knots TAS)

58
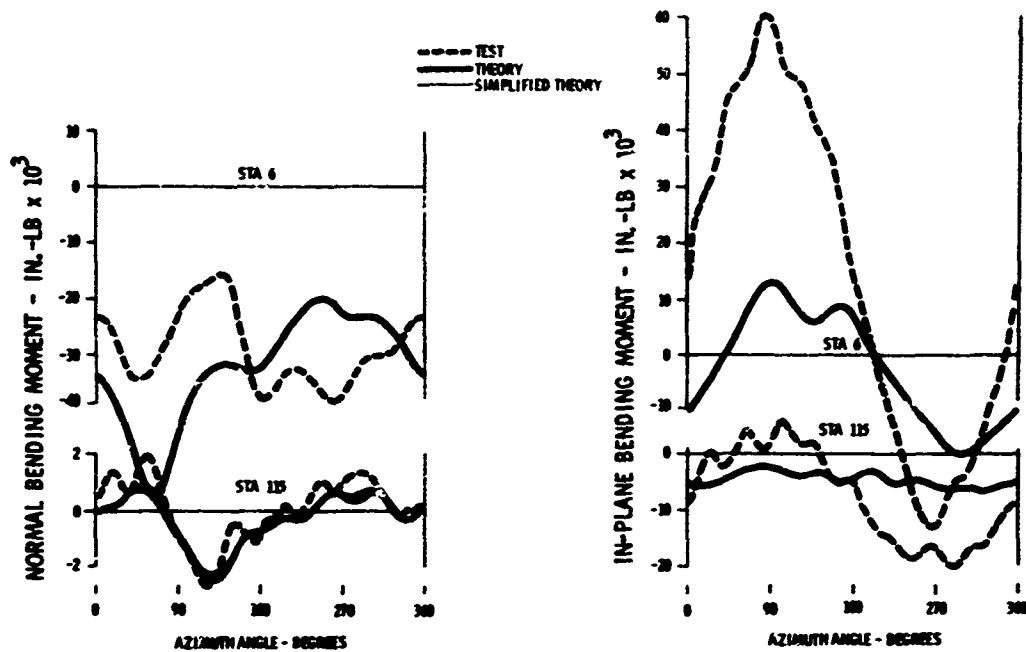
Figure 47. Response to Measured Airloads (13 Modes), Condition 35 (Level Flight at 219 Knots TAS)
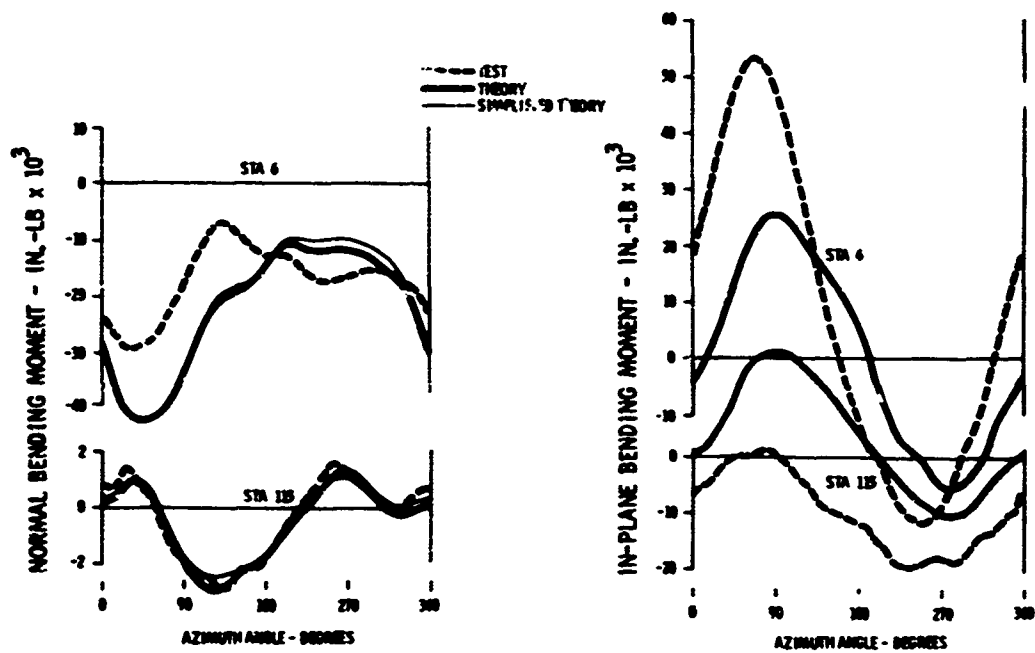
Figure 48. Response to Measured Airloads (13 Modes), Condition 38 (Pullup at 160 Knots TAS)
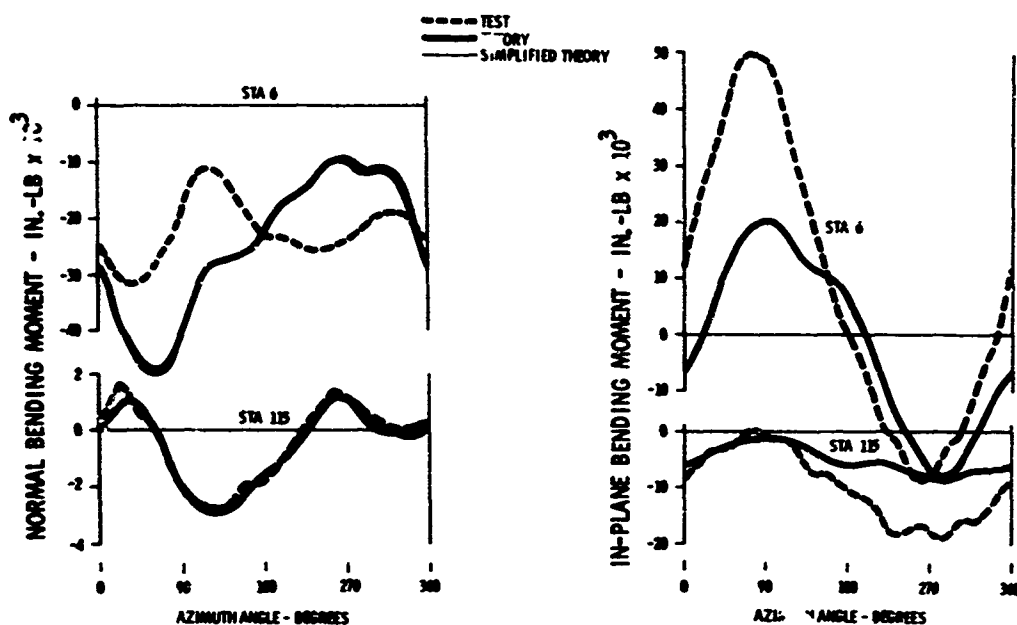
Figure 49. Response to Measured Airloads (13 Modes),
Condition 41 (Pullup at 83 Knots TAS)
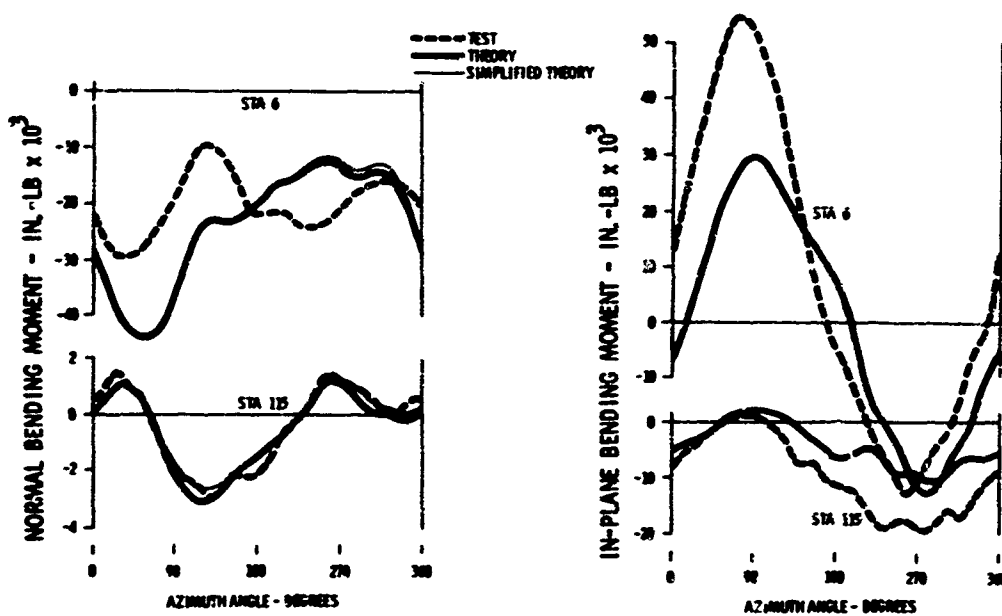
Figure 50. Response to Measured Airloads (13 Modes),
Condition 42 (Pullup at 166 Knots TAS)

60
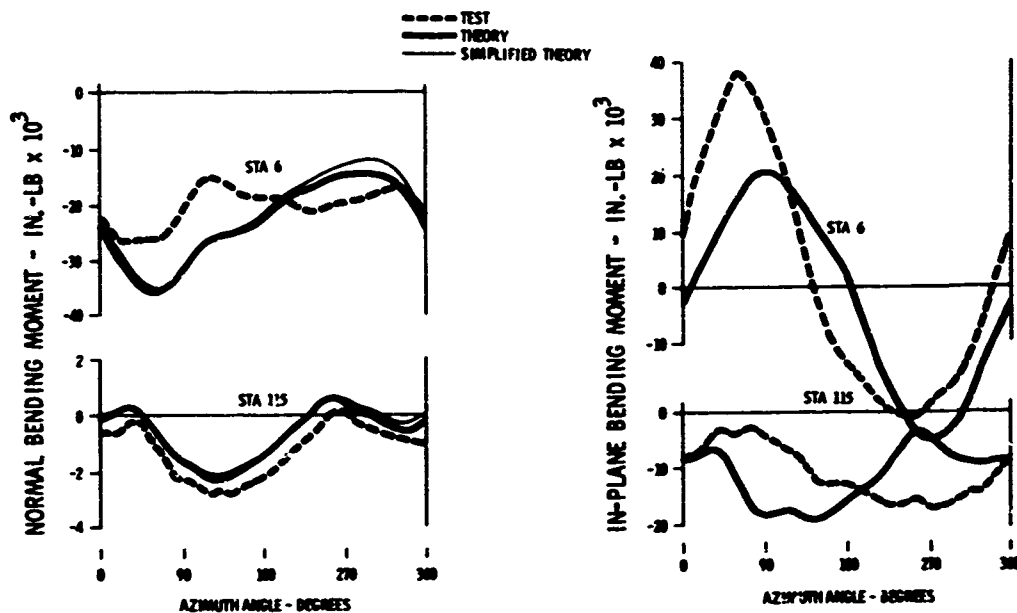
Figure 51. Response to Measured Airloads (13 Modes),
Condition 45 (Left Turn at 124 Knots TAS)
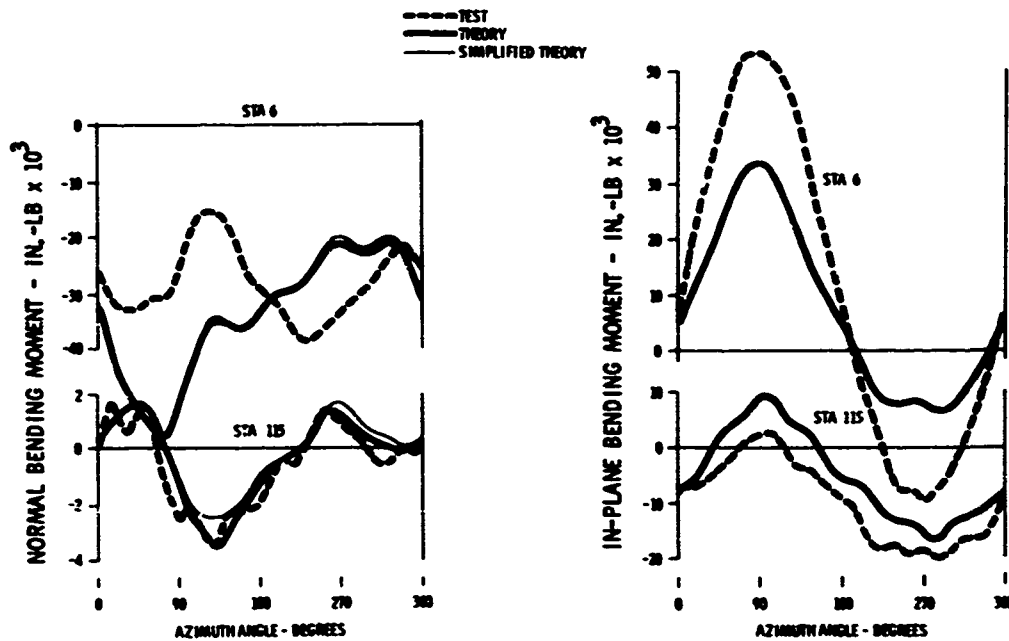
Figure 52. Response to Measured Airloads (13 Modes),
Condition 47 (Left Turn at 207.5 Knots TAS)

61
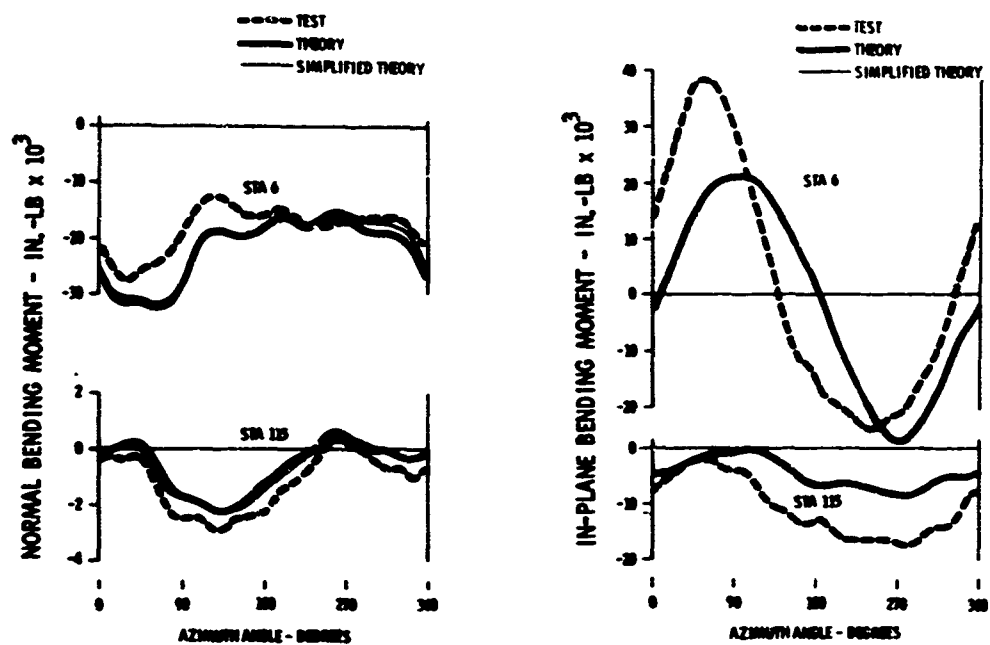
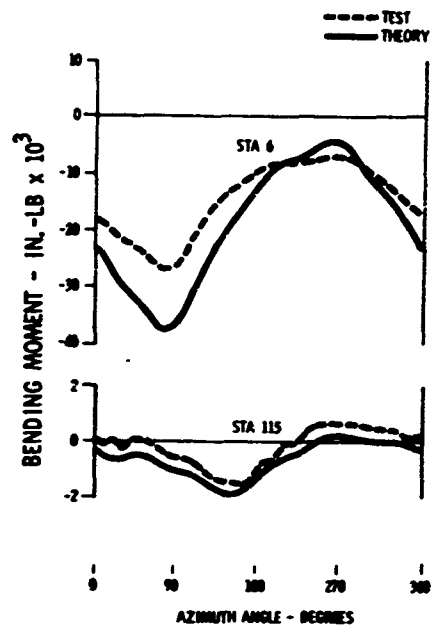Figure 53. Response to Measured Airloads (13 Modes),
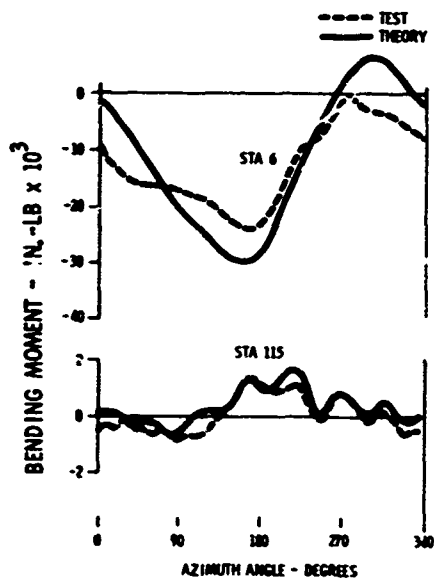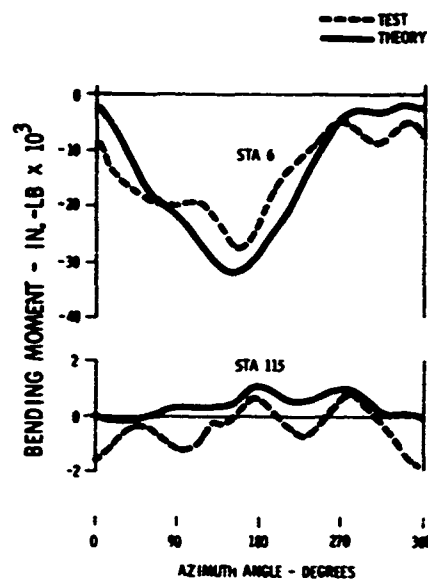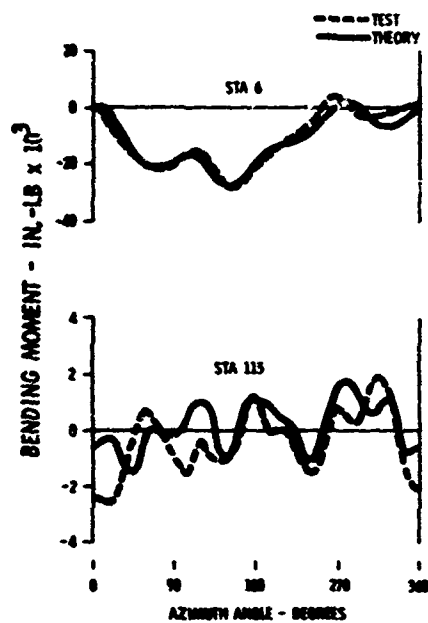Condition 48 (Right Turn at 124 Knots TAS)
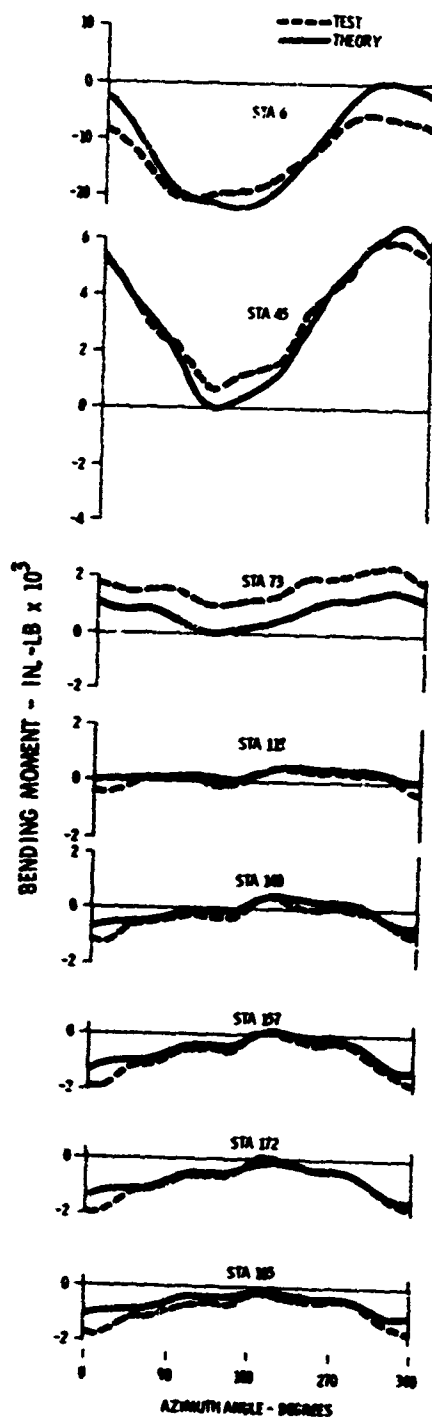
Figure 54. Normal Bending Response to Measured Airloads (5 Normal Bending Modes), Condition 1 (Hover)
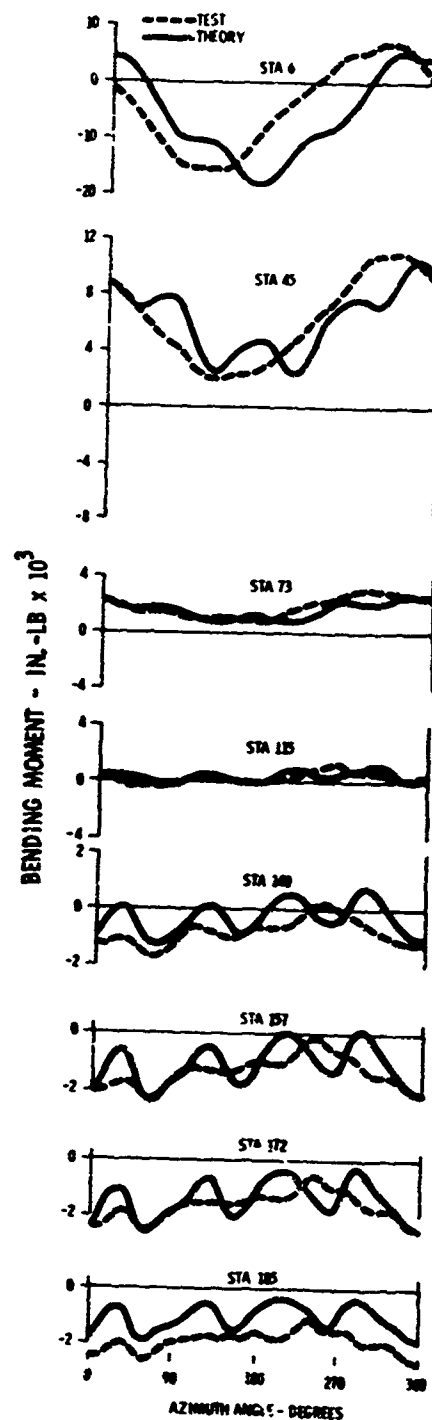
Figure 55. Normal Bending Response to Measured Airloads (5 Normal Bending Modes), Condition 4 (Collective Pullup at 0 Knot TAS)

63
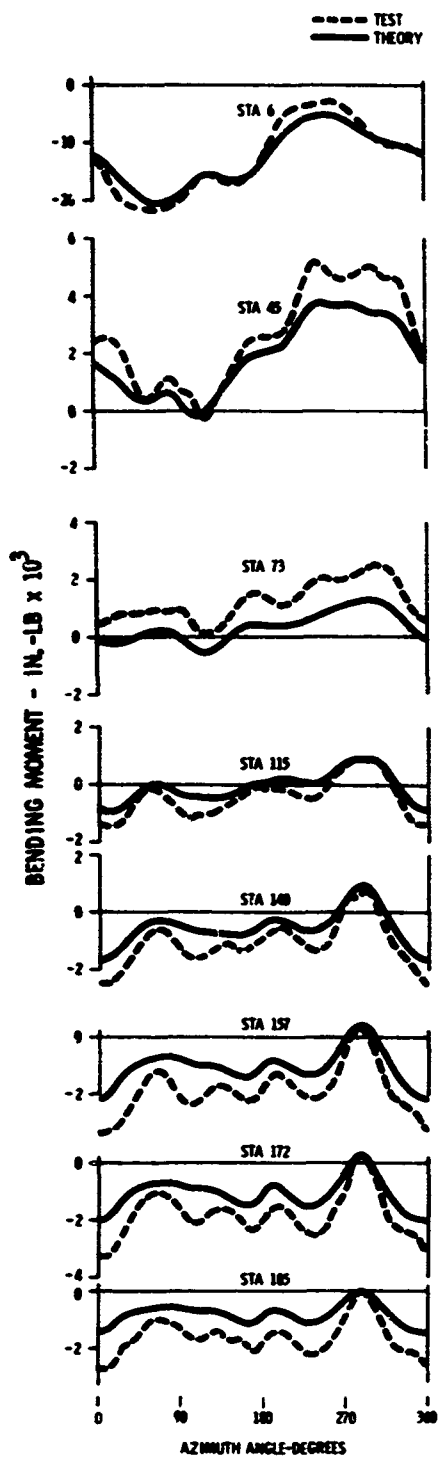
Figure 56. Normal Bending Response
to Measured Airloads (5 Normal
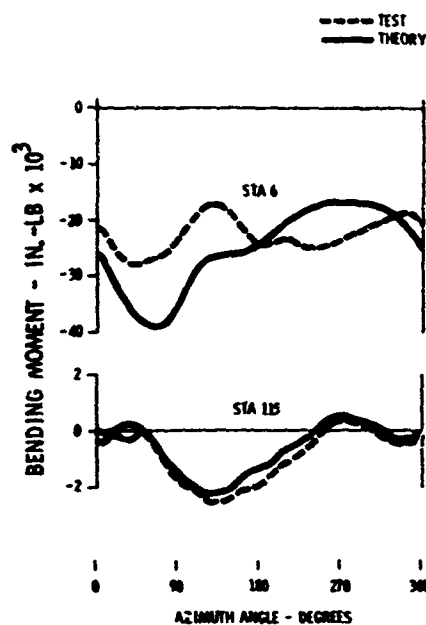Bending Modes), Condition 5
(Forward Flight at 51 Knots TAS)
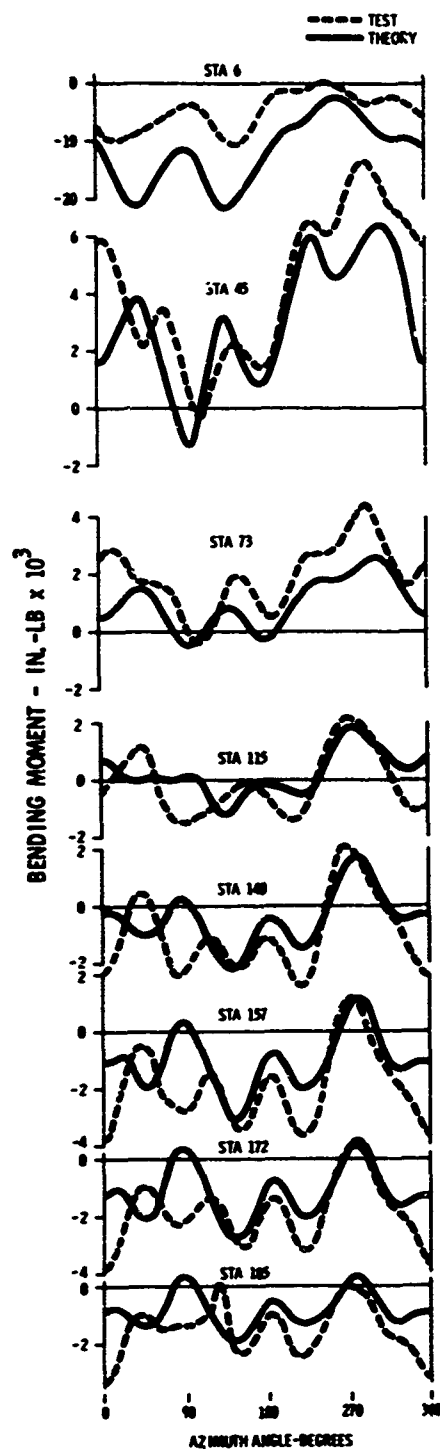
Figure 57. Normal Bending Response
to Measured Airloads (5 Normal
Bending Modes), Condition 8
(Forward Flight at 105 Knots TAS)
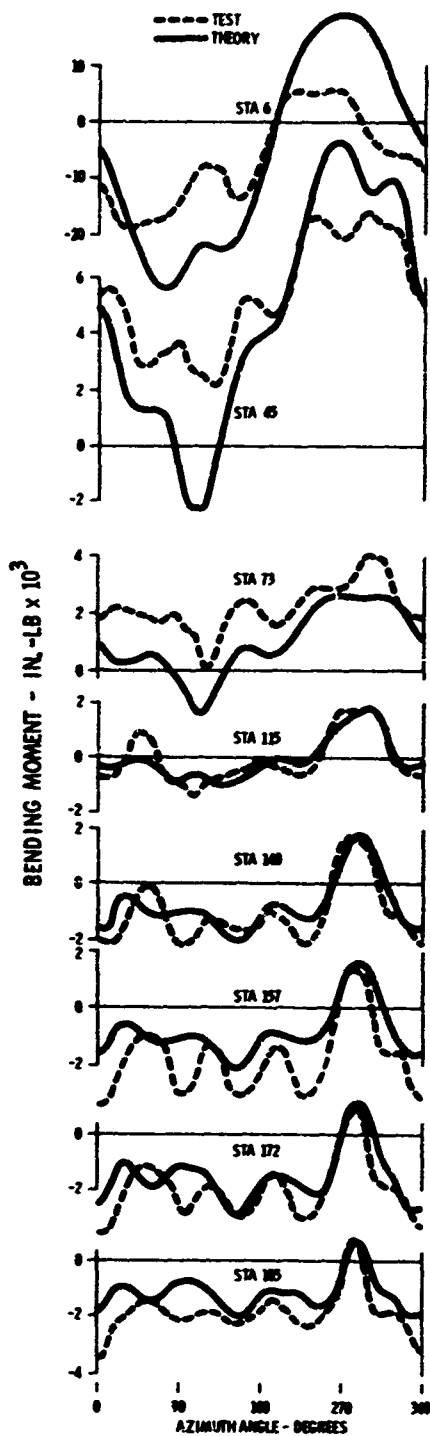
Figure 58. Normal Bending Response to Measured Airloads (5 Normal Bending Modes), Condition 11 (Left Turn at 84 Knots TAS)
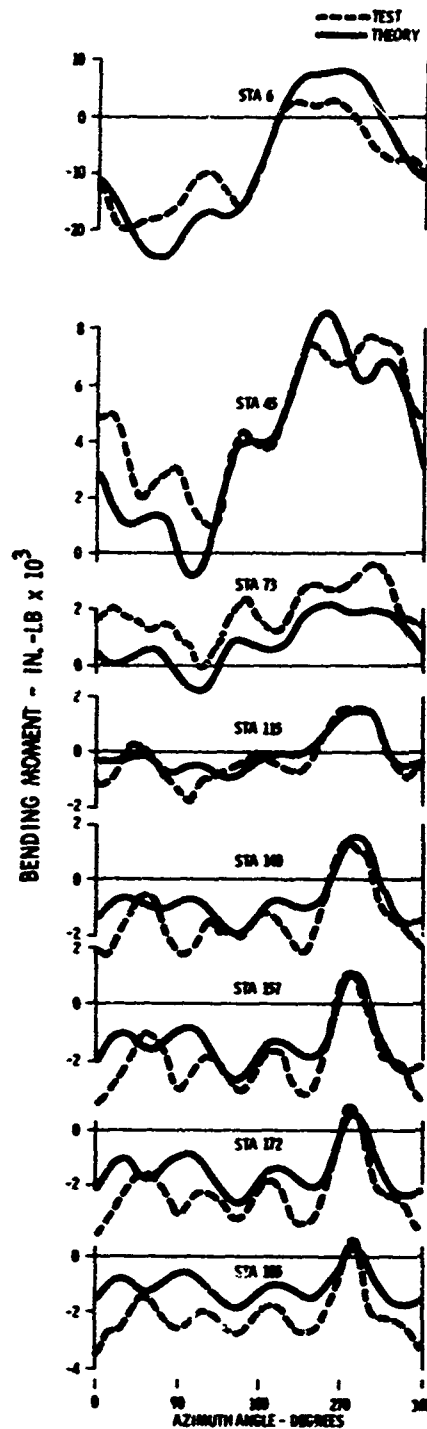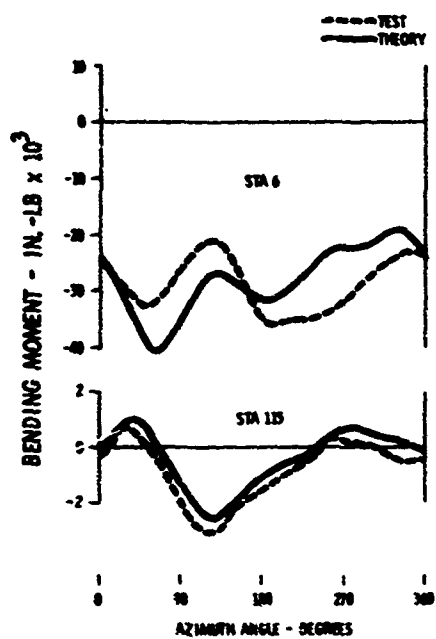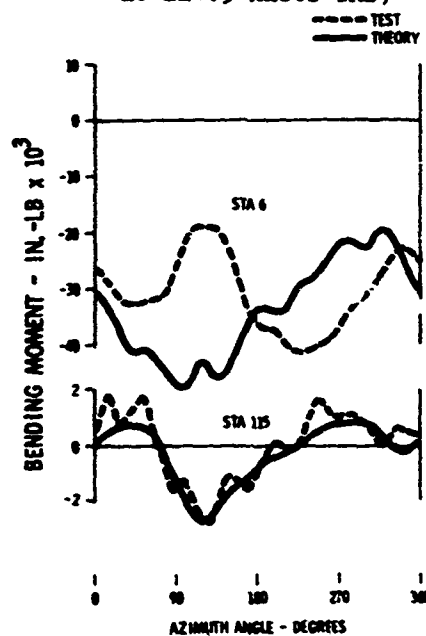
Figure 59. Normal Bending Response to Measured Airloads (5 Normal Bending Modes), Condition 12 (Right Turn at 82 Knots TAS)
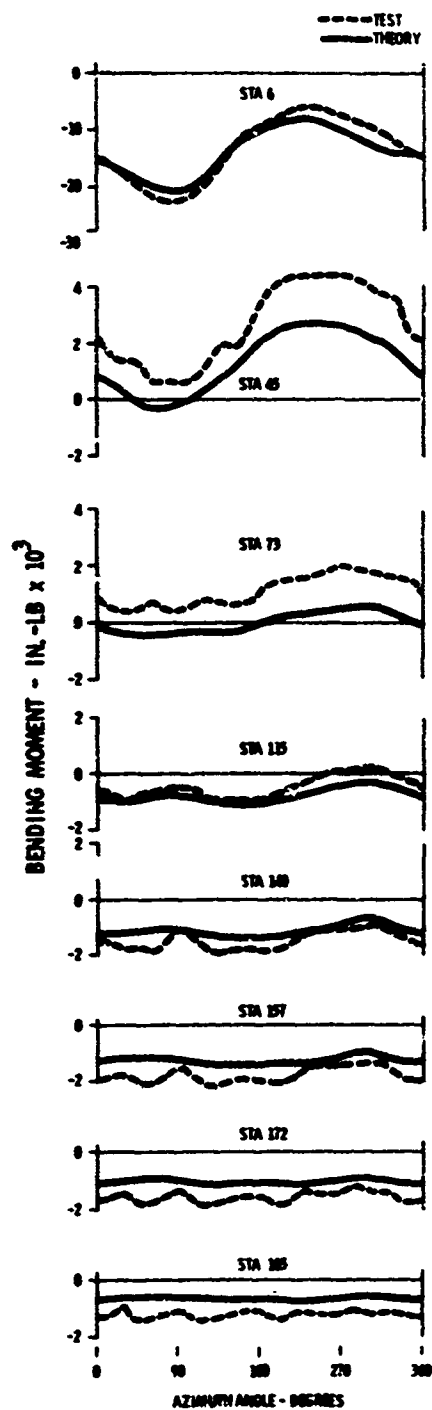
Figure 60. Normal Bending Response to Measured Airloads (5 Normal Bending Modes), Condition 16 (Autorotation)
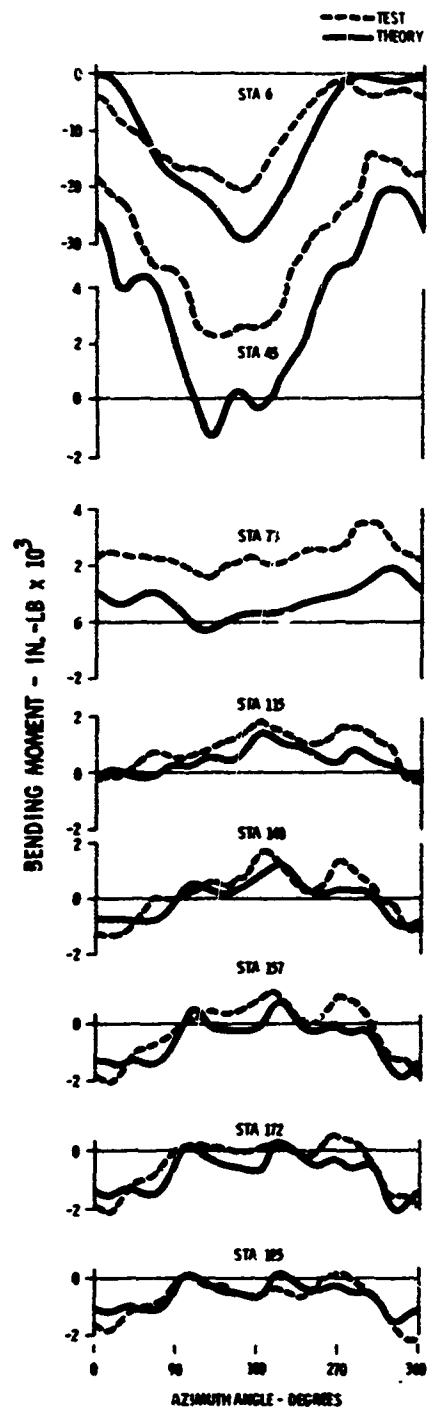
Figure 61. Normal Bending Response to Measured Airloads (5 Normal Bending Modes), Condition 19 (Transition)
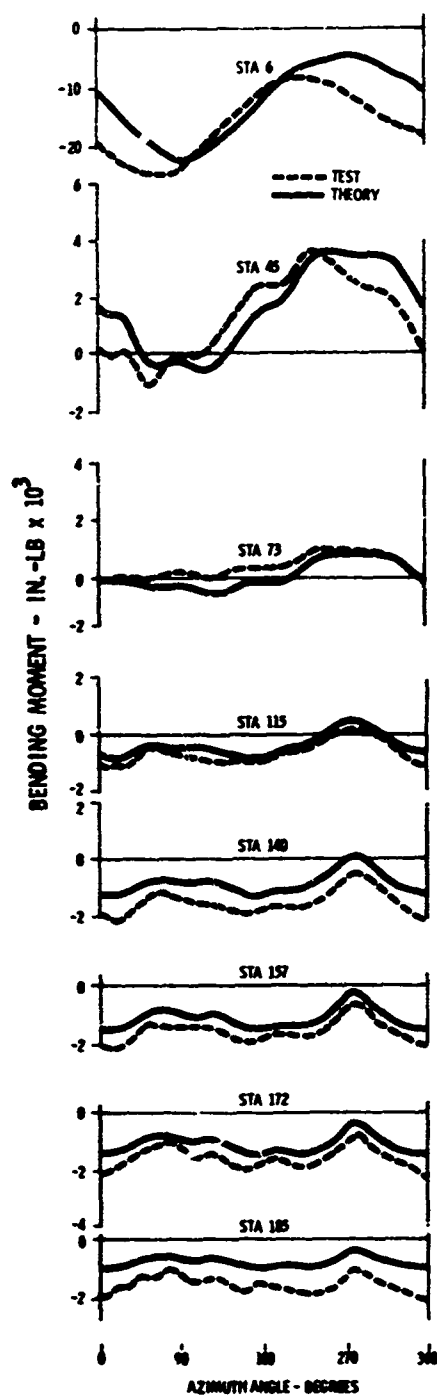
Figure 62. Normal Bending Response
to Measured Airloads (5 Normal
Bending Modes), Condition 21
(Flare at 60 Knots TAS)
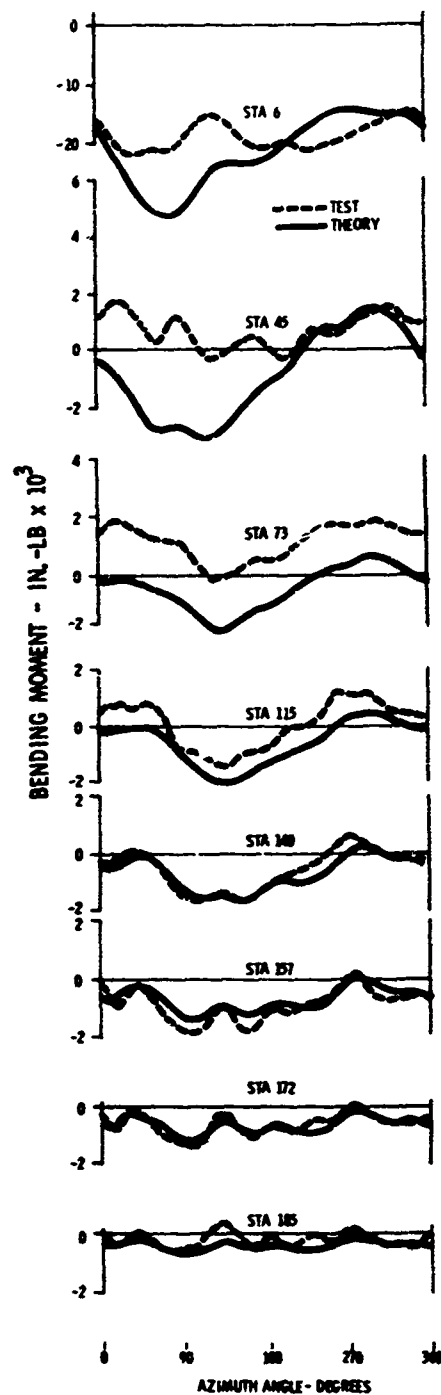
Figure 63. Normal Bending Response
to Measured Airloads (5 Normal
Bending Modes), Condition 23
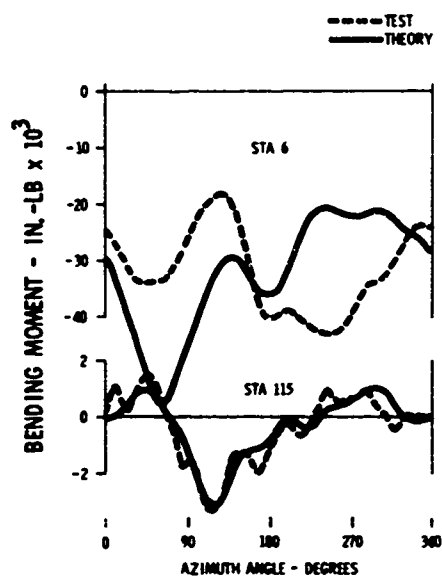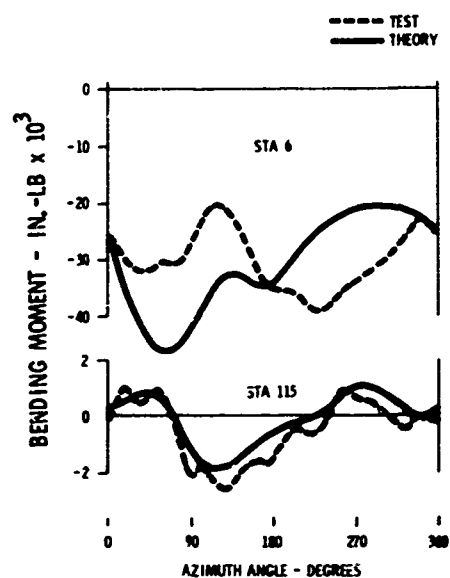(Level Flight at 109 Knots TAS)
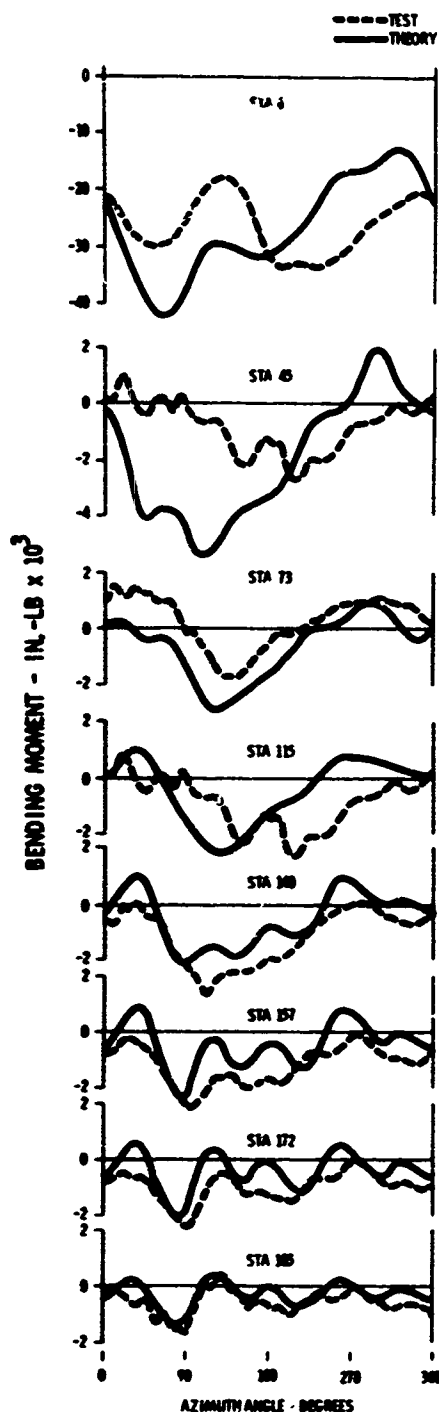
Figure 64. Normal Bending Response
to Measured Airloads (5 Normal
Bending Modes), Condition 25
(Level Flight at 163.5 Knots TAS)
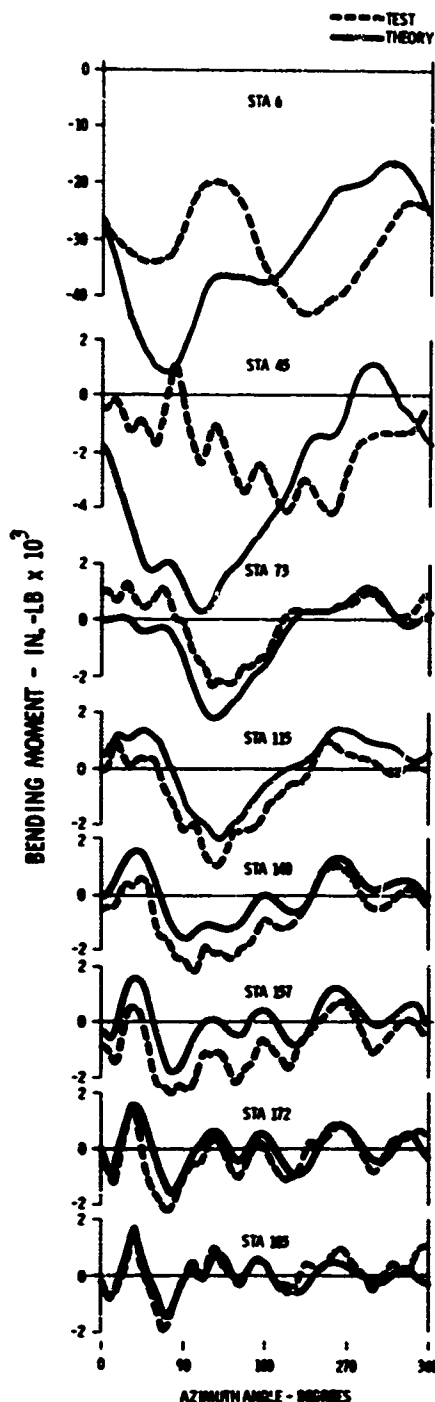
Figure 65. Normal Bending Response
to Measured Airloads (5 Normal
Bending Modes), Condition 26
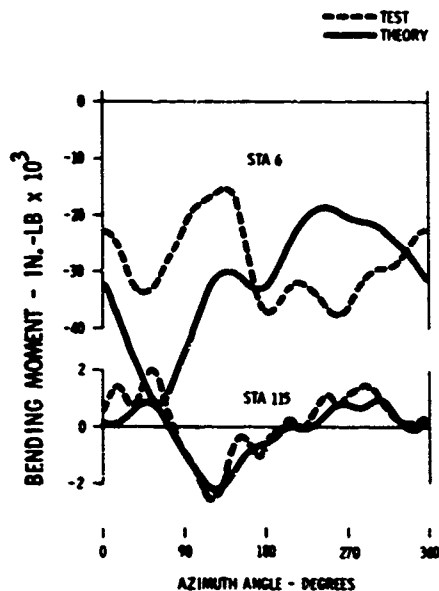(Level Flight at 207 Knots TAS)
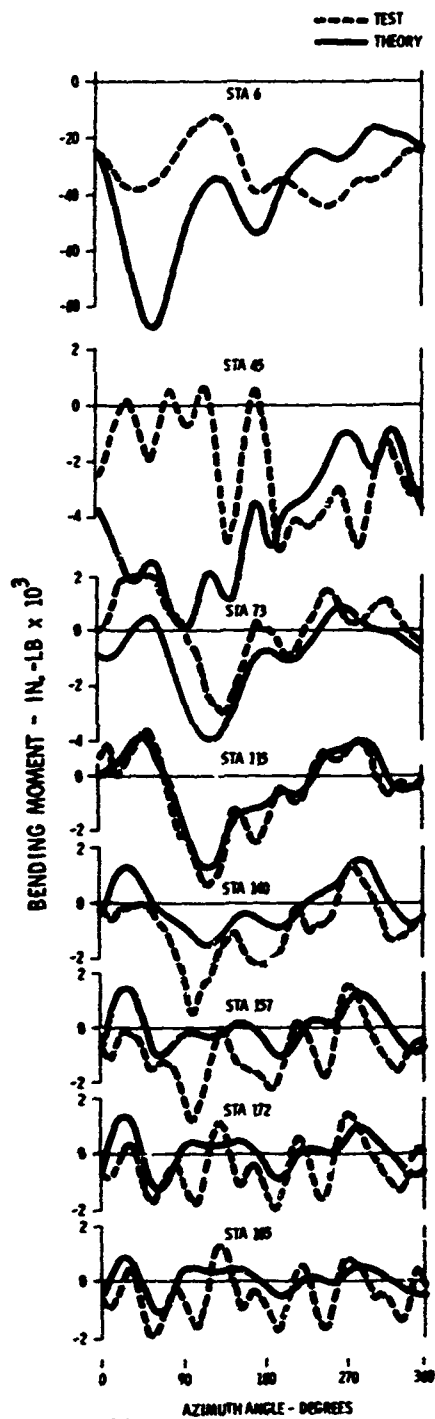
Figure 66. Normal Bending Response
to Measured Airloads (5 Normal
Bending Modes), Condition 27
(Level Flight at 227 Knots TAS)
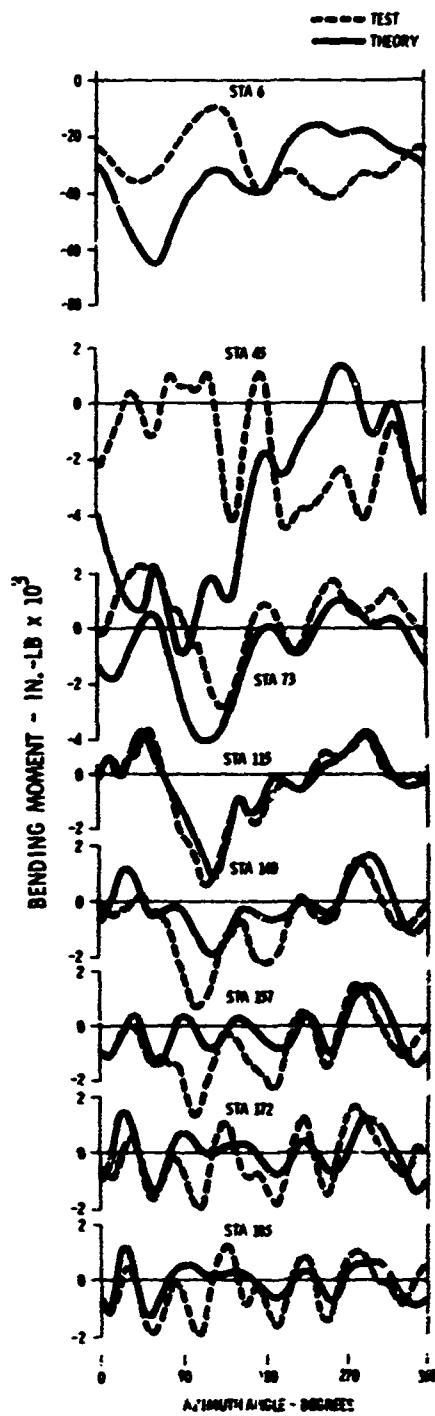
Figure 67. Normal Bending Response
to Measured Airloads (5 Normal
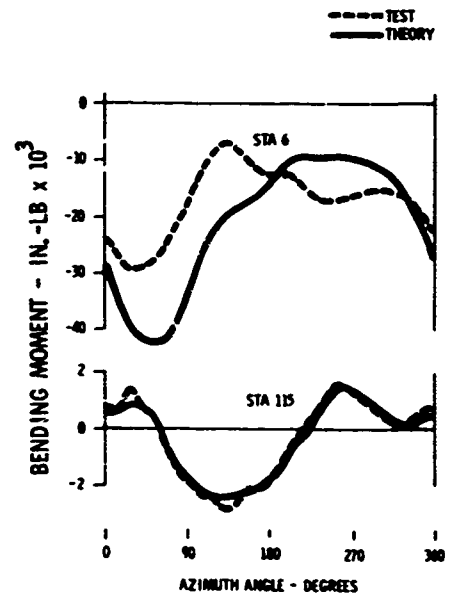Bending Modes), Condition 31
(Level Flight at 232 Knots TAS)

Figure 68. Normal Bending Response to Measured Airloads (5 Normal Bending Modes), Condition 33 (Level Flight at 157 Knots TAS)

Figure 69. Normal Bending Response to Measured Airloads (5 Normal Bending Modes), Condition 36 (Pullup at 126 Knots TAS)
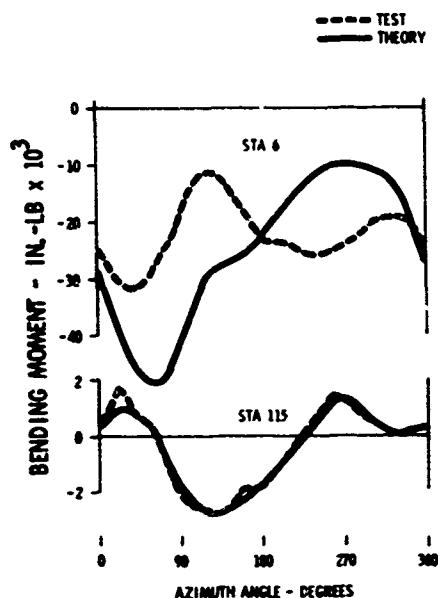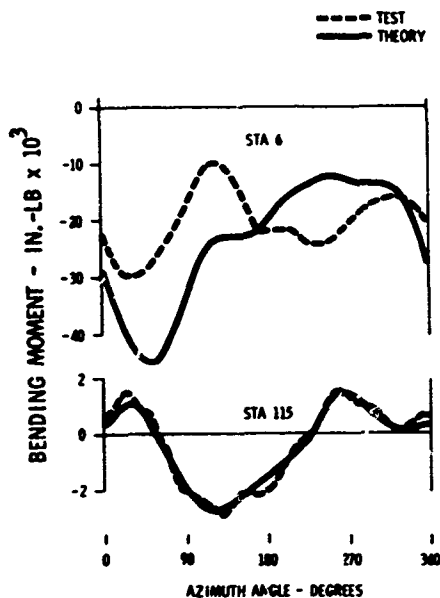
Figure 70. Normal Bending Response
to Measured Airloads (5 Normal
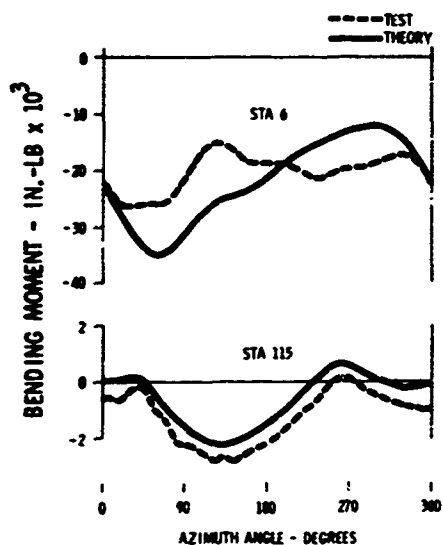Bending Modes), Condition 37
(Pullup at 124 Knots TAS)

Figure 71. Normal Bending Response
to Measured Airloads (5 Normal
Bending Modes), Condition 39
(Pullup at 206 Knots TAS)

Figure 72. Normal Bending Response to Measured Airloads (5 Normal Bending Modes), Condition 40 (Pullup at 203 Knots TAS)
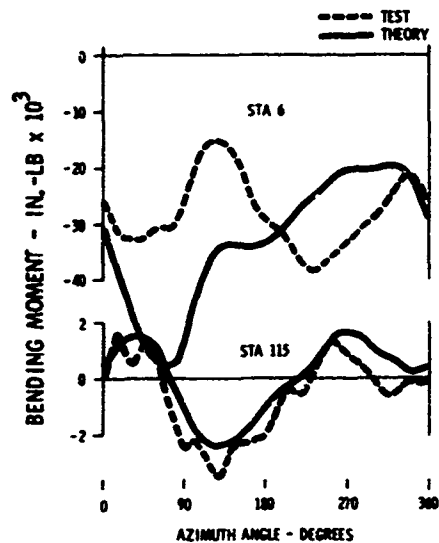
Figure 73. Normal Bending Response to Measured Airloads (5 Normal Bending Modes), Condition 43 (Pullup at 163 Knots TAS)
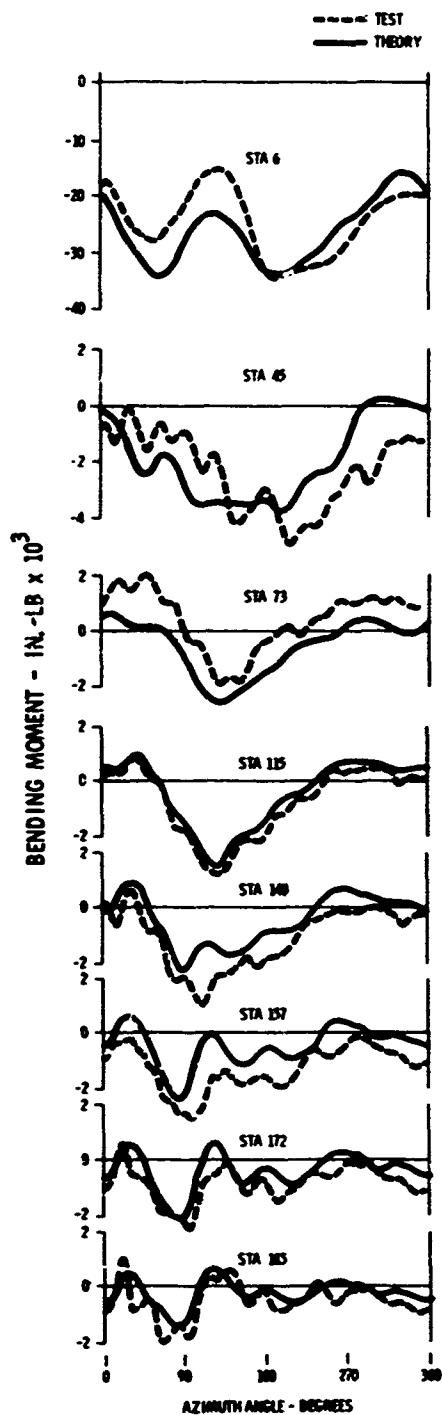
Figure 74. Normal Bending Response
to Measured Airloads (5 Normal
Bending Modes), Condition 44
(Pullup at 162 Knots TAS)
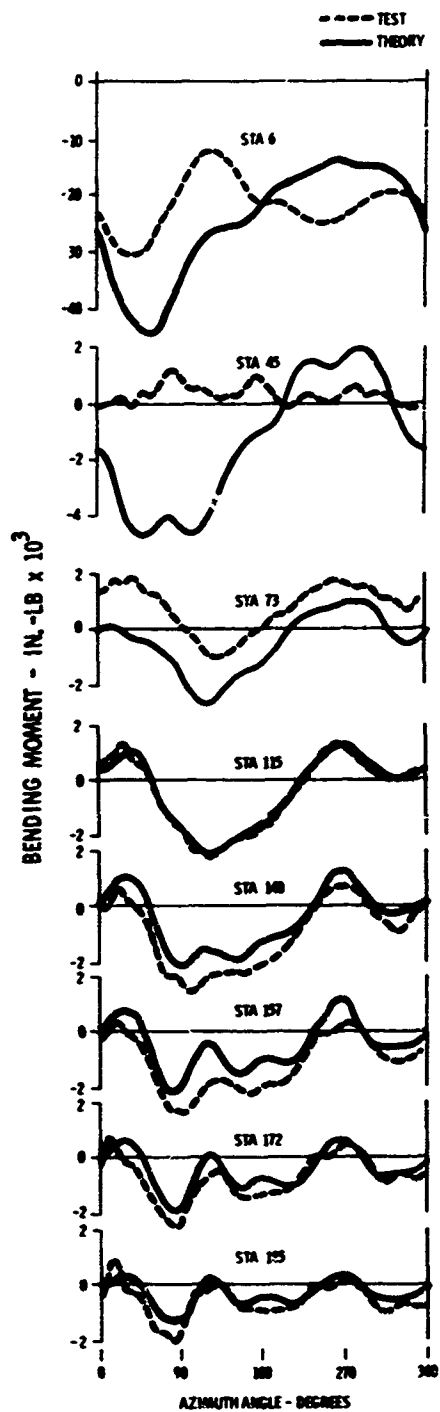
Figure 75. Normal Bending Response
to Measured Airloads (5 Normal
Bending Modes), Condition 46
(Left Turn at 161 Knots TAS)

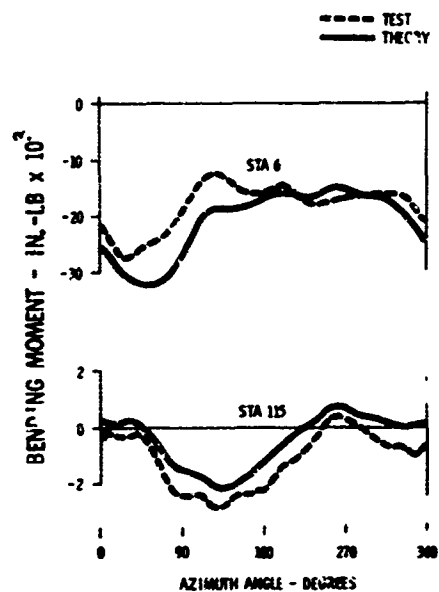Figure 76. Normal Bending Response
to Measured Airloads (5 Normal
Bending Modes), Condition 49
(Right Turn at 164 Knots TAS)
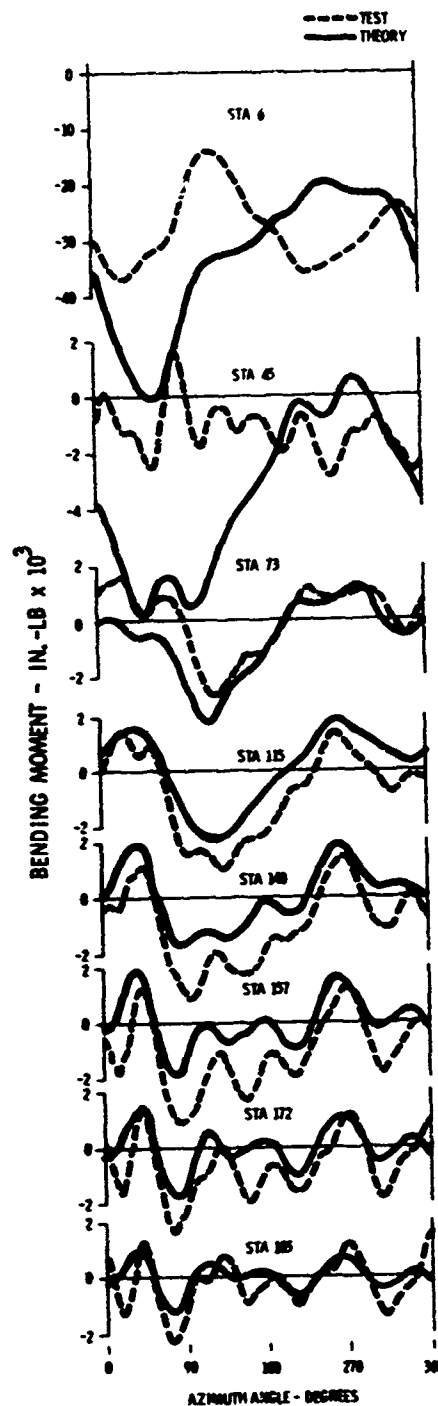
Figure 77. Normal Bending Response
to Measured Airloads (5 Normal
Bending Modes), Condition 50
(Right Turn at 208 Knots TAS)
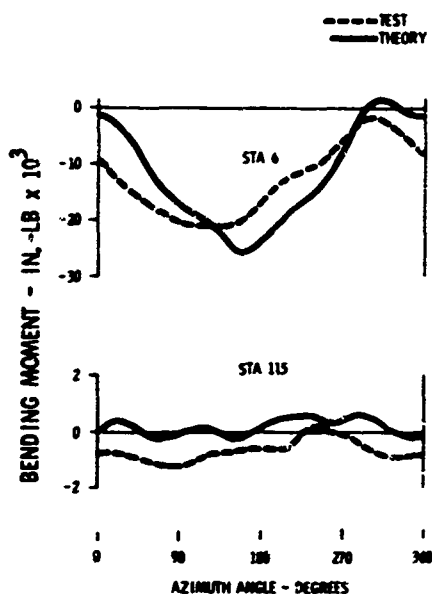
Figure 78. Normal Bending Response to Measured Airloads (5 Normal Bending Modes), Condition 2 (Collective Pullups at 0 Knot TAS)
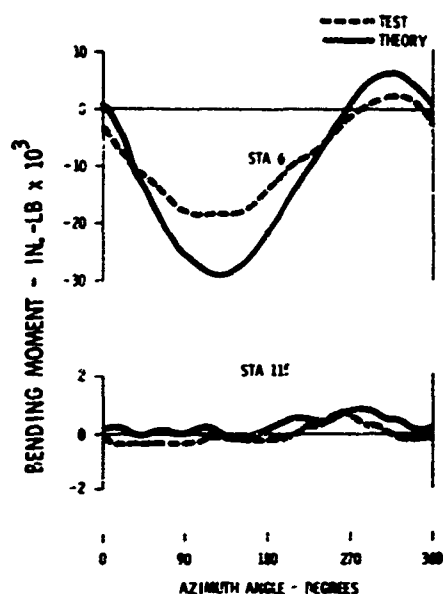
Figure 79. Normal Bending Response to Measured Airloads (5 Normal Bending Modes), Condition 3 (Collective Pullups at 0 Knot TAS)
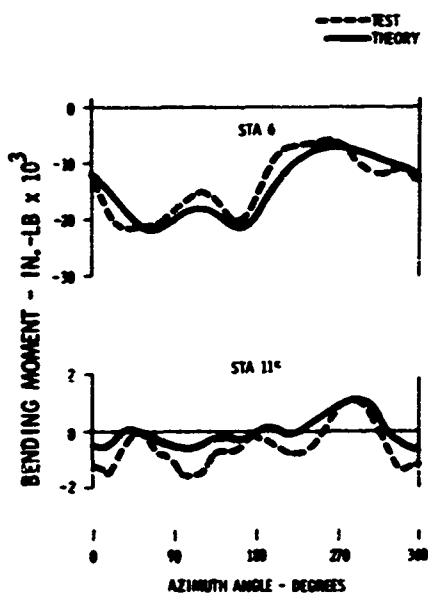
Figure 80. Normal Bending Response to Measured Airloads (5 Normal Bending Modes), Condition 6 (Forward Flight at 59.5 Knots TAS)
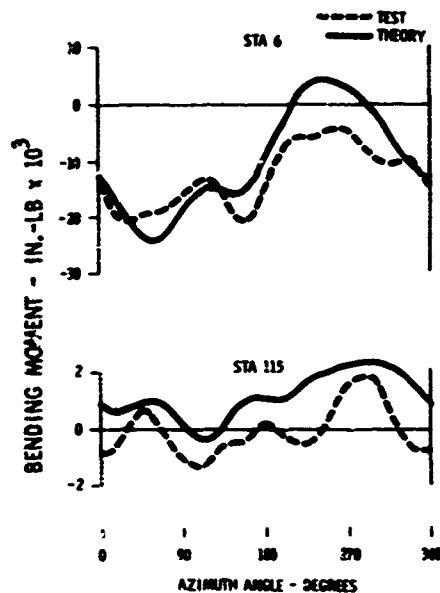
Figure 81. Normal Bending Response to Measured Airloads (5 Normal Bending Modes), Condition 7 (Forward Flight at 80.5 Knots TAS)

75
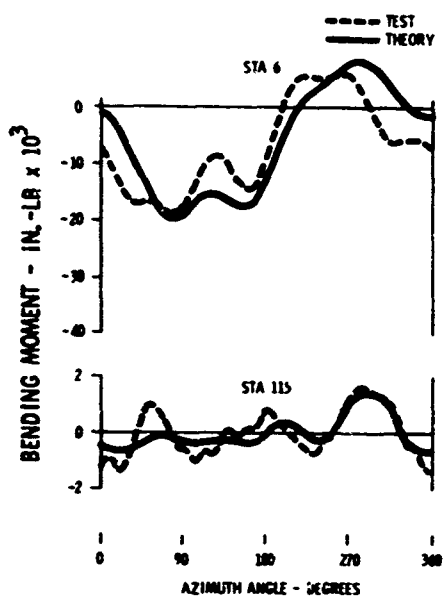
Figure 82. Normal Bending Response to Measured Airloads (5 Normal Bending Modes), Condition 9 (Left Turn at 61 Knots TAS)
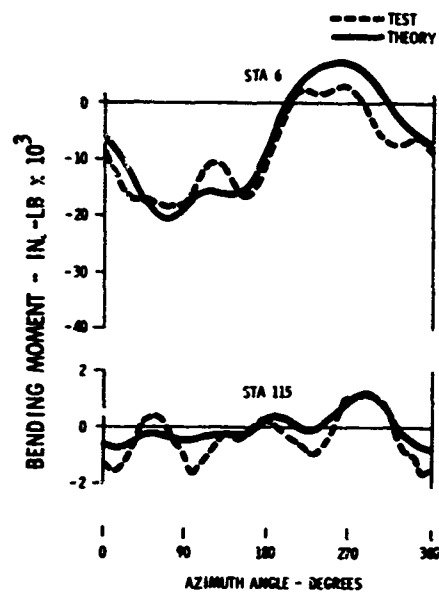
Figure 83. Normal Bending Response to Measured Airloads (5 Normal Bending Modes), Condition 10 (Right Turn at 58 Knots TAS)
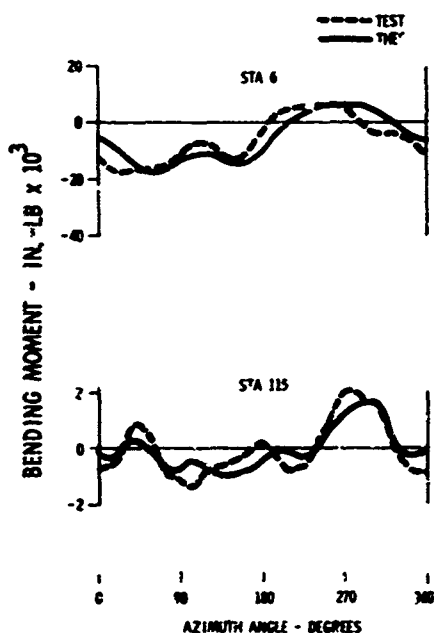
Figure 84. Normal Bending Response to Measured Airloads (5 Normal Bending Modes), Condition 13 (Collective Pullup at 84.5 Knots TAS)
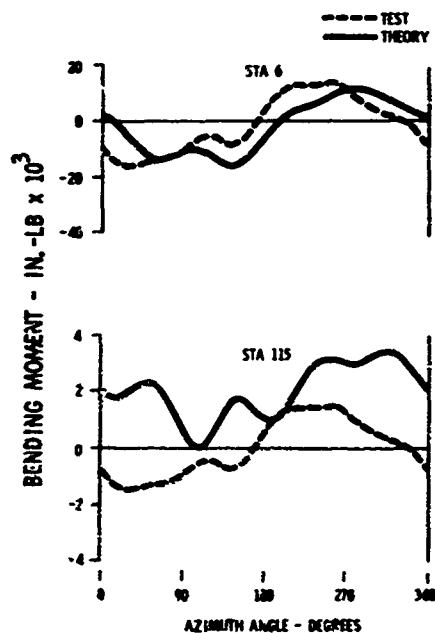
Figure 85. Normal Bending Response to Measured Airloads (5 Normal Bending Modes), Condition 14 (Collective Pullup at 86 Knots TAS)

76
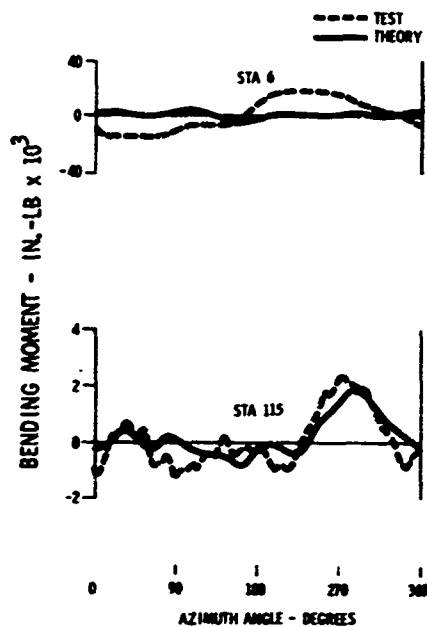
Figure 86. Normal Bending Response to
Measured Airloads (5 Normal Bending
Modes), Condition 15 (Collective
Pullup at 87 Knots TAS)

Figure 87. Normal Bending Response to
Measured Airloads (5 Normal Bending
Modes), Condition 17 (Autorotation
at 83 Knots TAS)

Figure 88. Normal Bending Response to
Measured Airloads (5 Normal Bending
Modes), Condition 18 (Transition)

Figure 89. Normal Bending Response to
Measured Airloads (5 Normal Bending
Modes), Condition 20 (Transition)

Figure 90. Normal Bending Response to
Measured Airloads (5 Normal Bending
Modes), Condition 22 (Flare)

Figure 91. Normal Bending Response to
Measured Airloads (5 Normal Bending
Modes), Condition 24 (Level Flight
at 124.5 Knots TAS)

Figure 92. Normal Bending Response to
Measured Airloads (5 Normal Bending
Modes), Condition 28 (Level Flight
at 170 Knots TAS)

Figure 93. Normal Bending Response to
Measured Airloads (5 Normal Bending
Modes), Condition 29 (Level Flight
at 215.5 Knots TAS)

Figure 94. Normal Bending Response to Measured Airloads (5 Normal Bending Modes), Condition 30 (Level Flight at 219.5 Knots TAS)

Figure 95. Normal Bending Response to Measured Airloads (5 Normal Bending Modes), Condition 34 (Level Flight at 202.5 Knots TAS)

Figure 96. Normal Bending Response to Measured Airloads (5 Normal Bending Modes), Condition 35 (Level Flight at 219 Knots TAS)

Figure 97. Normal Bending Response to Measured Airloads (5 Normal Bending Modes), Condition 38 (Pullup at 160 Knots TAS)

Figure 98. Normal Bending Response to Measured Airloads (5 Normal Bending Modes), Condition 41 (Pullup at 83 Knots TAS)

Figure 99. Normal Bending Response to Measured Airloads (5 Normal Bending Modes), Condition 42 (Pullup at 166 Knots TAS)

Figure 100. Normal Bending Response to Measured Airloads (5 Normal Bending Modes), Condition 45 (Left Turn at 124 Knots TAS)

Figure 101. Normal Bending Response to Measured Airloads (5 Normal Bending Modes), Condition 47 (Left Turn at 207.5 Knots TAS)

80

Figure 102.   Normal Bending Response to Measured Airloads (5 Normal
Bending Modes), Condition 48 (Right Turn at 124 Knots TAS)
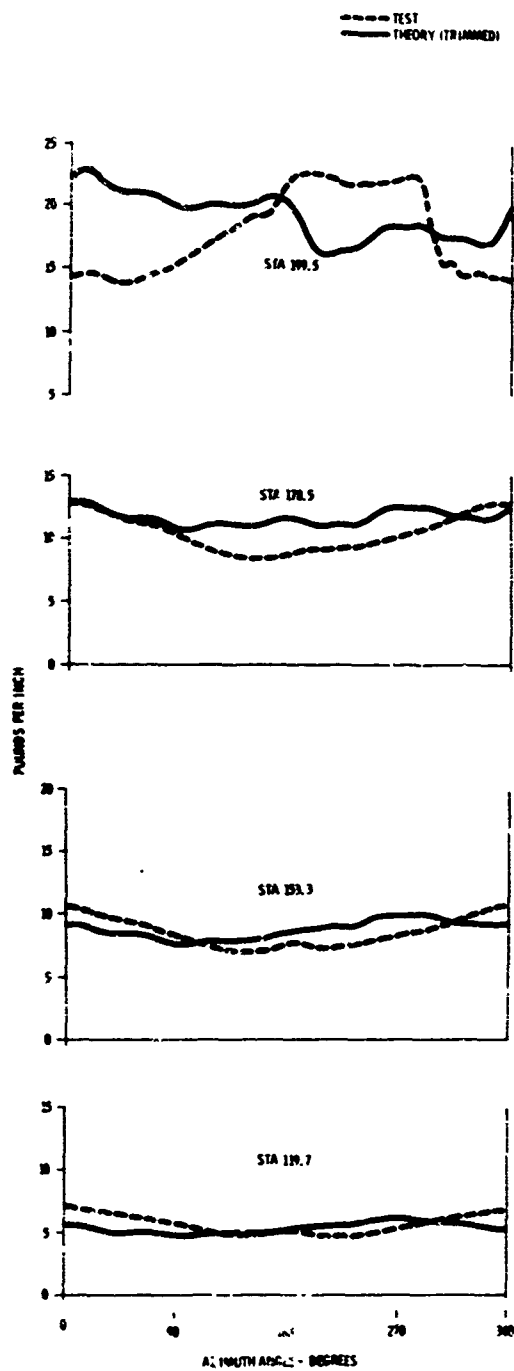
Figure 103. Measured and Computed Airloads, Lockheed Program, Condition 1 (Hover)
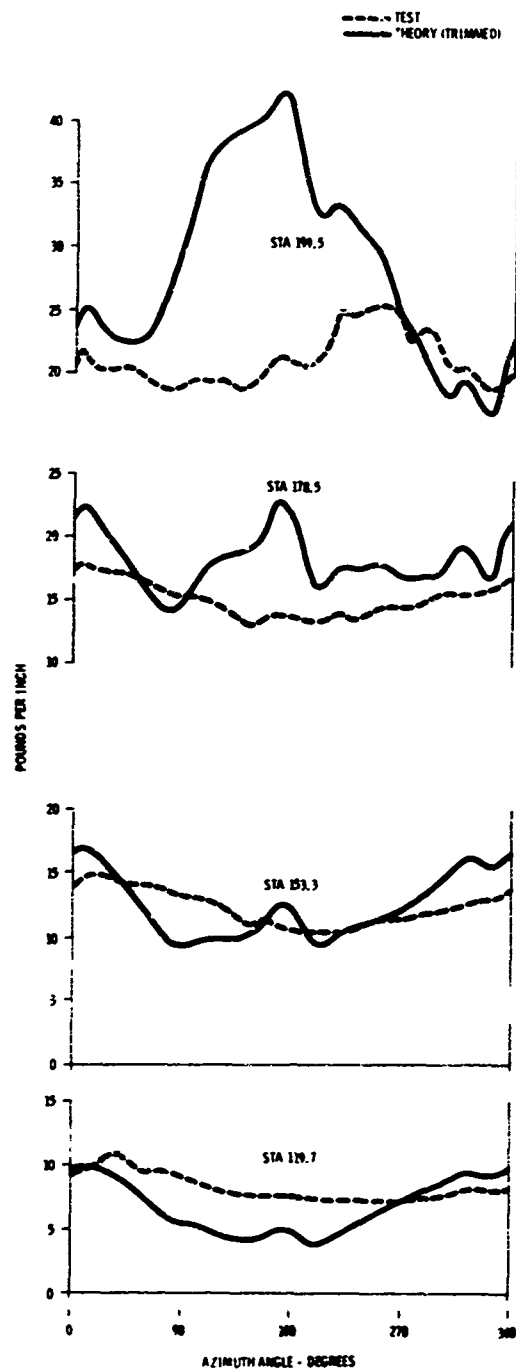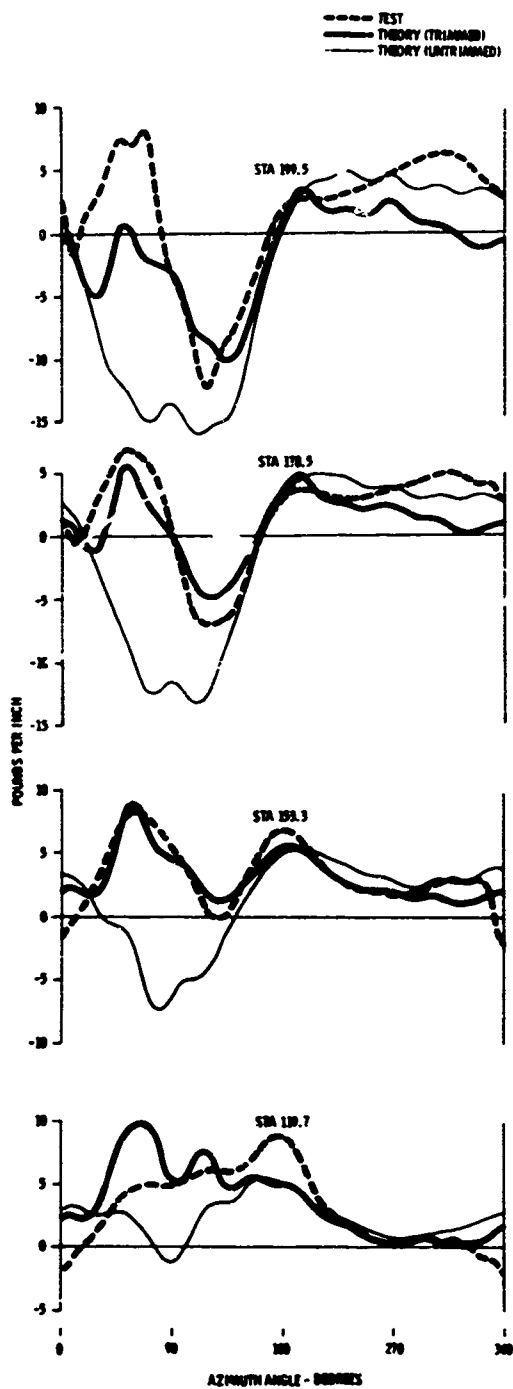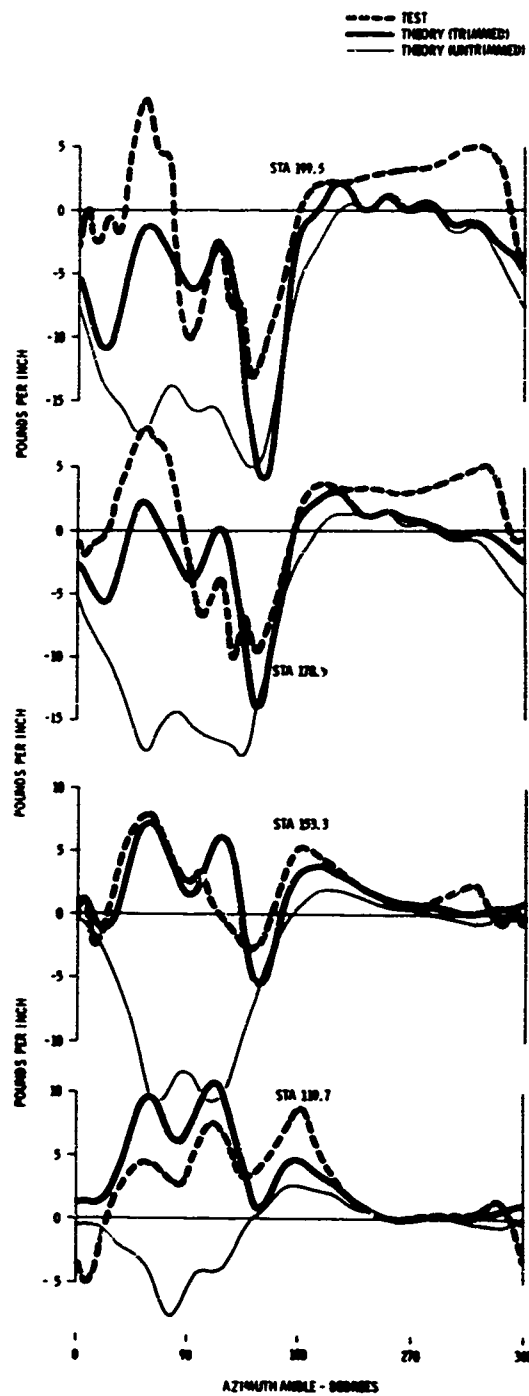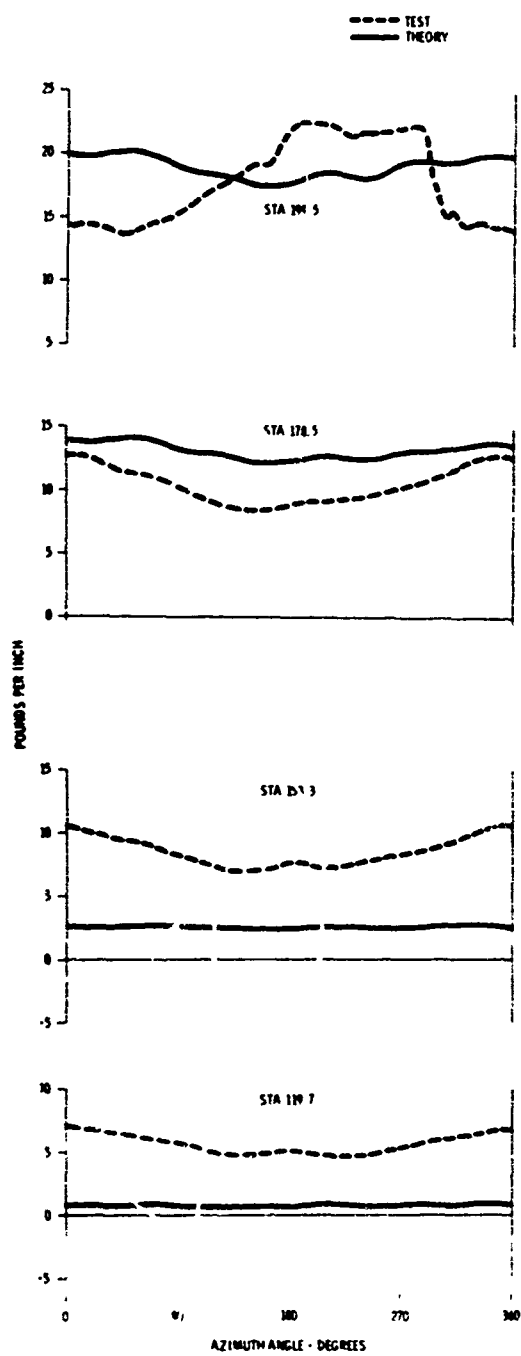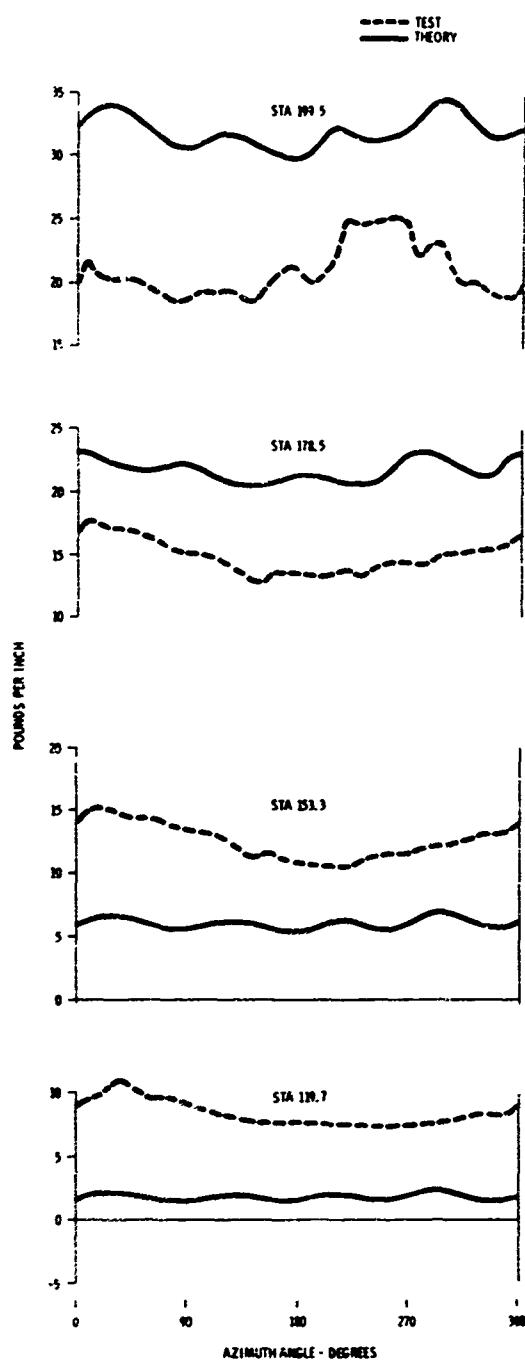
Figure 104. Measured and Computed Airloads, Lockheed Program, Condition 4 (Collective Pullup at 0 Knot TAS)
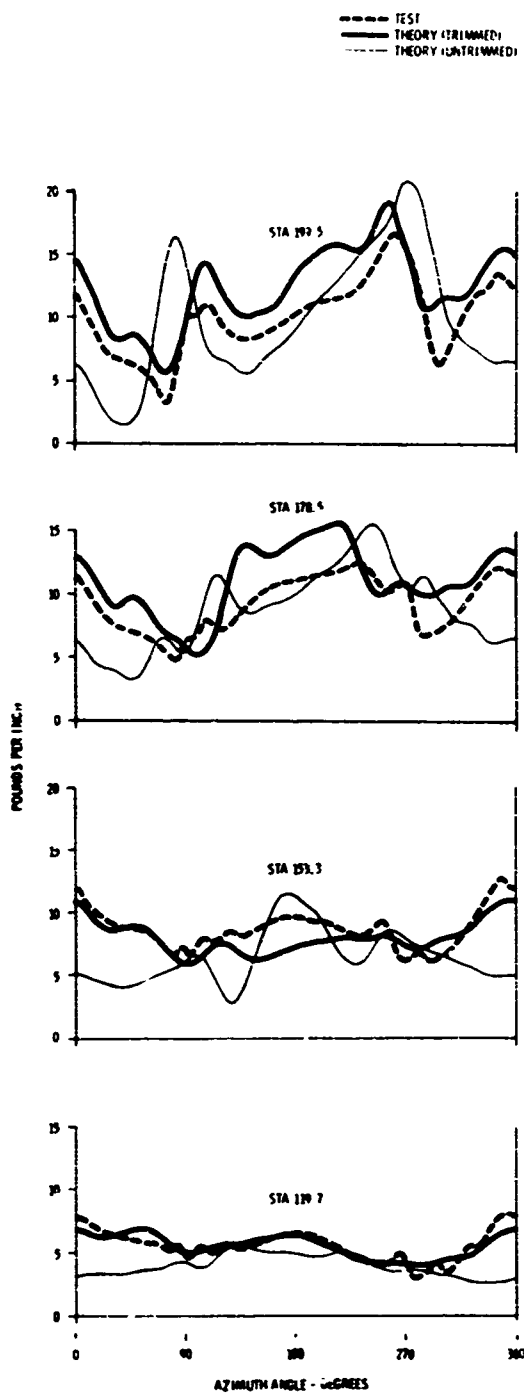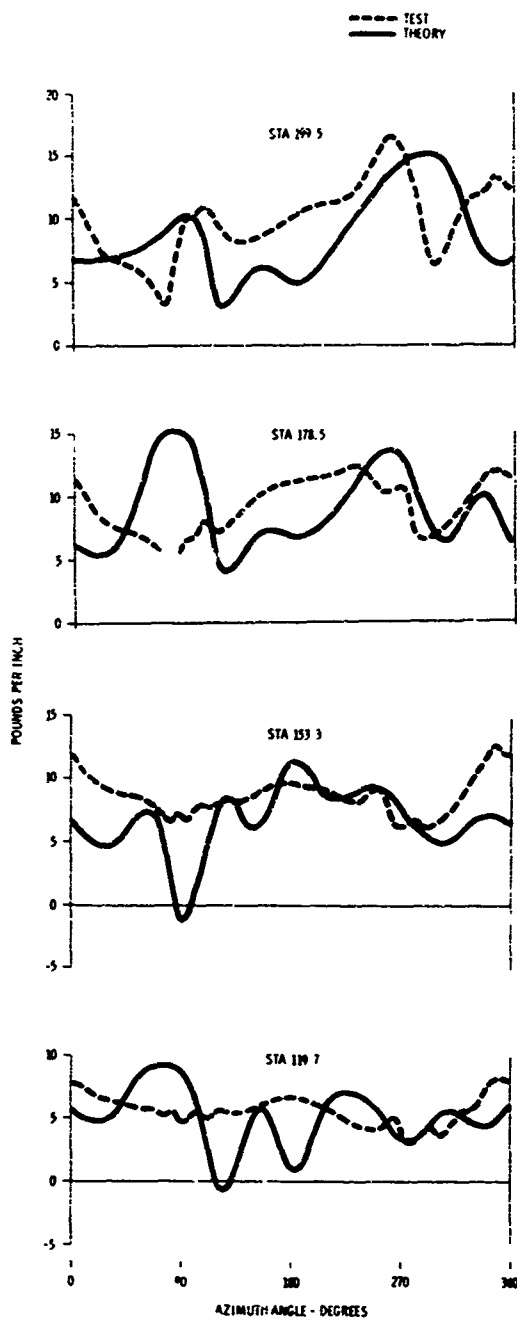
Figure 105. Measured and Computed
Airloads, Lockheed Program,
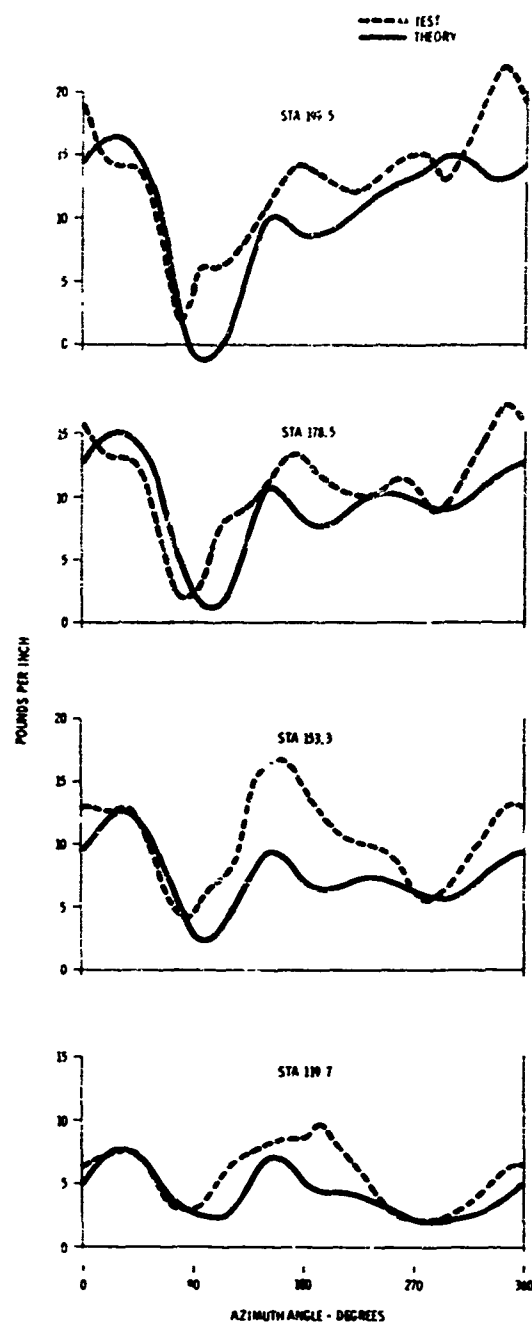Condition 5 (Forward Flight
at 51 Knots TAS)
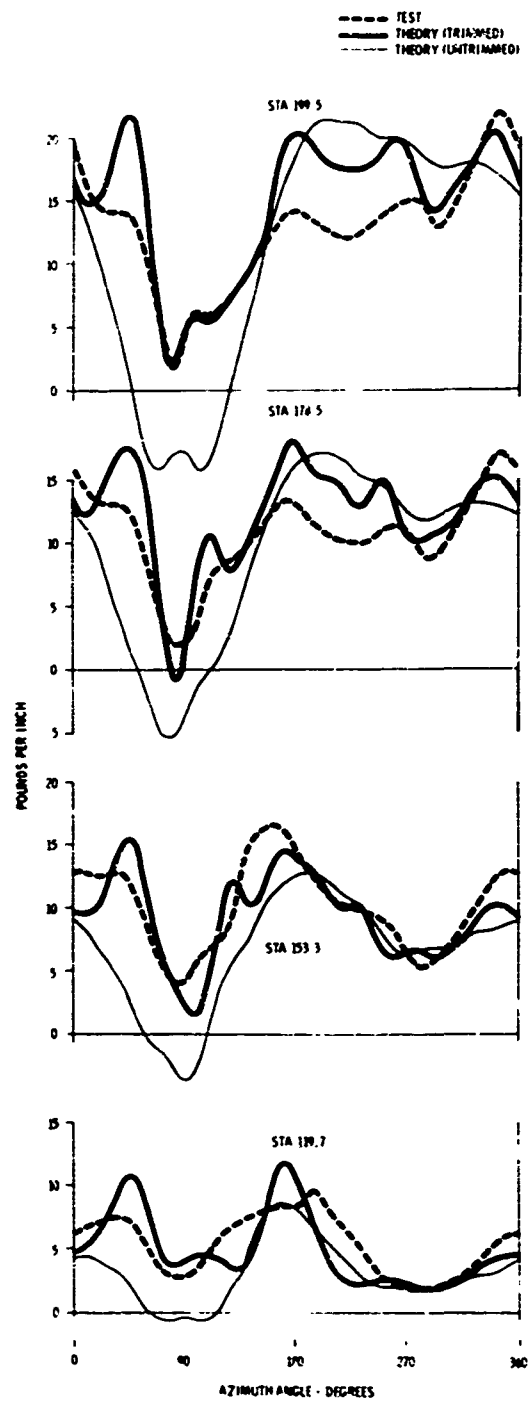
Figure 106. Measured and Computed
Airloads, Lockheed Program,
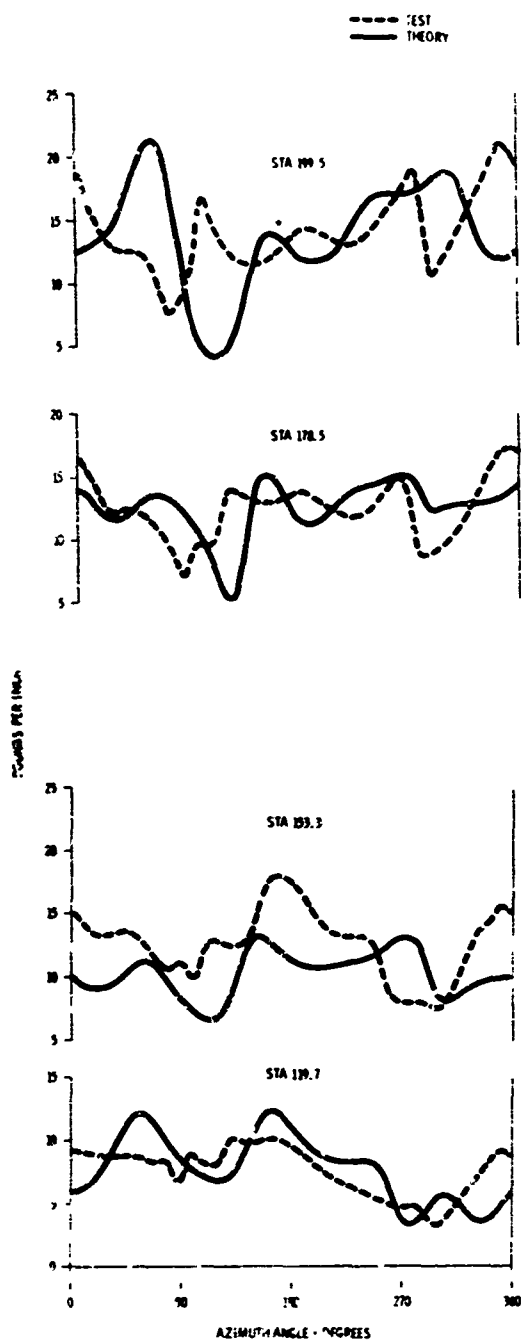Condition 8 (Forward Flight
at 95 Knots TAS)

83
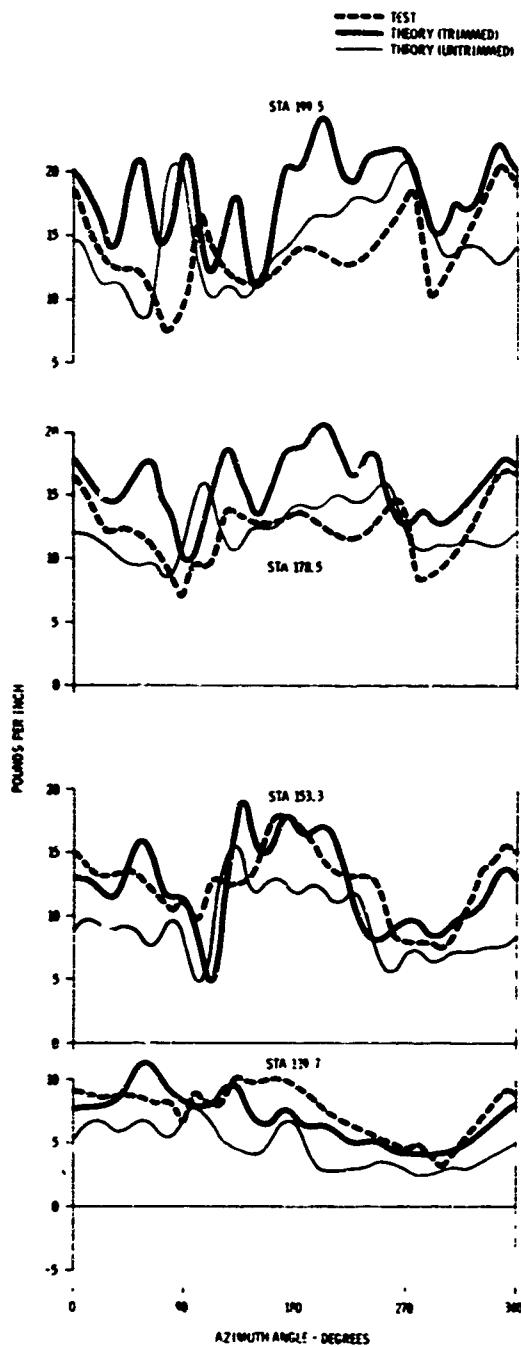
Figure 107. Measured and Computed
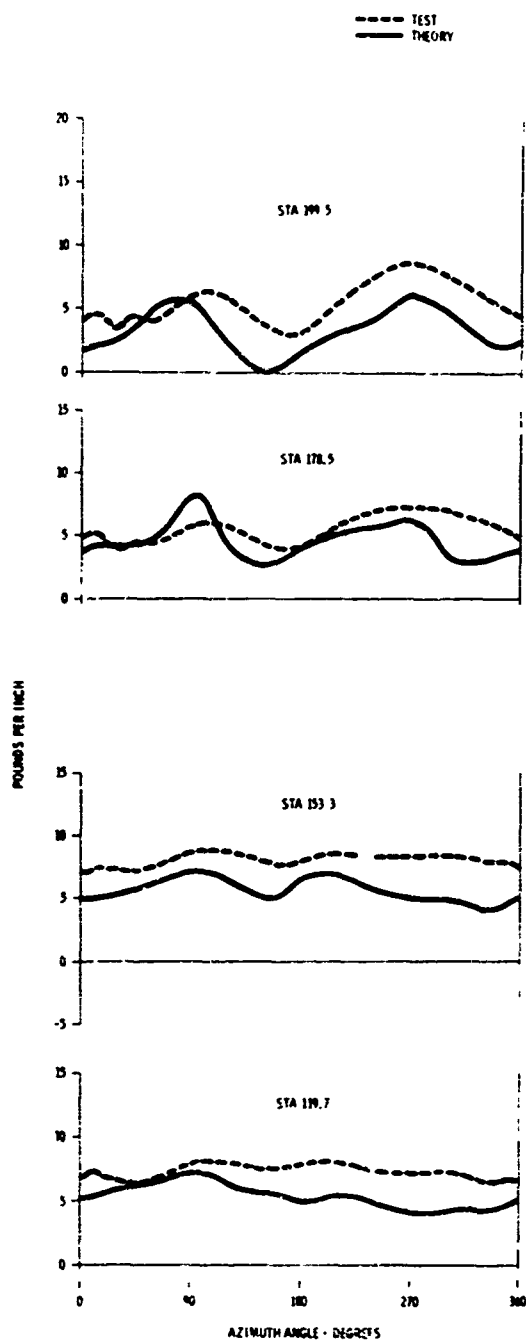Airloads, Lockheed Program,
Condition 11 (Left Turn
at 24 Knots TAS)
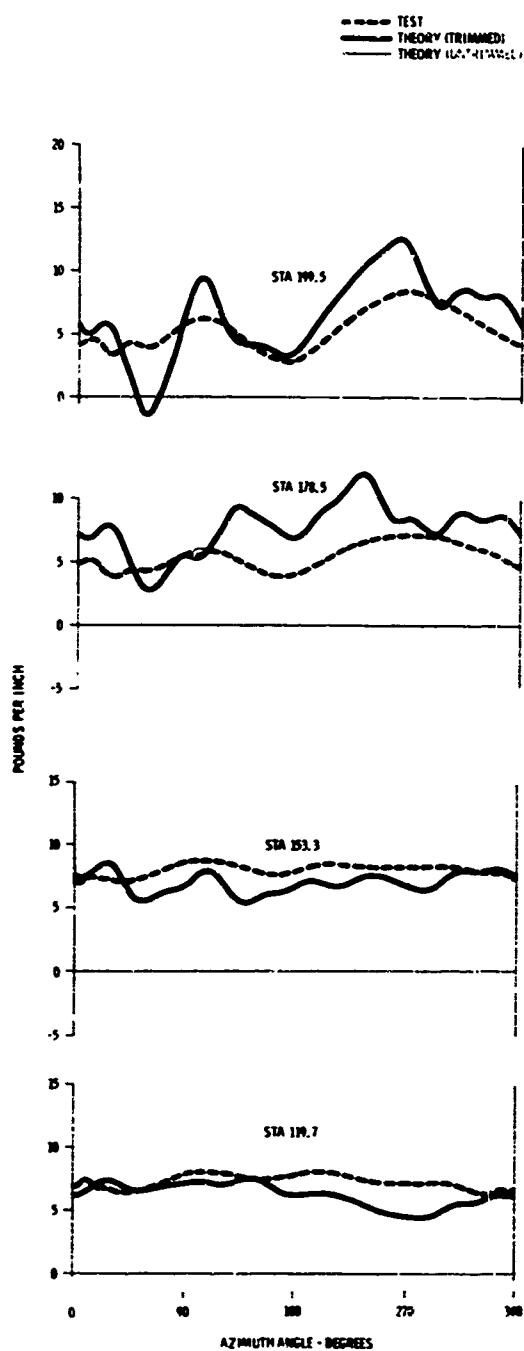
Figure 108. Measured and Computed
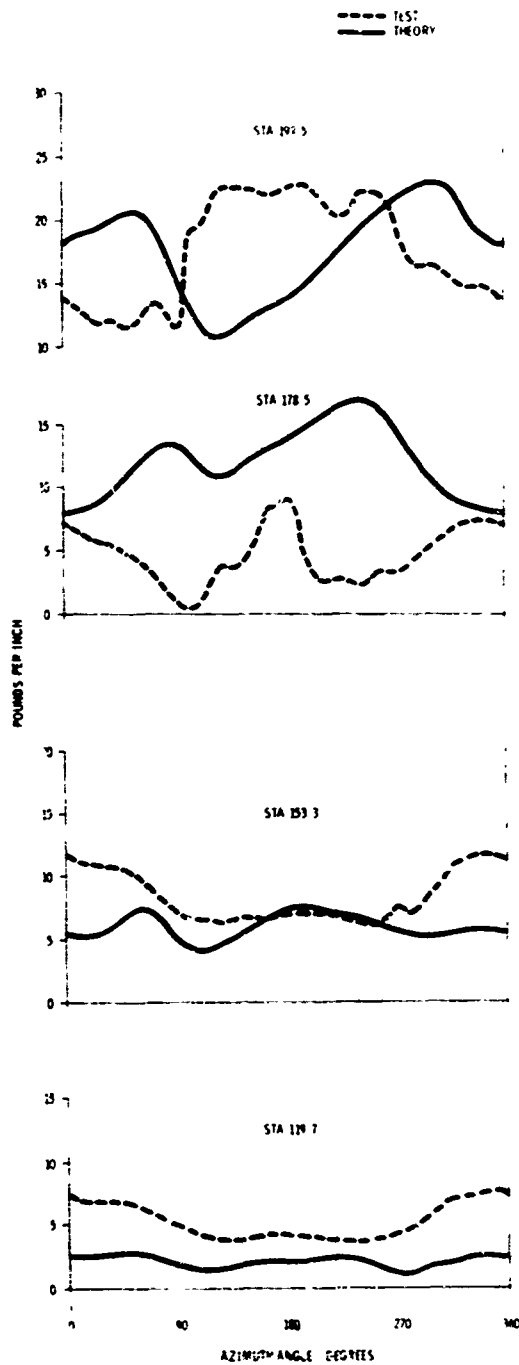Airloads, Lockheed Program,
Condition 16 (Autorotation)

84
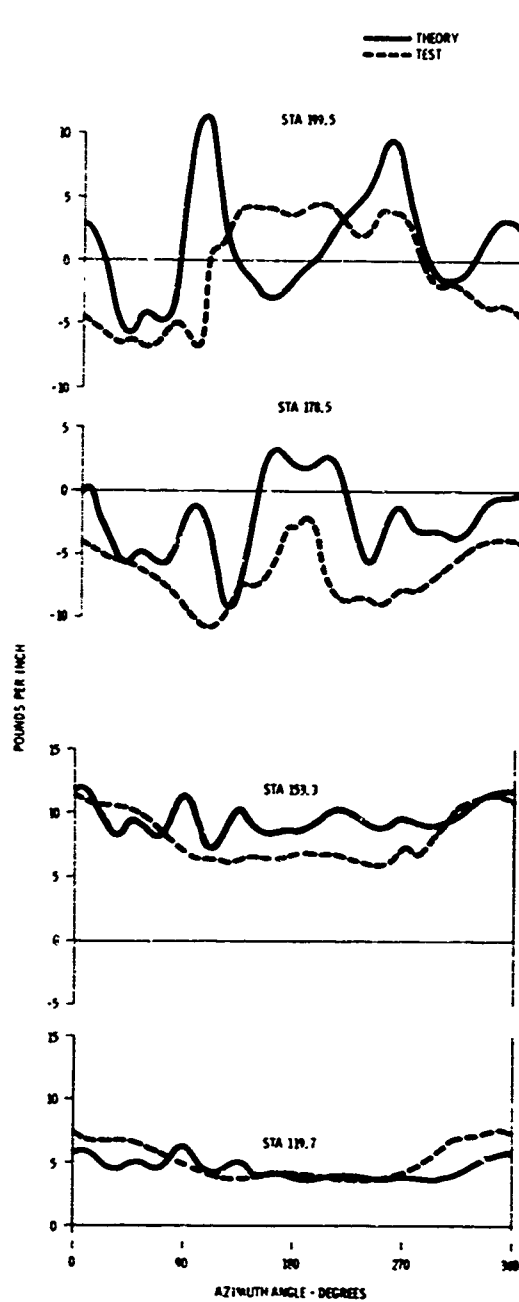
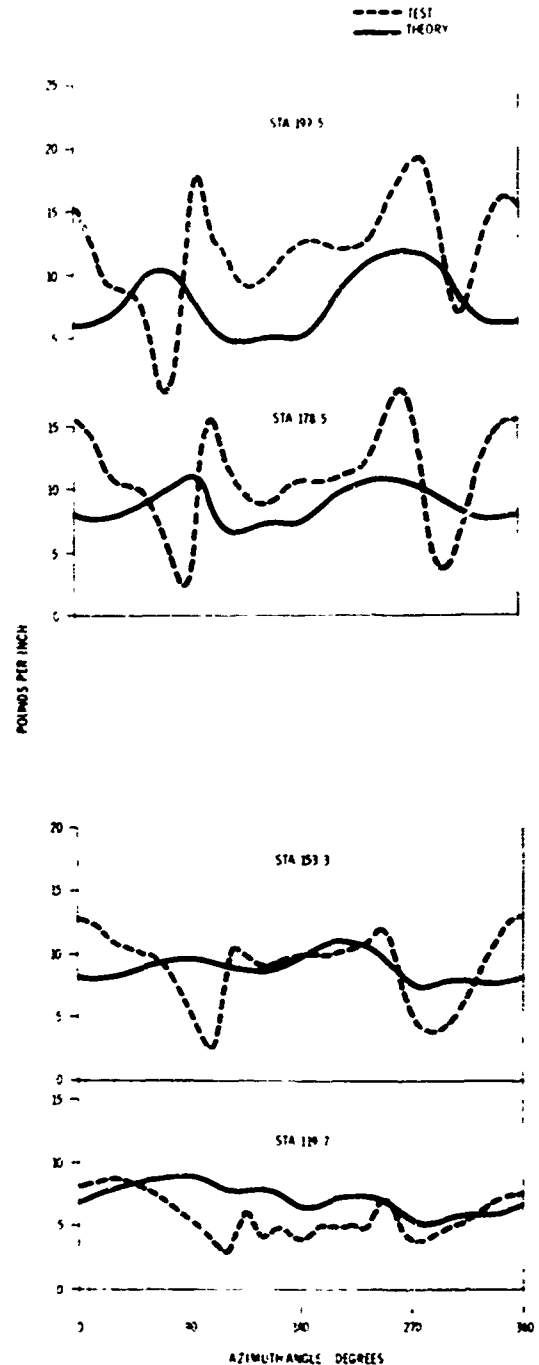Figure 109. Measured and Computed Airloads, Lockheed Program, Condition 19 (Transition)
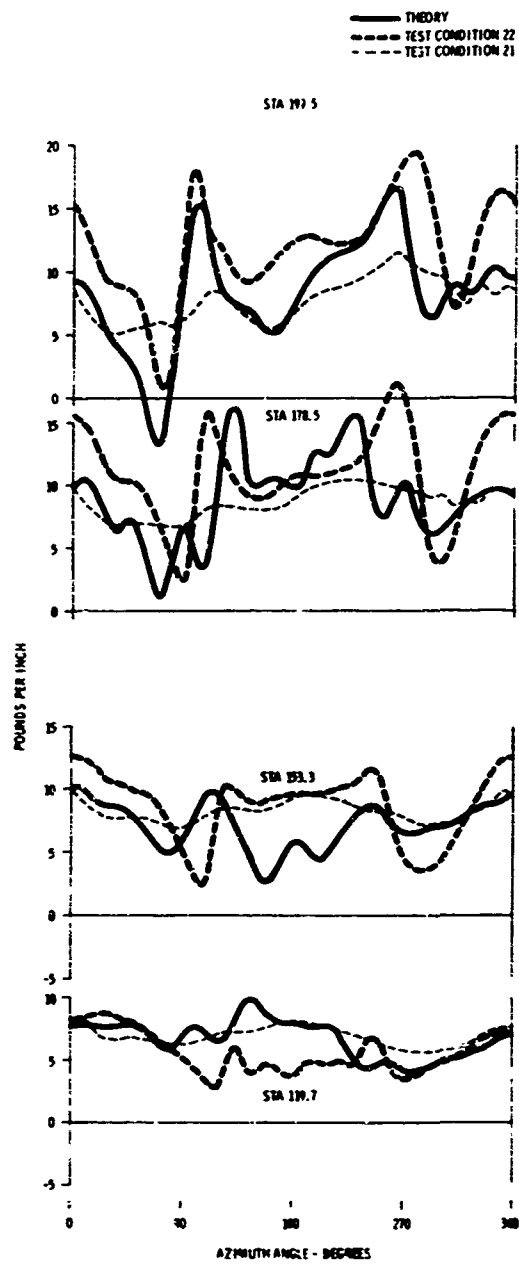
Figure 110. Measured and Computed Airloads, Lockheed Program, Conditions 21 and 22 (Flare at 60 Knots TAS)

85
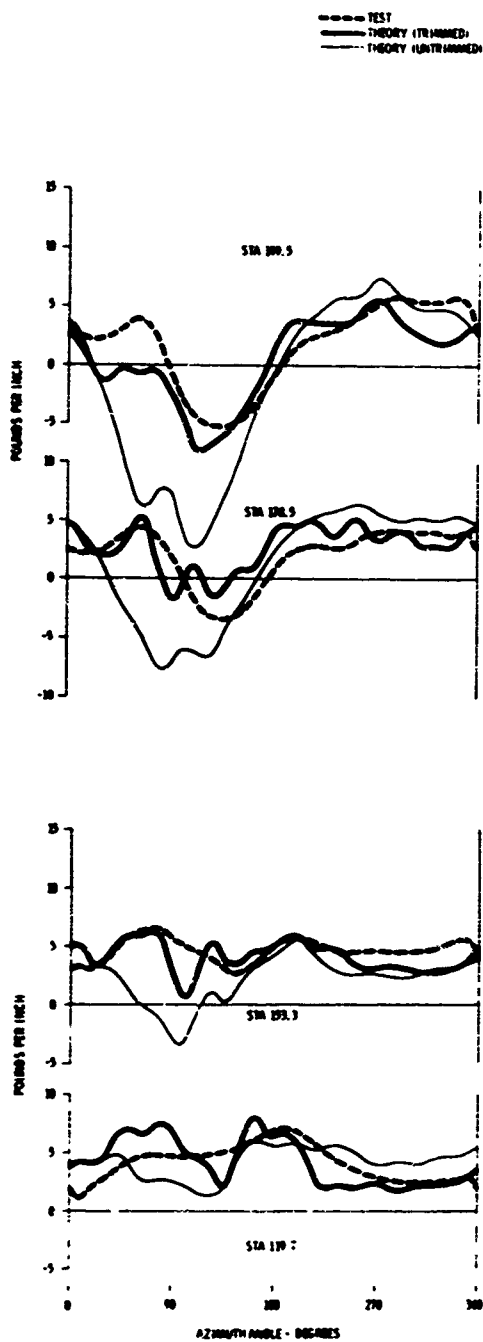
Figure 111. Measured and Computed
Airloads, Lockheed Program,
Condition 23 (Level Flight
at 109 Knots TAS)
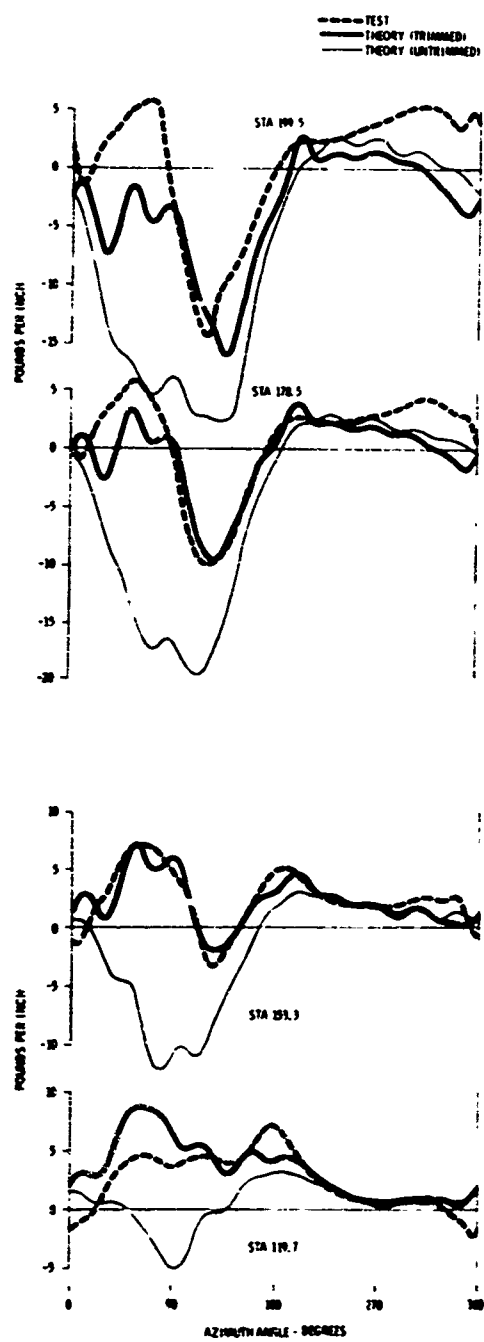
Figure 112. Measured and Computed
Airloads, Lockheed Program,
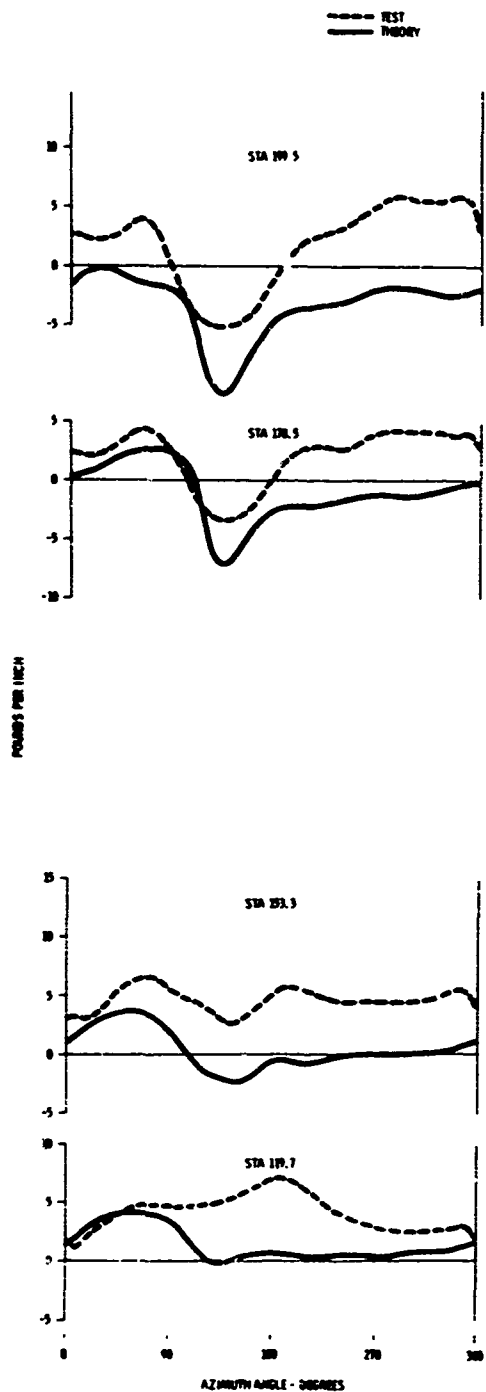Condition 25 (Level Flight
at 163.5 Knots TAS)

86
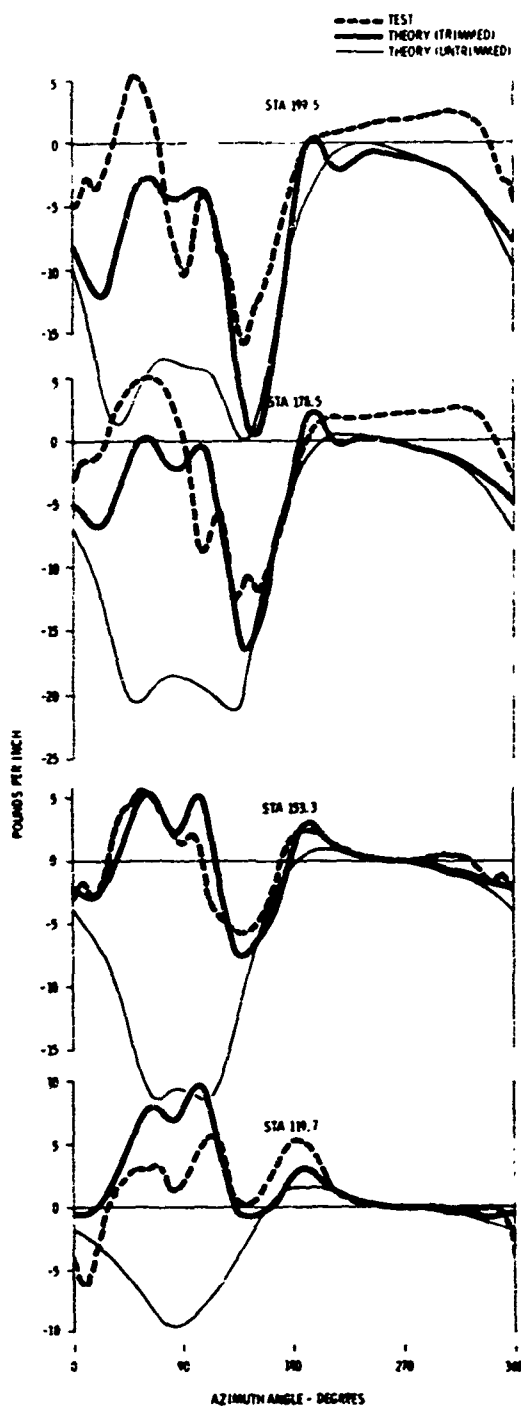
Figure 113. Measured and Computed
Airloads, Lockheed Program,
Condition 26 (Level Flight
at 207 Knots TAS)
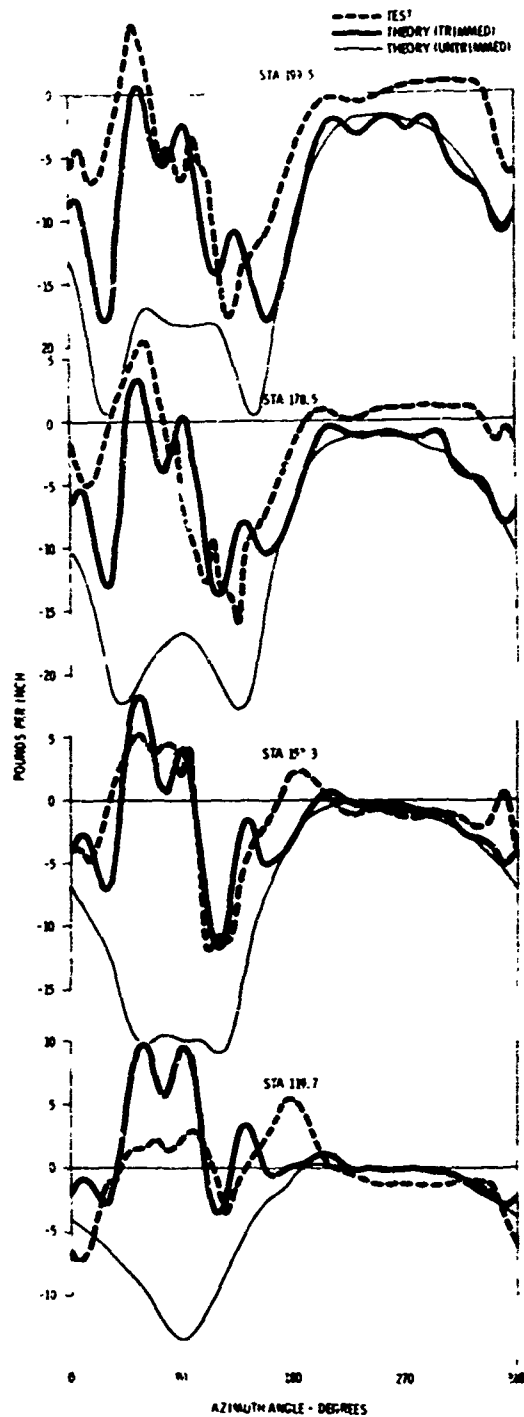
Figure 114. Measured and Computed
Airloads, Lockheed Program,
Condition 27 (Level Flight
at 227 Knots TAS)

87
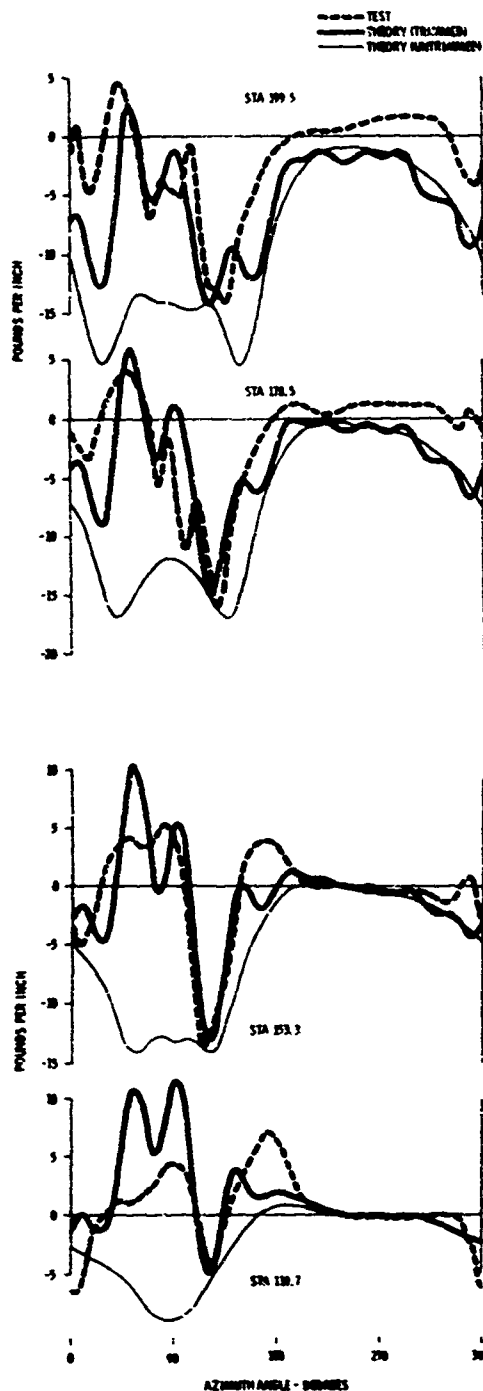
Figure 115.   Measured and Computed
Airloads, Lockheed Program,
Condition 31 (Level Flight
at 232 Knots TAS)
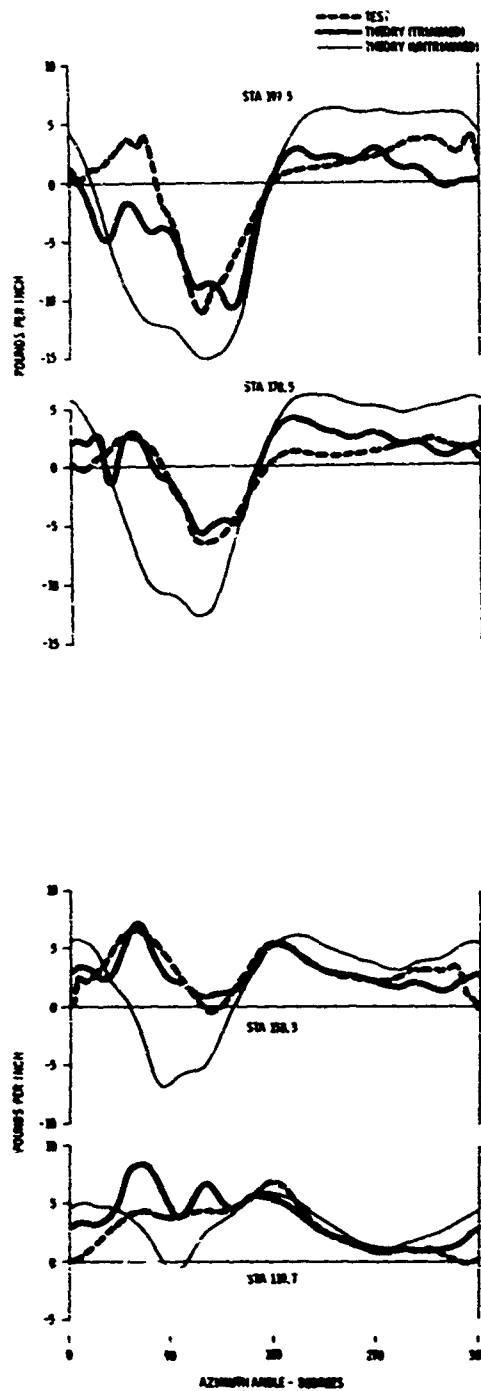
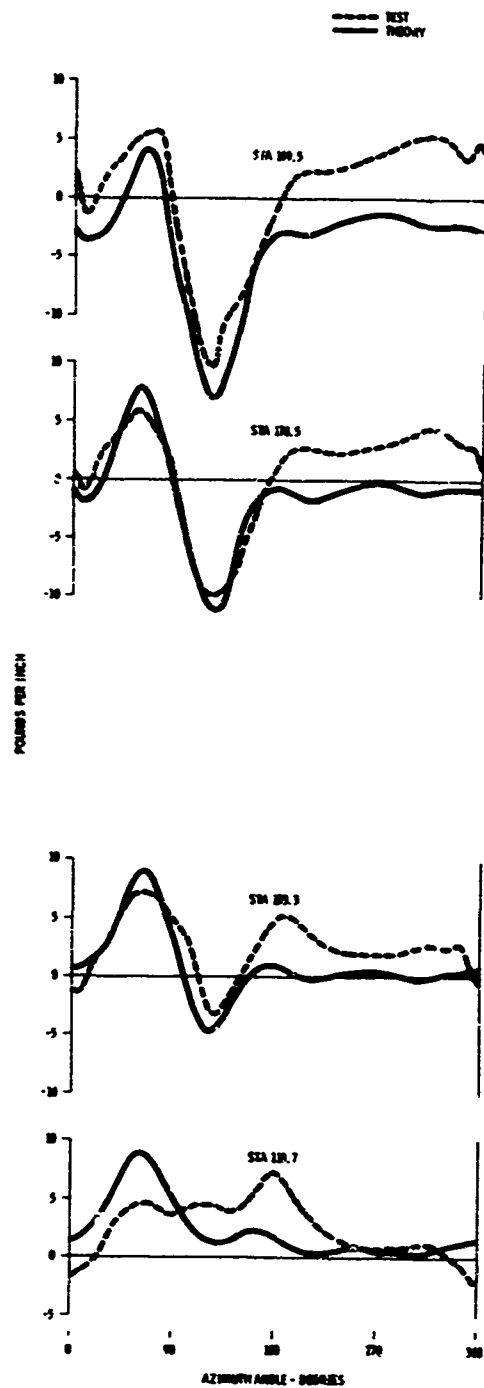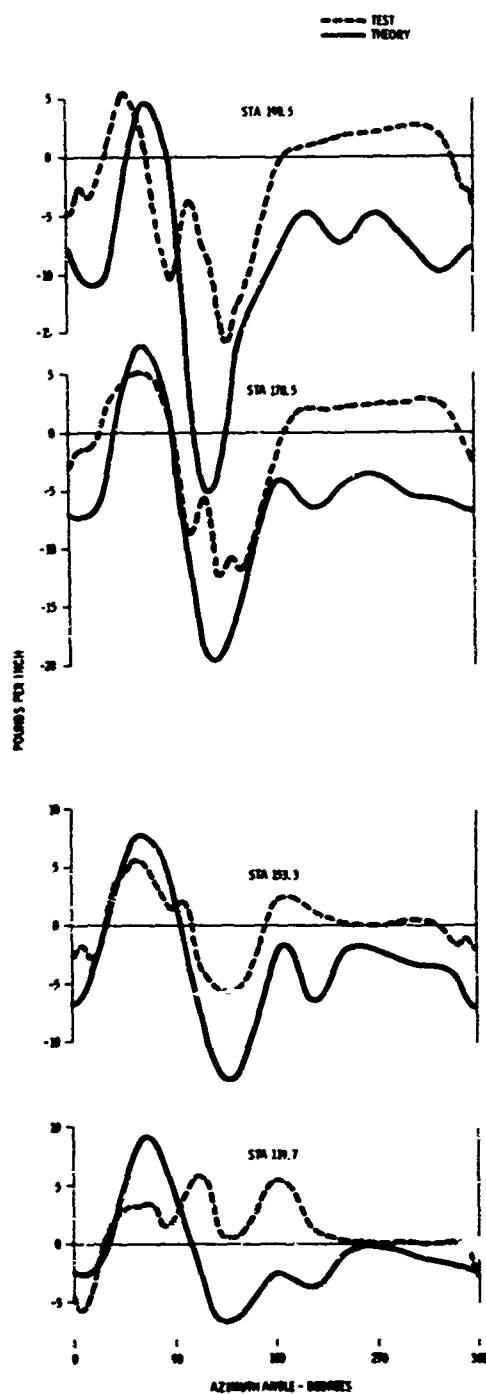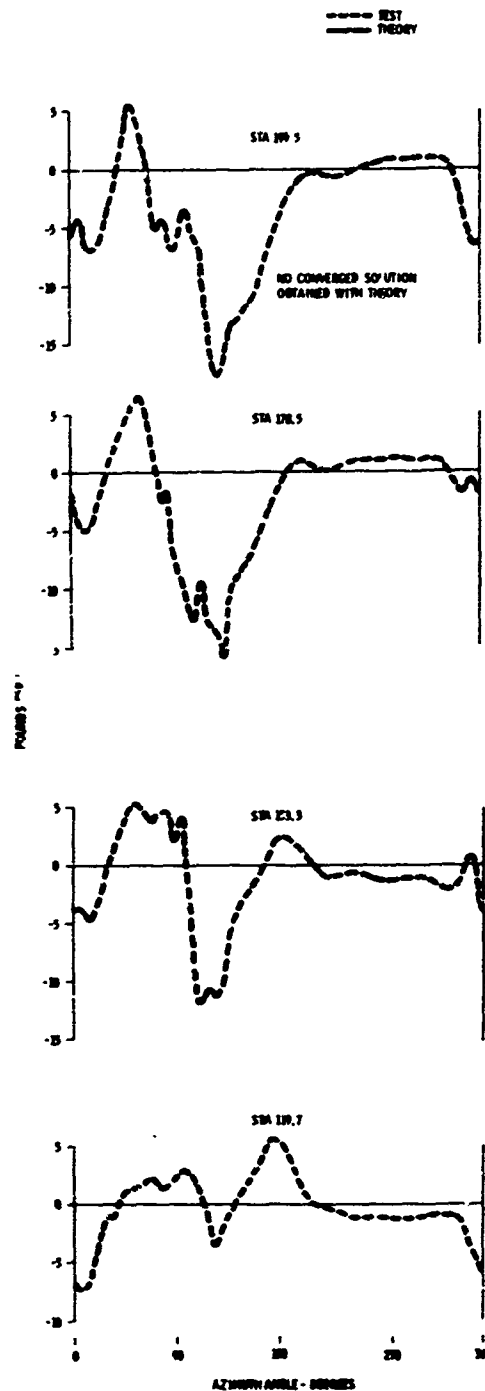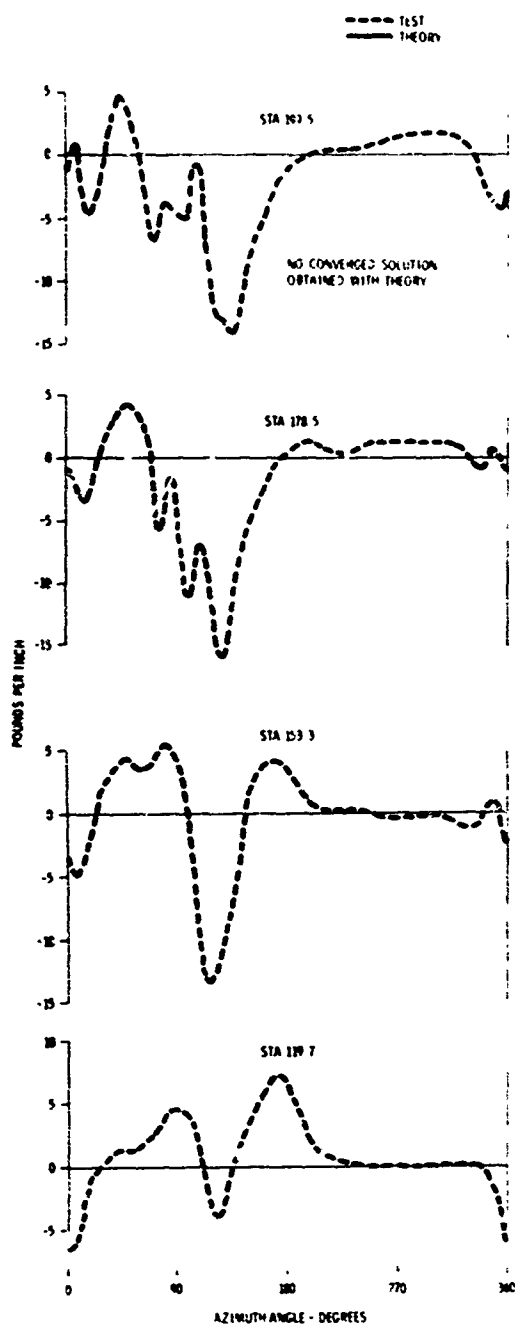Figure 116.   Measured and Computed
Airloads, Lockheed Program,
Condition 33 (Level Flight
at 157 Knots TAS)
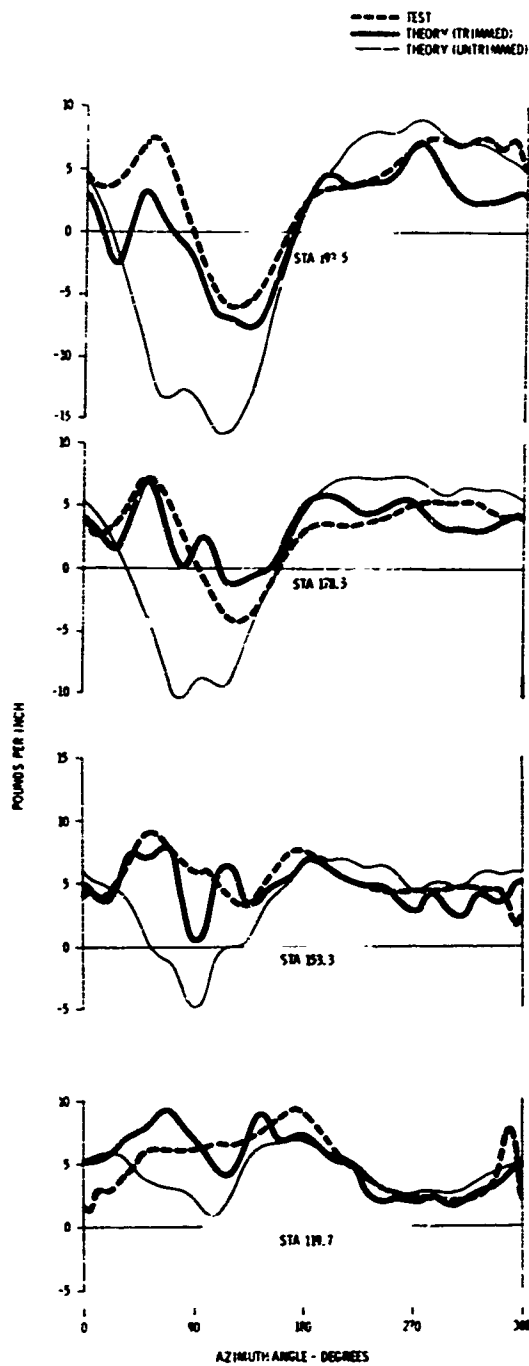
Figure 117. Measured and Computed Airloads, Lockheed Program, Condition 36 (Pullup at 126 Knots TAS)
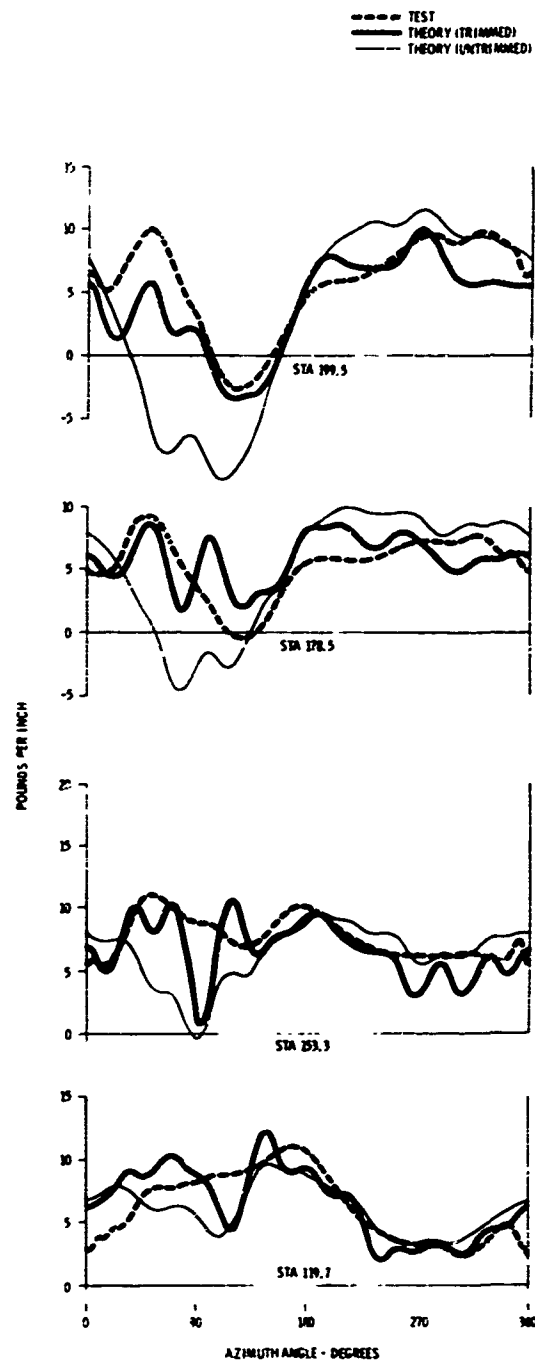
Figure 118. Measured and Computed Airloads, Lockheed Program, Condition 37 (Pullup at 124 Knots TAS)
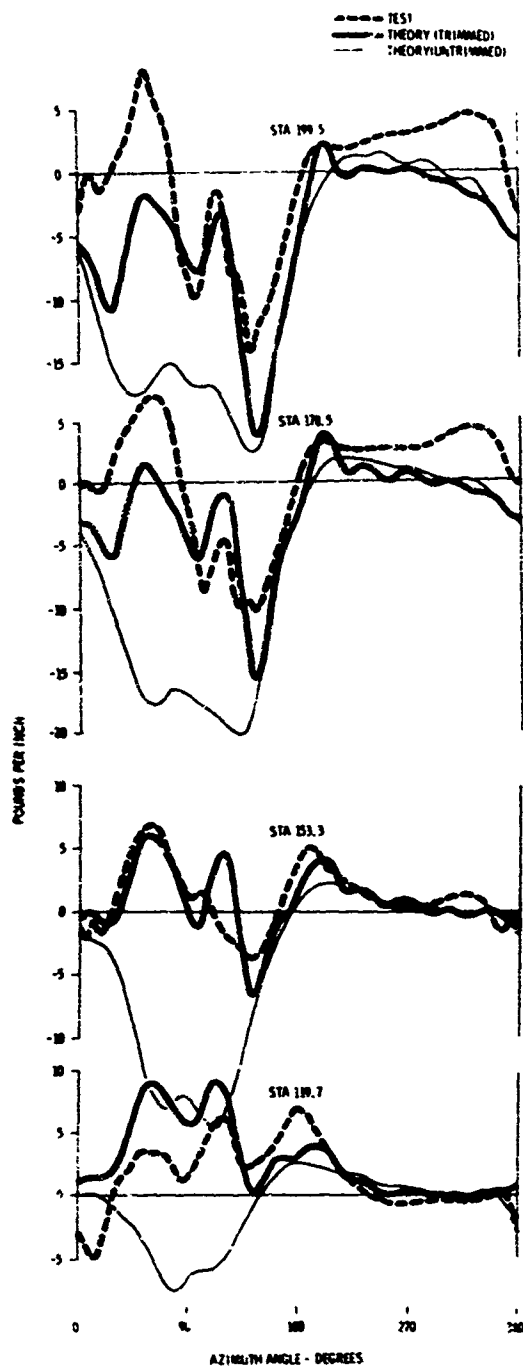
Figure 119. Measured and Computed Airloads, Lockheed Program, Condition 39 (Pullup at 206 Knots TAS)
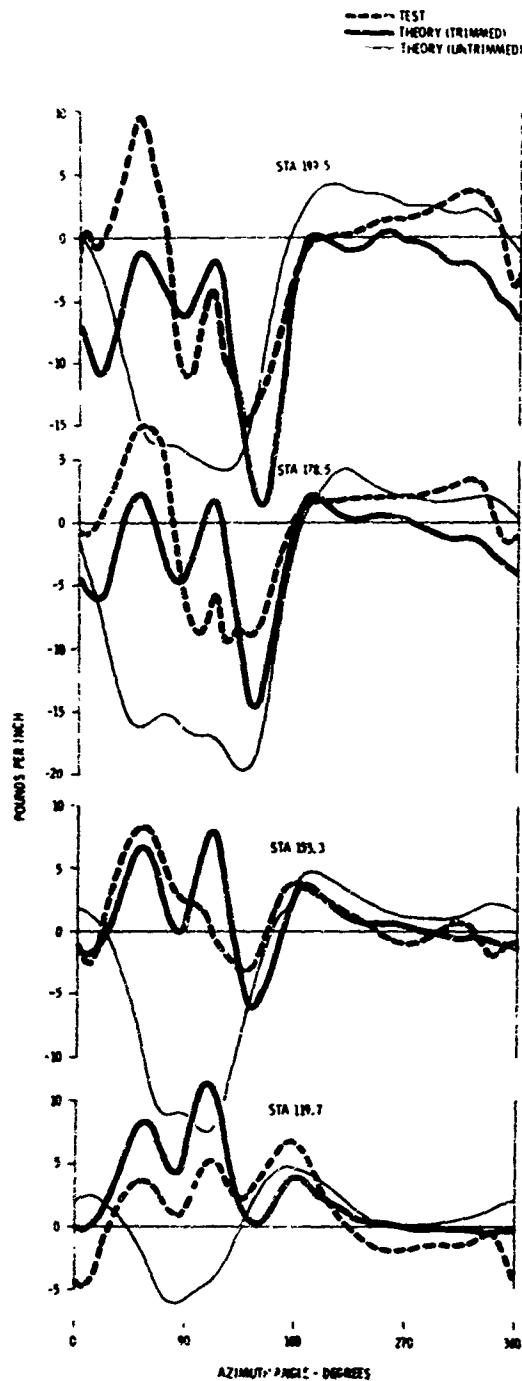
Figure 120. Measured and Computed Airloads, Lockheed Program, Condition 40 (Pullup at 206 Knots TAS)

90

Figure 121. Measured and Computed Airloads, Lockheed Program, Condition 46 (Left Turn at 161 Knots TAS)

Figure 122. Measured and Computed Airloads, Lockheed Program, Condition 50 (Right Turn at 208 Knots TAS)

91

Figure 123. Measured and Computed
Airloads, Cornell Program,
Condition 1 (Hover)

Figure 124. Measured and Computed
Airloads, Cornell Program, Condition
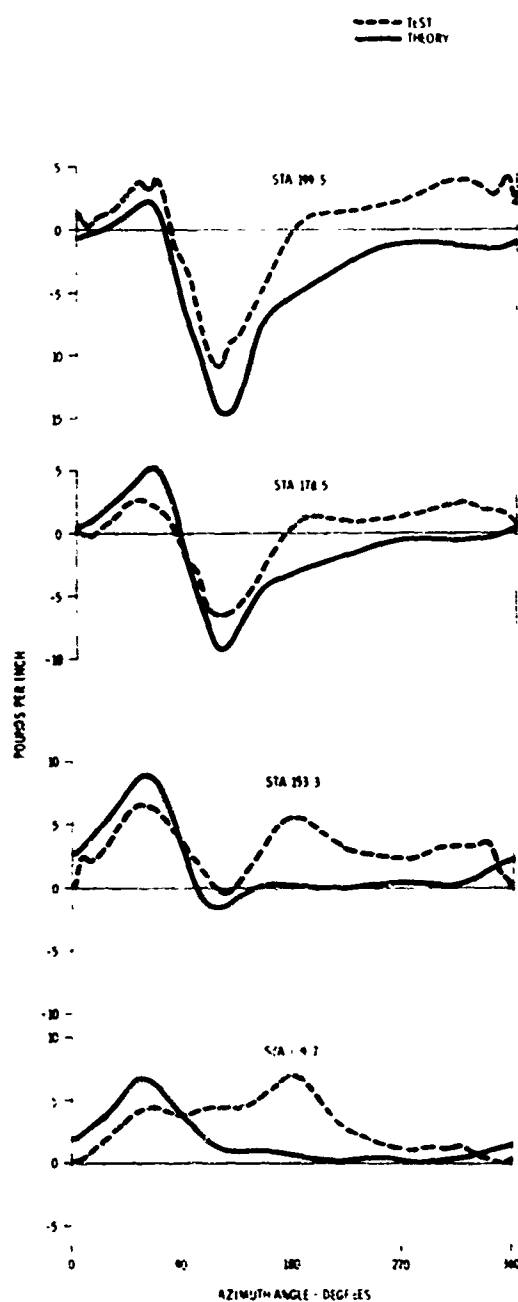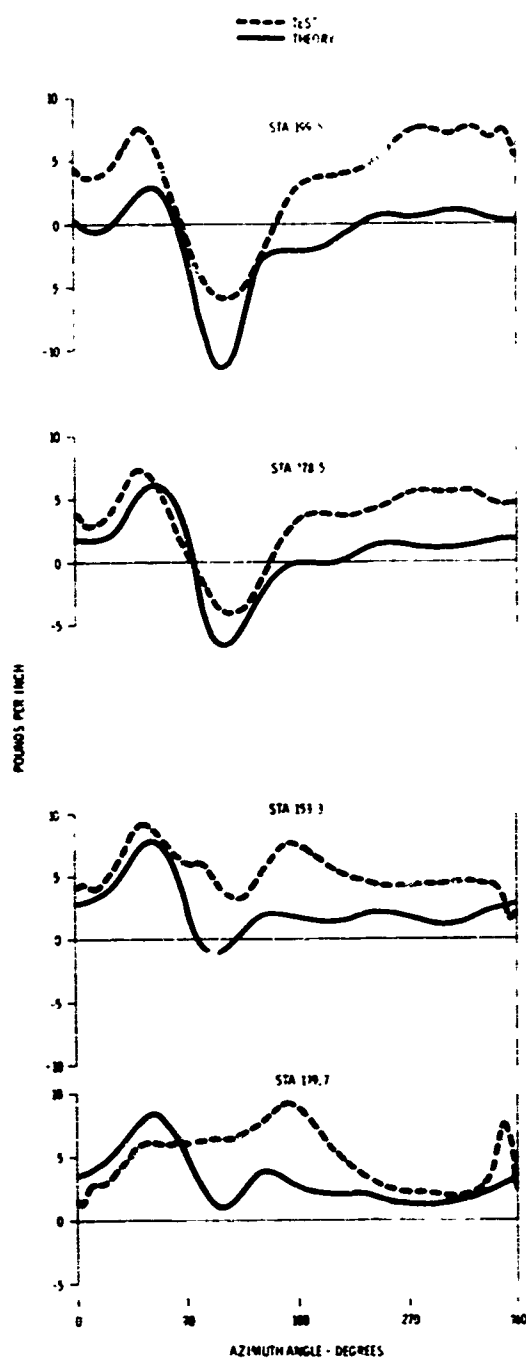4 (Collective Pullup at 0 Knot TAS)

Figure 125. Measured and Computed Airloads, Cornell Program, Condition 5 (Forward Flight at 51 Knots TAS)

Figure 126. Measured and Computed Airloads, Cornell Program, Condition 8 (Forward Flight at 105 Knots TAS)
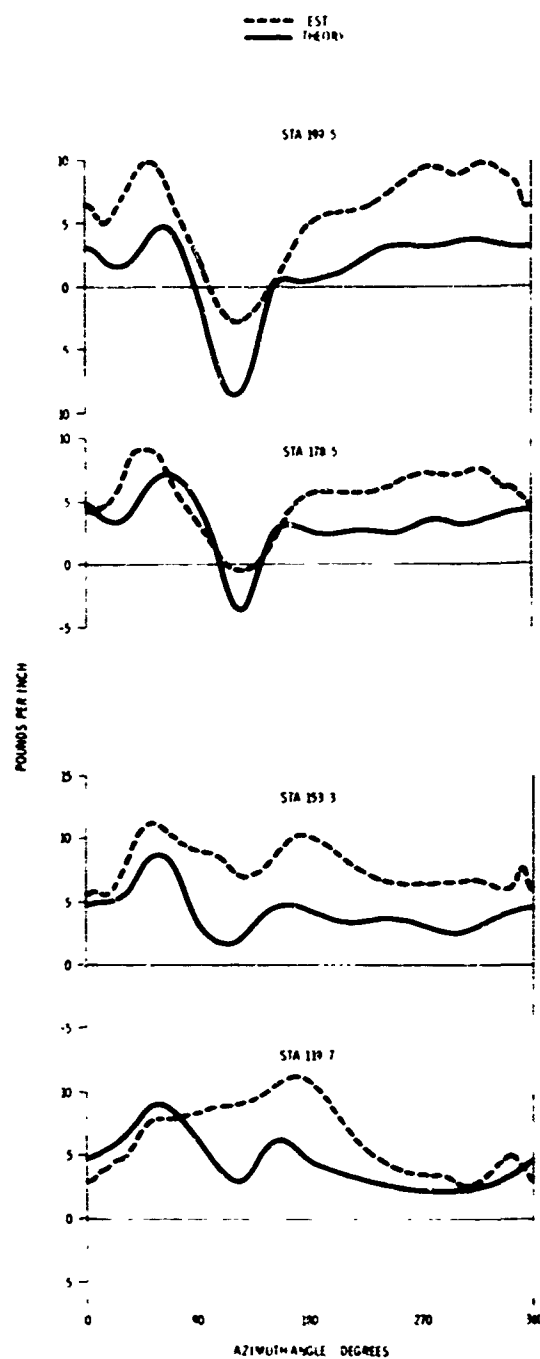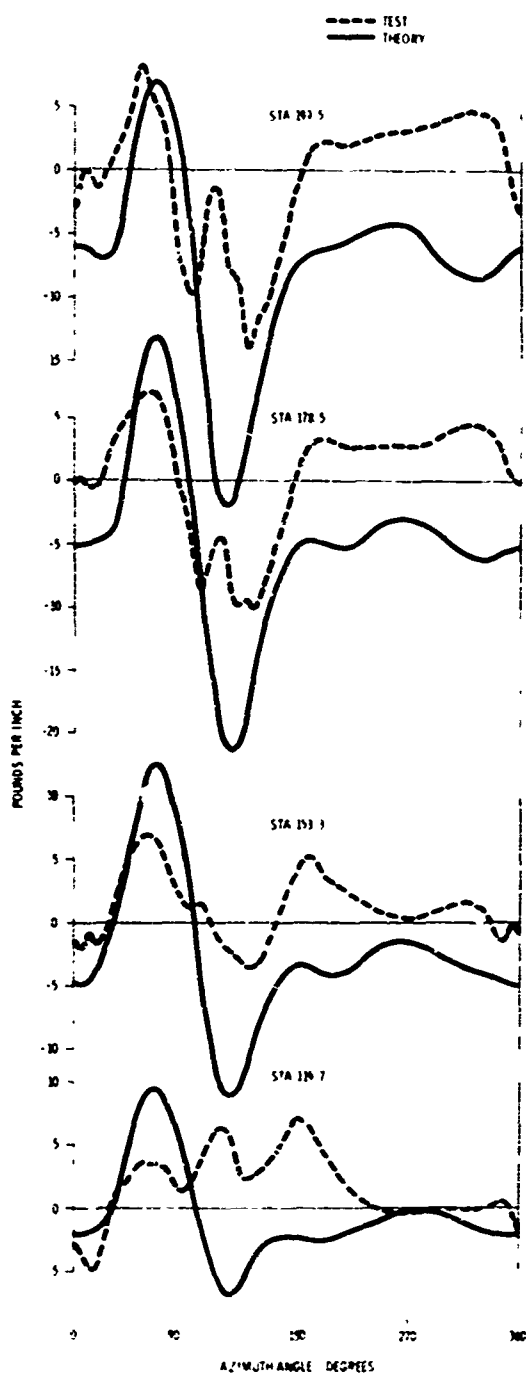
93

Figure 127. Measured and Computed
Airloads, Cornell Program,
Condition 11 (Left Turn
at 84 Knots TAS)

Figure 128. Measured and Computed
Airloads, Cornell Program,
Condition 16 (Autorotation)

94

Figure 129. Measured and Computed
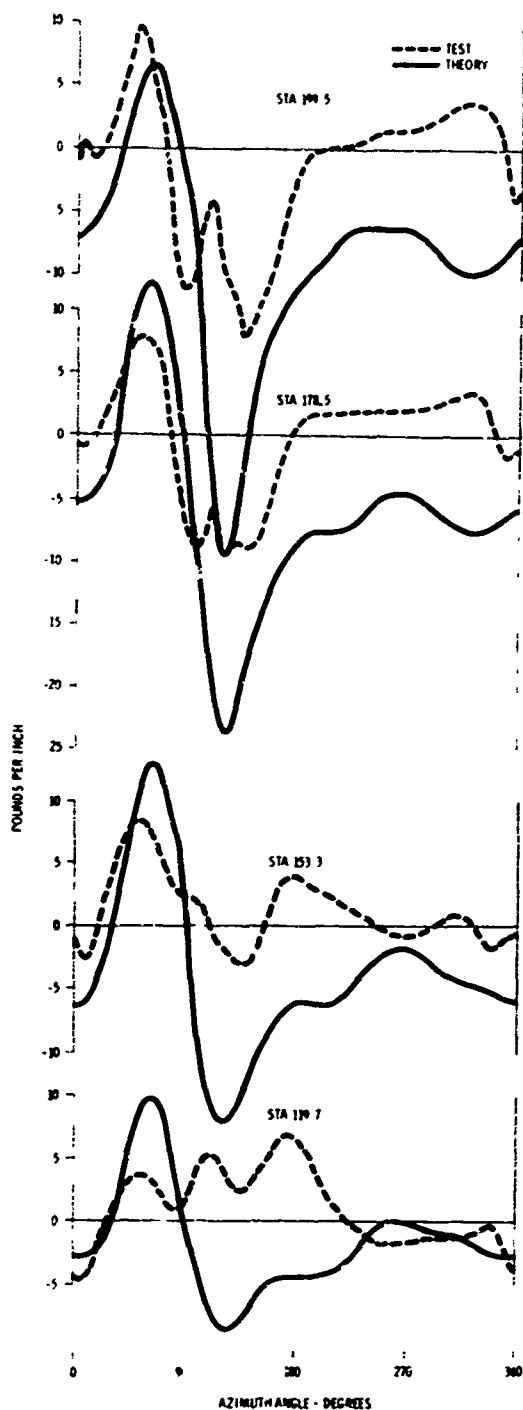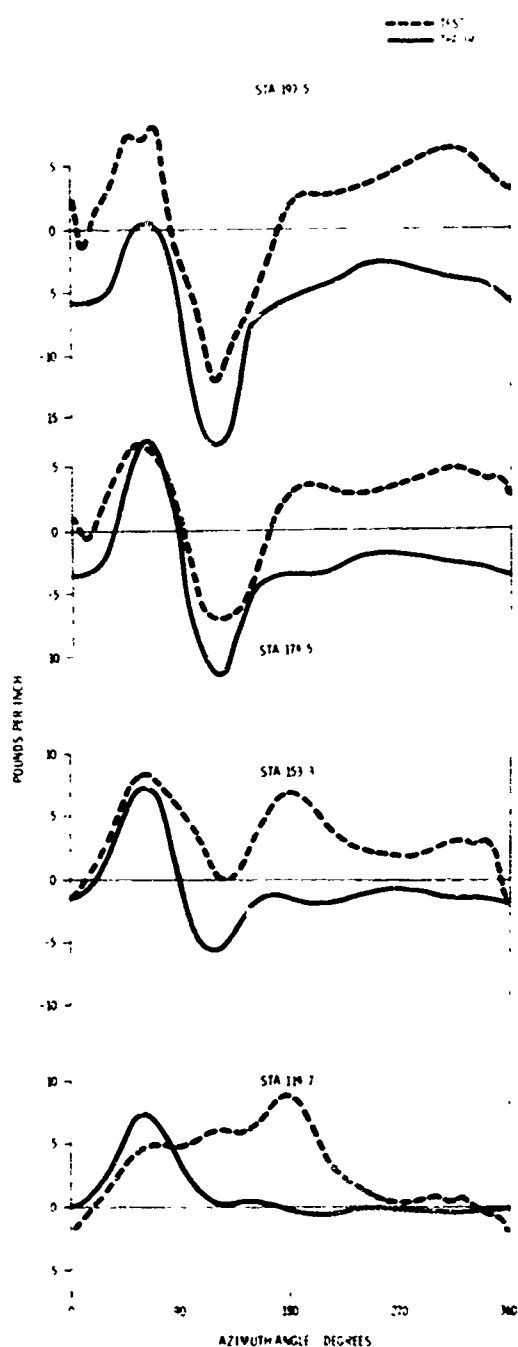Airloads, Cornell Program,
Condition 19 (Transition)

Figure 130. Measured and Computed
Airloads, Cornell Program,
Condition 21 (Flare
at 60 Knots TAS)

95

Figure 131. Measured and Computed
Airloads, Cornell Program,
Conditior 23 (Level Flight
at 109 Knots TAS)

Figure 132. Measured and Computed
Airloads, Cornell Program,
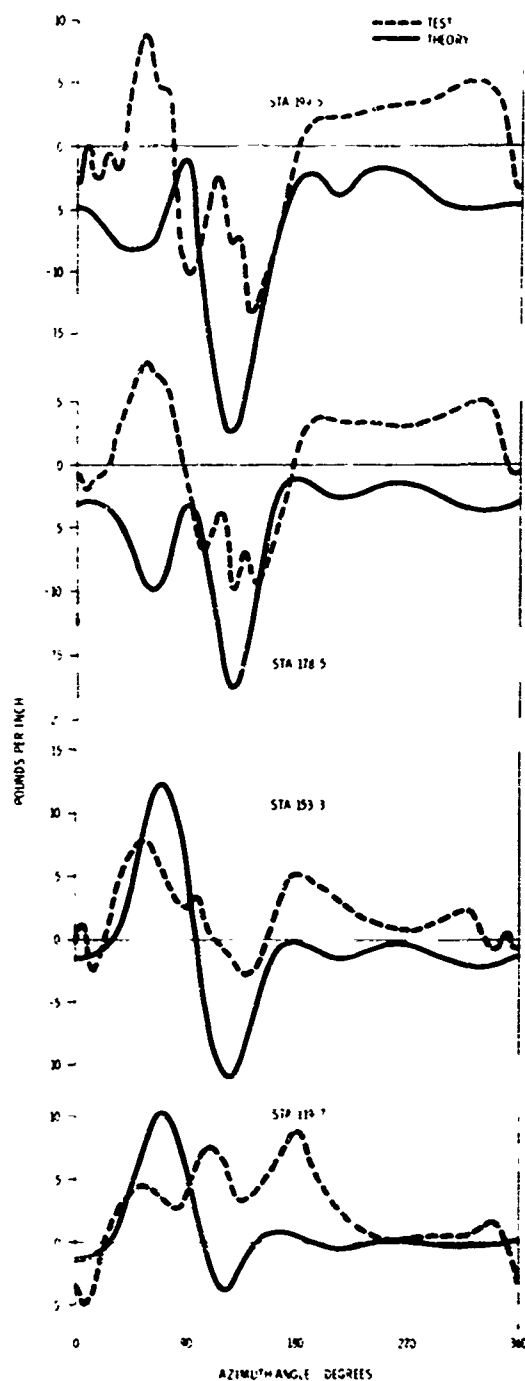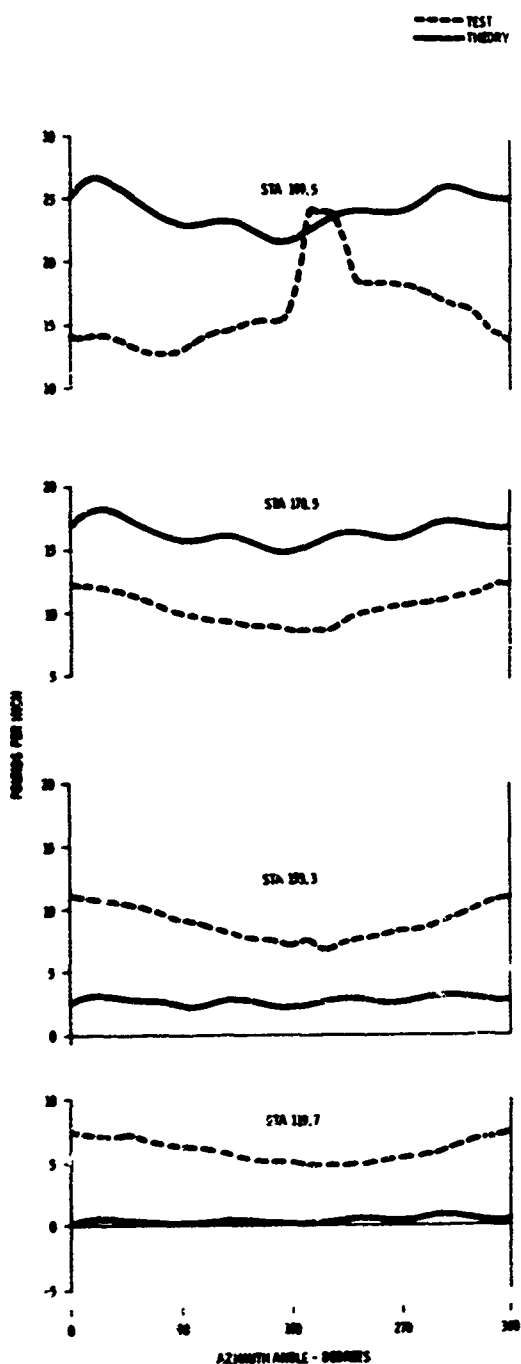Condition 25 (Level Flight
at 163.5 Knots TAS)

96

Figure 133. Measured and Computed
Airloads, Cornell Program,
Condition 26 (Level Flight
at 207 Knots TAS)

Figure 134. Measured and Computed
Airloads, Cornell Program,
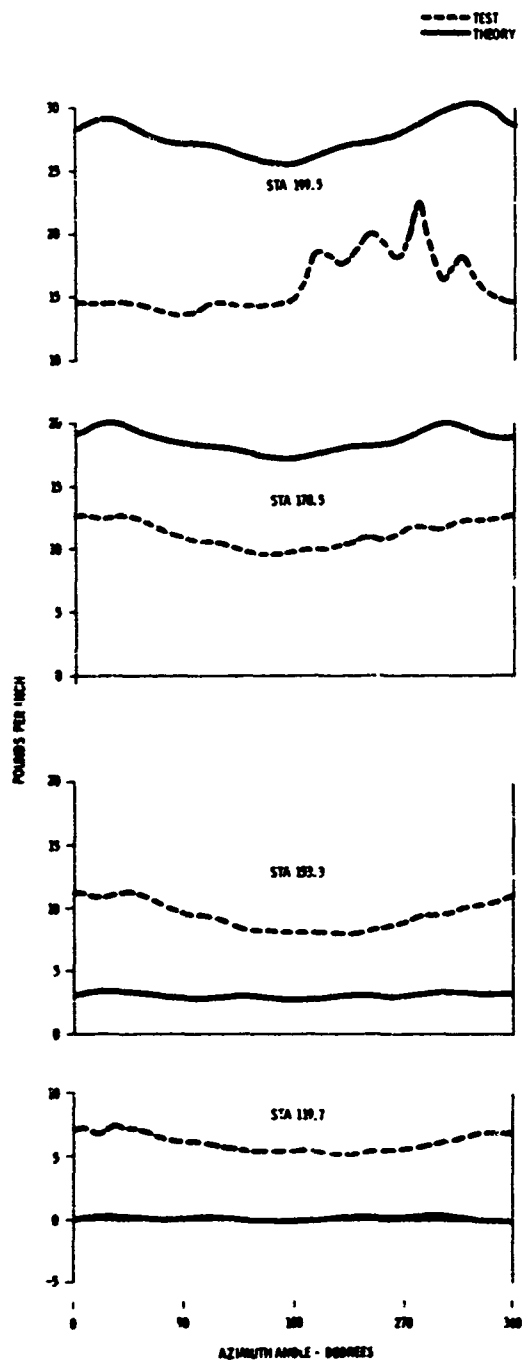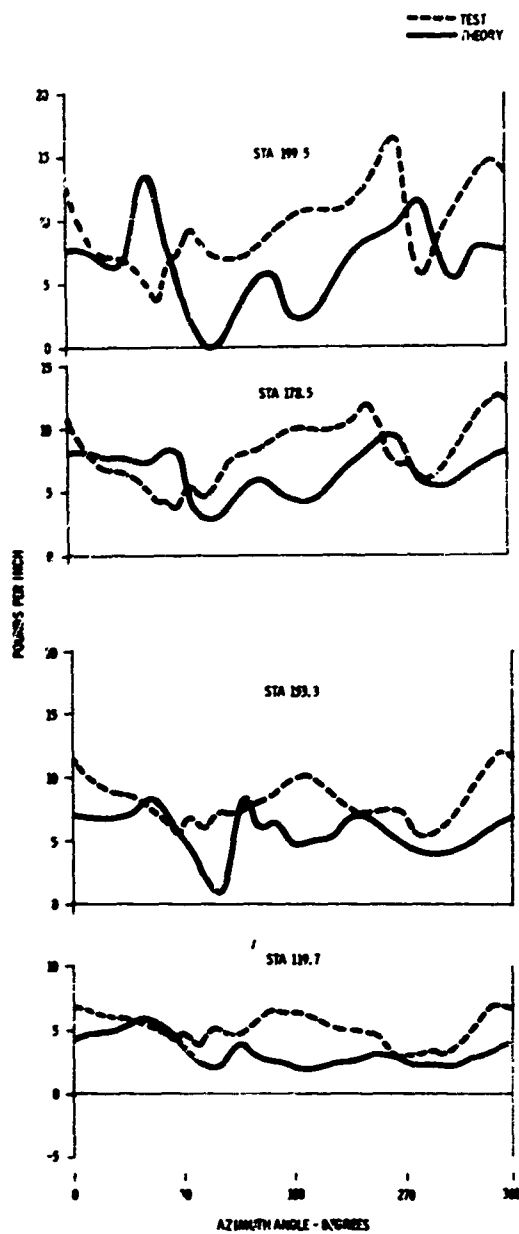Condition 27 (Level Flight
at 227 Knots TAS)

Figure 135. Measured and Computed
Airloads, Cornell Program,
Condition 31 (Level Flight
at 232 Knots TAS)

Figure 136. Measured and Computed
Airloads, Cornell Program,
Condition 3° (Level Flight
at 157 κ   TAS)

Figure 137. Measured and Computed
Airloads, Cornell Program,
Condition 36 (Pullup
at 126 Knots TAS)

Figure 138. Measured and Computed
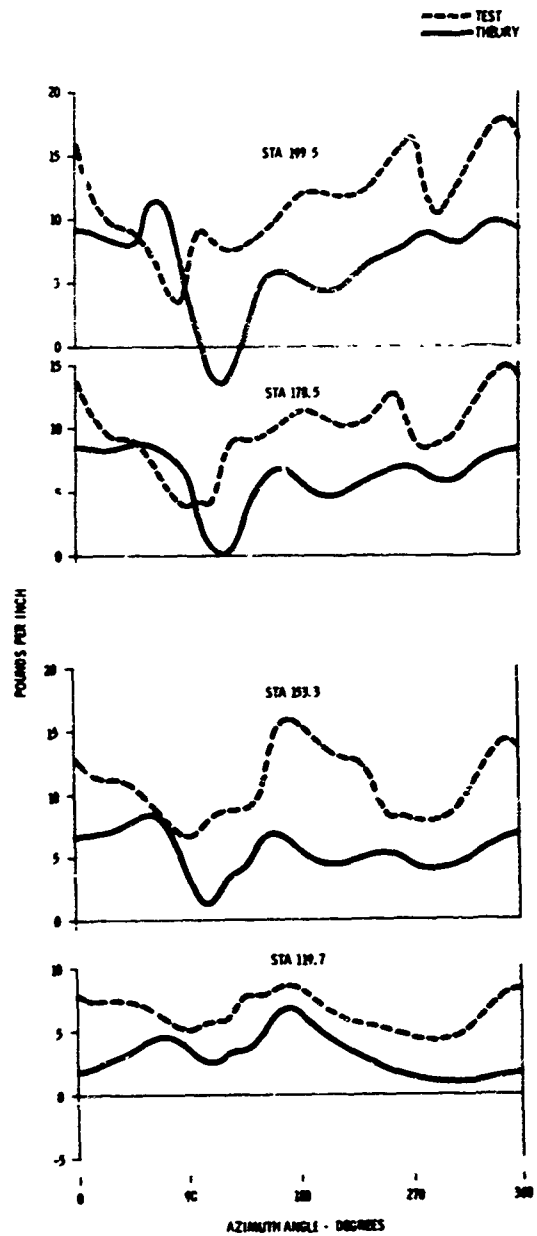Airloads, Cornell Program,
Condition 37 (Pullup
at 124 Knots TAS)

99

Figure 139. Measured and Computed
Airloads, Cornell Program,
Condition 39 (Pullup
at 206 Knots TAS)

Figure 140. Measured and Computed
Airloads, Cornell Program,
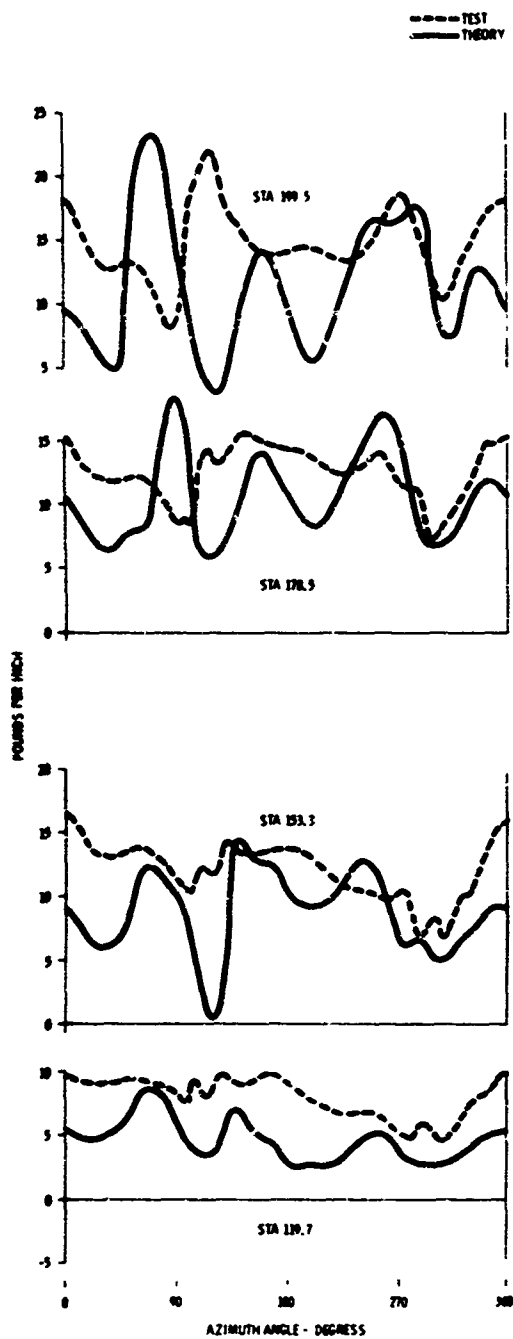Condition 40 (Pullup
at 206 Knots TAS)

100

Figure 141. Measured and Computed
Airloads, Cornell Program,
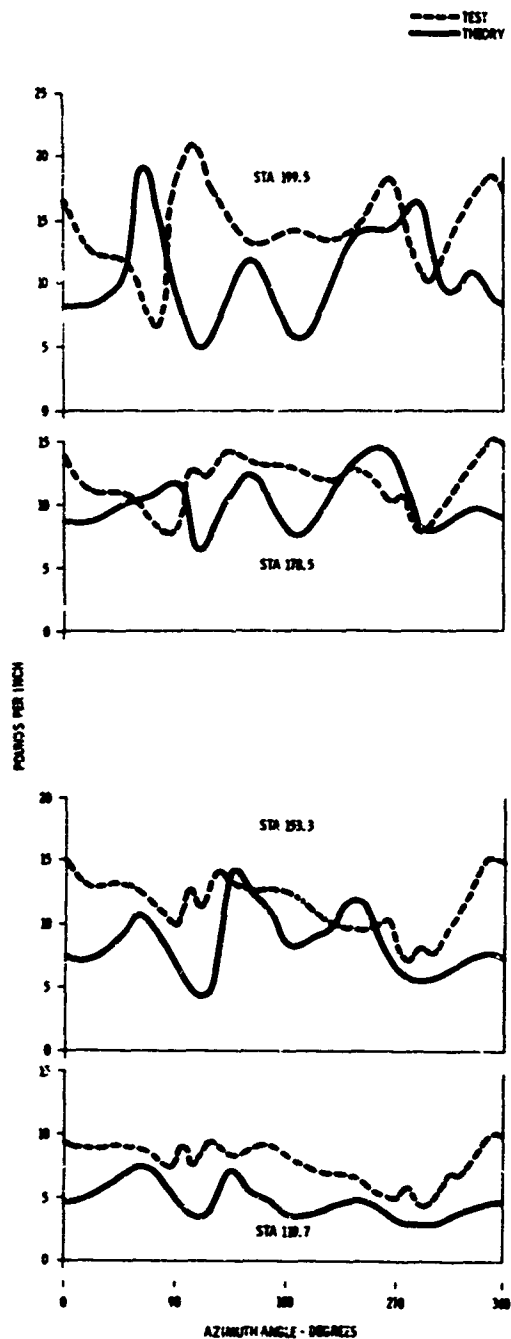Condition 46 (Left Turn
at 161 Knots TAS)

Figure 142. Measured and Computed
Airloads, Cornell Program,
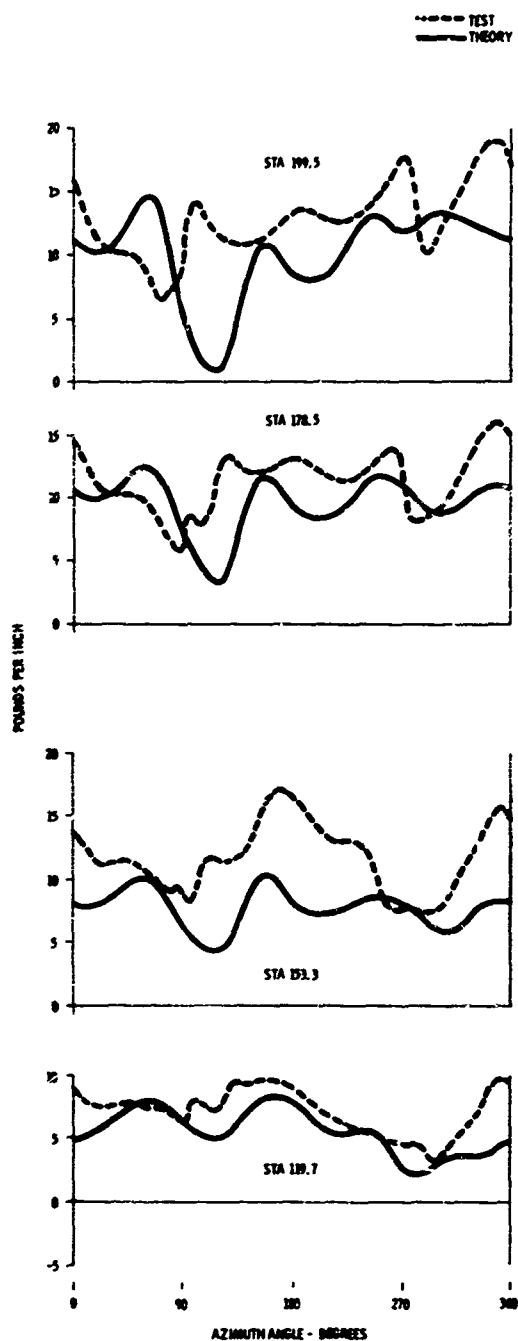Condition 50 (Right Turn
at 208 Knots TAS)

101

Figure 143. Measured and Computed
Airloads, Cornell Program,
Condition 2 (Collective
Pullup at 0 Knot TAS)
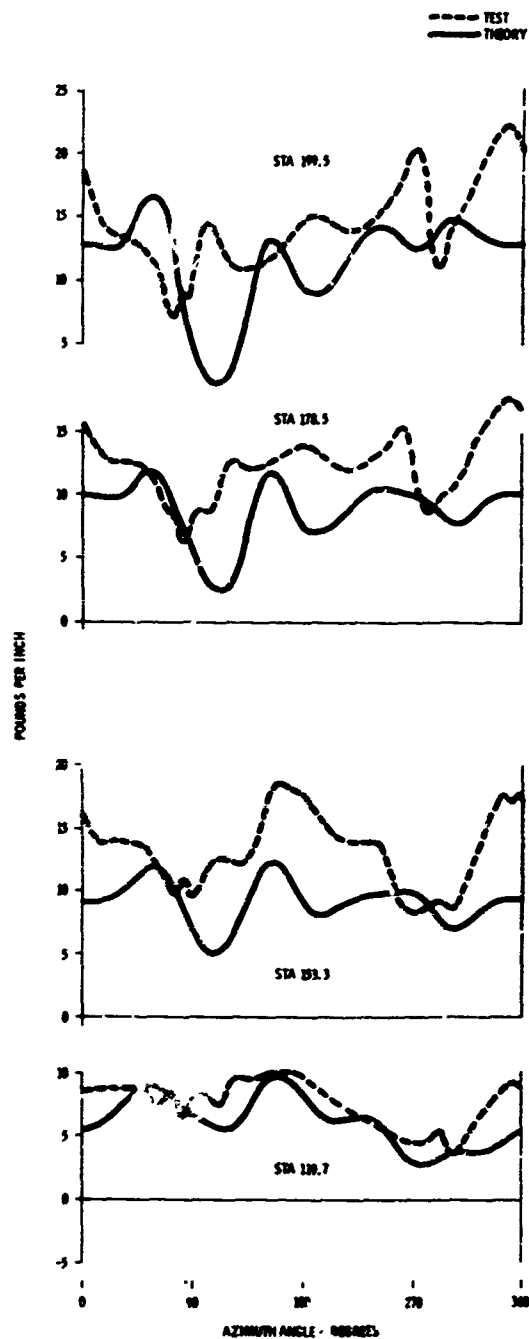
Figure 144. Measured and Computed
Airloads, Cornell Program,
Condition 3 (Collective
Pullup at 0 Knot TAS)

Figure 145. Measured and Computed
Airloads, Cornell Program,
Condition 6 (Forward Flight at
59.5 Knots TAS)

Figure 146. Measured and Computed
Airloads, Cornell Program,
Condition 7 (Forward Flight at
80.5 Knots TAS)

Figure 147. Measured and Computed
Airloads, Cornell Program,
Condition 9 (Left Turn at 61
Knots TAS)

Figure 148. Measured and Computed
Airloads, Cornell Program,
Condition 10 (Right Turn at 58
Knots TAS)

Figure 149. Measured and Computed
Airloads, Cornell Program,
Condition 12 (Right Turn at 82
Knots TAS)

Figure 150. Measured and Computed
Airloads, Cornell Program,
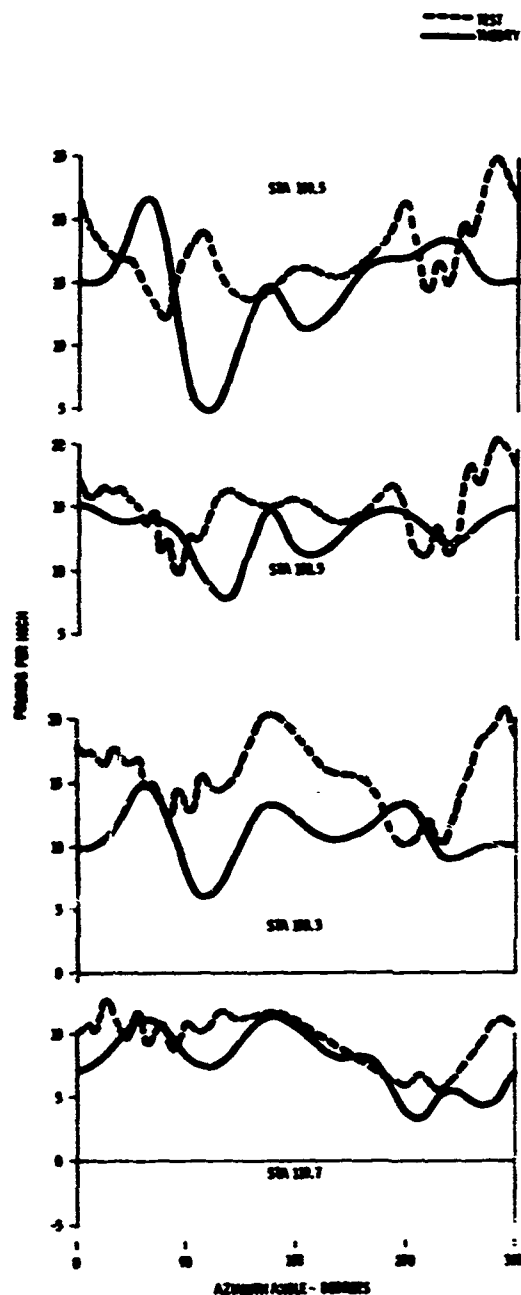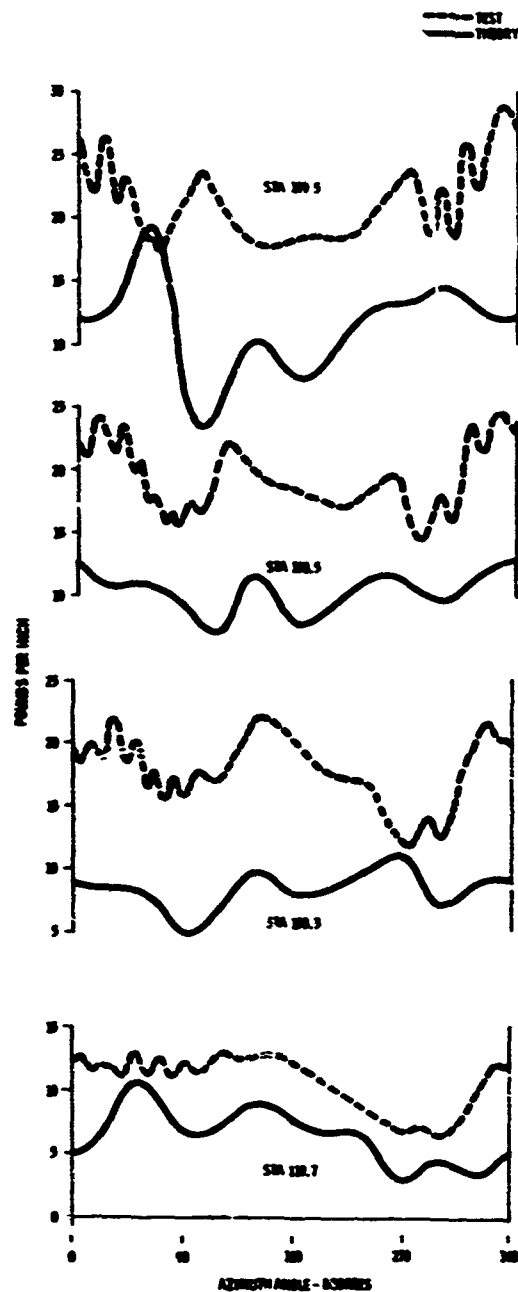Condition 13 (Collective Pullup
at 84.5 Knots TAS)

105

Figure 151. Measured and Computed
Airloads, Cornell Program,
Condition 14 (Collective Pullup
at 86 Knots TAS)

Figure 152. Measured and Computed
Airloads, Cornell Program,
Condition 15 (Collective Pullup
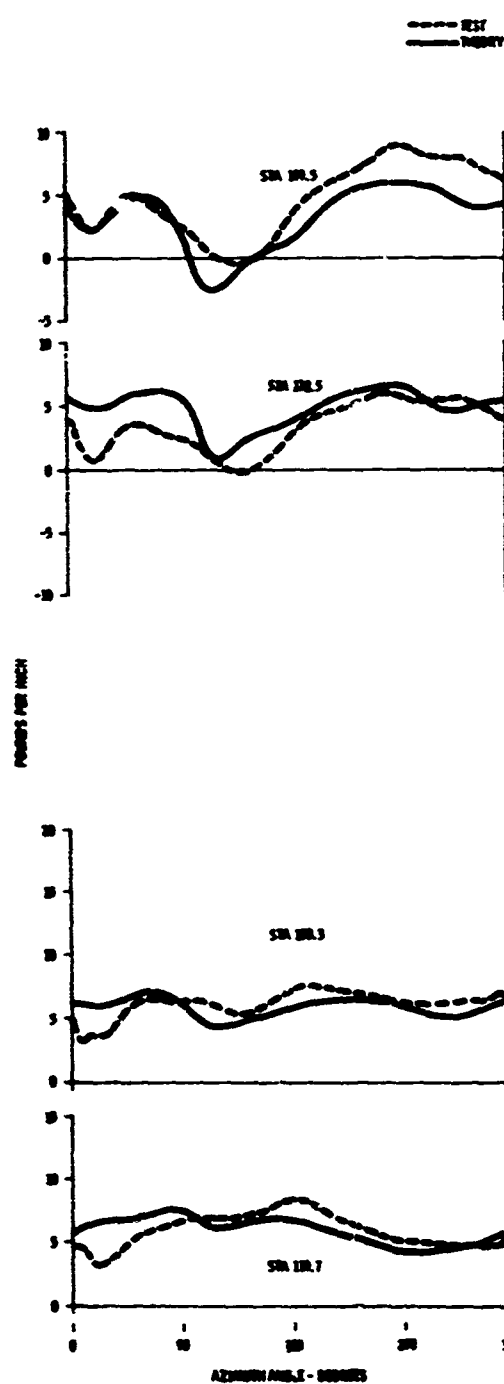at 87 Knots TAS)

Figure 153. Measured and Computed
Airloads, Cornell Program,
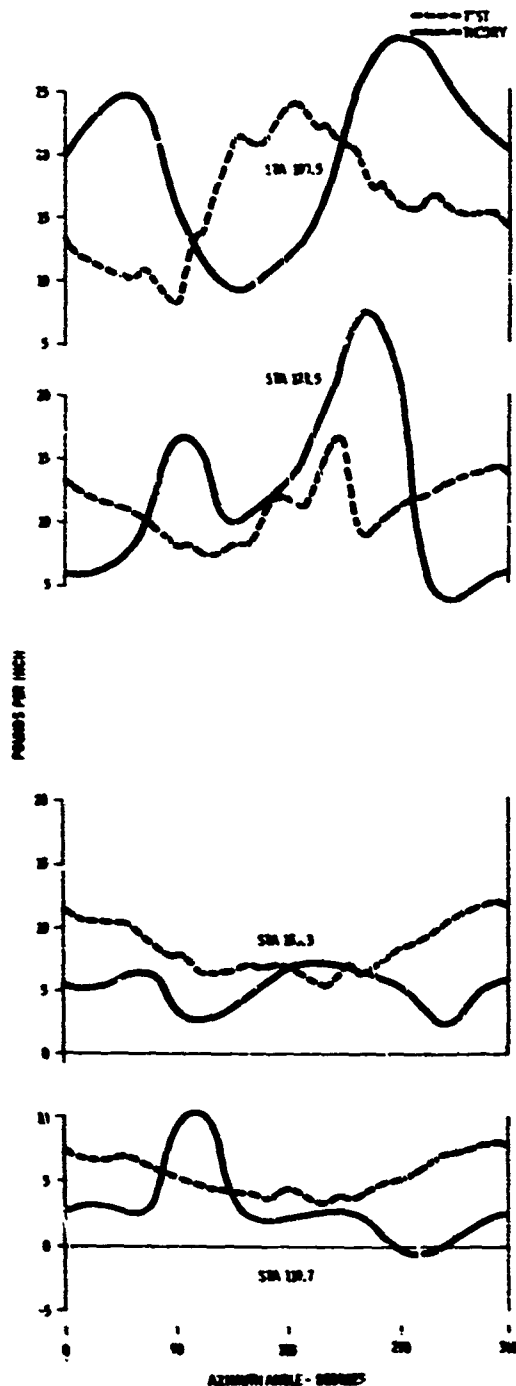Condition 17 (Autorotation at
83 Knots TAS)

Figure 154. Measured and Computed
Airloads, Cornell Program,
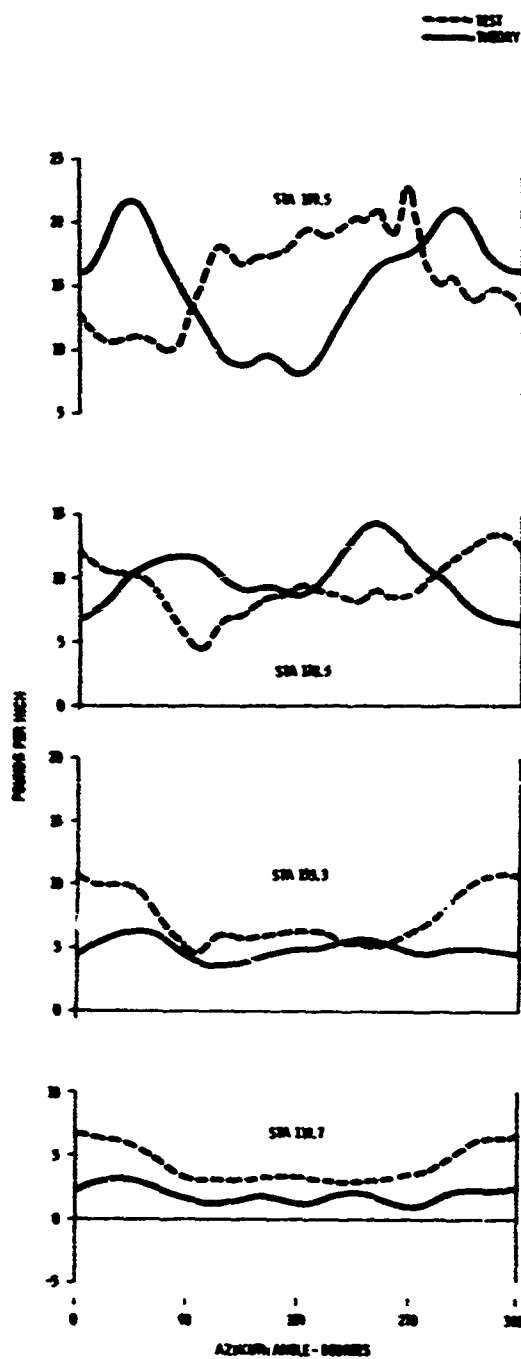Condition 18 (Transition)

Figure 155. Measured and Computed   Figure 156. Measured and Computed
Airloads, Cornell Program,   Airloads, Cornell Program,
Condition 20 (Transition)   Condition 22 (Flare)
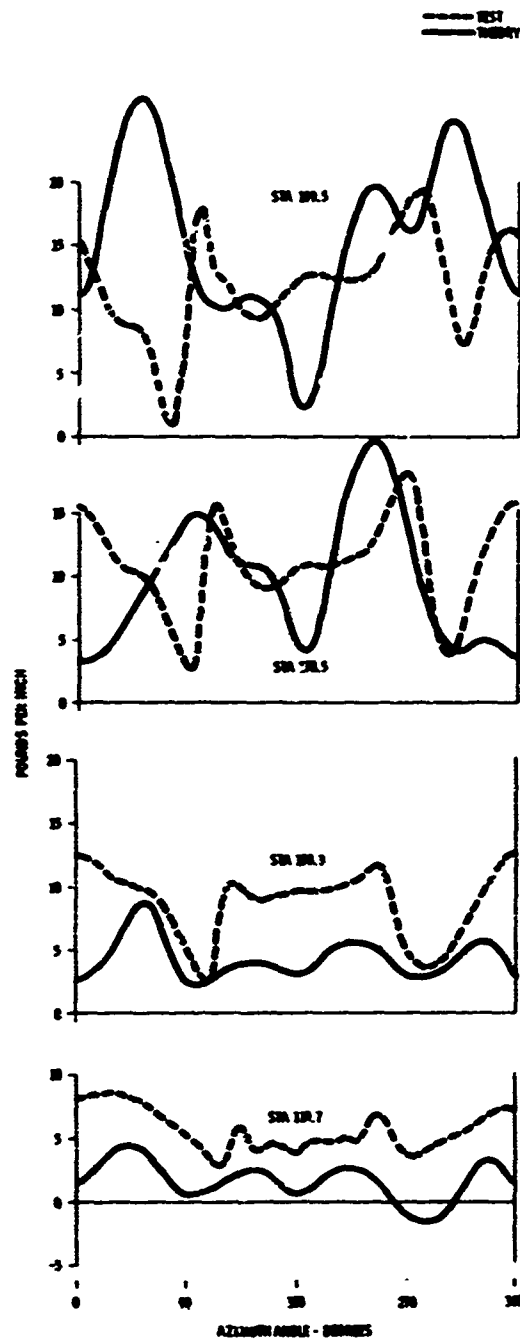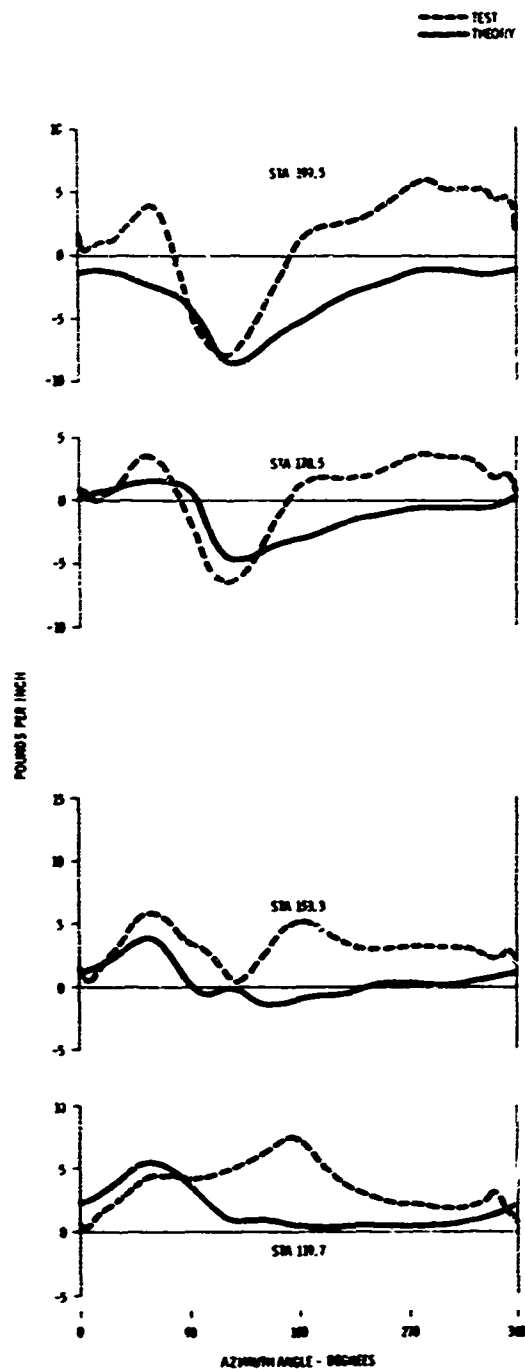
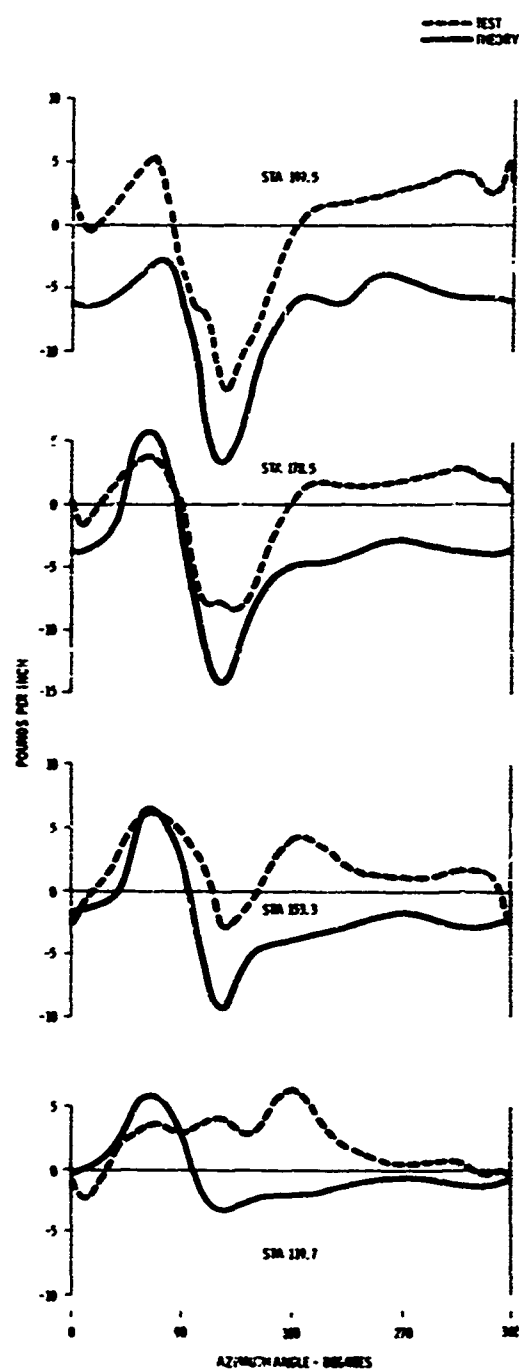Figure 157. Measured and Computed Airloads, Cornell Program, Condition 24 (Level Flight at 124.5 Knots TAS)

Figure 158. Measured and Computed Airloads, Cornell Program, Condition 28 (Level Flight at 170 Knots TAS)
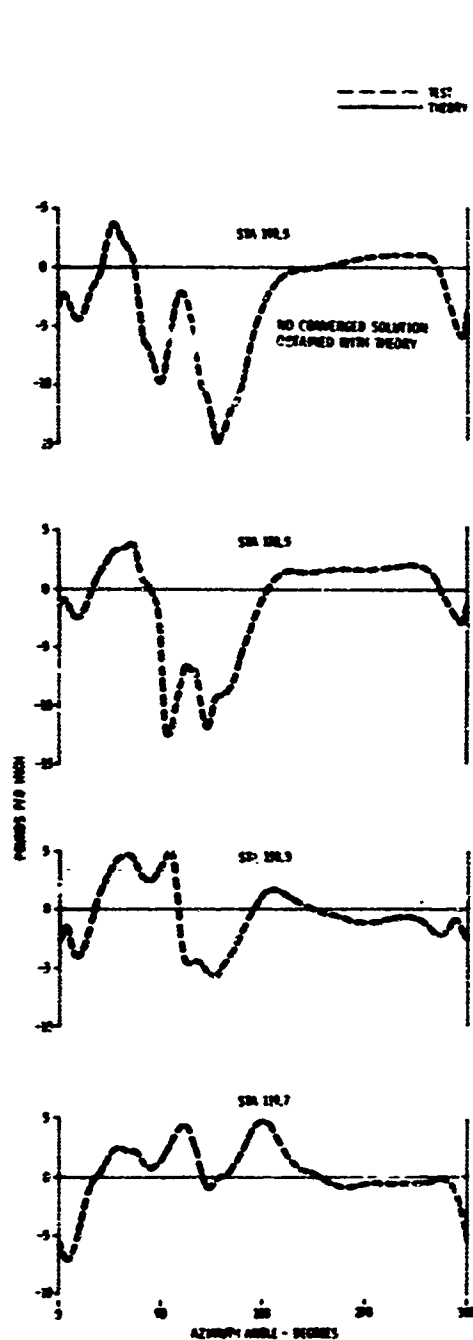
Figure 159. Measured and Computed
Airloads, Cornell Program,
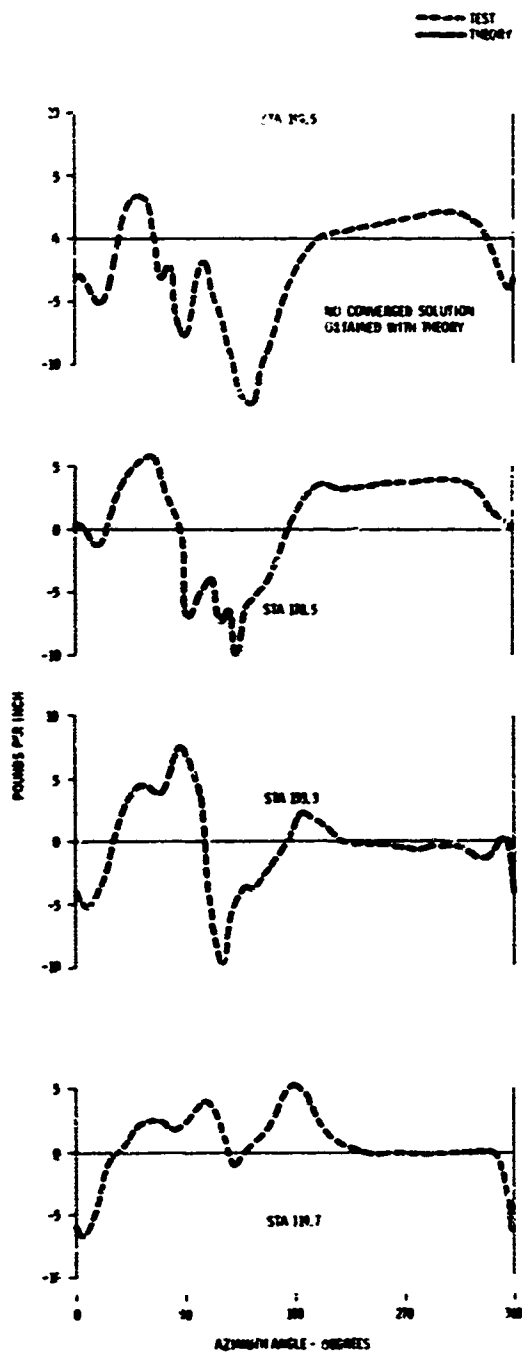Condition 29 (Level Flight at
215.5 Knots TAS)

Figure 160. Measured and Computed
Airloads, Cornell Program,
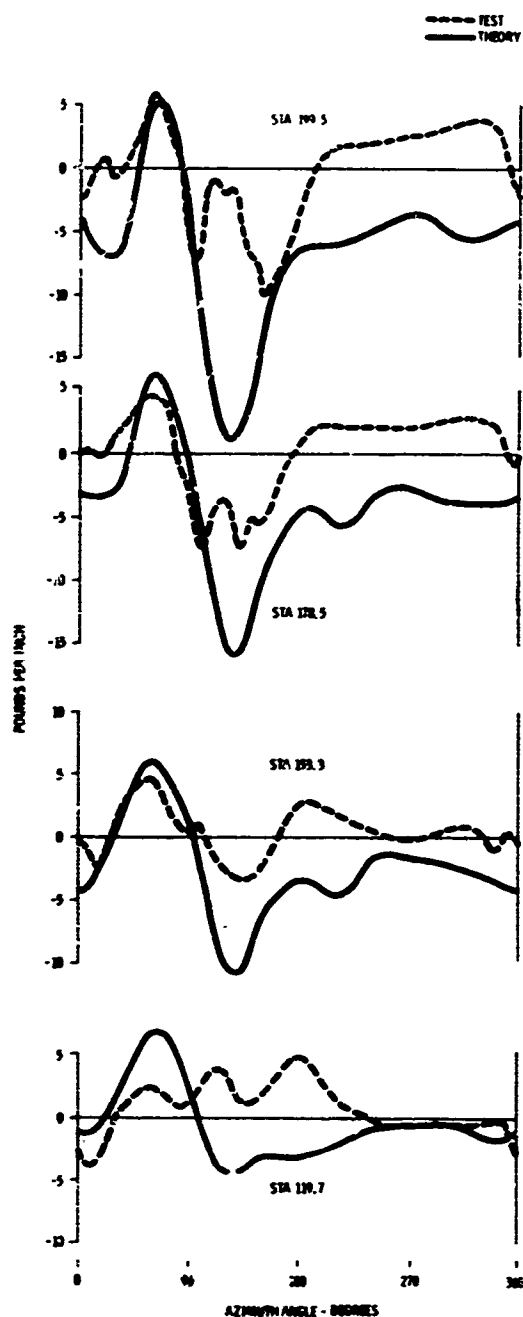Condition 30 (Level Flight at
219.5 Knots TAS)

Figure 161. Measured and Computed
Airloads, Cornell Program,
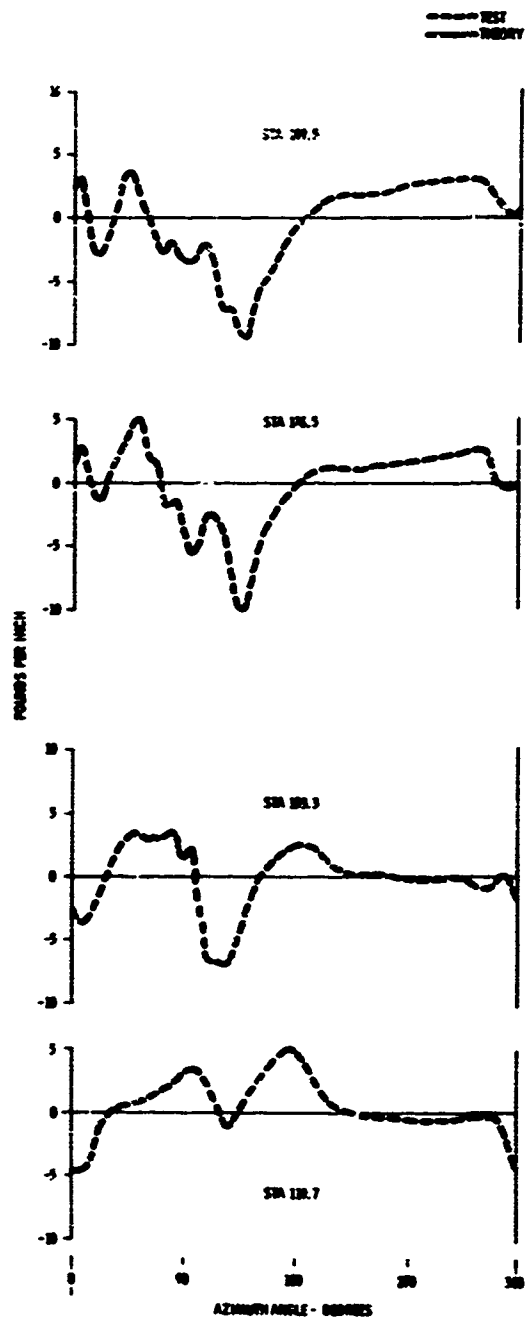Condition 34 (Level Flight at
202.5 Knots TAS)

Figure 162. Measured and Computed
Airloads, Cornell Program,
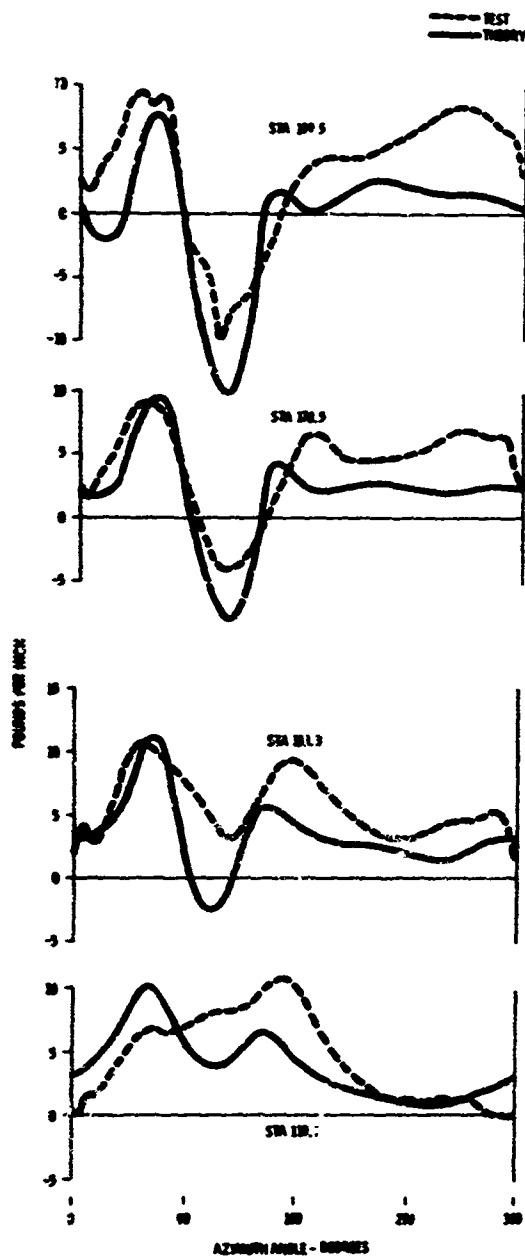Condition 35 (Level Flight at
219 Knots TAS)

111

Figure 163. Measured and Computed
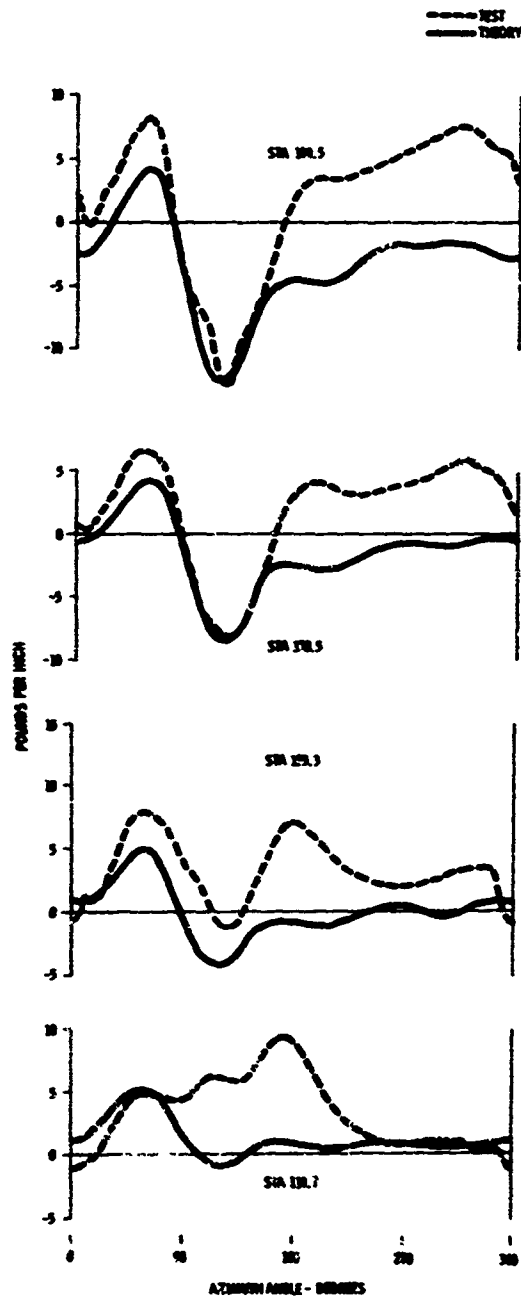Airloads, Cornell Program,
Condition 38 (Pullup at
160 Knots TAS)

Figure 164. Measured and Computed
Airloads, Cornell Program,
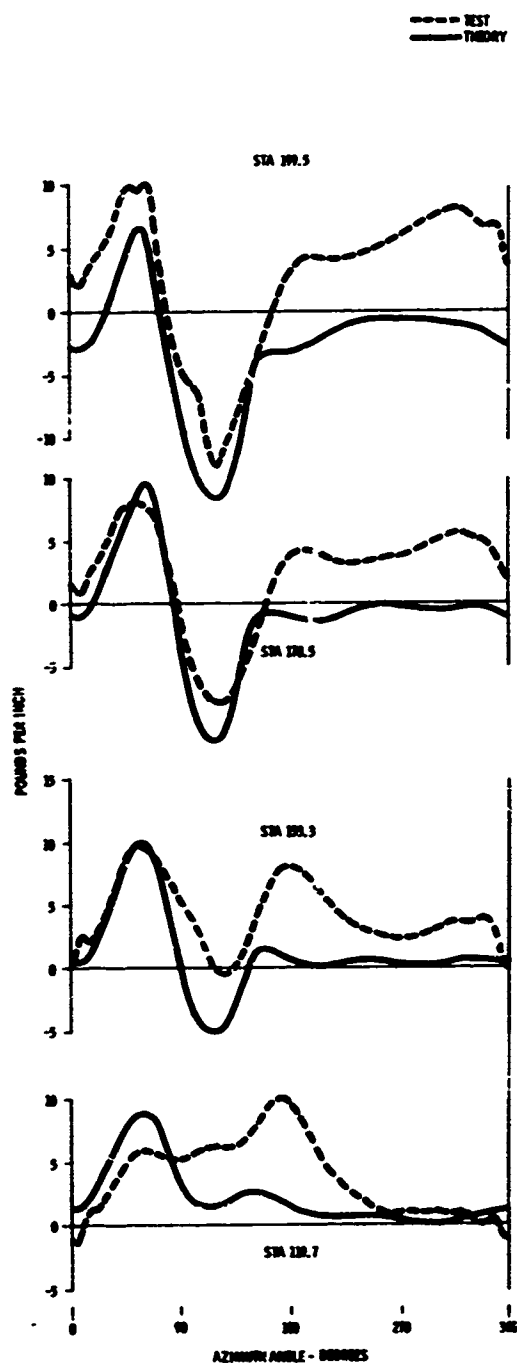Condition 41 (Pullup at
83 Knots TAS)

Figure 165. Measured and Computed
Airloads, Cornell Program,
Condition 42 (Pullup at
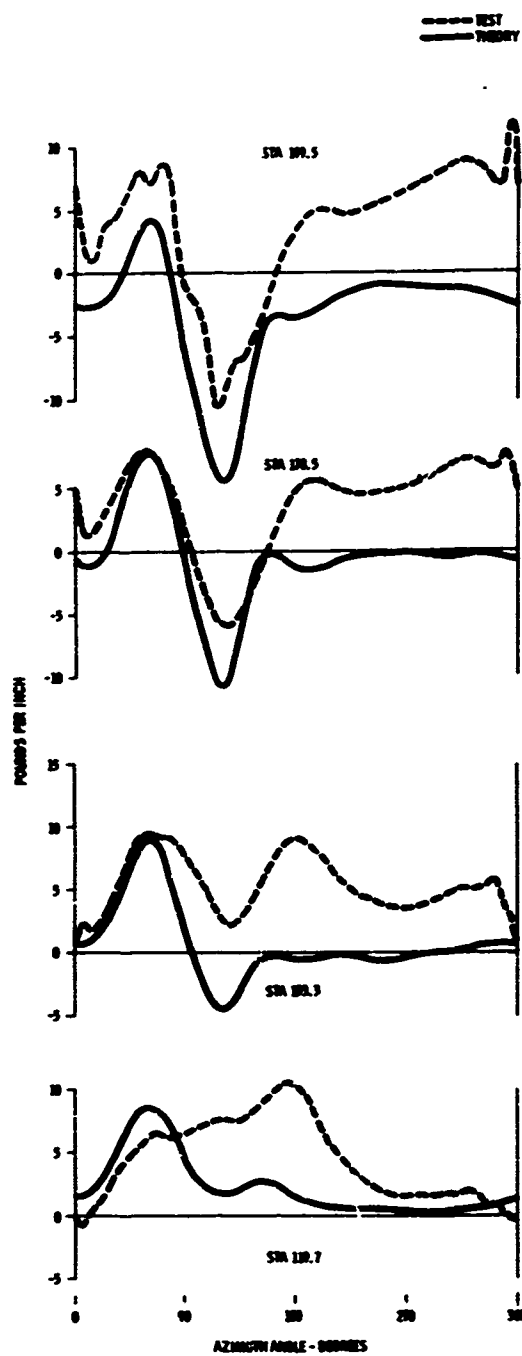166 Knots TAS)

Figure 166. Measured and Computed
Airloads, Cornell Program,
Condition 43 (Pullup at
163 Knots TAS)

113

Figure 167. Measured and Computed Airloads, Cornell Program, Condition 44 (Pullup at 162 Knots TAS)

Figure 168. Measured and Computed Airloads, Cornell Program, Condition 45 (Left Turn at 124 Knots TAS)
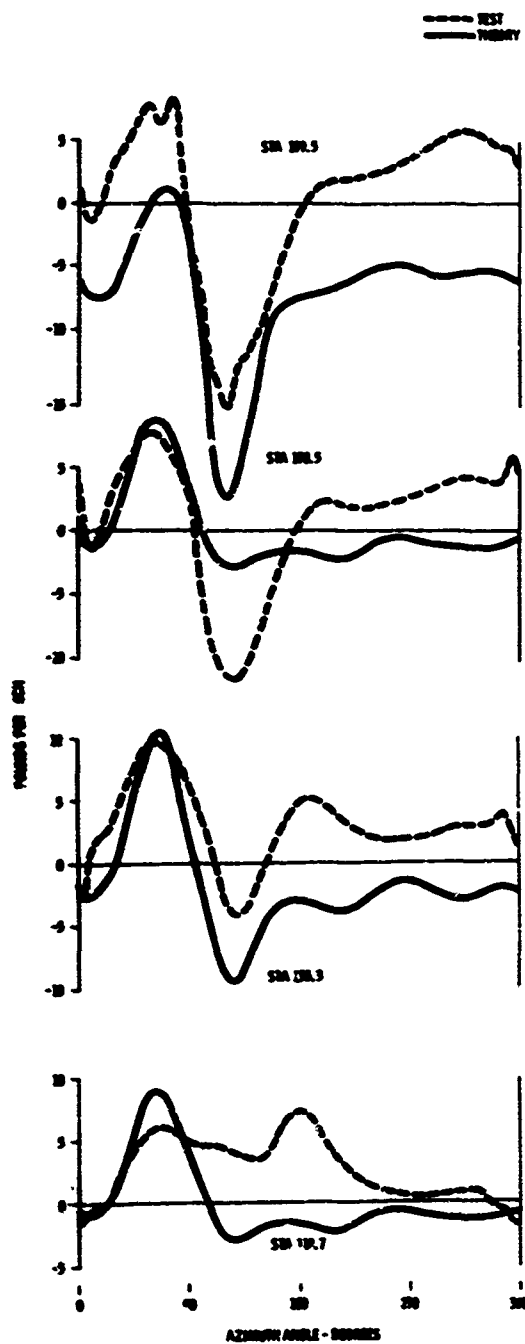
Figure 169. Measured and Computed
Airloads, Cornell Program,
Condition 47 (Left Turn at
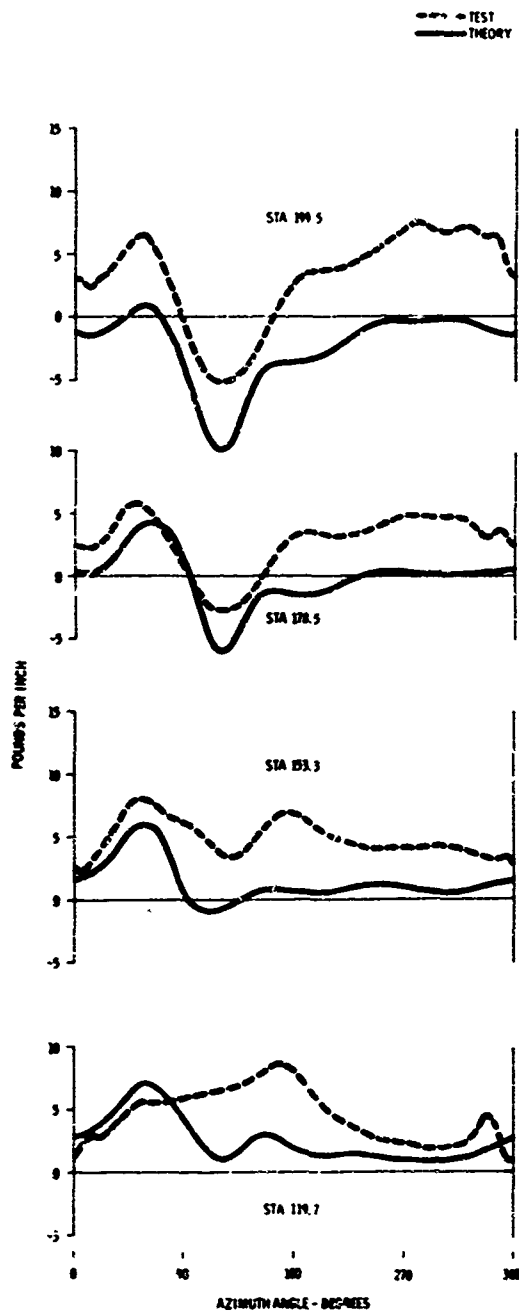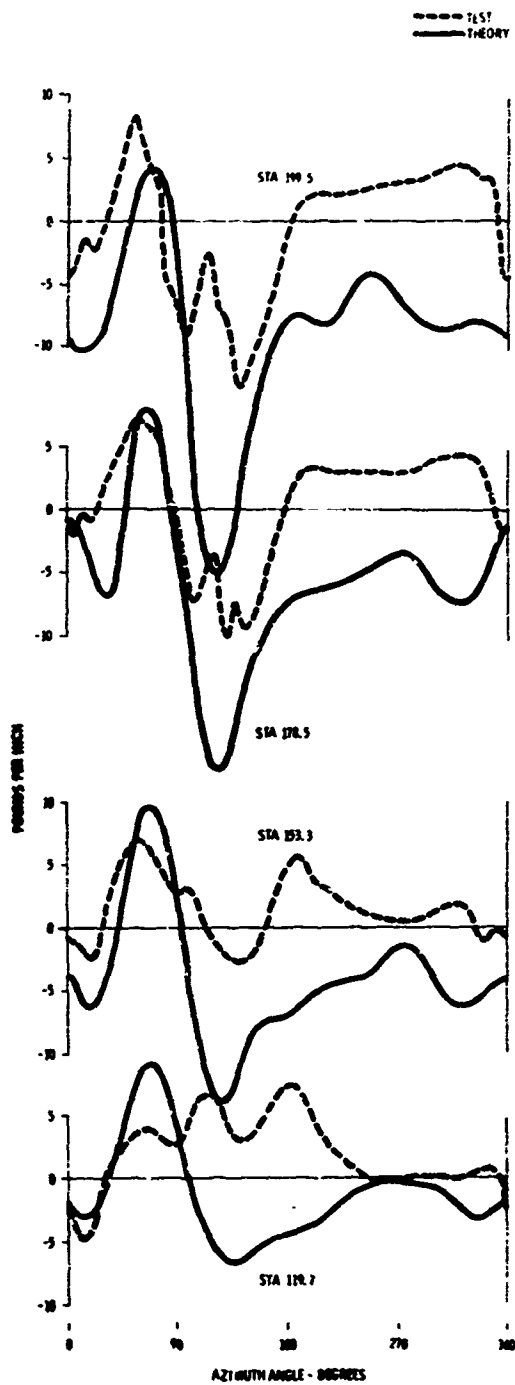207.5 Knots TAS)
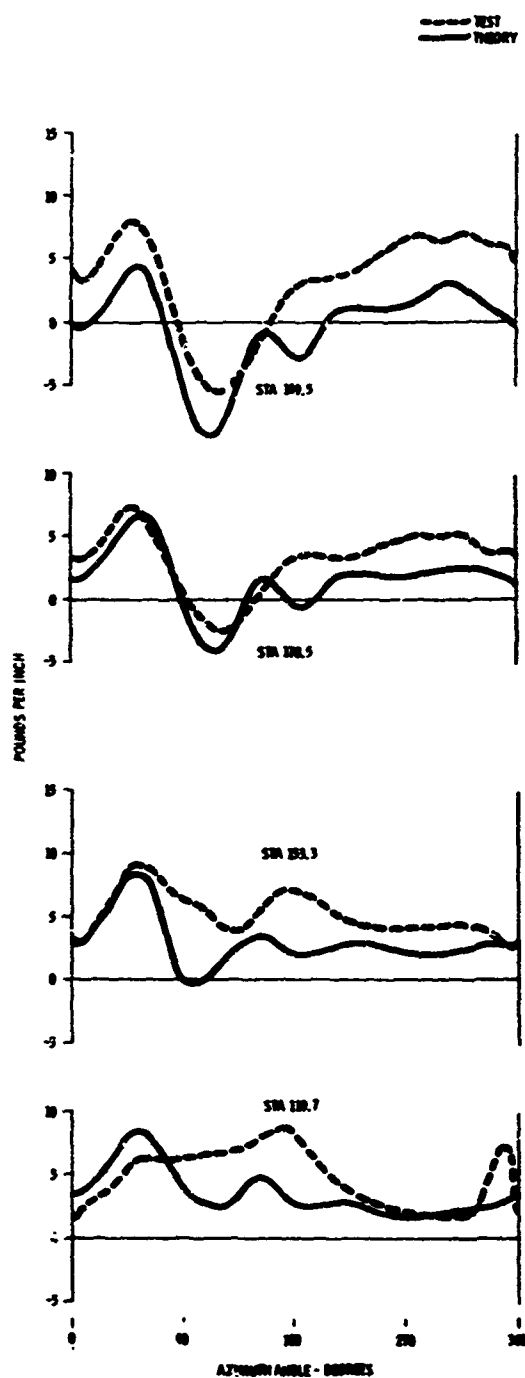
Figure 170. Measured and Computed
Airloads, Cornell Program,
Condition 48 (Right Turn at
124 Knots TAS)
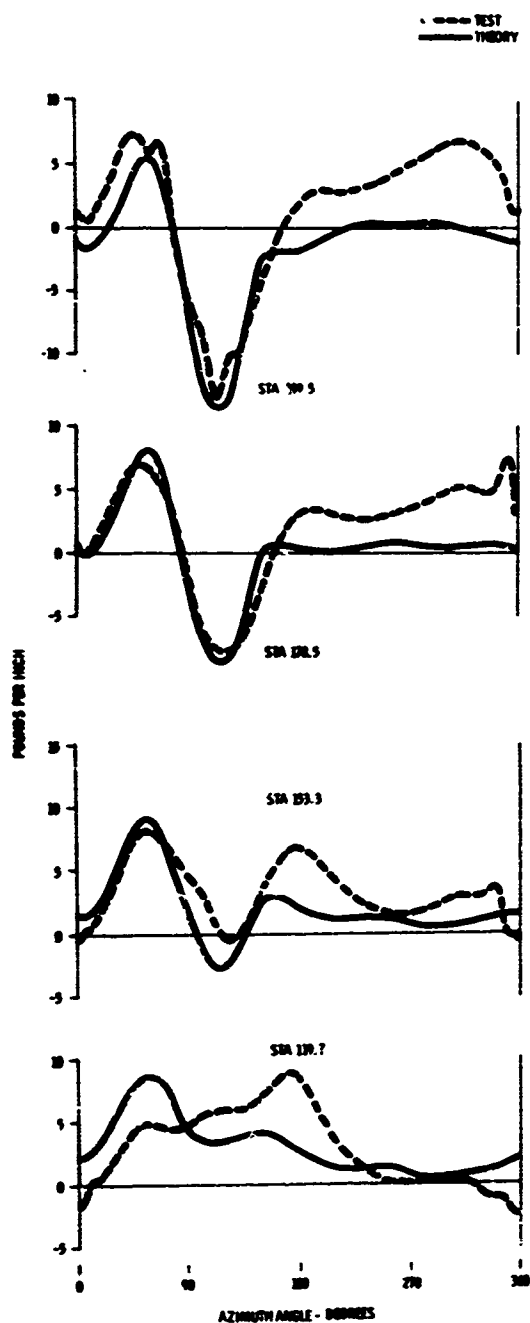
Figure 171. Measured and Computed Airloads, Cornell Program, Condition 49 (Right Turn at 164 Knots TAS)

Figure 172. Airloads Computed from Equilibrium, Condition 5 (Forward Flight at 51 Knots TAS)

116

<figure>

Figure 173. Airloads Computed from
Equilibrium, Condition 8
(Forward Flight at 105 Knots TAS)

Figure 174. Airloads Computed from
Equilibrium, Condition 25
(Level Flight at 163.5 Knots TAS)
</figure>

117
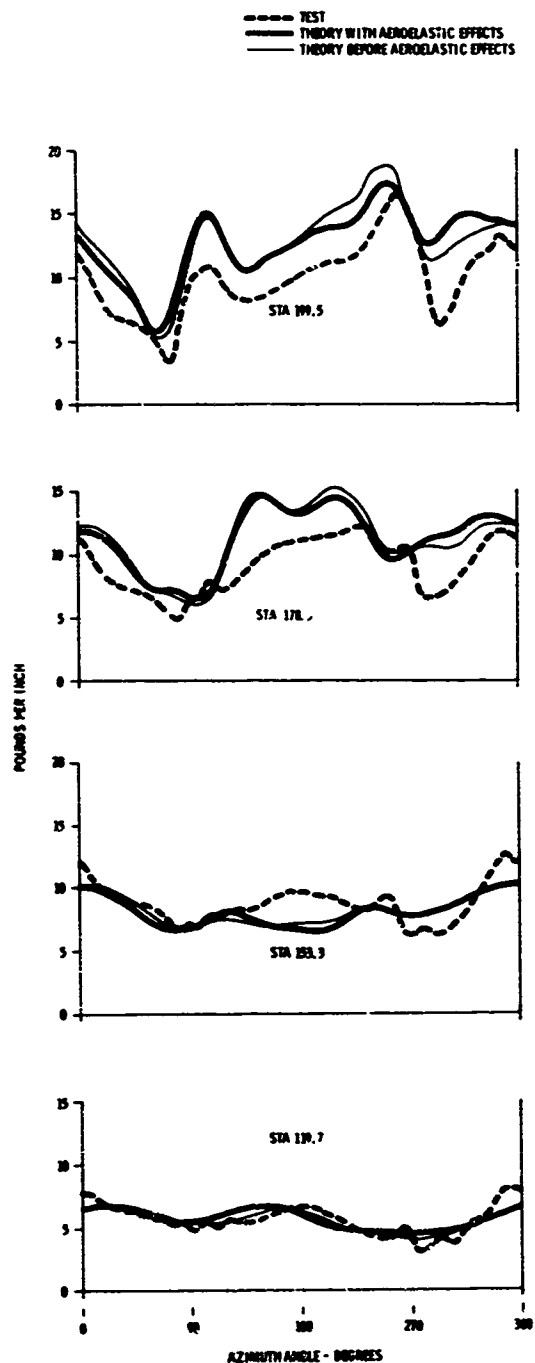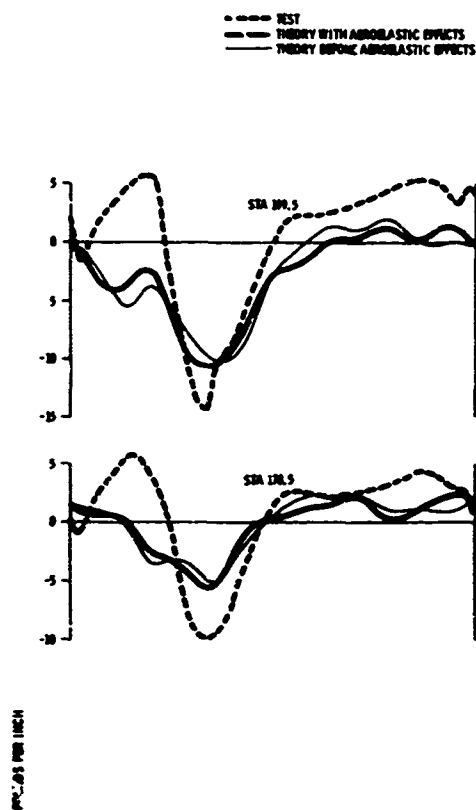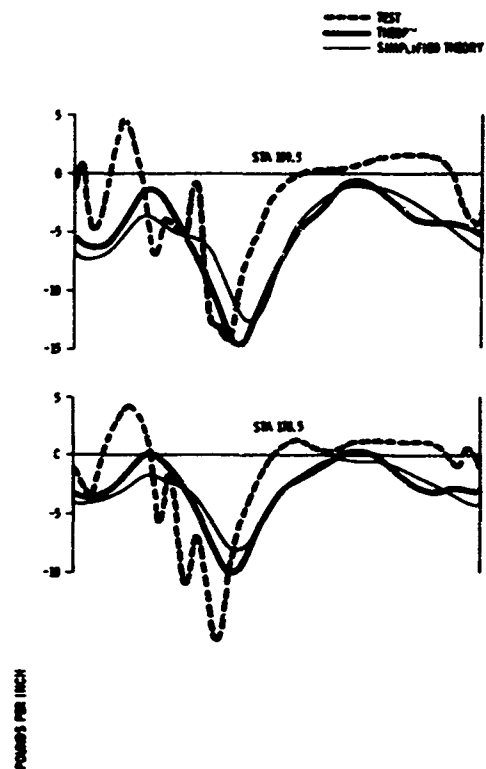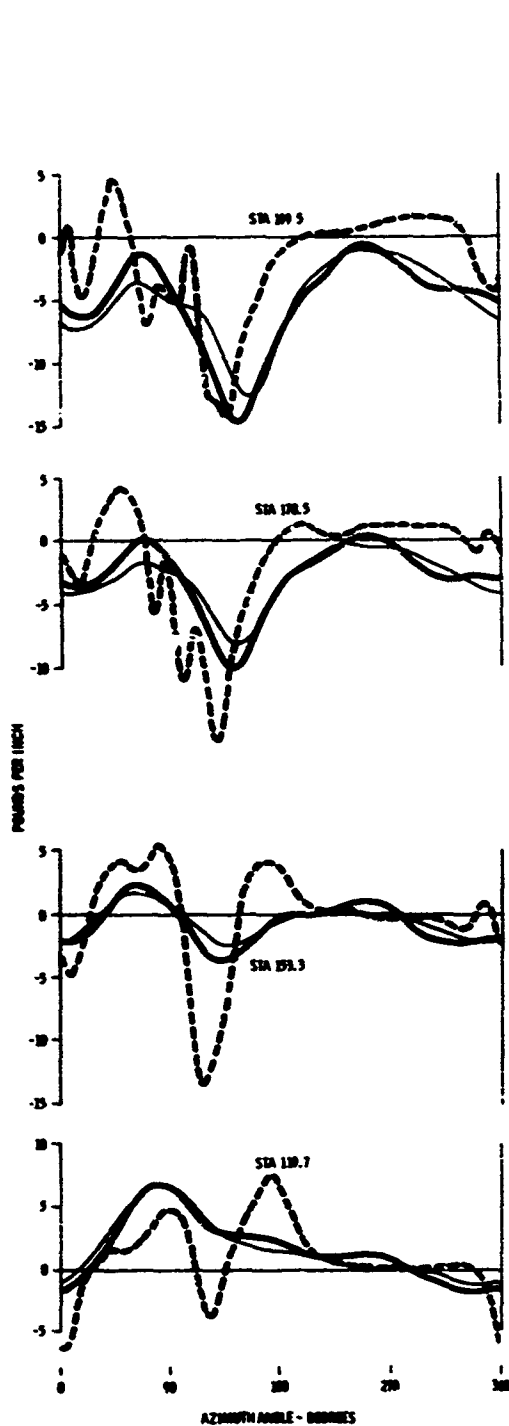
Figure 175. Airloads Computed from
Equilibrium, Condition 31
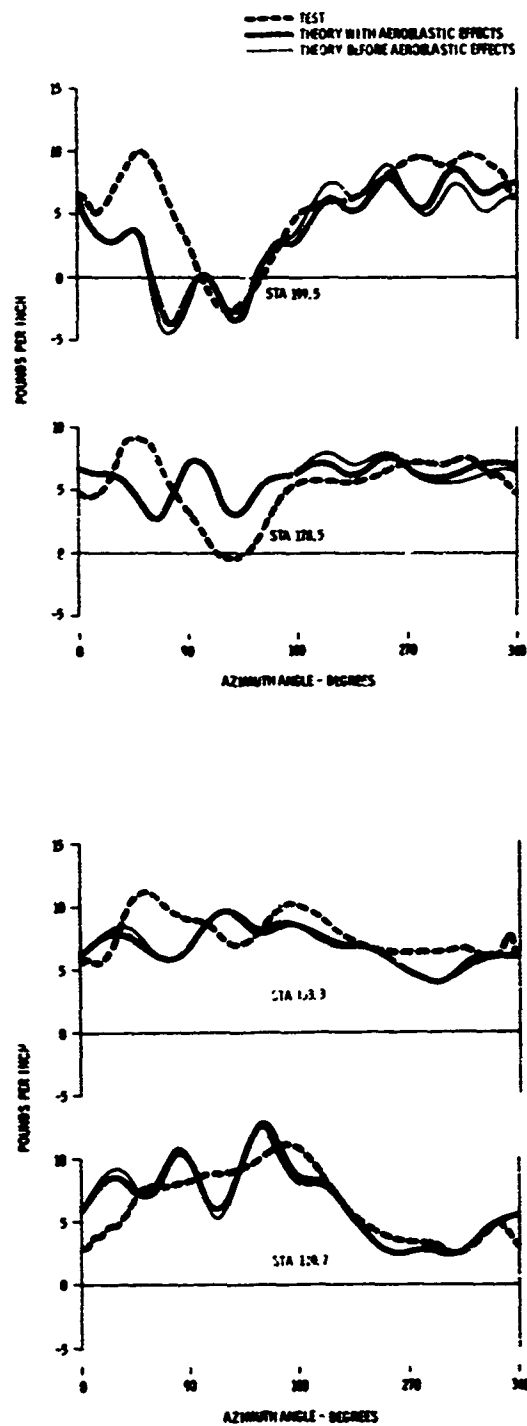(Level Flight at 232 Knots TAS)

Figure 176. Airloads Computed from
Equilibrium, Condition 37
(Pullup at 124 Knots TAS)

118

DOCUMENT CONTROL DATA - R & D

(Security classification of title, body of abstract and indexing annotation must be entered when the overall report is classified)

1. ORIGINATING ACTIVITY (Corporate author)	2a. REPORT SECURITY CLASSIFICATION
Lockheed-California Company	Unclassified
Burbank, California	2b. GROUP

3. REPORT TITLE

In-Flight Measurement and Correlation With Theory of Blade Airloads and Responses on the XH-51A Compound Helicopter Rotor-Volume III, Theoretical Prediction of Airloads and Structural Loads and Correlation With Flight Test Measurements

4. DESCRIPTIVE NOTES (Type of report and inclusive dates)

Final Technical Report

5. AUTHOR(S) (First name, middle initial, last name)

J. E. Sweers

6. REPORT DATE	7a. TOTAL NO. OF PAGES	7b. NO. OF REFS
May 1968	141	5

8a. CONTRACT OR GRANT NO.	9a. ORIGINATOR'S REPORT NUMBER(S)
DA 44-177-AMC-357(T)	
b. PROJECT NO.	USAAVLABS Technical Report 68-22C
TASK 1F125901A14608	
c.	9b. OTHER REPORT NO(S) (Any other numbers that may be assigned this report)
d.	LR 21072

10. DISTRIBUTION STATEMENT

This document has been approved for public release and sale; its distribution is unlimited.

11. SUPPLEMENTARY NOTES	12. SPONSORING MILITARY ACTIVITY
Volume III of a 3-volume report	U.S. Army Aviation Materiel Laboratories Fort Eustis, Virginia

13. ABSTRACT

This report presents the results of a two-phase research program consisting of (1) in-flight measurement of aerodynamic pressures and structural loads on a compound, rigid-rotor helicopter, and (2) correlation of these data with theoretical results.

Flight test data obtained in Phase I and recorded on an oscillograph were read on an oscillograph reading machine and were processed in an automatic data reduction program. This data processing consisted of integration of the pressure data to obtain the distribution of aerodynamic lift and pitching moments over the rotor blade, as functions of azimuth position. Airload and structural load data were harmonically analyzed.

Output of the data reduction program was used in Phase II as input to the correlation program. The measured airloads were used to compute the theoretical bending and torsion responses of the blade. The measured torsion moments were used in the theoretical prediction of the airloads. The results of the applied theories are compared with the flight measurements.

DD FORM **1473** REPLACES DD FORM 1473, 1 JAN 64, WHICH IS OBSOLETE FOR ARMY USE.

14. KEY WORDS	LINK A		LINK B		LINK C	
	ROLE	WT	ROLE	WT	ROLE	WT
Compound Helicopter. Differential Pressure Measurements Dynamic Response Harmonic Analysis Helicopter High Advance Ratio Modes of Vibration Pressure Measurements Rigid Rotor Rotor Loads XH-51A						